POLITECNICO DI TORINO

Corso di Laurea Magistrale

in INGEGNERIA MECCANICA

Tesi di Laurea Magistrale

Implementation of an off-road tyre model for real-time dynamic driving simulator

Relatori

Prof. Ing. Mauro Velardocchia

Ing. Antonio Tota

Candidato

Lorenzo Mancardi

Tutor aziendale

Ing. Pietro Ciadamidaro
(Danisi Engineering S.r.l)

Anno Accademico 2019/2020

"Che cos'è il genio?
È fantasia, intuizione, decisione e velocità d'esecuzione"
[Il Perozzi - Amici miei]

Abstract

The purpose of this thesis is to develop a tyre model for simulating the off-road driving, suitable to run in real-time on a professional dynamic driving simulator.

The dynamic phenomenon of tyre-soil interaction is complex; considering the fundamental equations of the "Terramechanics", the model aims to calculate forces and moments, which are generated by the wheel during the contact with a soft soil, such as sand, and loam.

The model has been developed in MATLAB/Simulink environment, using the co-simulation technique with a commercial 14 DoF vehicle dynamics software.

The tyre longitudinal forces (traction/braking) have been modelled with the assumption of considering the tyre as a rigid wheel. This is valid if the tyre deformation is negligible with respect to the terrain deformation and it is the case of sand soil.

The tyre lateral forces, in this study, do not consider the so-called "bulldozing effect", which is due to the wheel compacting the terrain in the lateral direction.

Using the same soil properties and an equivalent vehicle model, the results have been compared to those obtained by a commercial multibody software, capable of running reliable vehicle dynamics simulations on deformable terrains.

Once the comparison was satisfactory, the developed tyre model has been implemented on a real-time dynamic driving simulator and it has given the feeling of a realistic off-road driving.

In conclusion, real-time simulation results have been successfully compared with offline simulation results.

Ringraziamenti

Desidero ringraziare tutte le persone che in modi diversi mi hanno supportato in questo lavoro e durante gli anni di studio.

Ringrazio il mio relatore, Prof. Ing. Mauro Velardocchia, per la fiducia mostrata, dandomi la possibilità di svolgere questa Tesi e per avermi seguito con professionalità ed umanità.

Un ringraziamento particolare all' Ing. Antonio Tota che mi ha aiutato con grande disponibilità, competenza e preziosi consigli.

Inoltre, desidero ringraziare l'azienda "Danisi Engineering S.r.l", in particolare il team di "Advanced Vehicle Dynamics". Un sincero grazie per l'ottimo rapporto instauratosi all'Ing. Pietro Ciadamidaro che, con pazienza, competenza ed umiltà, mi ha sostenuto in questo lavoro di Tesi, dedicandomi parte del suo tempo.

Un grande grazie al gruppo di amici "Le Fase 'd…", sempre pronti ad accogliermi con un bicchiere (a volte due) dopo i classici periodi di clausura.

Un grazie a Marta e Anna per il supporto emotivo nei momenti di gioia e disperazione.

Come nel nuoto, se non fosse per i miei fratelli, mi sarei fermato alla terza media: grazie di cuore.

Infine, un grazie speciale ai miei genitori, presenza costante in questo percorso, pronti ad incoraggiarmi e supportami nei momenti più difficili.

Contents

Nomenclature

b	tyre width	[m]
b_{ti}	the smaller dimension of a rectangular plate	[m]
c	soil cohesion	[Pa]
c_0 c_1	coefficients related to the angle at which the maximum stress occurs	[-]
D	diameter (tyre)	[m]
F_{thrust}	tractive effort (tyre)	[N]
F_x	longitudinal force (tyre)	[N]
F_y	lateral force (tyre)	[N]
F_{ybd}	lateral force due to bulldozing effect (tyre)	[N]
F_z	vertical load (tyre)	[N]
j_x	longitudinal shear displacement	[m]
j_y	lateral shear displacement	[m]
k_c	cohesion modulus (soil properties)	[N/m^(n+1)]
k_φ	friction modulus (soil properties)	[N/m^(n+2)]
k_x	shear deformation modulus in the longitudinal direction (soil properties)	[m]
k_y	shear deformation modulus in the lateral direction (soil properties)	[m]
M_x	overturning moment (tyre)	[Nm]
My	driving torque (tyre)	[Nm]
n	exponent of sinkage (soil properties)	[-]
R_u	undeformed radius (tyre)	[m]
S_d	longitudinal slip	[-]
V_x	longitudinal speed of vehicle	[m/s]
V_y	lateral speed of vehicle	[m/s]
W	vertical load (weight)	[N]
z	sinkage	[m]
α_c	slip angle	[rad]
γ_s	soil density	[kg/m^3]
ϑ	angle	[rad]

ϑ_e	entry angle	[rad]
ϑ_r	exit angle	[rad]
ϑ_m	max stress angle, angle at which the maximum stress occurs	[rad]
σ_n	normal stress along the contact patch	[Pa]
τ_{max}	max longitudinal shear stress	[Pa]
τ_x	longitudinal shear stress	[Pa]
τ_y	lateral shear stress	[Pa]
ϕ	angle of internal friction of the soil	[rad]

List of figures

List of tables

1 Introduction

"The problem of wheel–terrain interaction may seem antiquated in this technologically advanced era of space exploration, nanotechnology, robotics and microelectronics. It is, nevertheless, a complex problem, at least from an analytical point of view, for the characteristics of wheel–terrain interaction are influenced by a large number of design and operational factors, as well as terrain characteristics" [1].

The tyre is responsible for transmitting the forces from the vehicle to the road and it allows to control the vehicle. The dynamic phenomenon of tyre-road interaction is complex and, since tyres were used on vehicles, researchers had attempted to create a representative model of energy transfer between pneumatic tyre and surface. The research has been concentrated on the on-road tyre model, thus getting enough realistic representation of the tyre behaviour. The on-road tyre model, with respect to the off-road tyre model, has the advantage that the soil is non-deformable, making it easier to formulate the interaction between them.

In the past fifty years, the increased interest in agriculture mobility, construction and cross-country transport industries, military vehicles, and rover vehicles has made the study of the off-road vehicle important; efforts have been directed to create a realistic off-road tyre model for dynamic simulation to assess vehicle performance.

With this in mind, the work of this thesis aims to develop a tyre model for simulating the off-road driving, with the purpose to represent the interaction between tyre and deformable soil. The fundamental characteristic of the developed tyre model is to run in real-time in order to be suitable on a professional dynamic driving simulator.

The science of analysing soil properties during interaction with tracked and wheeled vehicles is called "Terramechanics".

To create a model capable of interacting with a complete vehicle system during dynamic simulation, it is necessary to focus on two aspects: the first one is that the outcome to predict vehicle performance must be acceptable, and the second aspect is that the computational efficiency must be reasonable. If the model is implemented on a dynamic driving simulator, the computational effort will be further limited because the model must run in real time.

The following models are suitable to predict vehicle performance on soft soil:

- Empirical models;
- Analytical models (Finite/Discrete element methods);
- Semi-empirical models.

Based on laboratory and field test data, the empirical models give formulations which allow to measure vehicle performance: usually, these models are used to assess

simple vehicle mobility like go or no-go situations. An example of application of these empirical models is the WES (Waterways Experiment Station) method developed by the US Army [2].

Although empirical models are able to run in real time, their application is limited because they can only evaluate the performance of vehicles which are in conditions similar to the test tyre: due to this limit, empirical models cannot be used to give results regarding problems outside the scope of the experimental tests.

The analytical models use the physical principles of the interaction between the tyre and soil. The degree of complexity varies from the simple models that consider tyre as a rigid ring and terrain as a spring-damper system, to very detailed models that use finite/discrete element formulation for both tyre and terrain [2]. During the last three decades the increase of computational capability has allowed to implement the finite element method, which gives accurate and reliable results: this methodology is not suitable for performing real-time simulations because of high computation time.

The semi-empirical models, which combine empirical formulation, experimental data and analytical methods, are the most versatile and used because they represent well enough the tyre-soil interaction and, due to the low required computational effort, they can run in real time.

These models, on which this thesis is developed, are based on the formulation given by M. G. Bekker and J. Y. Wong, that, among others, are two of the most important researchers in Terramechanics.

Bekker's equation is based on the use of the apparatus called "Bevameter", that correlates the vehicle load, specifically the vertical pressure distribution in the contact patch, and the sinkage. The bevameter technique uses a sinkage plate of specified dimensions to parameterise the relationship between normal pressure and sinkage. Furthermore, Bekker provided a formulation for taking into account the soil shearing phenomenon, even if this formulation does not consider any correlation between the shear deformation of the soil and the normal stress produced by vehicle's weight.

In Terramechanics community there are other relations used to determine the shear stress, among which the most widely used formulations are those based on an empirical expression introduced by Janosi and Hanamoto. Their approach takes advantage of using the Mohr-Coulomb Failure Criterion to correlate the shear stress, which is tangential to the surface of the sinkage plate, with the normal stress. The formula developed by Janosi and Hanamoto, which properly models the shearing action at the soil-wheel interface, has been successfully applied to various studies: moreover, this formula, even if originally developed for tracked vehicles, has successfully been used on wheeled vehicles [3].

In this dissertation, starting from a literature overview (*chapter 2*), it is examined the characteristic equations of the interaction between tyre and soft soil and their implementation in MATLAB/Simulink environment, developing an off-road tyre model (*chapters 3-4-5*).

In *chapter 6* it is reported an analysis of the thrust and longitudinal forces available on off-road terrains.

In *chapter 7* it is described the developed external road model, which is necessary to simulate deformable soils; the tyre model and external road model constitute the developed off-road model, which can run in co-simulation with a commercial vehicle dynamics software.

In order to validate the developed off-road model, the results of the co-simulations are compared to the results obtained by a commercial multibody software, capable of running reliable vehicle dynamics simulations on deformable terrains: the comparison is reported in *chapter 8*.

After the validation through the simulations performed by the two software, in *chapter 9* it is described the implementation of the developed off-road model on a real-time dynamic driving simulator.

The data analysis of the tests, carried out on the driving simulator, are summarised in *chapter 10*, together with the feedback given by professional drivers.

The work of this thesis is developed in collaboration with the company "Danisi Engineering S.r.l".

2 Literature Review

This brief literature overview on off-road tyre model does not demand to be complete, but it focuses on most important concepts about tyre-terrain contact models, while for a thorough technical survey it is suggested to refer to Taheri's work [2]. Taheri's survey gives a picture of the most used models that have been developed for wheeled vehicles: he compares models with similar characteristics pointing out advantages and drawbacks.

In the book "Terramechanics and off-road vehicle engineering" [1] Wong presents the fundamentals of Terramechanics and focuses on the study of vehicle-terrain interaction from the traction perspective. Furthermore, he gives a brief review of the modelling of terrain behaviour: the fundamentals of the theories of elasticity, plastic equilibrium, and critical state soil mechanics are applied to the study of tyre-soil interaction. There is a description of techniques and instrumentation used to measure and parameterise terrain's properties. The application of both the pressure-sinkage relationship and the shear stress-shear displacement relationship on different types of terrain is explained. Wong describes empirical and semi-empirical methods for predicting wheeled vehicle performance.

The study "Development of a 3-D quasi-static tyre model for on-road and off-road vehicle dynamics simulations" (Part II and Part III) [4] [5]done by B. J. Chan and C. Sandu presents a semi-empirical model for an off-road tyre. This work analyses the dynamic behaviour of the vehicle during combined manoeuvres and it is based on the work done by Chan during his PhD (2008) [3]. These researchers deal with a simplified off-road wheel/tyre model that has the capability to revert back to on-road trend of behaviour on firmer soils [3].

The paper "Off-road tire modelling and the multi-pass effect for vehicle dynamics simulation" [6], done by C. Senatore and C. Sandu, obtains similar results to Chan and Sandu, but in this study they use a different formulation to calculate where the angle at which the maximum stress occurs. Moreover, they consider the longitudinal and the lateral dynamics for both rigid and flexible tyres, considering the multi-pass effect, which will be briefly reported in this thesis at a later stage. Their study is mainly based on works done by Wong, Reece, and Chan.

3 Equations of Tyre-Terrain Interaction (Terramechanics)

The purpose of this chapter is to report and to analyse the main physical characteristics and formulae applied to the proposed model which has been developed for the real-time driving simulator.

The main variables considered in following equations are reported in *Fig. 1*,

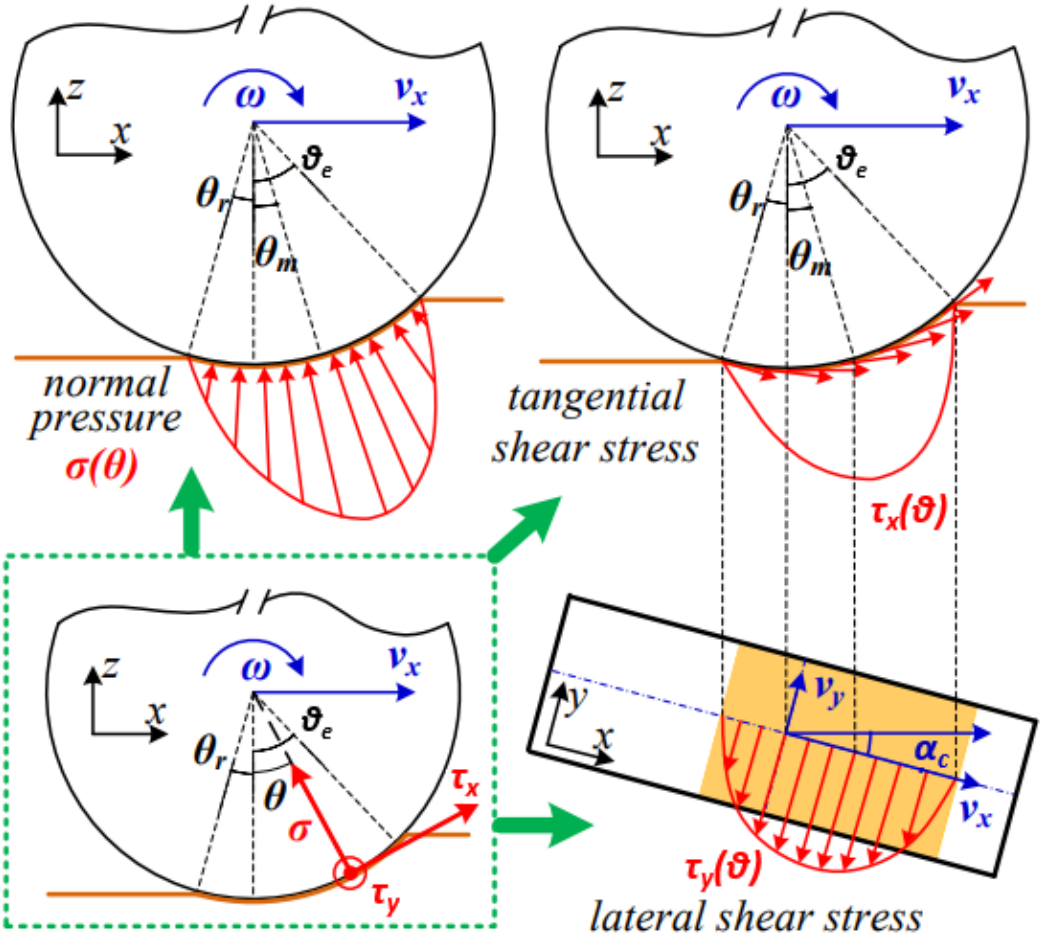

Figure 1: main variables in Terramechanics [7]

where:

- ϑ_e is the entry angle that defines the position where a point on the tyre circumference first comes into contact with the terrain [1];
- ϑ_r is the exit angle;
- ϑ_m is the angle where the maximum value of normal stress is reached;
- α_c is the slip angle, it is defined by *Eq. 3.5;*

- σ is the normal stress;
- τ_x is the longitudinal shear stress;
- τ_y is the lateral shear stress.

The following *Fig. 2* describes main angles of the wheel, in which z represents the sinkage in the terrain and R_u is the undeformed radius of the wheel. Based on the wheel running direction, the origin of angles is the vertical diameter and it starts at the point under the wheel centre, while the value of angles in the forward part of the wheel is positive and it is negative in the rear part.

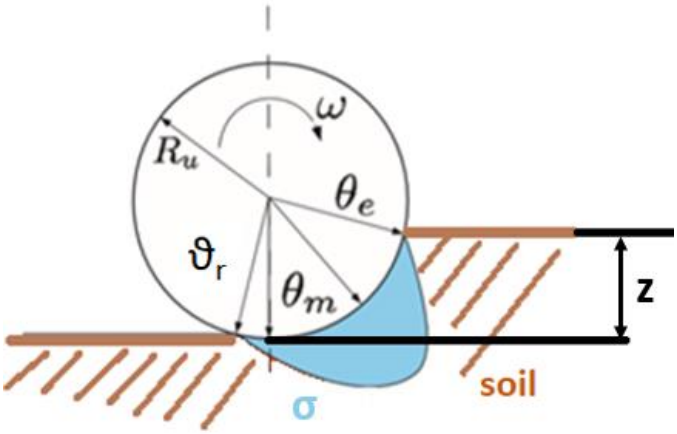

Figure 2: focus on main variables [6]

3.1 Modelling terrain as a plastic medium

The terrain behaviour can be modelled as an elastic medium (theory of elasticity) or as a rigid and perfectly plastic material (theory of plastic equilibrium) [1].

The theory of elasticity is only applicable if the normal load does not exceed a certain level (point A in *Fig. 3*).

The theory of plastic equilibrium may be applied only to estimate the maximum load which can be supported by the terrain without causing its failure, but it cannot predict the sinkage due to normal vehicle load. This theory is used to estimate the maximum traction developed by off-road vehicles.

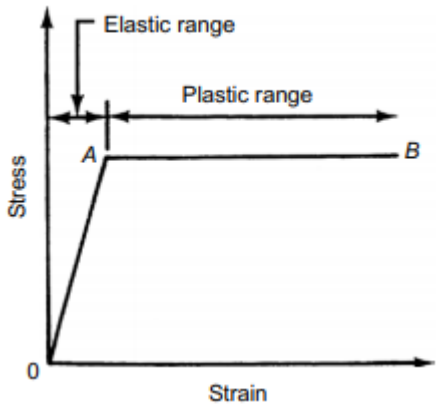

Figure 3: stress-strain relationship of an idealize elastoplastic material [1]

When the load on the soil reaches the value at the point A (*Fig. 3*), a small increase in stress produces a rapid increase in strain: this state represents the plastic flow. Before reaching the state of plastic flow, the terrain is considered to be in the state of plastic equilibrium: the transition from the state of plastic equilibrium to the one of plastic flow represents the failure of the terrain material.

When the terrain works like a plastic medium, the Mohr-Coulomb criterion is widely used to define the maximum shear stress value that soils, or other types of terrain material, can bear at given normal load.

This criterion establishes that the material will fail if the shear stress satisfies the following condition:

$$\tau_{max} = c + \sigma_n \, tan\phi \tag{3.1}$$

where:

- τ_{max} is the max shear stress;
- c is the cohesion of the material (soil properties);
- σ_n is the normal stress;
- ϕ is the angle of internal shearing resistance of the material (soil properties).

3.2 Shear displacement

The shear displacement of the terrain is calculated for any arbitrary angle ϑ and it is estimated considering the slip of the tyre. The longitudinal slip is defined as the ratio of the difference between the tangential tyre speed and the longitudinal axle velocity over the tangential tyre speed (*Eq. 3.2*). The shear displacement can be determined by integrating the shear velocity of the terrain in contact with the tyre, assuming that

the velocity of terrain particles at the interface matches the velocity of the tyre (*Eq. 3.3*) [6].

Considering that any slip can originate different slip rates, which is an important factor to be considered when modelling wheel-soil interaction on rate-dependent soil, it is common practice to avoid the use of slip to directly calculate the shear deformation and to use the interface velocity instead [4].

Following equations are used to calculate the slip (S_d), the tangential slip velocity (V_{Sd}), and the longitudinal shear displacement (j_x):

$$S_d = 1 - \frac{V_x}{R_u w} \tag{3.2}$$

$$V_{Sd} = R_u w - V_x cos\vartheta = R_u w[1 - (1 - S_d)cos\vartheta] \tag{3.3}$$

$$j_x = R_u[(\vartheta_e - \vartheta) - (1 - S_d)(sin\vartheta_e - sin\vartheta)] \tag{3.4}$$

where:

- R_u is the undeformed wheel radius;
- w is the angular speed;
- V_x is the longitudinal velocity.

The value of soil shear displacement continuously increases form the entry angle to the exit one.

In a similar manner it is possible calculate the lateral shear displacement:

$$\alpha_c = \tan^{-1}\left(\frac{V_y}{V_x}\right) \tag{3.5}$$

$$V_y = V_x \tan(\alpha_c) \tag{3.6}$$

$$j_y = R_u(1 - S_d)(\vartheta_e - \vartheta)tan(\alpha_c) \tag{3.7}$$

where:

- α_c is the lateral slip angle;
- V_y is the lateral slip velocity.

3.3 Pressure – sinkage relationship

Vehicle's vertical load is balanced by soil's reaction forces. The normal load on a soft soil produces a sinkage, that causes motion resistance. Bekker formulated the pressure-sinkage relationship which can be used to characterized soil's interaction with vertical load:

$$p = \left(\frac{k_c}{b_{ti}} + k_\phi\right) z^n \tag{3.8}$$

where:

- p is the pressure on soil;
- z is the sinkage;
- n is the sinkage exponent;
- k_c and k_ϕ are the cohesive and frictional moduli respectively;
- b_{ti} is the smaller dimension of a rectangular plate.

This equation is applied only to homogeneous terrain, because in a non-homogeneous terrain the data extrapolation may be influenced by the plate dimension used to put pressure on soil.

The normal stress value at the start of the contact region is ideally zero; then, it increases until a maximum value between the entry and exit angles, and finally it goes down until zero in the exit angle. When the wheel is stopped, the angle of the maximum value of normal stress is directly under the centre of the wheel, but when the wheel runs the point shifts forward and it further moves forward if the slip increases.

The following linear function is widely used to predict the angle at which the maximum normal stress occurs (ϑ_m) [8], [6], [1]:

$$\vartheta_m = (c_0 + c_1 S_d)\vartheta_e \tag{3.9}$$

where c_0 and c_1 are two empirical constants.

It must be said that Wong has suggested a different definition of ϑ_m for negative slip [6]; however, considering that this definition creates discontinuity issues around zero slip, this thesis only refers to the absolute value of the longitudinal slip.

So, using the pressure-sinkage relationship proposed by Bekker, the normal stress is defined like a piece-wise function:

$$\sigma(\vartheta) = R_u^n \left(\frac{k_c}{b}\ k_\Phi\right)(\cos\vartheta - \cos\vartheta_e)^n \qquad \text{for } \vartheta_m \le \vartheta < \vartheta_e \qquad (3.10)$$

$$\sigma(\vartheta) = R_u^n \left(\frac{k_c}{b}\ k_\Phi\right)\left(\cos\left(\vartheta_e - \frac{\vartheta - \vartheta_r}{\vartheta_m - \vartheta_r}(\vartheta_e - \vartheta_m)\right) - \cos\vartheta_e\right)^n \qquad \text{for } \vartheta_r \le \vartheta < \vartheta_m \qquad (3.11)$$

3.3.1 Multi-pass effect

For an accurate prediction of vehicle performance, the repetitive loading must be considered. When front wheels pass on terrain, they apply a normal load, which will be reduced after their passage. If rear wheels pass on the same path, a normal load is again applied. The loading-unloading-reloading cycles are defined as multi-pass effect and, when they are carried out on soft soils, results of pressure-sinkage relationship will be affected: in this case, the repetitive normal load should be measured.

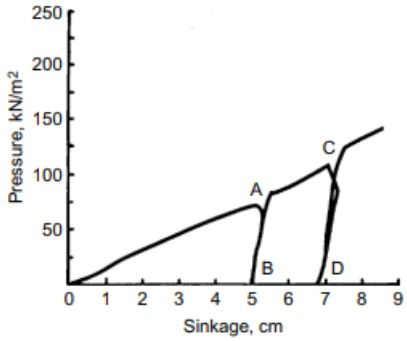

Figure 4: response to repetitive normal load [1]

In *Fig. 4* the section 0-A of the curve represents the first load on terrain, while the A-B section is the unload zone where it is possible to note the return of elastic deformation because the sinkage shows a little decrease. After having reloaded the soil, the section B-C reports the new load on soil with the respective sinkage.

In *Fig. 5* a pattern of multi-pass effect with two wheels is reported.

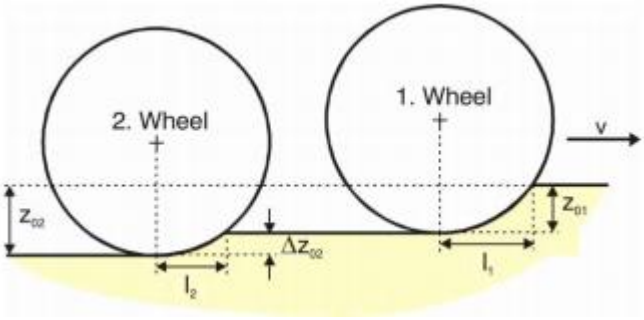

Figure 5: multi-pass effect [9]

With reference to the multi-pass effect, Wong proposed the following expression:

$$p = p_u - k_u(z_u - z) \tag{3.12}$$

where:

- p_u is the pressure when unloading cycle begins;
- z_u is the sinkage when unloading cycle begins;
- k_u is the pressure-sinkage parameter representing the average slope of the unloading-reloading line A-B [1].

This multi-pass effect model introduced by Wong to analyse repetitive loading cycles is tricky and it cannot be directly implemented into the model because the normal stress is represented by a piecewise function [6]. For this reason, a lot of multi-pass effect models, as the one developed by Senatore and Sandu, are based on Holm's studies: Holm showed that the terrain changes its properties after each pass and variations are a function of the slip [6], [10].

3.4 Shear stress – shear displacement

The measurement of the shear stress-shear displacement is fundamental to predict the tractive performance of an off-road vehicle. In fact, a vehicle, through its running wheels, applies shear load to the soil surface, which results in the development of the thrust and associated slip [1].

The most important equation used to describe this relationship was proposed by Janosi and Hanamoto (1961):

$$\tau = \tau_{max}\left(1 - e^{\frac{-j}{k}}\right) = (c + \sigma_n tan(\Phi)\left(1 - e^{\frac{-j}{k}}\right) \tag{3.13}$$

where:

- j is the above-mentioned displacement;

- τ is the stress;
- τ_{max} is the maximum shear stress that terrain can support (*Eq. 3.1*);
- k is the shear deformation modulus to be estimated experimentally and it is a measure of the magnitude of the shear displacement required to develop the maximum shear stress, on which it has a strong impact [6], [1].

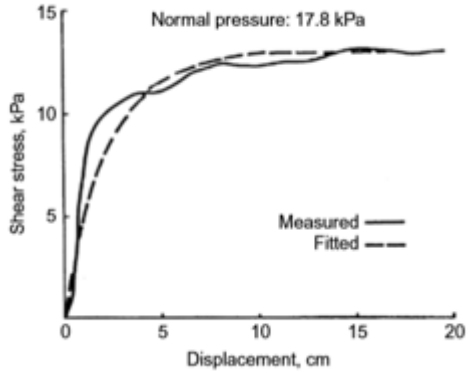

Figure 6: Shear stress-shear displacement [1]

Eq. 3.13 describes fairly well tyre behaviour on certain types of sand, saturated clay and also fresh snow. In literature there are other complex, but similar, equations used to describe different types of terrain, but, considering all the Janosi and Hanamoto's equations, this is the most used in Terramechanics.

3.5 Rigid wheel or flexible wheel

As above-mentioned, rigid wheels have been replaced by pneumatic tyres as the running gear of off-road wheeled vehicles in normal operation; however, pneumatic tyres, in case of a high inflation pressure and when used on a soft soil, may behave like a rigid rim. Usually, when tyre deformations are negligible compared to terrain deformations, it is possible to consider the tyre as a rigid wheel. This is the case when the tyre is on an extremely soft terrain (e.g. dry desert sand).

Wheel's behaviour depends on a combination of the following factors: the tyre inflation pressure, the pressure due to the stiffness of tyre carcass, and the terrain condition.

As for tyre characteristics, since it is difficult to measure the pressure due to the carcass stiffness, the average ground pressure is ordinarily used; it represents the sum of tyre inflation pressure and carcass stiffness pressure; moreover, the ground average pressure is estimated for a given tyre in a particular condition (load and inflation pressure) and it is reported in the "generalise deflection chart", normally available from the tyre manufacturer.

Bekker prosed a method to predict the critical ground pressure, which was derived from the analysis of forces and moments acting on a tyre. If the average ground pressure is greater than critical ground pressure, the tyre can be considered like a rigid wheel [1].

Wong also studied the prediction of the operating mode of a pneumatic tyre on soft soil, improving Bekker's method in order to obtain a smooth transition from rigid mode to flexible mode.

3.6 Normal and longitudinal forces and drive torque

Knowing normal and tangential stresses distribution and integrating them across the entire length of the tyre contact with soil surface, it is possible to calculate normal and longitudinal forces and the wheel drive torques.

The normal force is the first one to be estimated, because it ensures that the vertical load, which is applied by the vehicle to the soil, is balanced by soil's reaction forces. This balance allows to determine the entry angle and exit angle with iterative calculations. Usually, the exit angle is in a range between -20° and -5° and it is generally assumed to be constant, therefore it is quite easy to identify the entry angle [1], [4], [6].

The following equation is used to calculate the normal force (F_z):

$$F_z = bR_u \int_{\vartheta_r}^{\vartheta_e} \{\tau_x(\vartheta) \sin\vartheta + \sigma(\vartheta) \cos\vartheta\} d\vartheta \tag{3.14}$$

After having set a value of the exit angle and having iteratively determined the entry angle, it is possible to calculate the longitudinal force (F_x), the lateral force (F_y), and the drive torque (M_y) with equations reported below:

$$F_x = bR_u \int_{\vartheta_r}^{\vartheta_e} \{\tau_x(\vartheta) \cos\vartheta - \sigma(\vartheta) \sin\vartheta\} d\vartheta \tag{3.15}$$

$$F_y = bR_u \int_{\vartheta_r}^{\vartheta_e} \tau_y(\vartheta) d\vartheta \tag{3.16}$$

$$M_y = bR_u^2 \int_{\vartheta_r}^{\vartheta_e} \tau_x(\vartheta) d\vartheta \tag{3.17}$$

In the equations (*Eqs. 3.14 – 3.17*) b is the width of the wheel.

It is worth to point out that these equations are only applicable when the wheel behaves like a rigid rim because the radius R_u is assumed to be constant.

Stress and forces developed by wheel-soil interaction are illustrated in *Fig. 7*.

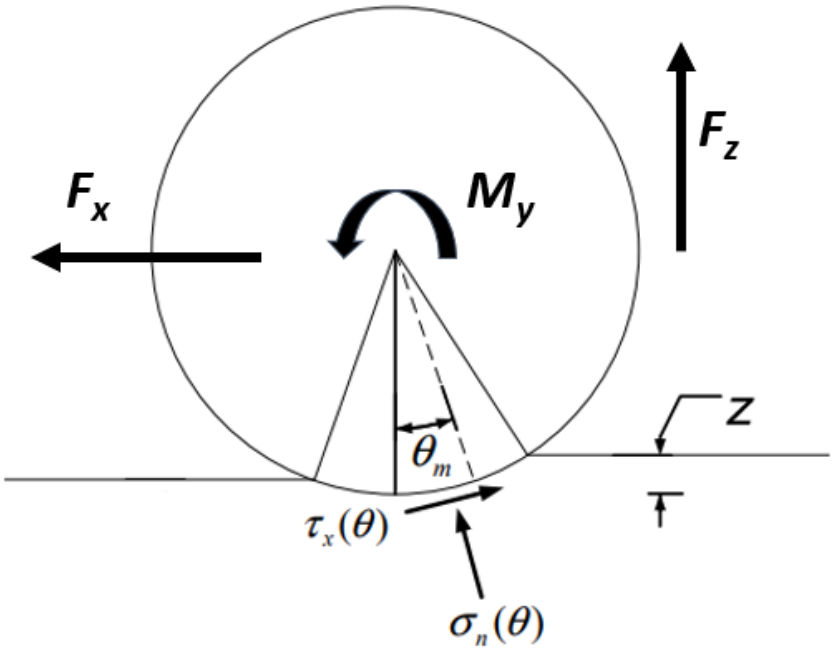

Figure 7: tyre forces and moments

3.6.1 Bulldozing effect

For an accurate prediction of the lateral forces, the bulldozing effect must be considered.

It is named "Bulldozing effect" because the phenomenon generates a resistance similar to one generated by a bulldozer blade.

The bulldozing effect is due to the wheel compacting the terrain in the lateral direction; in particularly the tyre sinkage and soil surcharge influences this phenomenon. The bulldozing effect generates a bulldozing force which acts on the side of the tyre in the lateral direction.

In *Fig. 8* it is possible to observe the bulldozing effect.

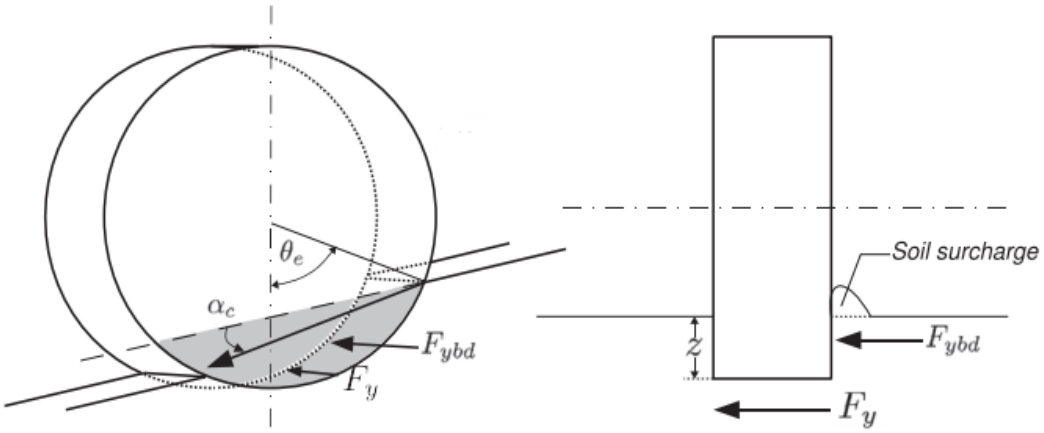

Figure 8: bulldozing effect

To estimate the bulldozing force (F_{ybd}) several methods have been developed based on the soil mechanics and geotechnical principles. For example, some models are based on the Hegedus's estimation [11] while others are based on the Terzaghi bearing capacity equation [12] and the Hettiarachi-Reece equation [13]. The Terzaghi equation and the Hettiarachi-Reece equation are used in the Senatore and Sandu's paper [6] and in the Chan's study [3].

In conclusion, the total lateral force is generated by the lateral shear displacement (j_y) and by the bulldozing effect.

4 Soil's Properties

4.1 Measurement of soil's properties

The most used techniques for measuring mechanical properties of terrain are the cone penetrometer technique and the bevameter technique. The first one is used for empirical models, while the second method is employed for detailed parametric analysis of vehicle performance [1].

The bevameter, designed and developed by Bekker, simulates both the normal and the shear load exerted by a vehicle, performing two different tests: penetration test and shear test.

In the penetration test, a plate, whose size is comparable to the contact patch of a tyre, simulates the normal load done by a vehicle, putting pressure on soil, and measuring the pressure-sinkage relationship of the terrain.

To measure the shear stress-shear displacement relationship, a shear plate with grouser is used. This simulates the shear stress when applying different normal loads [1].

Figure 9: shear test using a vehicle-mounted bevameter [1]

With some sensors (e.g. potentiometer) and using computer technology, it is possible to record and to process data. After processing data with a curve fitting method, it is possible to extrapolate soil's parameters that characterise the terrain behaviour in terms of pressure-sinkage constants.

Here below, some parameters used to describe terrain properties are reported:

- cohesion (c) is the bond that cements particles of the material together, regardless of the normal pressure between the particles [1];
- the angle of internal shearing resistance of the material (ϕ) that represents the slope of the straight line that is tangent to the circle in the Mohr-Coulomb failure criteria (see *Fig. 10* below) [1].

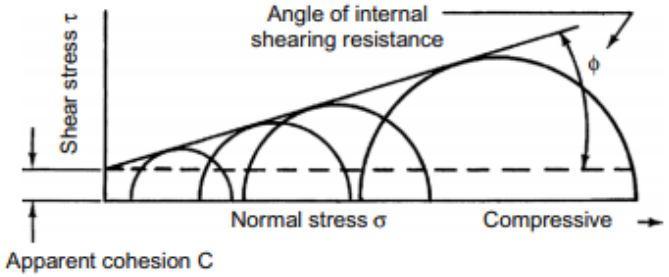

Figure 10: Mohr-Coulomb failure criterion [1]

4.2 Data soil's properties

In this thesis, three types of terrain are simulated and here below the parameters of each type of soil are reported. The data soil's properties are taken from the soil's database of Adams/Car, which uses a formulation based on Bekker and Wong's equations [14].

The *Tab. 1* contains the parameters of a dry sand, this type of soil is similar a desert sand.

k_x	0.036	[m]
k_y	0.013	[m]
C	1040	[Pa]
ϕ	0.489	[rad]
k_c	950	[N/m^(n+1)]
k_ϕ	1530000	[N/m^(n+2)]
n	1.1	[-]
γ	1555	[Kg/m^3]
c_0	0.4	[-]
c_1	0.15	[-]

Table 1: dry sand properties

The *Tab. 2* contains the parameters of a friable dirt soil, this type of sand is more compact respect to the dry sand.

k_x	0.036	[m]
k_y	0.013	[m]
c	1150	[Pa]
ϕ	0.5498	[rad]
k_c	6940	[N/m^(n+1)]
k_ϕ	505800	[N/m^(n+2)]
n	0.71	[-]
γ	1555	[Kg/m^3]
c_0	0.4	[-]
c_1	0.15	[-]

Table 2: LETE sand properties

The *Tab. 3* contains the parameters of a sandy loam soil, this type of terrain is found near some banks of rivers.

k_x	0.036	[m]
k_y	0.013	[m]
c	3700	[Pa]
ϕ	0.520	[rad]
k_c	6900	[N/m^(n+1)]
k_ϕ	752000	[N/m^(n+2)]
n	0.66	[-]
γ	1280	[Kg/m^3]
c_0	0.4	[-]
c_1	0.15	[-]

Table 3: loam sand properties

5 Tyre Model Development

The equations, described in *chapter 3*, are implemented in Simulink environment.

Simulink is a graphical environment for multidomain simulations: it provides blocks library customisable and solvers for modelling dynamic systems. Simulink is integrated with MATLAB software, allowing to use MATLAB algorithms into the model and to analyse simulation results in MATLAB interface. It is worth to point out that Simulink simulates considering the time evolution; thus, all variables are integrated with respect to the time.

The tyre model to simulate the off-road driving is developed in Simulink and it works together with the VI-CarRealTime core, making a co-simulation in MATLAB/Simulink environment.

VI-CarRealTime is a software for modelling and simulating vehicles, suitable also for running in real-time in professional driving simulators.

Simulink environment and the co-simulation technique with VI-CarRealTime were chosen because of the developed model implementation for driving simulator; in fact, as we will see in *chapter 7*, this choice allows to create the proper executables for the integration within driving simulator environment.

In this chapter the off-road tyre model, developed in Simulink, is described.

The interaction between tyre model and VI-CarRealTime car model for co-simulation will be described in *chapter 7*.

5.1 Tyre model hypothesis

The tyre developed in this thesis is based on the following assumptions:

- the tyre behaves like a rigid rim, so the radius is assumed to be constant;
- soil properties are homogenous and isotropic;
- the multi-pass effect is not considered;
- the bulldozing effect is not considered;
- the exit angle is assumed to be constant for the entire time of simulation; a further description about this assumption will be reported later.

5.2 Entry angle

As mentioned in *chapter 3*, the first step for calculating tyre forces and moments is to determine the entry angle, which has been calculated through a MATLAB function,

developed during this thesis and called "Find ϑ_e"; moreover, it can also be implemented in Simulink.

Starting from the equation (*Eq. 3.14*), shown here again in *Eq. 5.1*,

$$F_z = bR_u \int_{\vartheta_r}^{\vartheta_e} \{\tau_x(\vartheta)\sin\vartheta + \sigma(\vartheta)\cos\vartheta\} d\vartheta \tag{5.1}$$

the normal force, which balances the vehicle vertical load, can be calculated only if both the longitudinal shear stress and the normal stress are known. These variables can be calculated only if both the entry angle and the exit angle are known.

In this study, the value of the exit angle is assumed to be constant. At first, this value was approximated on the basis of the available literature, which provided a range of values that was not specific for a particular type of soil. Then, when comparing the developed model to the one available in a commercial software (Adams/Car), the exit angle value was derived from simulations performed on the latter one; in fact, considering also that the vehicle model is nominally the same, it is possible to perform a more reasonable and accurate comparison.

The "Find ϑ_e" function, through an iterative calculation, determines the value of the entry angle at which the normal force is equal to the vehicle vertical load. During the iterative calculation, the value of the exit angle remains constant.

"Find ϑ_e" is a nested function which uses the MATLAB "fzero" function to find the value x at which the given objective function of the respective x is zero. The "fzero" function needs at least two inputs: the objective function (fun) and an initial value (x_0) from where the research of the zero value starts.

An example of how "fzero" function works is reported here below:

$$x = @fzero(fun, x_0) \;\rightarrow\; fun(x) = 0$$

In the "Find ϑ_e" the difference between the normal force and the vehicle vertical load represents the objective function: therefore, "fzero" finds the value of entry angle at which the difference is zero.

All the variables necessary to calculate the entry angle using "Find ϑ_e" are known; they are soils properties or tyre properties or outputs of the vehicle model (e.g longitudinal slip).

Here below, all the variables needed in "Find ϑ_e" are reported with their sources in brackets:

- Ru tyre radius (tyre properties);

- b tyre width (tyre properties);
- soil properties (soil data sheet);
- W vehicle normal load (vehicle model);
- Sd longitudinal slip (vehicle model);
- ϑ_{e_zero} is the initial value from where "Find ϑ_e" starts the research of the correct value of the entry angle (imposed by user);
- ϑ_r exit angle (imposed by user).

It is worth to highlight that the longitudinal slip is indirectly provided by the vehicle model: *Eq. 3.2* is used to calculate the longitudinal slip, thus the longitudinal vehicle speed and the angular wheel speed are provided by the vehicle model.

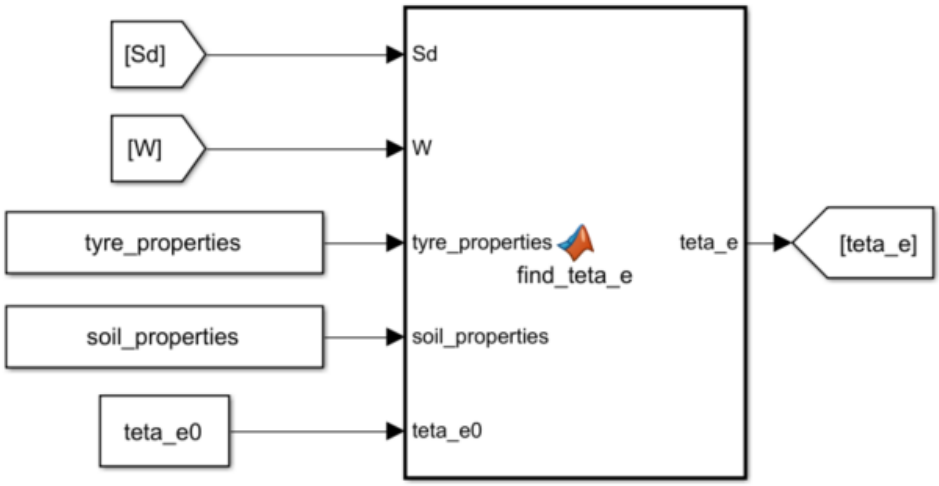

Figure 11: block of function "Find θ_e"

The term "soil_properties" refers to all the variables, related to soil data, needed in the equations reported in *chapter 3* (e.g. soil cohesion, sinkage exponent, etc.).

For any instant time of the simulation, both the longitudinal slip (S_d) and the vehicle vertical load (W) are provided by the vehicle model; the obtained value of the entry angle changes at each moment, therefore the iterative calculation is performed within any time step. Moreover, this repetitive calculation is carried out for each wheel.

The iterative calculation at any time step represents an issue because it increases the computational effort, slowing the cycle time which is too long for real-time simulation. Furthermore, the nested functions are not always numerically stable.

To avoid these problems which affected the real-time simulation it has been decided to use lookup tables to determine the entry angle for the tyre model.

5.3 Lookup table for the entry angle

A lookup table is a Simulink block which uses arrays of data to map input values to output values. Input values and output values are set using block parameters. Moreover, the output can be estimated using interpolation between arrays of data.

To generate the lookup tables, it is used the function "Find ϑ_e" in offline mode.

Both the longitudinal slip and the vehicle vertical load inputs depend on vehicle characteristics and manoeuvre simulated: it is necessary to generate lookup tables as much generic as possible.

For generating lookup tables, both the longitudinal slip and the vertical load are represented by a vector of real number and they are given as inputs. For each value of longitudinal slip and each value of vertical load the function "Find ϑ_e" respectively creates an array of value for the entry angle.

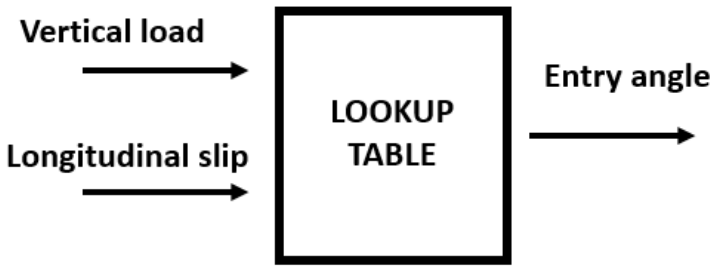

Figure 12: conceptual lookup table

Fig. 12 is a conceptual representation of how the lookup table works.

The chart, reported in *Fig. 13*, represents normal forces trend with changes in the longitudinal slip and the entry angle.

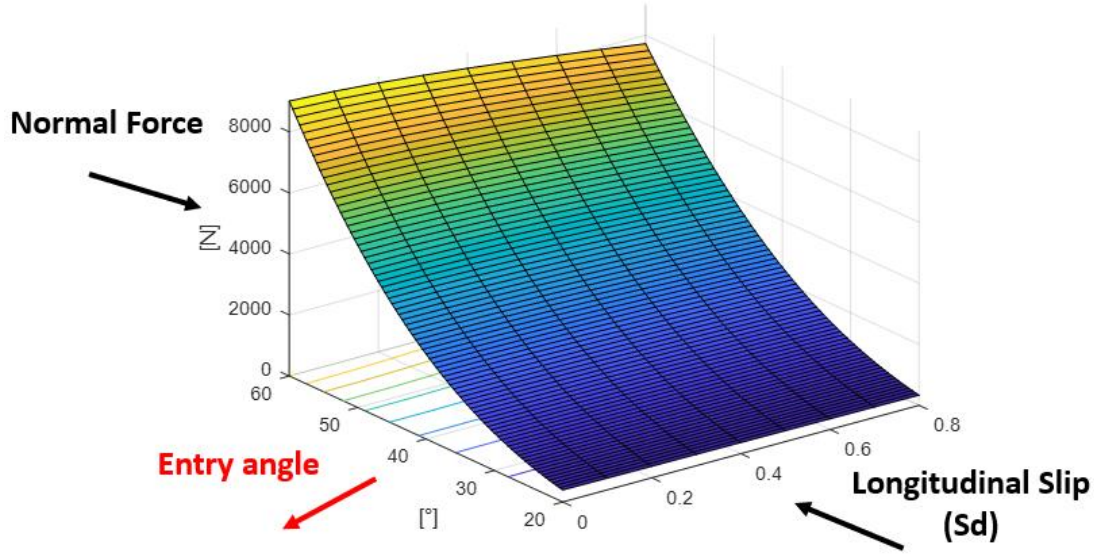

Figure 13: normal forces trend

Observing the charts (*Fig. 13*), it is clear that the entry angle change has the greatest impact in influencing the normal force. The next two charts better show this observation: in *Fig. 14*, at different value of longitudinal slip, normal forces are plotted as a function of the entry angle, while in *Fig. 15*, at different value of entry angle, normal forces are plotted as a function of the longitudinal slip.

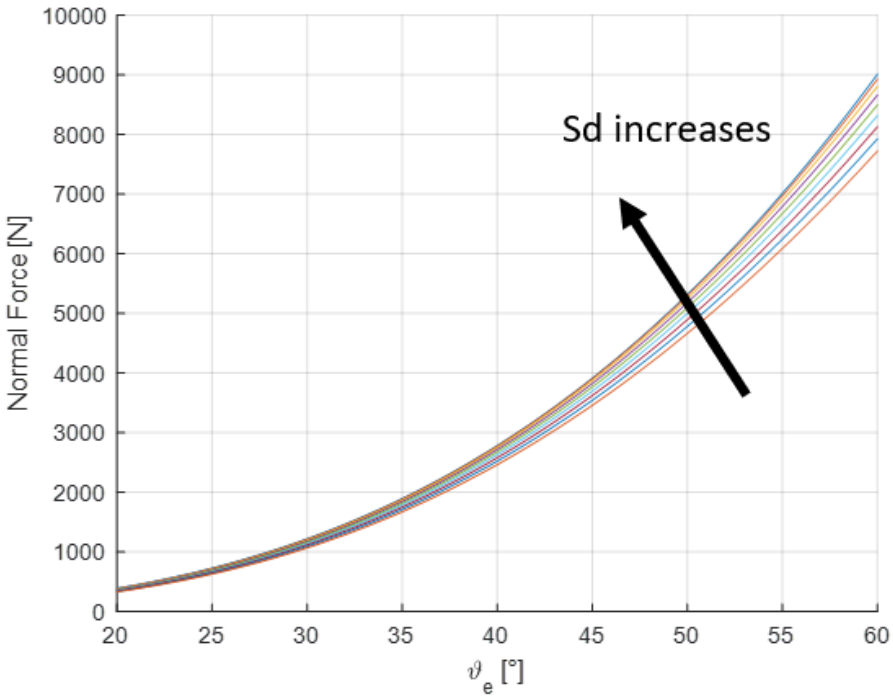

Figure 14: normal forces as a function of entry angle

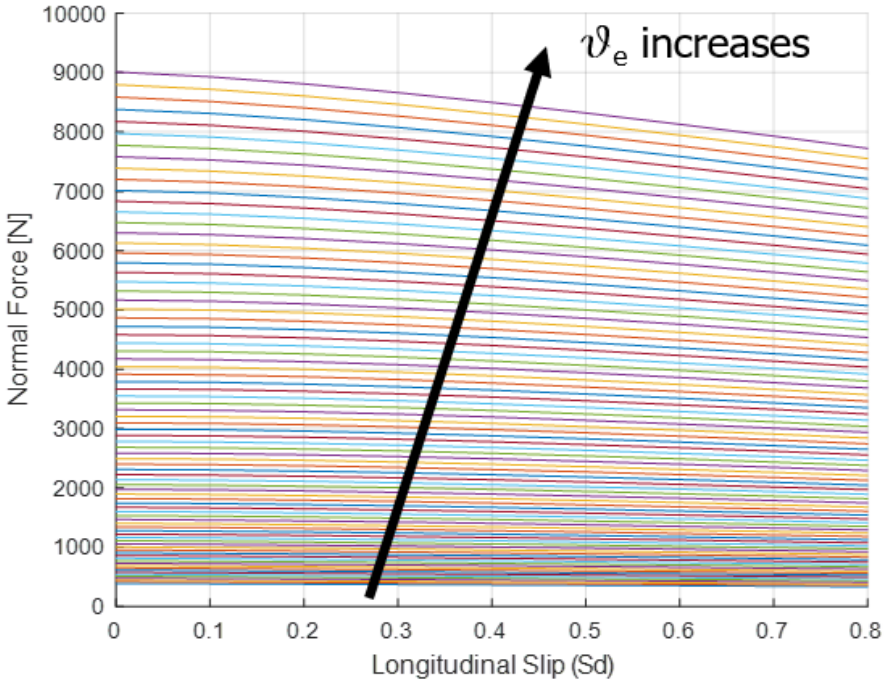

Figure 15: normal forces as a function of longitudinal slip

It is worth to point out that the lookup tables must be generated for each type of soil that the user want to simulate.

As mentioned above, the value of the exit angle is assumed constant during lookup tables creation.

Comparing different simulated driving manoeuvres, it is possible to observe that the value of the exit angle remains constant. For example, in *Fig. 16* two driving manoeuvres are compared: in the first one the speed is constant while the second one is an acceleration full throttle starting at 15 seconds. The values of the exit angle are very similar making the comparison between constant speed driving and acceleration driving, while they are different if they refer to front wheels or to rear wheels. The difference of value between front axle and rear axle is due to the different vertical load between them.

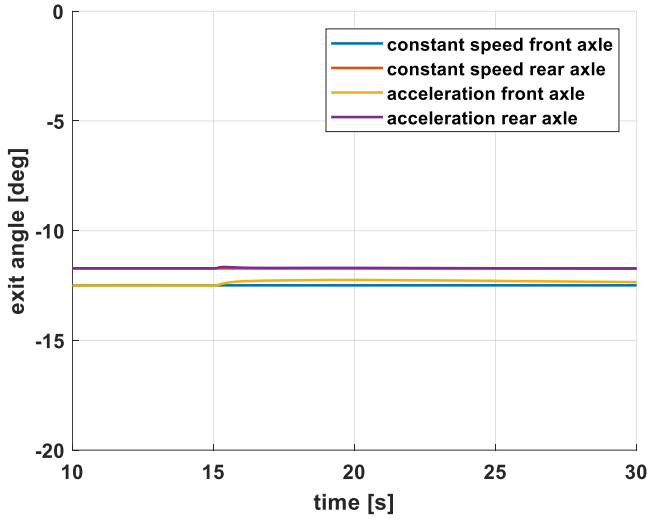

Figure 16: exit angle comparison

In this study, the lookup tables are generated based on the following assumptions:

- the exit angle is assumed to be constant for each simulation, but it has different value for front wheels and rear wheels respectively and for each type of simulated soils;
- the vertical load varies from 250 [N] to 10000 [N];
- the longitudinal slip varies from -0.2 to 0.8.

The negative longitudinal slip is limited to 0.2 because the thesis is focused on the longitudinal traction conditions.

In the tyre model developed the lookup tables have the following characteristics:

- number of table dimension is 2;
- the interpolation method is "Cubic spline": this method fits a cubic spline to the adjacent breakpoints and it returns the point on that spline corresponding to the input [15];
- the extrapolation method is "Clip": this method disables extrapolation and it returns the table data corresponding to the end of the breakpoint data set range [15]; This is done also to increase the numerical stability, avoiding unexpected extrapolation.

Fig. 17, herein below, represents the lookup table block in Simulink.

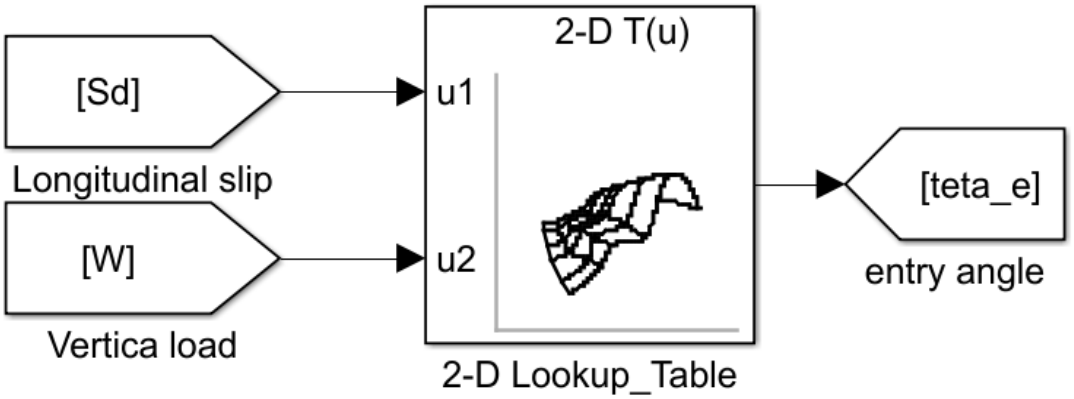

Figure 17: lookup table Simulink block

5.4 Tyre forces and moments

Knowing the entry angle, in the Simulink model it is implemented a MATLAB function, developed in this thesis, to calculate the tyre forces and moments. The MATLAB function makes use of the equations described in *chapter 3*.

Here below, all the necessary inputs in the MATLAB function are reported with their sources in brackets:

- Ru tyre radius (tyre properties);
- b tyre width (tyre properties);
- soil properties (soil data sheet);
- longitudinal slip (vehicle model);
- lateral slip angle (vehicle model);
- ϑ_e entry angle (Lookup table);
- ϑ_r exit angle (imposed by user).

Also, for the lateral slip angle, like the longitudinal slip, the value is calculated using *Eq. 3.5*, therefore it is indirectly provided by the vehicle model.

The outputs obtained from the MATLAB function are reported below:

- longitudinal forces (F_x);
- lateral forces (F_y);
- normal forces (F_z);
- drive torque.

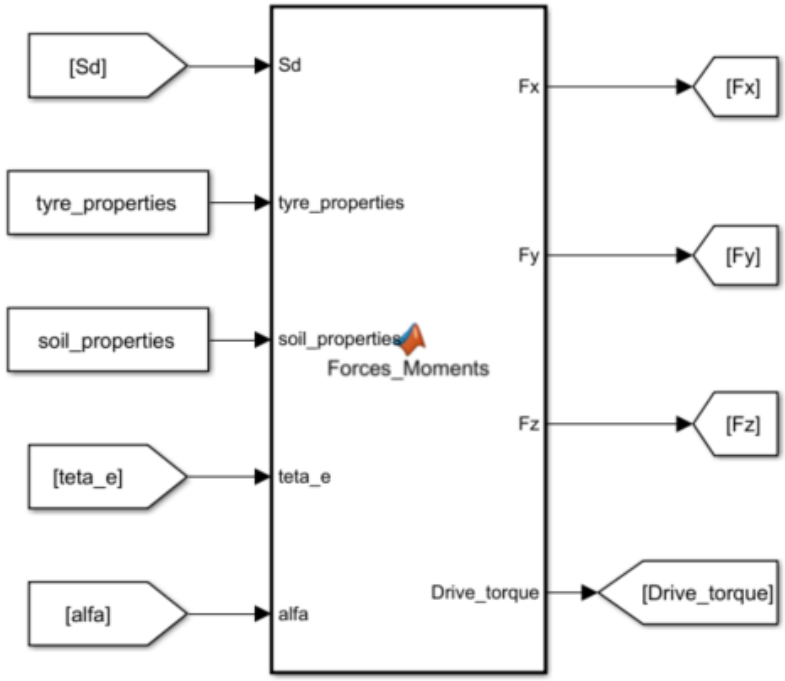

Figure 18: MATLAB function block (tyre forces and moments)

The script of the MATLAB function is reported in the *Appendix A*.

6 Analysis of Thrust and Longitudinal Forces

6.1 Thrust

In Terramechanics the analysis of the tractive effort (thrust), which allows vehicle movements, is important to improve the vehicle design process, early detecting some possible issues.

The thrust, which is the sum of tangential forces that act on the contact patch (A), is defined by the following equation:

$$F_{thrust} = \tau_{max} A = (c + \sigma_n \, tan\phi) A = cA + W tan\phi \tag{6.1}$$

The F_{thrust} is the maximum tractive effort available for the vehicle because it considers the maximum shear stress ($\tau_{\max}$), calculated using *Eq. 3.1*, that soils can bear.

Hereafter, whether "thrust" or "tractive effort" always refer to their maximum value.

The most important parameters (see *chapter 4.1*) that influence soil characteristics are the soil cohesion (c) and the internal friction angle (ϕ).

Considering a purely cohesive terrain, such as saturated clay or "heavy" snow, the internal friction angle is negligible ($\phi \cong 0$): therefore, the thrust of a vehicle is independent of its normal load (W), while it only depends on both the contact area (A) and the value of the soil cohesion (c). Assuming constant the contact area, the tractive effort remains constant (*Fig. 19*) [1]; therefore, *Eq. 6.1* becomes:

$$F_{thrust} = cA \tag{6.2}$$

Eq. 6.2 means that a higher cohesive soil and a bigger contact area increase the thrust available for the vehicle.

On the other hand, considering a purely frictional terrain, such as dry sand (desert sand) or cold snow, the cohesion parameter is negligible ($c \cong 0$): therefore, the tractive effort only depends both on the vehicle normal load and the internal friction angle (*Fig. 19*) [1]. In this case, *Eq. 6.1* becomes:

$$F_{thrust} = W tan\phi \tag{6.3}$$

These above-mentioned cases, available in literature, are simplifications according to which particular types of terrains are treated as purely cohesive or purely frictional together, and they are only used to better examine some particular tyre-terrain

interactions; in reality, most of soils are characterised by both cohesion and internal friction angle parameters.

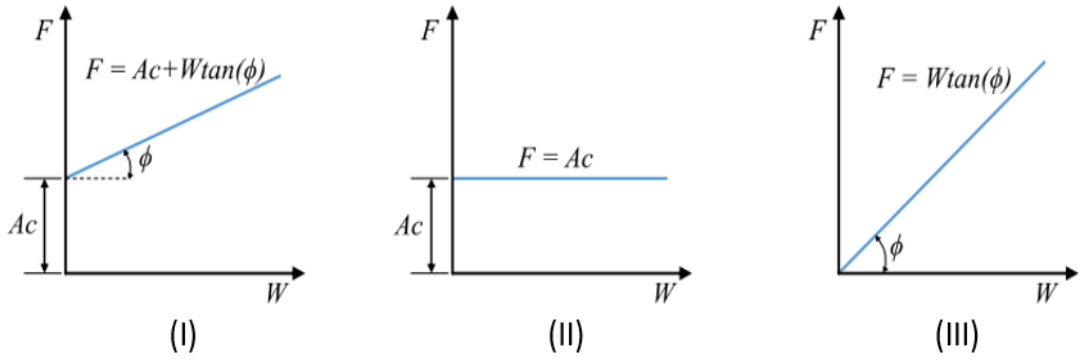

Figure 19: Thrust for (I) general soil, (II) purely cohesive soil, (III) purely frictional soil

An analysis on the tractive effort has been carried out in order to compare the data given by the developed tyre model with the theory described above.

Using *Eq. 6.1*, with reference to the "dry sand" soil only, the thrust has been examined by varying the value of the cohesion and setting to zero the value of the internal friction angle; then, the analysis has been repeated setting to zero the value of the cohesion and varying the internal friction angle.

The two obtained charts are reported in *Fig. 20* and *Fig. 21*.

The variables (A and σ_n), necessary for Eq. 6.1, are provided by the developed tyre model, which presents two significant differences with respect to the simplifications explained above:

- for each value of normal load, the tyre model calculates the right entry angle: therefore, the length of the contact patch changes, causing the variations of the contact area; on the contrary, in the simplification it remains constant for any vertical load;
- the vertical load (W) is calculated using *Eq. 3.14*, that considers the normal stress and the contribute given by the tangential stress; conversely, in the simplification it is considered the normal stress (σ_n) only.

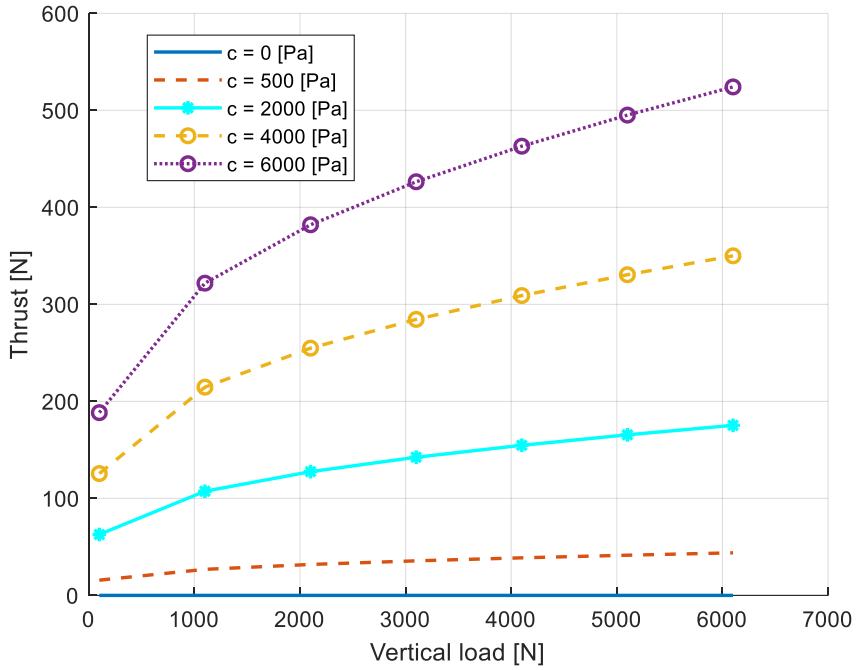

Figure 20: thrust vs vertical load – dependency on cohesion parameter

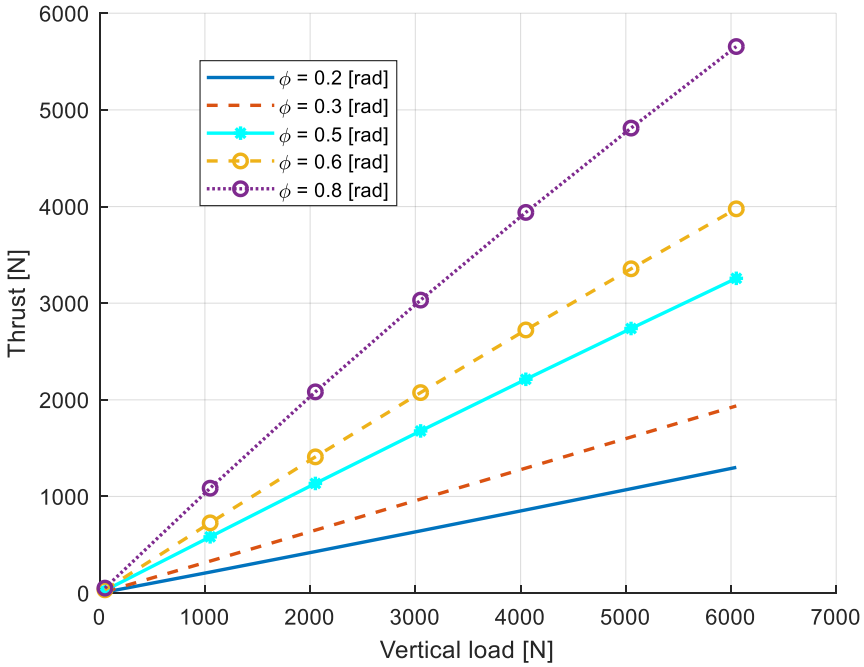

Figure 21: thrust vs vertical load - dependency on internal friction angle

The different trend of the second graph of *Fig. 19* with respect to *Fig. 20* is mainly because the contact area is not constant.

Despite the differences between the analysis carried out in this thesis and the analysis available in literature, the cohesion soil variation influences the thrust as it was

expected: indeed, the increase of the cohesion value allows to obtain a higher value of thrust; in the graph it is represented by an upward translation of the relevant line.

The trend of *Fig. 21* is similar to the third chart of *Fig. 19* because *Eq. 6.3* does not consider the contact area and because the above-mentioned difference between the developed tyre model and the simplifications given by literature to determine the vertical load has a minor impact on the results. A gradual increase of the internal friction angle causes an increase of the available thrust, which is coherent with the literature.

The trend of thrust, shown in *Fig. 20-21*, remains the same even considering different types of soil.

6.2 Longitudinal forces

In this section, it has been analysed the trend of longitudinal forces (F_x) (*Eq. 3.15*), given by the off-road tyre model, and it has been compared with the trend obtained by the Pacejka tyre model; in particular, the analysis has been focused on the effect of the variation of normal forces.

On off-road terrain, the vertical load variation has different effects, and the analysis of the results is not immediate and direct; moreover, contrary to the thrust analysis, the type of soil influences the trend of the results.

The first effect, observable in *Fig. 22*, is that a higher value of vertical load causes an increase of the entry angle, that means a longer length of the contact patch.

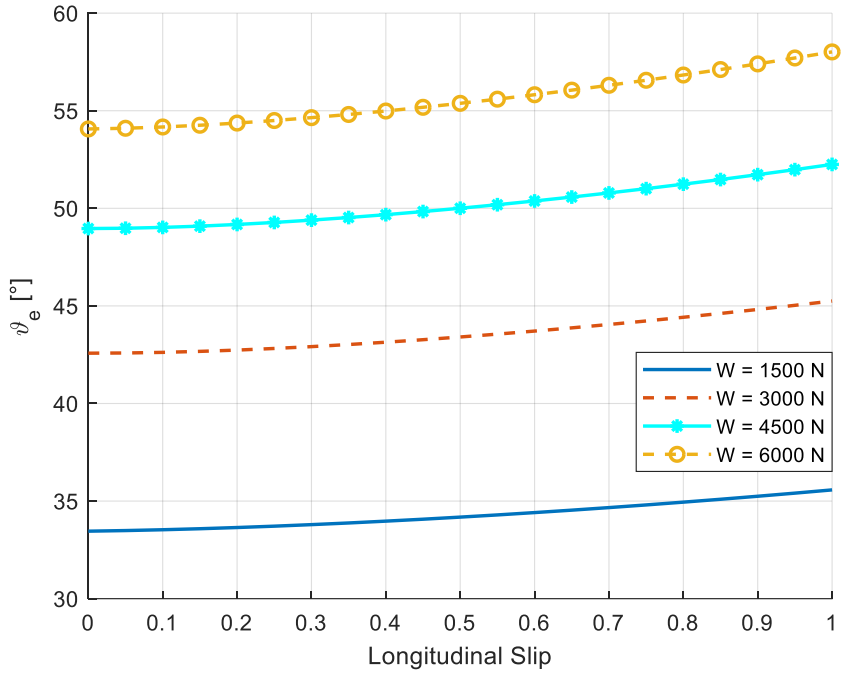

Figure 22: entry angle vs longitudinal slip – dependency on W

The sinkage variable (*Fig. 23*) is correlated to the entry angle; indeed, they both have the same trend. Furthermore, confirming expectations, increasing the vertical load, the vehicle sinkage into the soil increases.

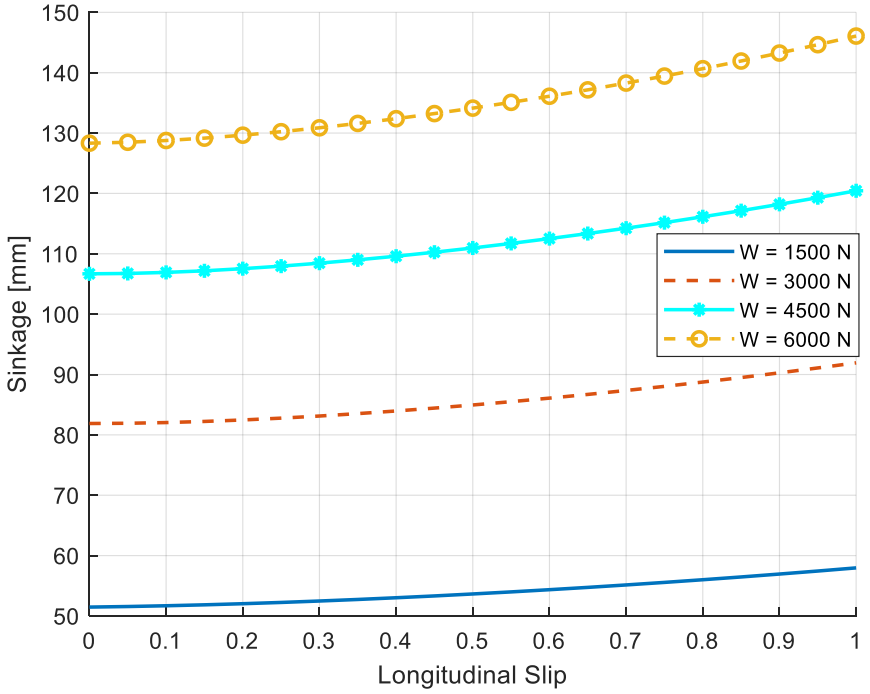

Figure 23: sinkage vs longitudinal slip – dependency on W

In the off-road model, the longitudinal forces are calculated using *Eq. 3.15*, shown here again in *Eq. 6.4*:

$$F_x = bR_u \int_{\vartheta_r}^{\vartheta_e} \{\tau_x(\vartheta)\cos\vartheta - \sigma(\vartheta)\sin\vartheta\} d\vartheta \tag{6.4}$$

The first term of the integral represents the shear thrust, while the second it is the compaction resistance caused by the soil deformation. It is necessary to analyse these two terms to understand the trend of longitudinal forces given by the off-road model.

Furthermore, it is worth to point out that the shear stress (τ_x) in *Eq. 6.4* is calculated using *Eq. 3.13*, while in thrust equation the shear stress is obtained using *Eq. 3.1*.

In the following sections, the analysis has been developed in two steps: the first one evaluates the shear and normal stresses, while the second part is focused on the shear thrust and the compaction resistance.

6.2.1 Shear stress and normal stress

Both shear and normal stresses are studied by varying the value of the vertical load (W) and the value of the longitudinal slip (S_d), one by one; furthermore, the combined effect given by simultaneously varying the vertical load and the longitudinal slip have been analysed and plotted on the same graph.

In *Fig. 24*, the vertical load changes, while the S_d remains constant at 0%: it is possible to observe that the tangential stress increases when the vertical load increases.

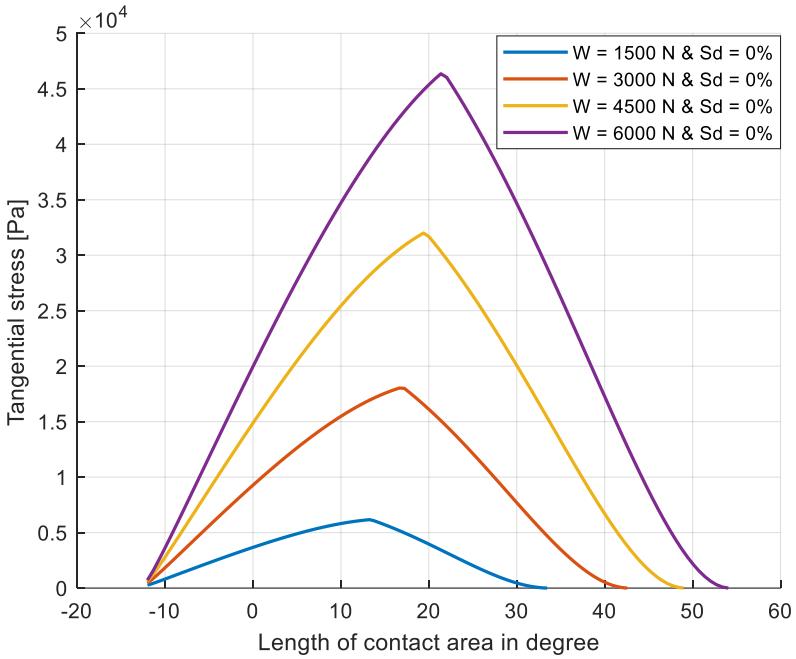

Figure 24: shear stress distribution – dependency on W

In *Fig. 25*, the longitudinal slip changes, while the vertical load remains constant at 3000 N; the slip has the same impact of the vertical load: indeed, they both increase the value of shear stress.

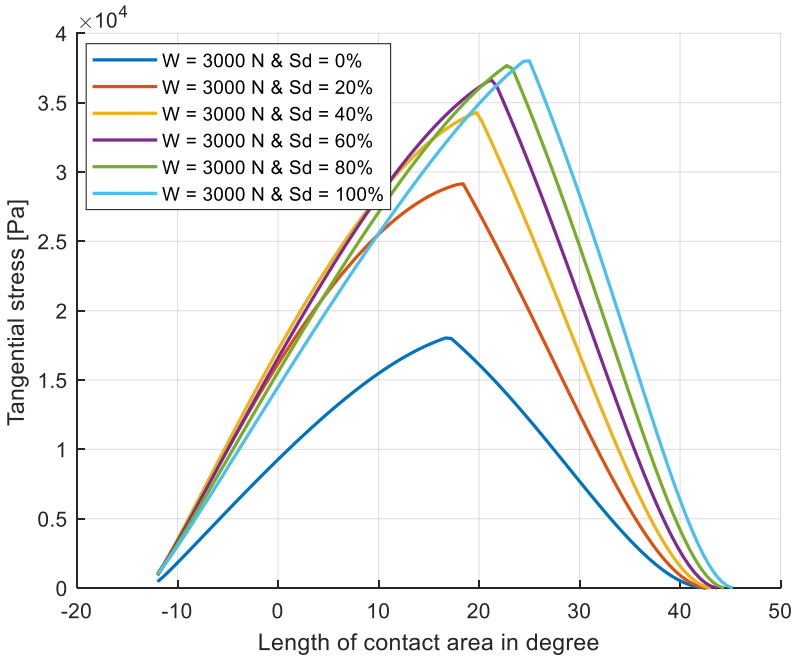

Figure 25: shear stress distribution – dependency on S_d

Moreover, in both cases, the peak of curves moves toward the entry angle: it means that the angle, where the maximum stress (called max stress angle) occurs, is closer

to the entry angle than the exit one. To evidence this behaviour, all variables have been plotted as a function of contact patch length, which corresponds to the distance, expressed in degree, from the exit angle up to the entry angle.

The translation toward the entry angle is due to two different reasons:

- in the first case (*Fig. 24*), the length of contact patch increases for bearing the vertical load;
- in the second case (*Fig. 25*), the longitudinal slip directly impacts on the max stress angle, which is determined using *Eq. 3.9*.

The combined effect of vertical load and slip is shown in *Fig. 26*.

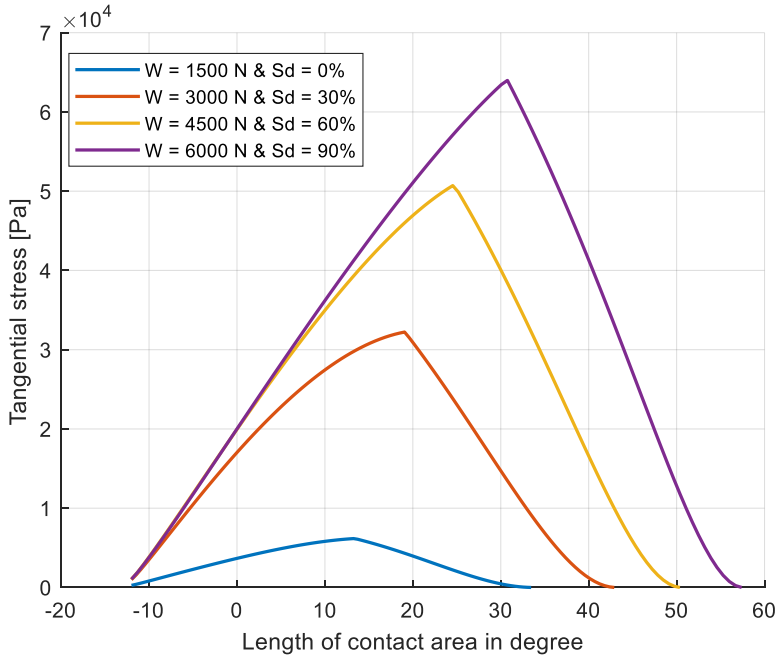

Figure 26: shear stress distribution – combined dependency on W and S_d

In the following charts (*Fig. 27-29*), the trend of the normal stress (σ) has been analysed and plotted as in the case of the tangential stress.

Based on the variation of the vertical load (*Fig. 27*), peaks move toward the entry angle and the normal stress increases; furthermore, the variation of the vertical load influences the normal stress in the same manner as occurred to the shear stress.

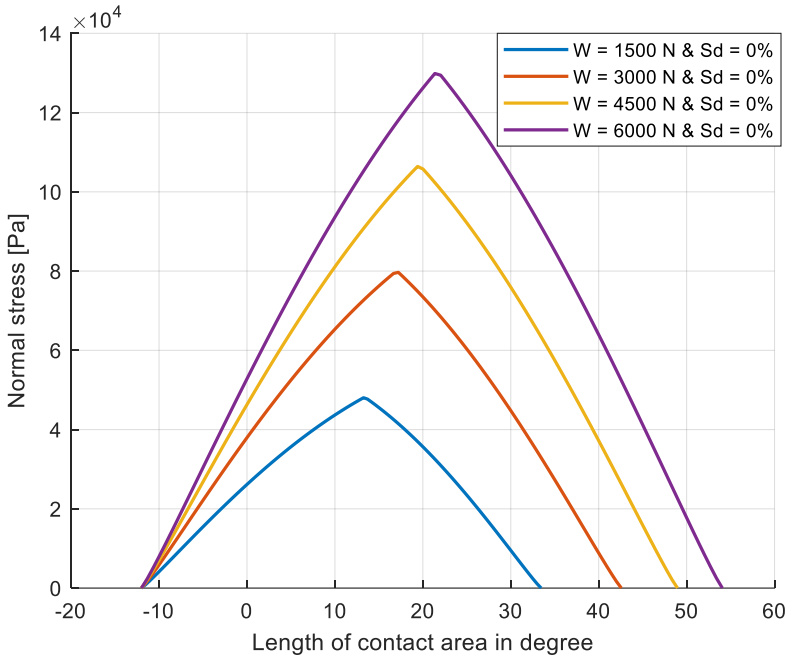

Figure 27: normal stress distribution – dependency on W

Contrary to the tangential stress, increasing the longitudinal slip (*Fig. 28*), the normal stress peak decreases, although the peak moves toward the entry angle: indeed, the normal stress decreases because the vertical load is given by the sum of vertical components of both the shear stress and the normal stress (see *Eq. 3.14*). Thus, being constant the vertical load, if the shear stress increases (*Fig. 25*) because of the slip increase, the normal stress must decrease.

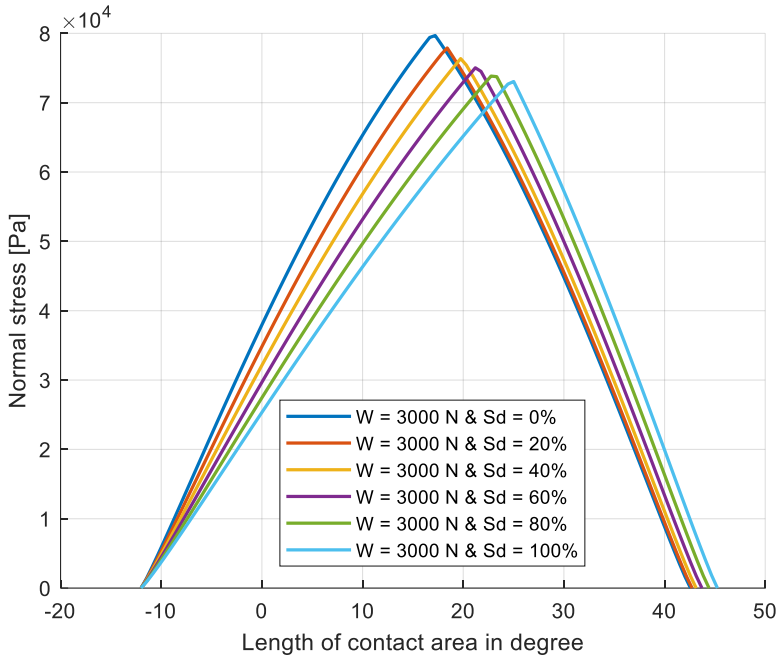

Figure 28: normal stress distribution – dependency on S_d

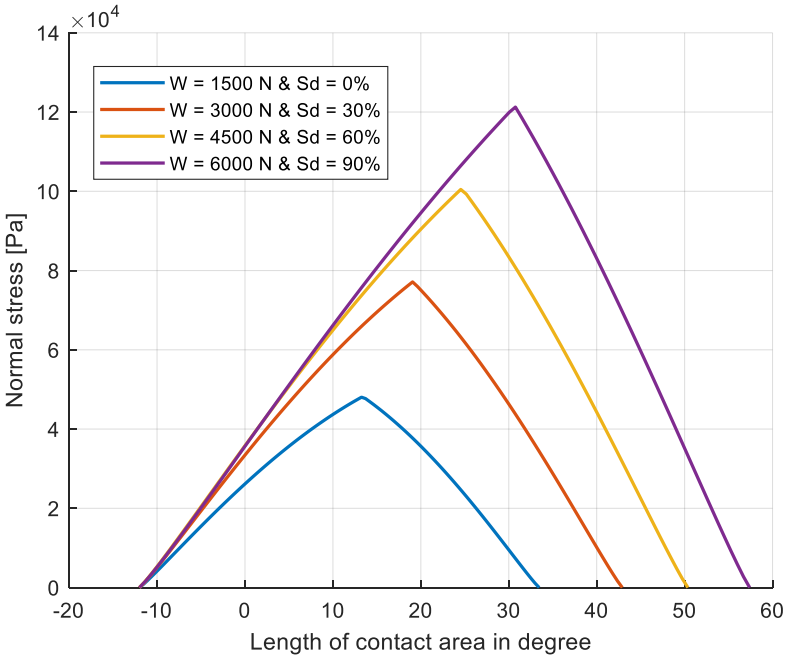

Figure 29: normal stress distribution – combined dependency on W and S_d

It is worth to point out that, based on the analysis of the combined effect of the vertical load and the longitudinal slip, observable in *Fig. 29*, the vertical load impacts the trend of the normal stress more than the longitudinal slip: indeed, even if the increase of the longitudinal slip has to cause the decrease of the normal stress, because of the increasing of the vertical load the normal stress increases.

6.2.2 Shear thrust and compaction resistance

Shear thrust and compaction resistance are the core of the longitudinal slip: indeed, the vehicle movement is allowed only if the difference between shear thrust and compaction resistance is positive.

The shear thrust is the horizontal component of the shear stress, while the compaction resistance is the horizontal component of the normal stress.

Normal and shear stress, as described in *section 6.2.1*, are influenced by both the vertical load and the slip; moreover, also the entry angle, which is influenced by the same factors, takes part in the calculation of the longitudinal force. The entry angle is important because it determines the sinkage and the length of the contact patch, considering that the exit angle is assumed to be constant.

It is worth to point out that the compaction resistance can have a positive contribution in the longitudinal forces. The normal stress is direct to the centre of the wheel: therefore, in the forward part of the wheel, the horizontal component of the normal stress has opposite direction with respect to the shear thrust, while it has the same direction in the rear part of the wheel.

Normal stress components are shown in *Fig. 30*.

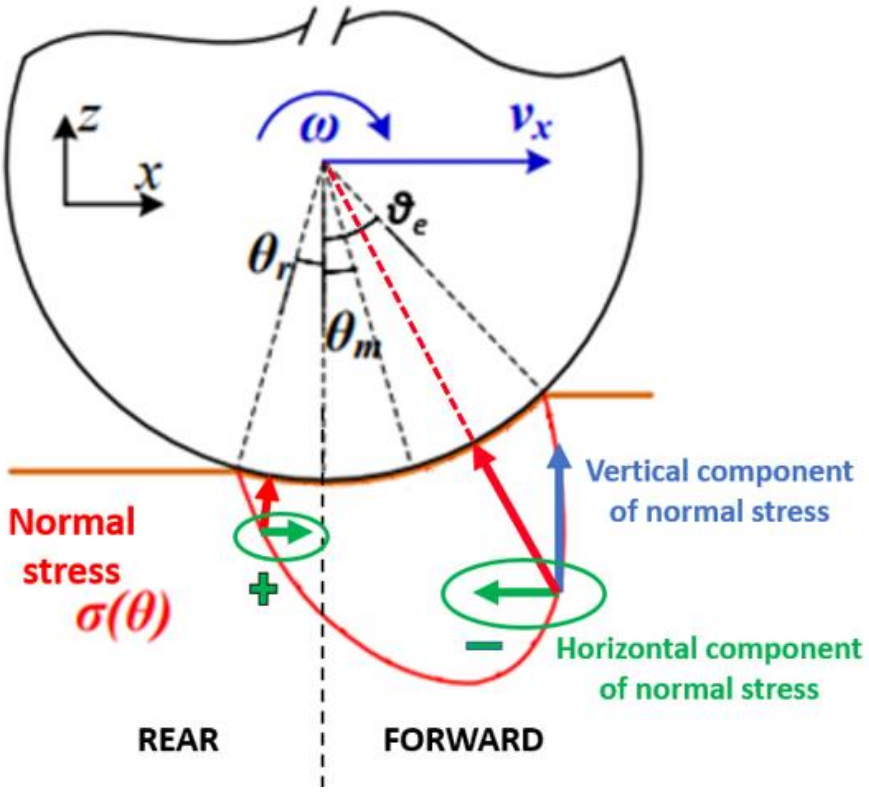

Figure 30: focus on horizontal component of normal stress

Here below, the charts show the combined effect of the vertical load and the longitudinal slip on the shear thrust (*Fig. 31*) and on the compaction resistance (*Fig. 32*).

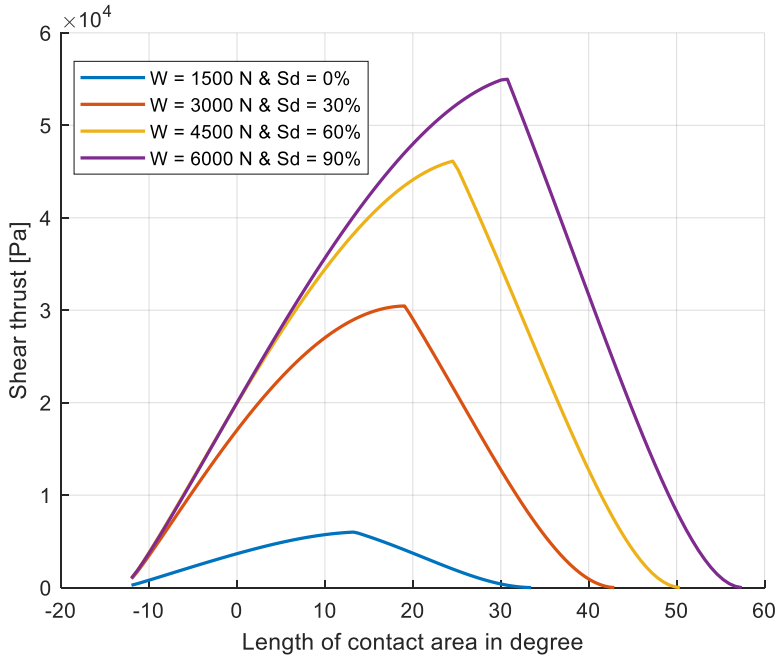

Figure 31: shear thrust distribution – combined dependency on W and S_d

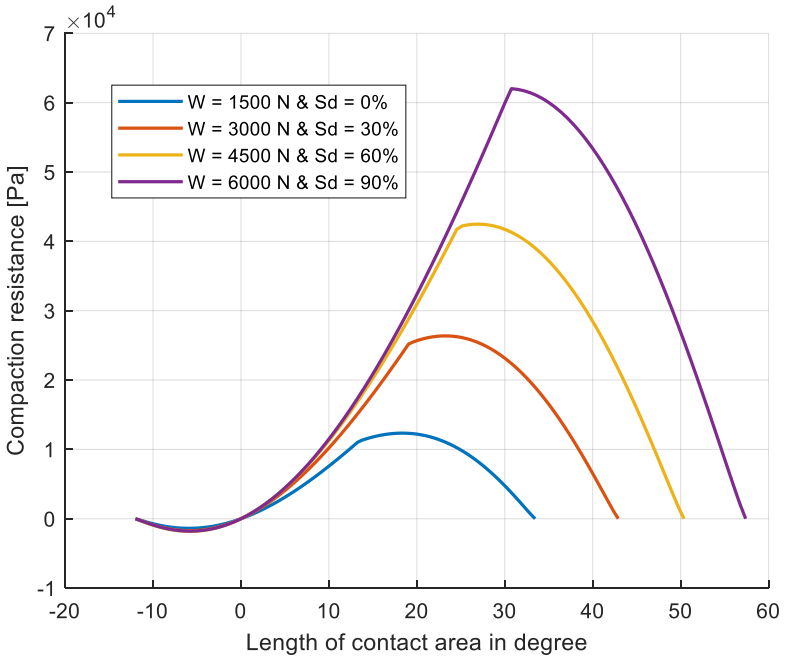

Figure 32: compaction resistance distribution – dependency on W and S_d

The negative values of the compaction resistance in the rear part of the wheel (range between -12° - 0°), shown in *Fig. 32*, represent the positive contribute to the longitudinal forces.

The positive values of the compaction resistance in the forward part of the wheel (0° - ~50°) can be imagined like a wall of soil under the wheel, which represents an obstacle to the movement of the vehicle.

6.2.3 Comparison of longitudinal forces

After this preliminary analysis it is possible to compare the trend of the longitudinal forces given by Pacejka's model and the trend given by the off-road model.

In *Fig. 33*, using the common Pacejka's model, the longitudinal forces vs longitudinal slip are plotted.

It is possible to observe that the longitudinal maximum force increases with increasing the vertical load, in a non-linear way. Moreover, the chart shows that the peak of forces occurs at about 0.1 longitudinal slip. The slope increase means that it is necessary a reduced slip to obtain the same value of the longitudinal force.

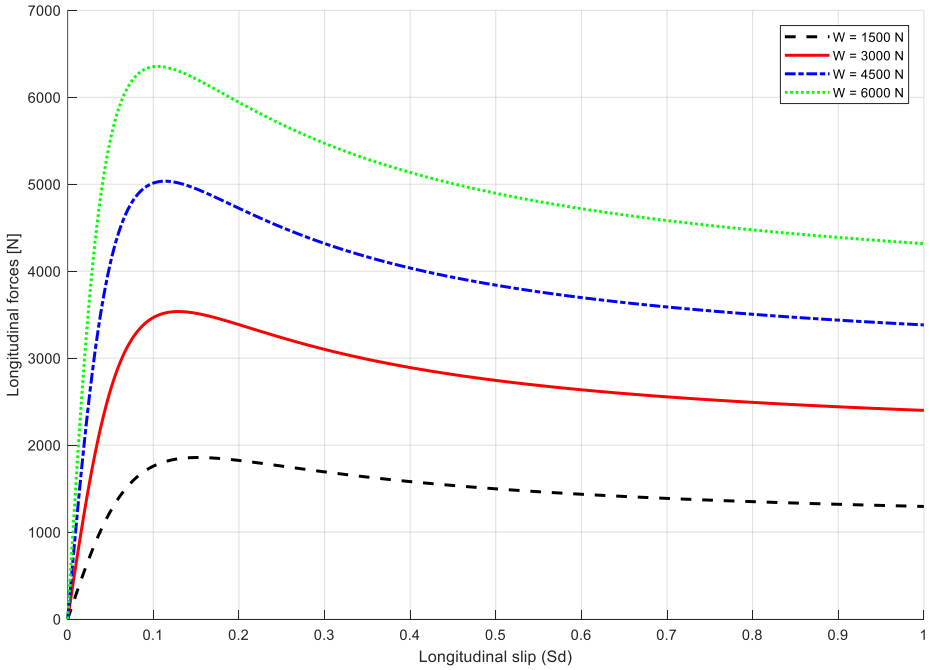

Figure 33: F_x vs S_d – dependency on W (Pacejka's model)

The trend of the F_x, shown in *Fig. 34*, is quite similar to the one given by Pacejka's model (*Fig. 33*), even if the influence of the vertical load variation is different.

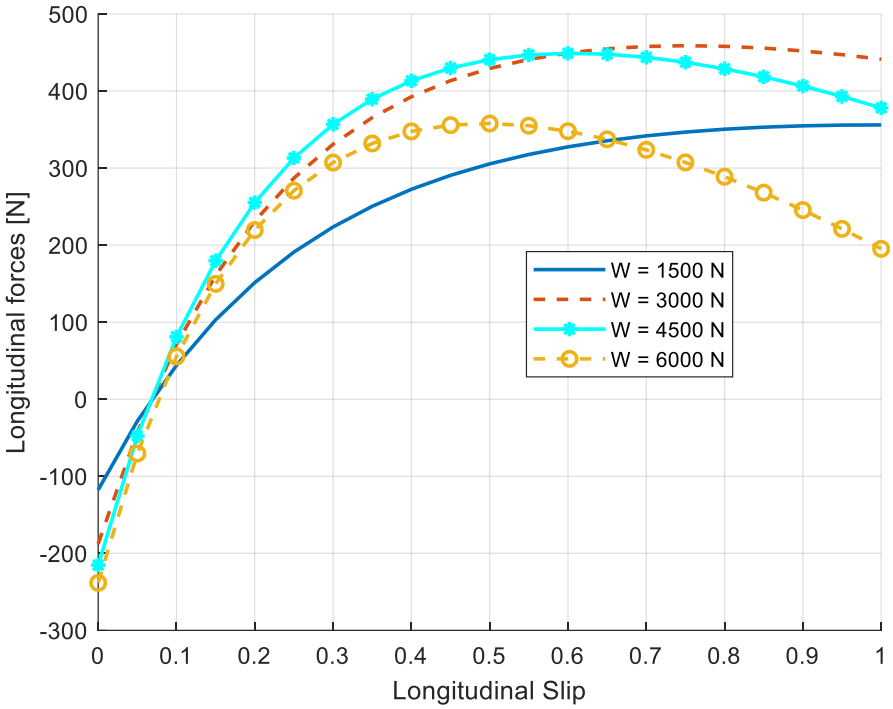

Figure 34: F_x vs S_d – dependency on W (off-road model – dry sand)

Fig. 34 shows that:

- at 0% of slip, for any vertical load, the value of F_x is negative because the compaction resistance is higher than the shear thrust: indeed, in *Fig. 35*, it is evident that the area under the compaction resistance line is bigger than the one under the shear thrust line;
- for the maximum vertical load (W = 6000 N), when the value of the slip is higher than 45%, the compaction resistance increases more than the shear thrust, therefore the longitudinal force curve has a negative slope.

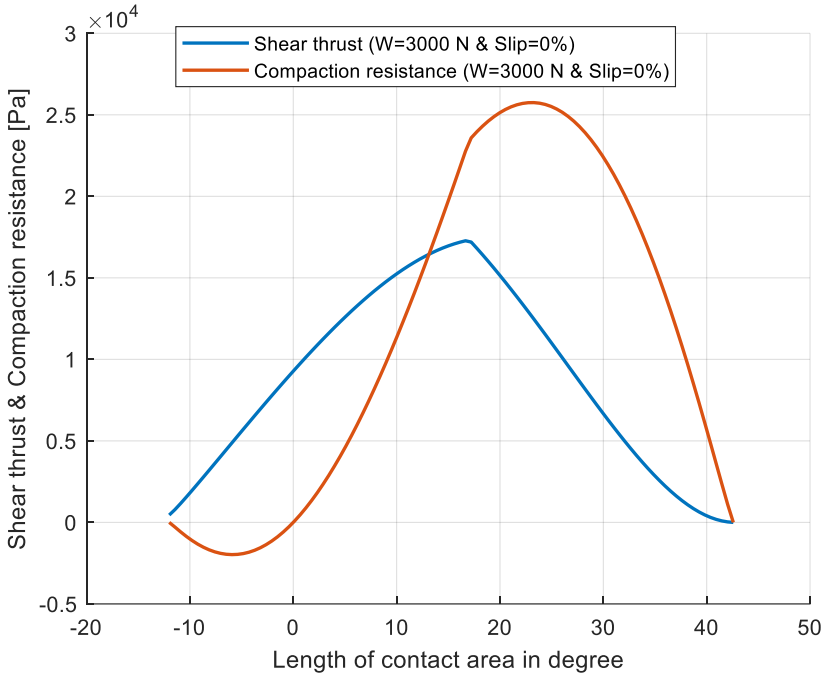

Figure 35: shear thrust and compaction resistance (0 % slip)

In *Fig. 36*, it is shown an example in which the area under the shear thrust line is bigger than the one under the compaction resistance.

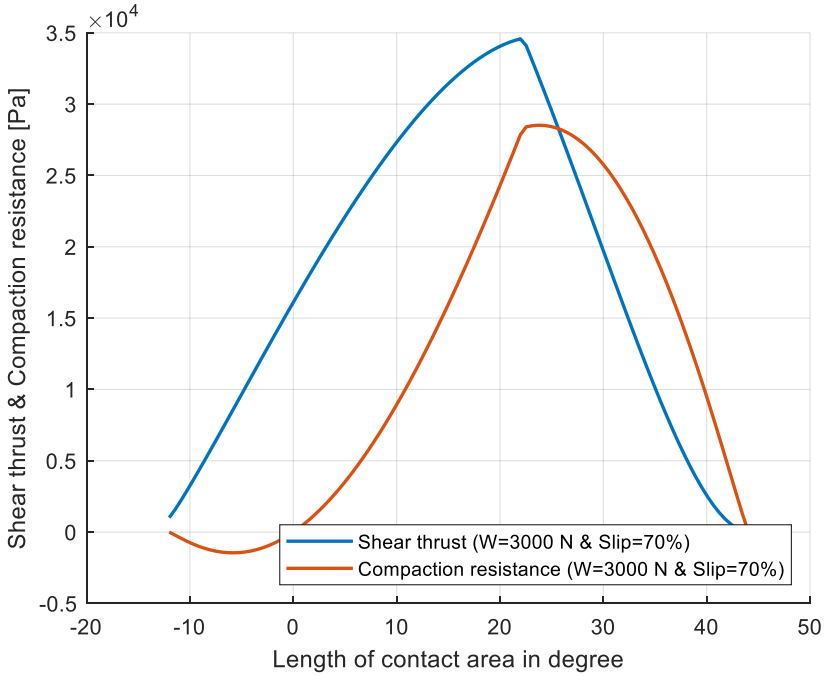

Figure 36: shear thrust and compaction resistance (70 % slip)

All charts, above reported in this chapter, refer to the "dry sand" soil.

Contrary to the thrust analysis, the type of soil influences the trend of the longitudinal forces; therefore, for the sake of completeness, graphs, in which longitudinal forces are plotted for "LETE sand" soil and for "Loam sand" soil, are reported here below.

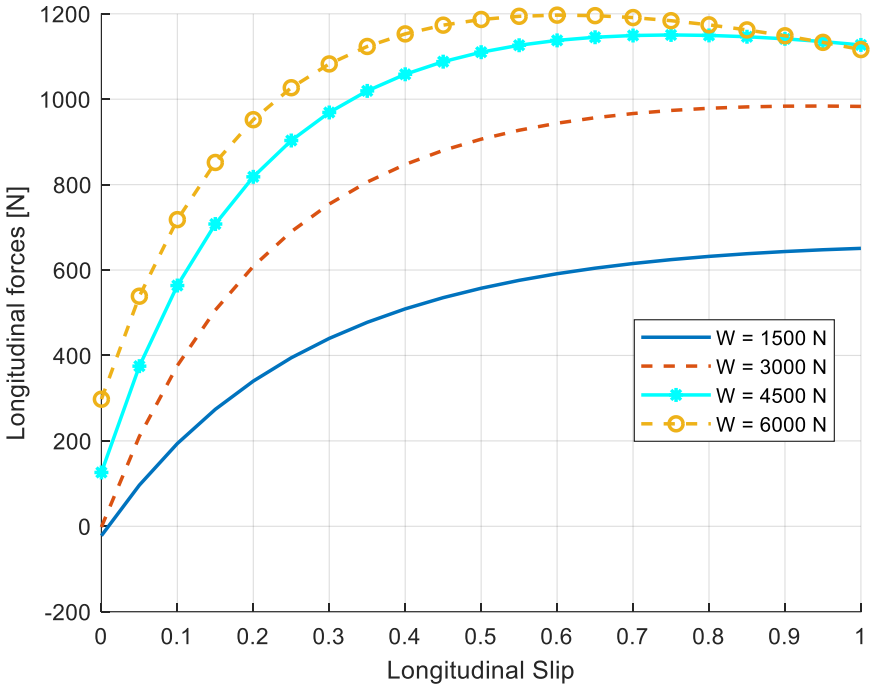

Figure 37: F_x vs S_d – dependency on W (off-road model – LETE sand)

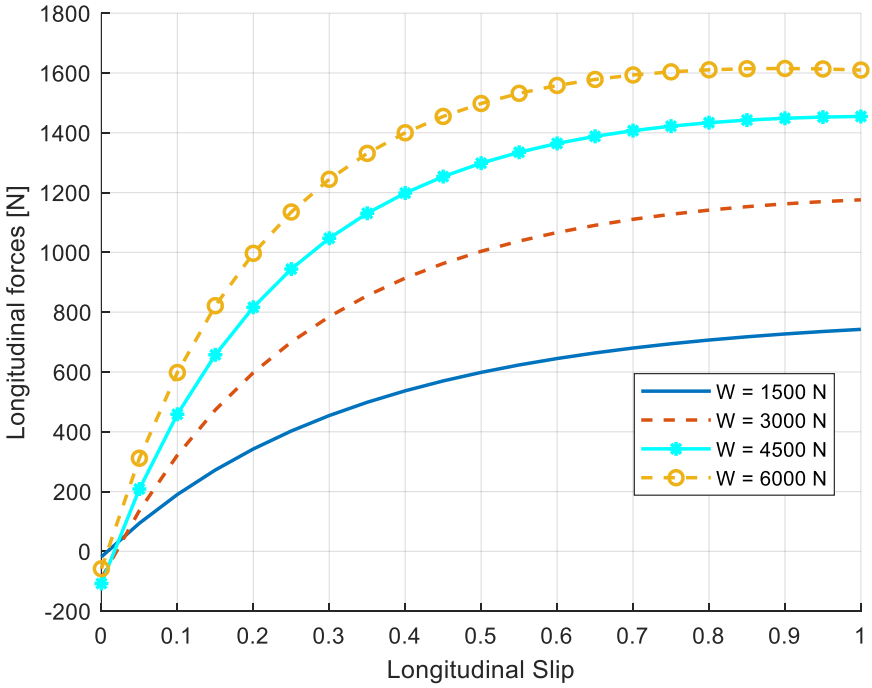

Figure 38: F_x vs S_d – dependency on W (off-road model – loam sand)

The same analysis carried out for "dry sand" soil can be developed for "LETE sand" and "loam sand" to examine the trend of both the shear thrust and the compaction resistance, using the same assumptions.

In conclusion, considering constant the vertical load (W = 5000 N), the longitudinal forces of the three types of soil are plotted in the following graph.

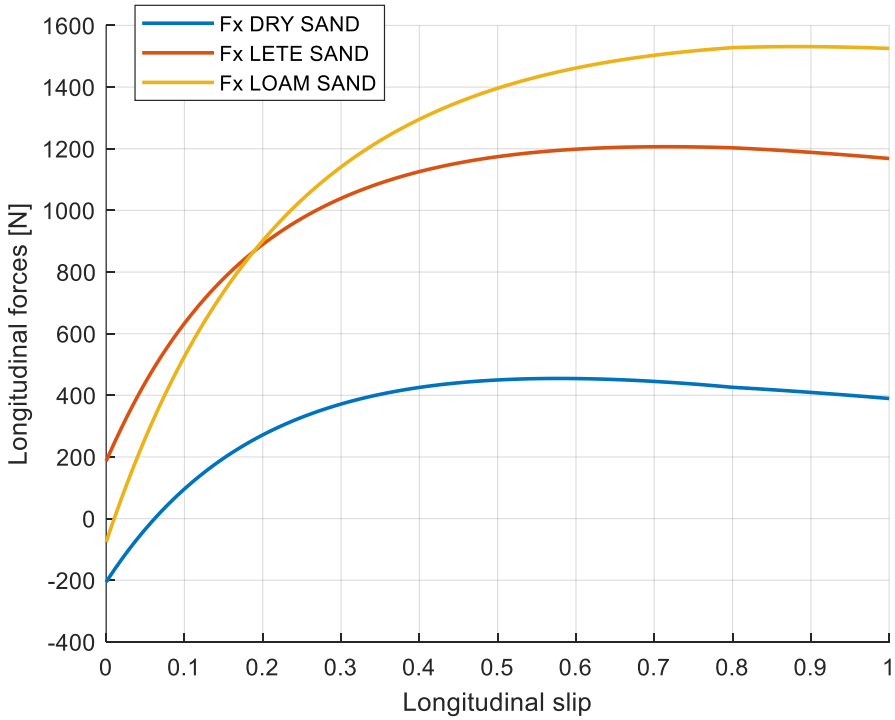

Figure 39: F_x vs S_d – different type of soils

Fig. 39 shows the influence of the soil on longitudinal forces by varying the slip.

For example, the "loam sand" soil is the one that allows higher longitudinal forces: this means higher vehicle acceleration and speed. On the other hand, when the slip is 0%, the "dry sand" is the soil that slows down the vehicle more than the other terrains because of the higher negative value of F_x.

The above-mentioned analysis of the graph has been confirmed by results of both offline and real-time simulations and by driver's feedback (reported in *chapter 10.1*).

In *Fig. 40* values of sinkage and both the entry angle and the exit angle are reported for all the three types of soil; it is worth to highlight that, since the slip variation determines a change of the entry angle, for each type of soil it has been considered an average value of the entry angle.

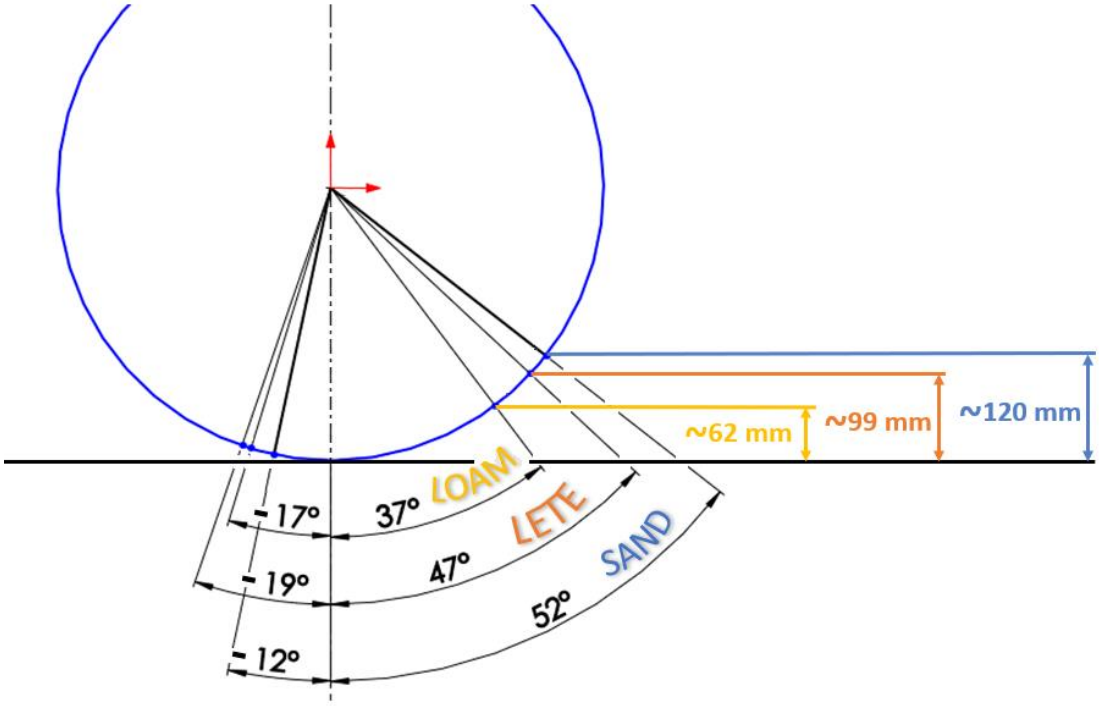

Figure 40: contact length for different type of soils

7 Off-Road Model

In this thesis, it has been decided to validate the developed off-road model using the results obtained by a commercial multibody software (Adams/Car), capable of running reliable vehicle dynamics simulations on deformable terrains.

The decision to validate the model through simulations was necessary because of Covid-19 outbreak: indeed, field tests were not feasible.

To achieve the final goal to obtain an off-road driving on dynamic simulator, it has been decided to use VI-CarRealTime because, contrary to Adams/Car, it is capable to run on the dynamic simulator software, allowing to run the model in real-time.

7.1 VI-CarRealTime interface

VI-CarRealTime is a software capable to model and to simulate a complete vehicle targeted to a simplified 4 wheels vehicle model. It is possible to create the vehicle system by collecting its fundamental subsystems, specifying dynamic manoeuvre schedules, launching standalone or MATLAB/Simulink embedded simulations, and post-processing obtained results [16].

The vehicle model has overall 14 degrees of freedom (DoF), distributed as follows:

- the vehicle chassis (sprung mass) has 6 DoFs;
- the wheel parts (unsprung mass) have 2 Dofs each (one for describing the motion with respect to the vehicle body and the other for the wheel spin) [16].

The vehicle system is composed by the following subsystems: front suspension, rear suspension, steering, body, powertrain, front wheels and tyres, rear wheels and tyres, and brakes. The behaviour of the suspensions and the steering subsystems is described by lookup tables, while other vehicle subsystems (such as powertrain and brakes) can be parameterised by the user and are described using differential and algebraic equations [16].

The simplified, but detailed, vehicle model used in VI-CarRealTime allows to run faster than real-time simulations and this is useful for controller design and for the optimisation of vehicle performance. Last but not least, VI-CarRealTime model is used for real-time applications, such as Hardware-in-the-Loop (HiL), Software-in-the-Loop (SiL) and, most important for this thesis, professional driving simulators.

In VI-CarRealTime, there is a tool named "Event Builder" which allows the user to create a series of mini-manoeuvres. In each created event, it is possible to set main vehicle parameters like speed, throttle, gear, steering, and others.

7.2 Vehicle model

To compare the simulation results given by both software, the vehicle must be aligned in terms of vehicle dynamics behaviour.

Starting from a reference vehicle model in Adams/Car (main characteristics reported in *Tab. 4*), it is possible to automatically translate it into a VI-CarRealTime model, using a dedicated plug-in tool.

Mass	1828 [kg]	57.75 % front	42.25 % rear
Traction	AWD	50 % front	50 % rear
Differential type	open		

Table 4: vehicle data

Even if the model generation procedure is automatic, it is necessary to check if all vehicle parameters are properly exported into the VI-CarRealTime model; it is possible to refine the VI-CarRealTime model so as to align it to the starting Adams/Car model.

This sort of mini-validation has been performed carrying out standard dynamic manoeuvres; specifically, simulation results of the following driving manoeuvres have been compared:

- constant speed: vehicle goes straight on at the speed of 80 km/h; vehicle weight, weight distribution and gear ratios have been evaluated;
- slow ramp steer: vehicle at the speed of 80 km/h steers 20°/s; steady state lateral dynamics: vertical position of the CoG, roll stiffness distribution, and so on; in particular, the most common handling diagrams have been evaluated;
- braking: vehicle at the speed of 80 km/h brakes until stop; brake pressure, pitch angle, longitudinal transient and steady state dynamics have been evaluated;
- acceleration: vehicle starts at the speed of 30 km/h, after 2 seconds the virtual driver accelerates full throttle for 20 seconds; longitudinal transient and steady state dynamics and gear ratios have been evaluated.

To avoid deformable soil influences, the above manoeuvres have been simulated on a flat road, using the same Pacejka tyre model.

In this case, it was not necessary to perform any adjustment to the VI-CRT model: the vehicle models are aligned in terms of both longitudinal and steady state lateral dynamics, as it can be seen in the following charts (*Fig. 41-46*), showing the comparison between Adams vehicle model and CRT vehicle model. In some charts,

because of the different initialization techniques performed by both software, it is possible to observe a non-perfect overlapping of the curves representing both models.

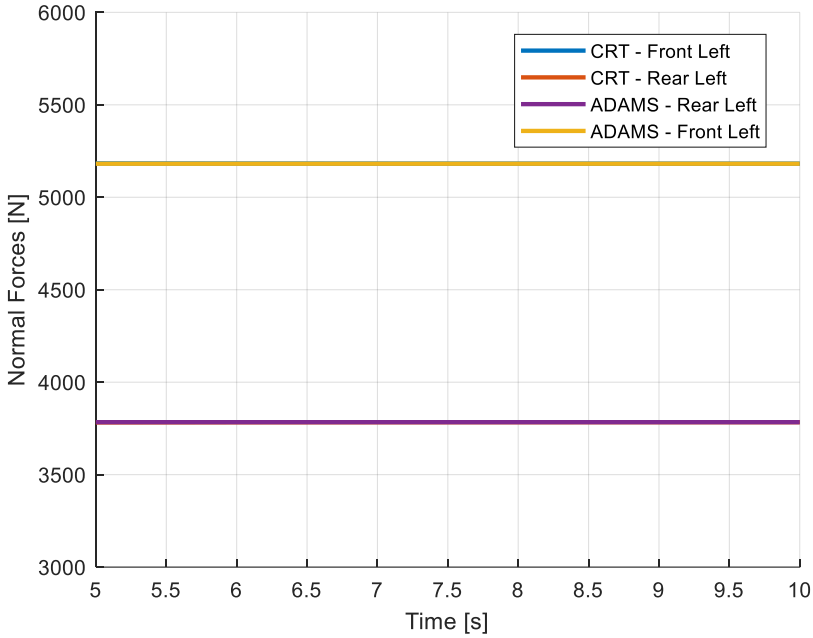

Figure 41: weight distribution (constant speed manoeuvre)

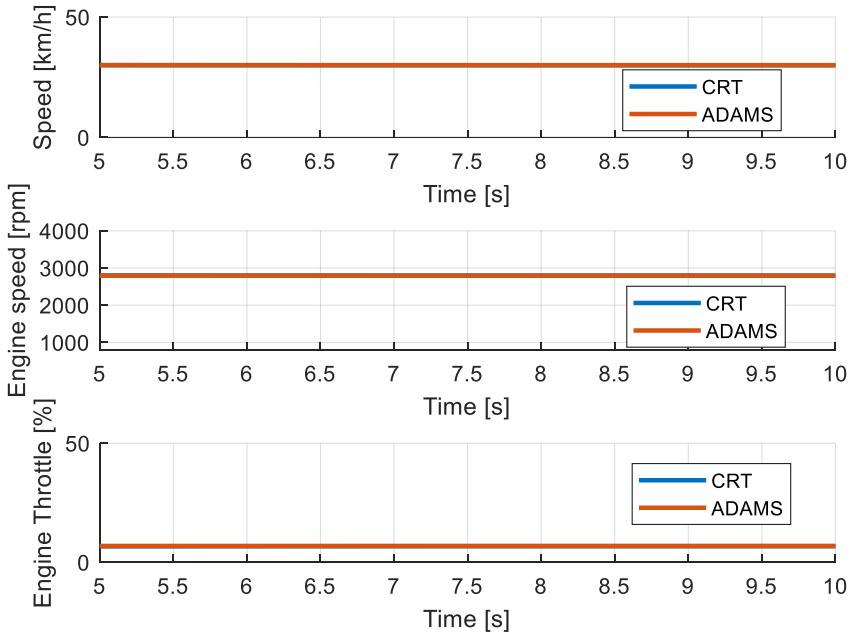

Figure 42: speed - engine speed - throttle (constant speed manoeuvre)

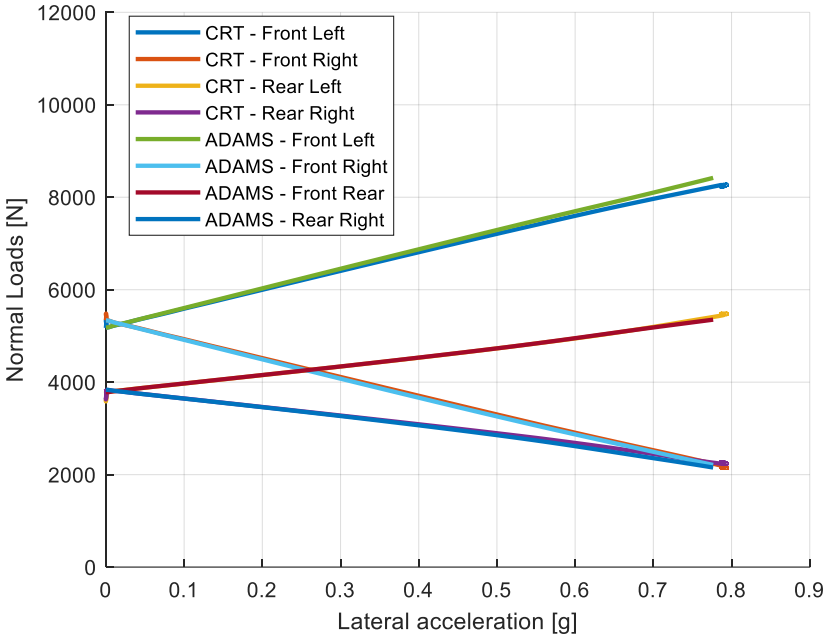

Figure 43: weight distribution (slow ramp steer manoeuvre)

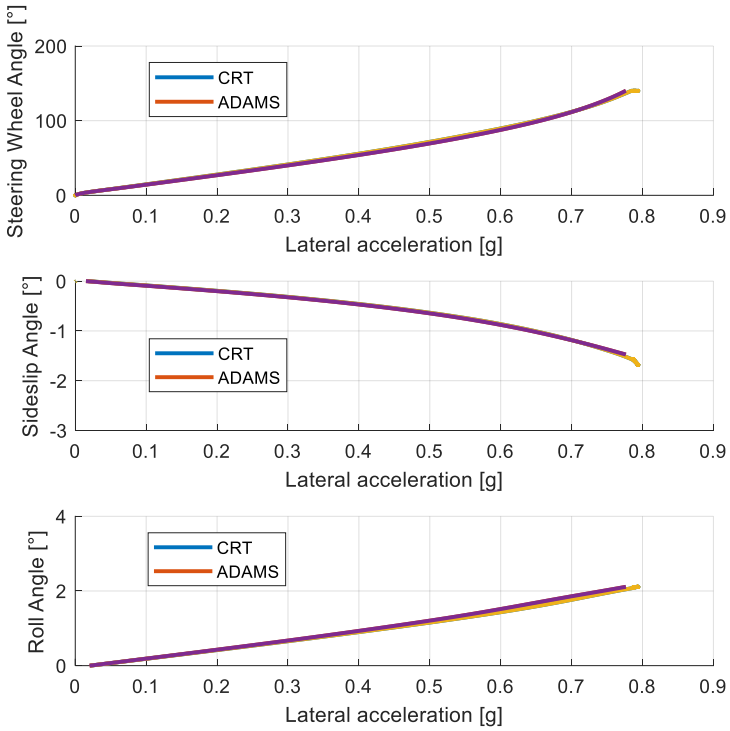

Figure 44: steering wheel angle – sideslip angle - roll angle (slow ramp steer manoeuvre)

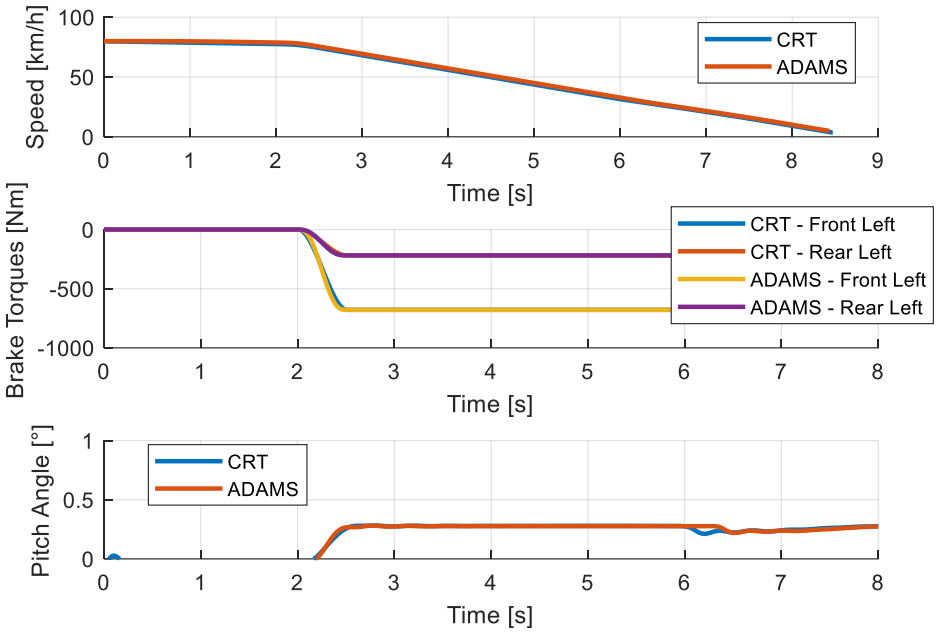

Figure 45: speed - brake torque - pitch angle (braking manoeuvre)

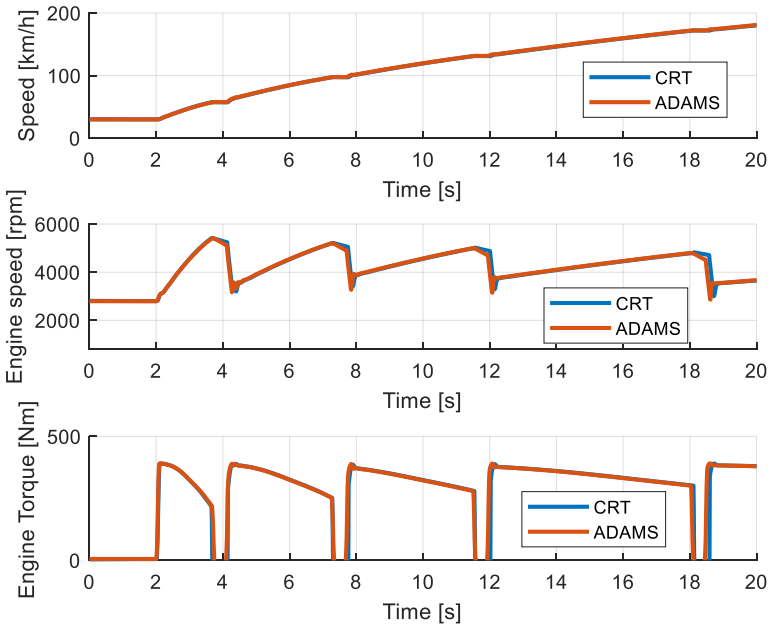

Figure 46: speed - engine speed - engine torque (acceleration manoeuvre)

7.3 Co-simulation: MATLAB/Simulink interface

The developed tyre model must be connected to the VI-CarRealTime car model in order to run the co-simulation of the off-road driving.

Control systems or custom models can be connected to the vehicle model using the VI-CarRealTime solver interface.

The tyre model developed in this thesis is an example of custom model.

In MATLAB/Simulink the VI-CarRealTime vehicle model is represented by a "s-function", which has completely configurable inputs and outputs (I/O); outputs can be connected to other blocks in Simulink. Moreover, through the s-function, the user can analyse and track over 900 outputs variables during the simulation and it is possible to pass over 100 inputs optionally.

Both the car data and the driving manoeuvre are set from a file that is passed to the s-function as a parameter [16]. After that, using standard methods in MATLAB/Simulink, the simulation can be started.

In Simulink the block, which represents the VI-CarRealTime MATLAB/Simulink interface (*Fig. 47*), can be completely configured to set up I/O (*Fig. 48*) that the user needs.

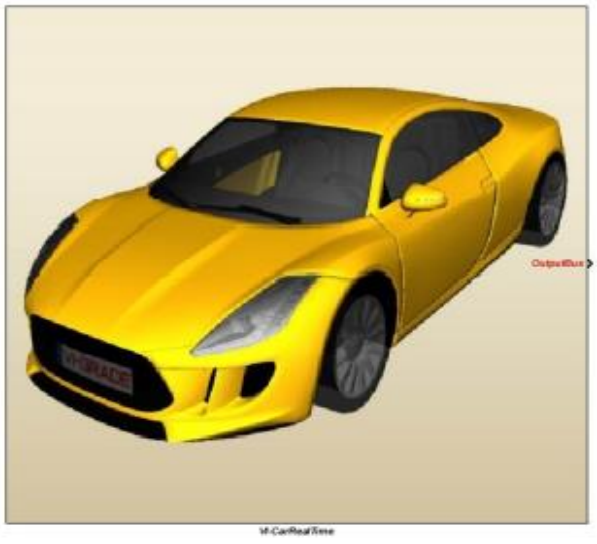

Figure 47: VI-CarRealTime MATLAB/Simulink interface [16]

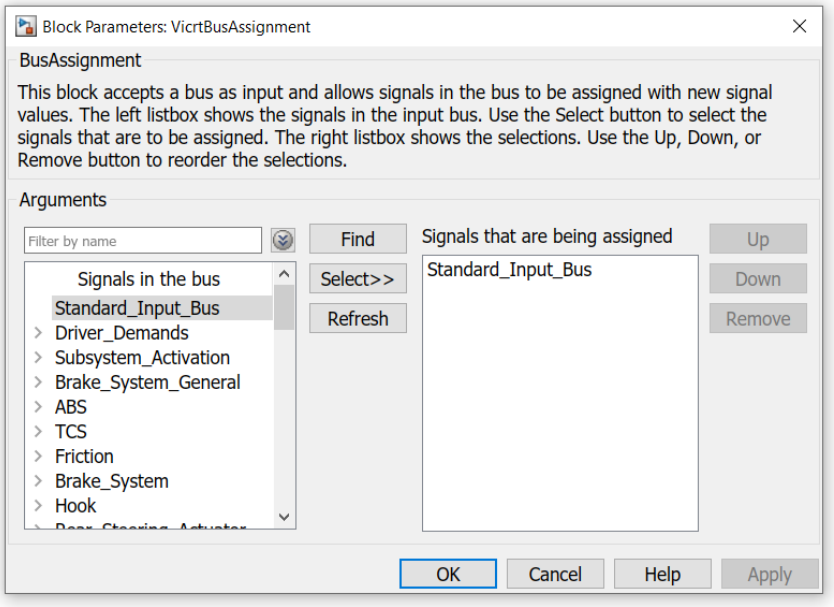

Figure 48: VI-CarRealTime S-function input ports

The s-function allows to define an output prefix, that gathers all the outputs, which can be used for a post-processing in MATLAB.

7.4 External road model

To simulate off-road driving, the soft-soil tyre model needs to interact with a proper soft-soil model, which is not provided by VI-CarRealTime. Furthermore, to obtain a realistic feeling of the off-road driving on dynamic simulator, it is important to simulate the sinkage of the wheel into deformable soil. When the soil is very soft, the sinkage can be considerable: for these reasons, it was necessary to create at least a simplified "deformable road" model.

VI-CarRealTime, in co-simulation environment, allows the usage of an external (user defined) road model. To characterise an external road, VI-CarRealTime solver needs contact patch information for all the tyres. Activating this feature, the s-function (VI-CarRealTime interface) enables a list of inputs; through these inputs the user can provide the contact patch information for all the tyre.

The contact patch information consists of:

- the absolute position of the wheel contact patch (x, y, z);
- the absolute orientation of the normal to the road surface provided by the direction cosines.

Fig. 49, here below, represents an example of a flat external road (to simplify, inputs and outputs of the VI-CarRealTime demo are reported for one wheel only).

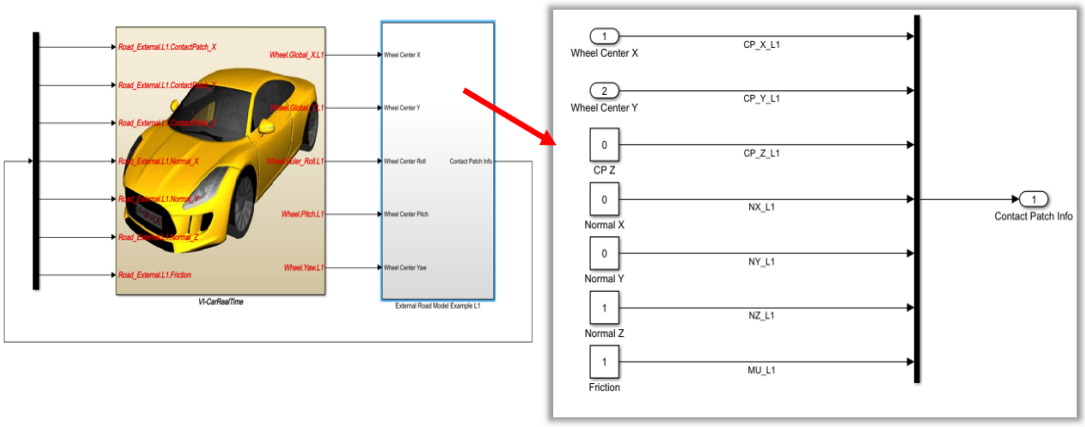

Figure 49: Simulink block of external road

The developed external road model is used to transmit the information of how much the vehicle sinks into the soil; furthermore, this model allows to use the coordinates of a real road.

Knowing the entry angle, the sinkage (Z) is calculated using a simple geometrical formulation:

$$Z = R_u(1 - \cos \vartheta_e) \tag{7.1}$$

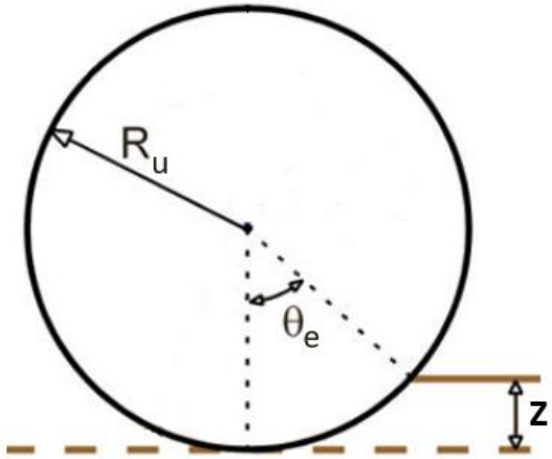

Figure 50: sinkage and entry angle

After determining the sinkage of each wheel, it is possible to give the information to the vehicle model; therefore, the new position of the contact patch is known.

In order to improve numerical stability, during the development of this model, a first order delay (0.05s) was introduced before transmitting the contact patch vertical position input.

The effect of this delay is to smooth abrupt vertical position changes, due to numerical solution, without causing an unrealistic delay.

7.4.1 Soil damping

During the work development, it was noted that, especially at the beginning of the simulation, the normal forces oscillate before stabilising. These oscillations are due to the sinkage of the wheel because it occurs immediately; therefore, the vertical forces are not dampened from the soil, since the equations shown in *chapter 3* do not consider any damping effect.

To obtain a more realistic off-road model and to reduce the oscillation phenomenon, a viscous damping, associated with wheel sinkage, has been introduced. In fact, since the wheel is considered as rigid, in this thesis it is assumed that the damping contribution must be given by the soil. This aspect would require a further investigation, both from an experimental and a modelling point of view, but it is out of the scope of this thesis. For these reasons, a simple viscous damping was considered.

It is possible to determine sinkage velocity and to introduce a viscous damping force, limiting the oscillations. The damping coefficient value was decided on the basis of co-simulations, with the aim to reasonably reduce oscillations due to sudden vertical load changes.

Fig. 51 shows the effect of the introduced soil damping.

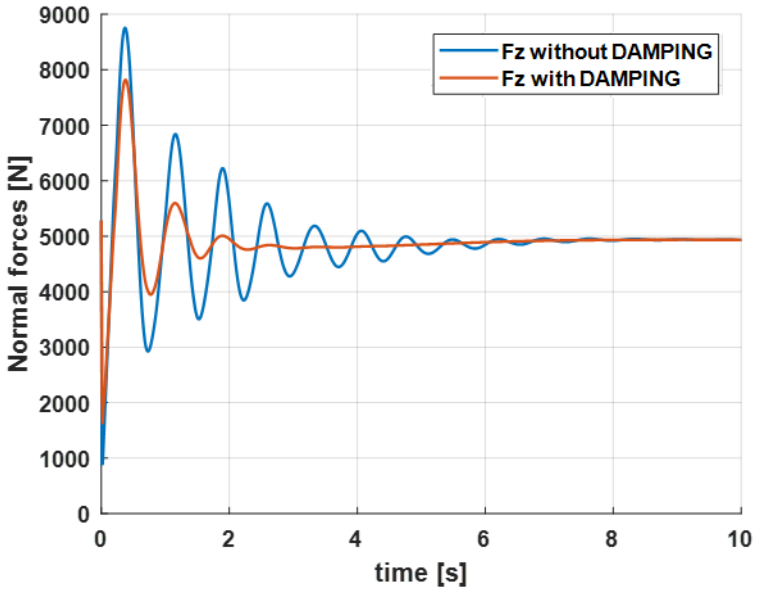

Figure 51: soil damping effect

7.5 Overview of the complete Off-Road Simulink model

The tyre model (described in *chapter 5*) and the external road model (*chapter 7.4*) constitute the developed off-road model, which, through the co-simulation, can be connected either with the vehicle model block on Simulink or on the simulator.

Fig. 52 represents the interaction between the vehicle model, the lookup table, the developed tyre model, and the external road model.

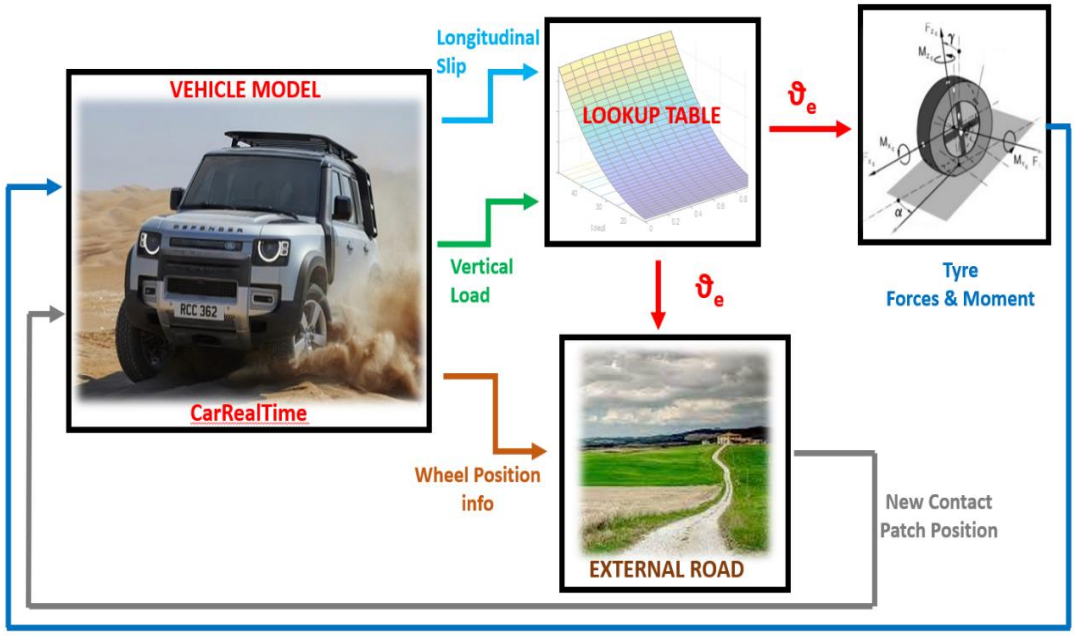

Figure 52: conceptual off-road model

The vehicle model provides the following outputs:

- the vehicle vertical load which acts on each wheel;
- variables for calculating the longitudinal slip for each wheel;
- the absolute position and orientation of each wheel.

The first two outputs listed above become the inputs for the lookup table. In the off-road model there are four lookup tables, one for each wheel.

Each lookup table has one output only, which is the entry angle.

Using the entry angle from the lookup table and other variables (described in *paragraph 5.4*) the MATLAB function calculates longitudinal, lateral, and normal forces, and the drive torque. Also, there are four MATLAB functions, one for each wheel.

The outputs of the MATLAB function become the inputs in the vehicle model and the loop is closed; this loop is run for each time step of the simulation.

7.5.1 Deactivation VI-CarRealTime forces and moments

It is worth to point out that the vehicle model, provided by VI-CRT, calculates forces and moments of the wheel without considering the external added models; therefore, it is necessary to deactivate this calculation otherwise tyre forces and moments, calculated by the off-road model, are added to the VI-CRT forces.

The inputs "Subsystem activation", available from the VI-CarRealTime interface (S-function), allow to deactivate the force/moment of interest, by selecting them (*Fig. 53*).

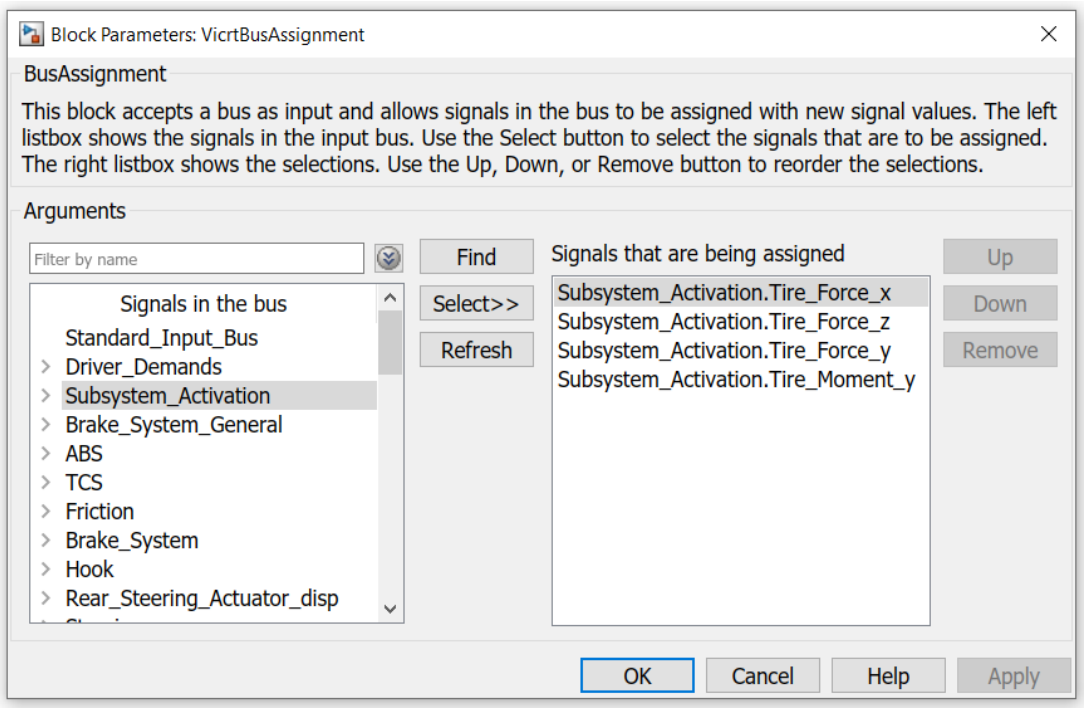

Figure 53: subsystem activation inputs

Subsystem activation inputs accept only two real numbers: if the value is 0, the selected force/moment is active, otherwise if the value is 1, the selected force/moment is deactivated.

8 Analysis of Offline Simulation Results

In this chapter it is shown the comparison between the results obtained by the offline simulation of the developed off-road model and those obtained by Adams/Car.

The term "offline simulation" refers to the offline test carried out without the dynamic simulator, while "real-time simulation" refers to the test carried out on the dynamic simulator.

8.1 Offline simulation set-up

To obtain results, which can be comparable to the ones given by Adams/Car, the co-simulation, performed by MATLAB/Simulink and VI-CarRealTime, must be set in similar way to the Adams/Car set-up. Here below, the main parameters of the co-simulation set-up are reported:

- the simulated vehicle model;
- the simulated soil;
- the driving manoeuvres.

Using VI-CarRealTime, especially the tool "Event Builder", it has been created the same driving manoeuvres simulated in Adams/Car. The imposed parameters of both simulated driving manoeuvres are reported here:

- **constant speed**: the vehicle goes straight on, in 2nd gear at the speed of 50 km/h for 30 seconds;
- **acceleration**: the vehicle starts, and it remains in 2nd gear at the speed of 30 km/h for 15 second; then the virtual driver accelerates full throttle for 45 seconds; during the acceleration, the selection of the gear is decided by the virtual driver.

The vehicle model has been loaded in VI-CarRealTime environment; then, the necessary events have been created for the co-simulations in VI-CarRealTime Test mode. In VI-CarRealTime, events are class objects defining a specific type of simulation [16].

The output of VI-CarRealTime Test mode is so-called send-file, that becomes the input parameter for the s-function (VI-CarRealTime solver in Simulink Off-road model). The send file contains the information about both the vehicle model and the driving manoeuvres that the user wants to simulate. Moreover, with the send file the external road inputs for the s-function are enabled.

The three types of soil, reported in *chapter 4.2*, are simulated and the soil parameters necessary for the co-simulation are imposed using an initialization MATLAB script, through which the lookup tables of the entry angle are also setup.

8.2 Offline Simulation Results

In this section, the results of preliminary simulations are compared to those obtained by Adams/Car, selecting the most important variables for off-road driving.

The performed simulations are six because the two driving manoeuvres, described above, are simulated for each type of terrain: for the sake of clarity, only the simulations on "dry sand" are reported in the following paragraphs, while the other simulations are available in *Appendix B*.

The plots show data only after 10s, due to the different initialization techniques performed by the two software.

In every charts legend, the name "CRT" indicates the results provided by the co-simulation of the off-road model, while the name "Adams" labels the results provided by the software Adams/Car.

Both the names "CRT" or "Adams" use the following prefixes:

- L1, it refers to the front left wheel;
- R1, it refers to the front right wheel;
- L2, it refers to the rear left wheel;
- R2, it refers to the rear right wheel.

In some charts, it is possible to see only one line because the results given by the two models are identical, therefore the result curves are overlapping.

8.2.1 Offline Simulation: constant speed – dry sand

The first offline simulation evaluates the driving manoeuvre at "constant speed" on a "dry sand" (soil data reported in *Tab. 1*).

Based on the following four charts (*Fig. 54-57*), it is possible to observe that both the virtual driver of VI-CarRealTime and the one of Adams/Car carry out the same driving manoeuvre: the speed and the longitudinal acceleration are the same, and the driver demands are also very similar.

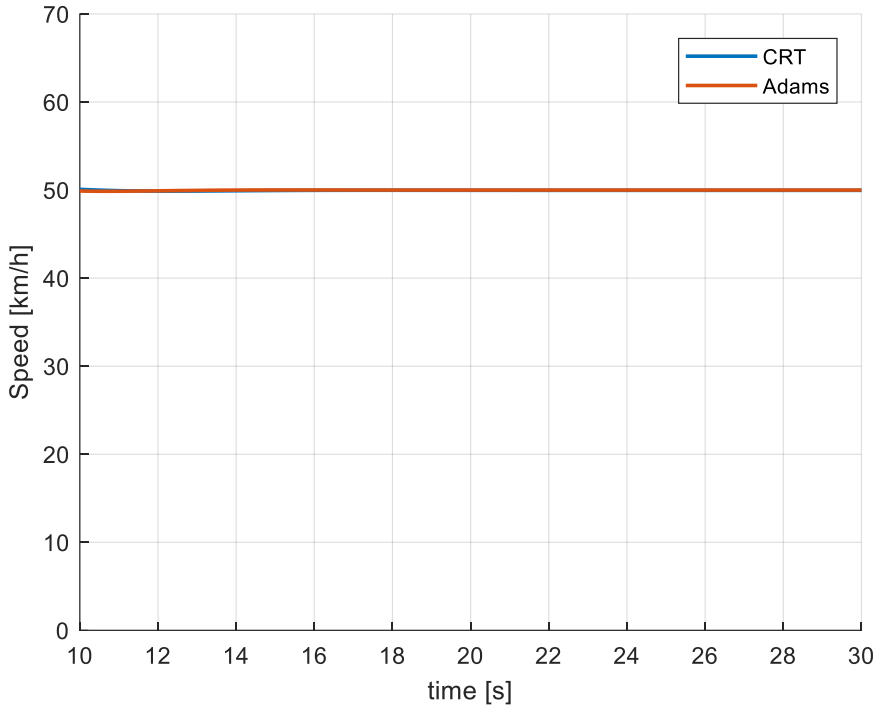

Figure 54: speed (Offline - Constant Speed - Dry Sand)

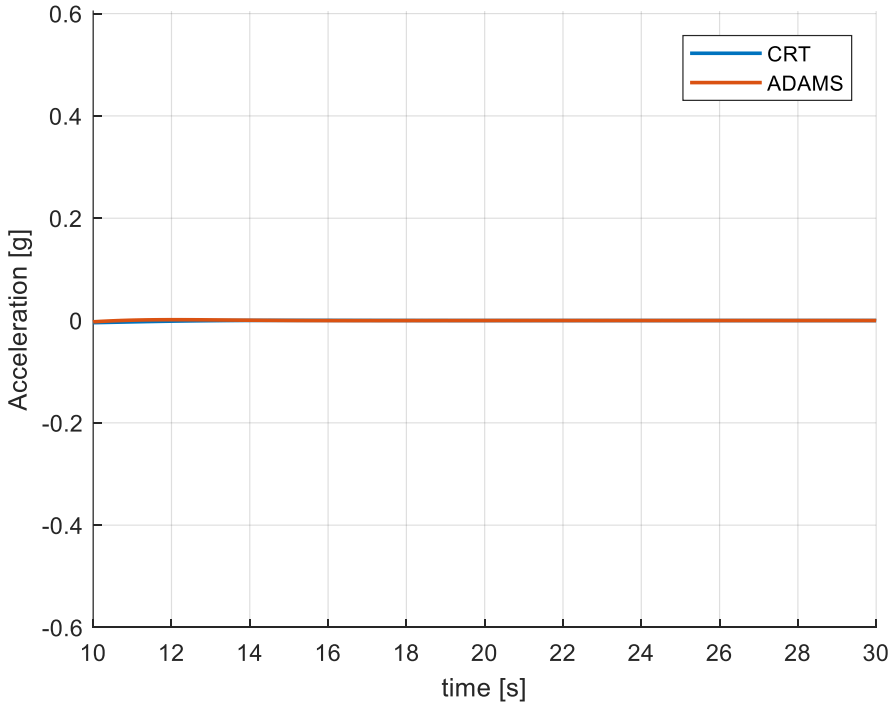

Figure 55: longitudinal acceleration (Offline - Constant Speed - Dry Sand)

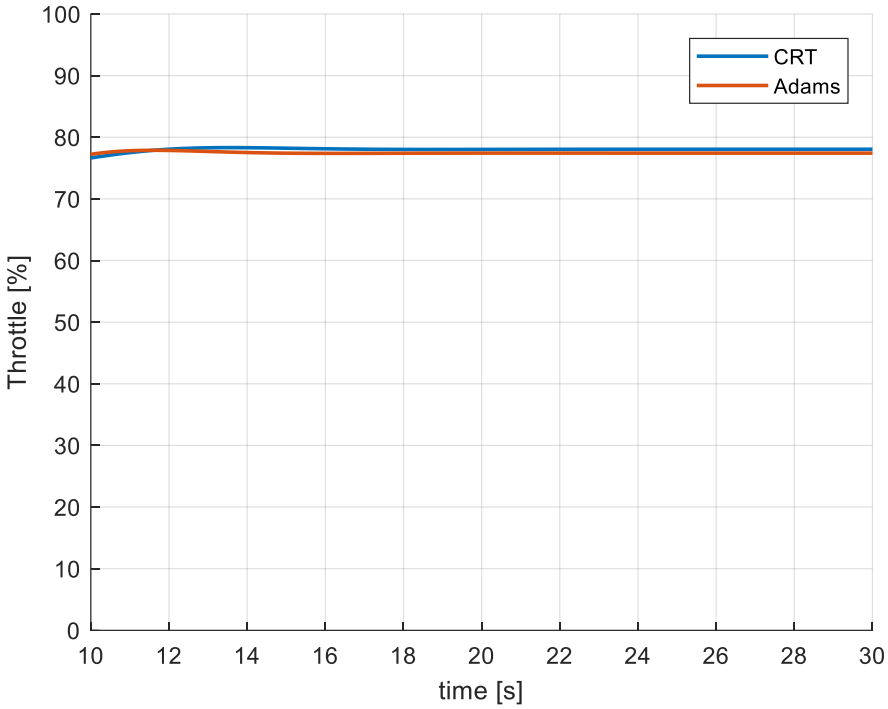

Figure 56: throttle demand (Offline - Constant Speed - Dry Sand)

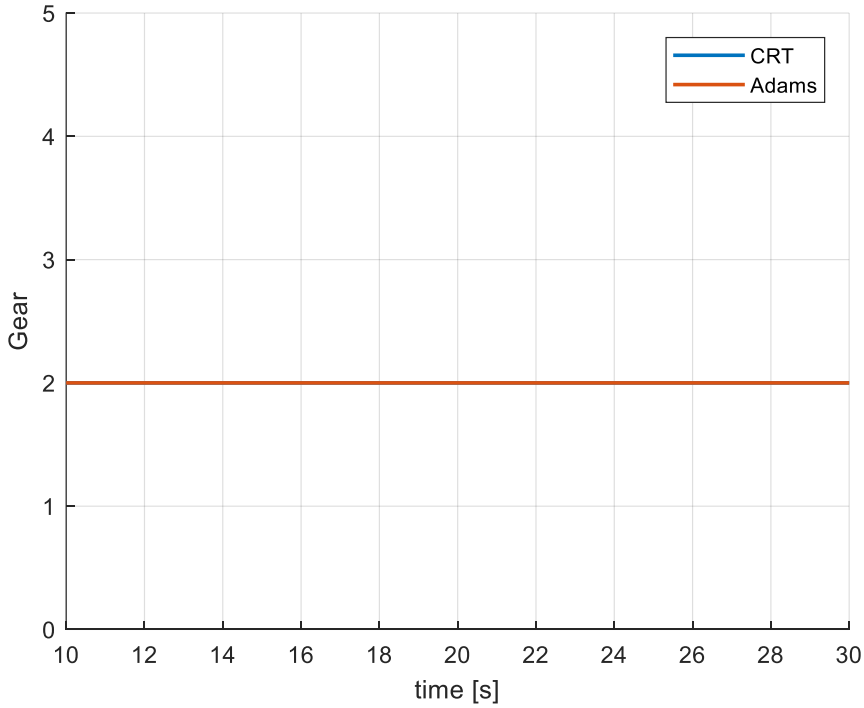

Figure 57: gear demand (Offline - Constant Speed - Dry Sand)

In *Fig. 58,* it is possible to observe the longitudinal slip: for the front wheels, the value is almost identical, while for the rear wheels, the variance between simulations is around 10% as a maximum.

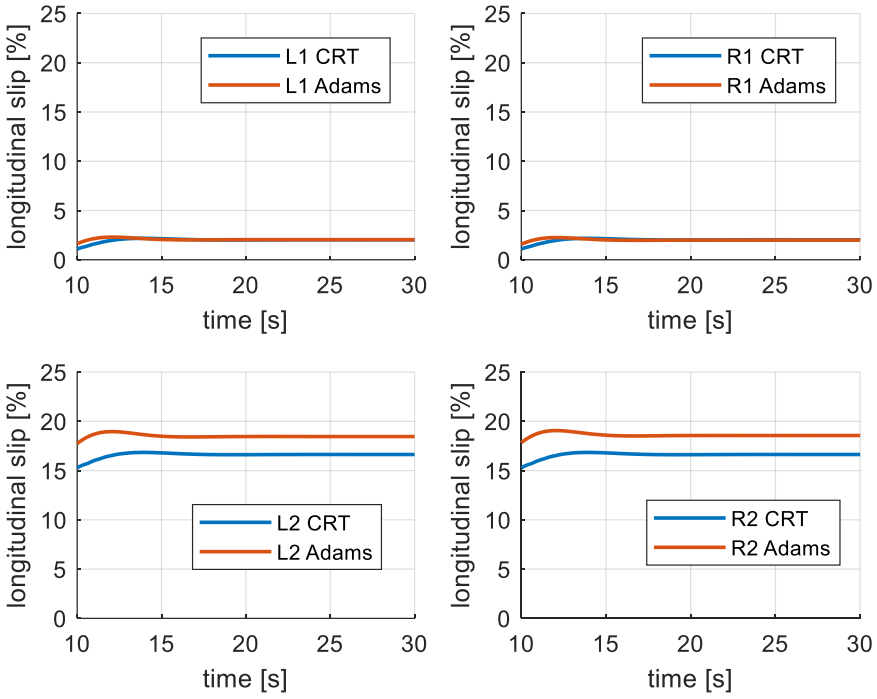

Figure 58: longitudinal slip (Offline - Constant Speed - Dry Sand)

The accuracy of the created lookup tables, therefore the precision of the function "Find ϑ_e", can be observed in *Fig. 59*: indeed, the value of the entry angle is almost the same to the one obtained by Adams/Car.

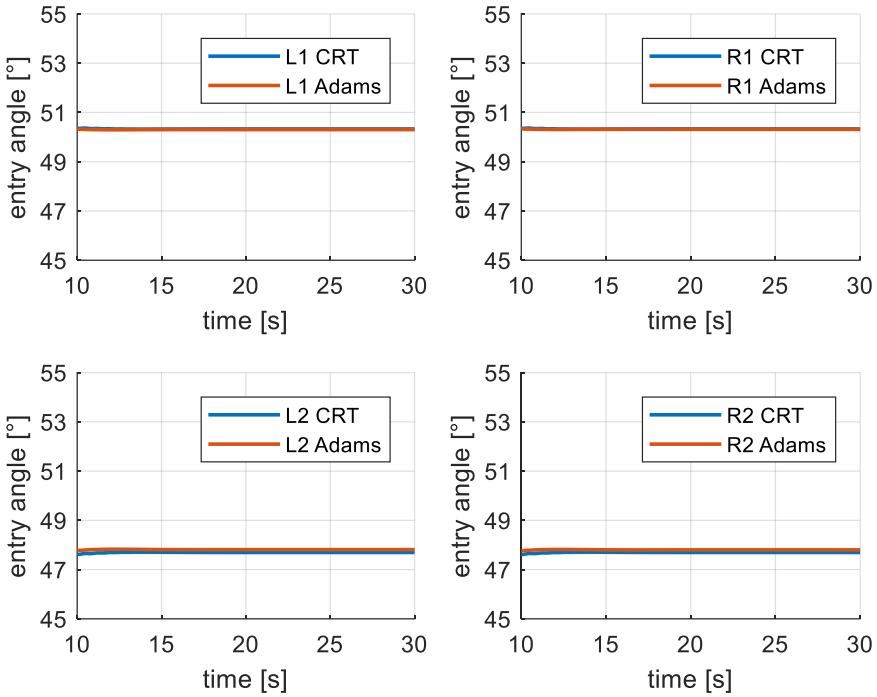

Figure 59: entry angle (Offline - Constant Speed - Dry Sand)

The angle at which the maximum normal stress occurs is considered important for the analysis of the off-road vehicle performance; also, in this case, the values given by the two software are identical (*Fig. 60*).

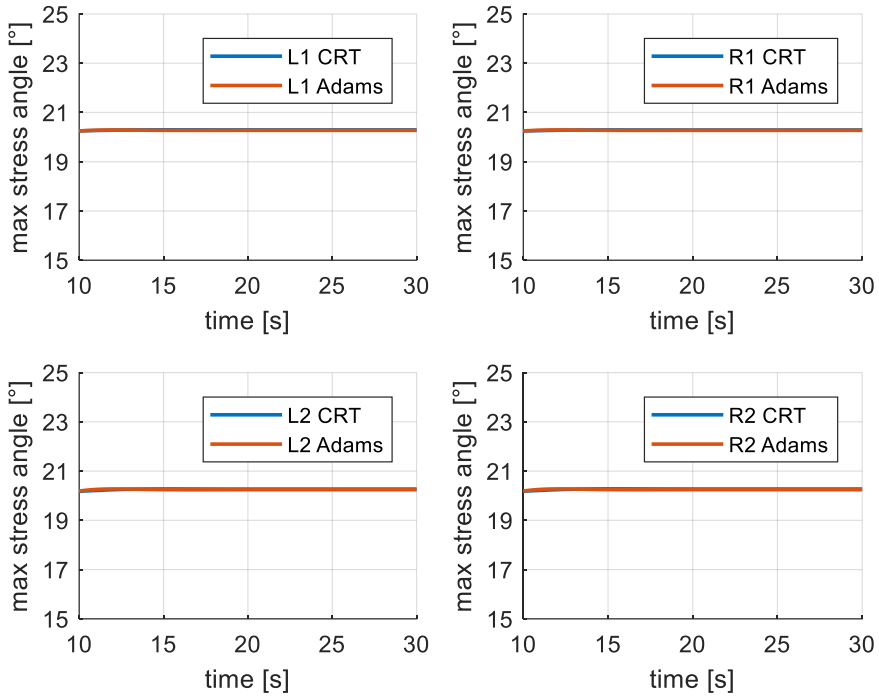

Figure 60: max stress angle (Offline - Constant Speed - Dry Sand)

In *Fig. 61,* it is shown that the vehicle sinks into the soil in the same manner.

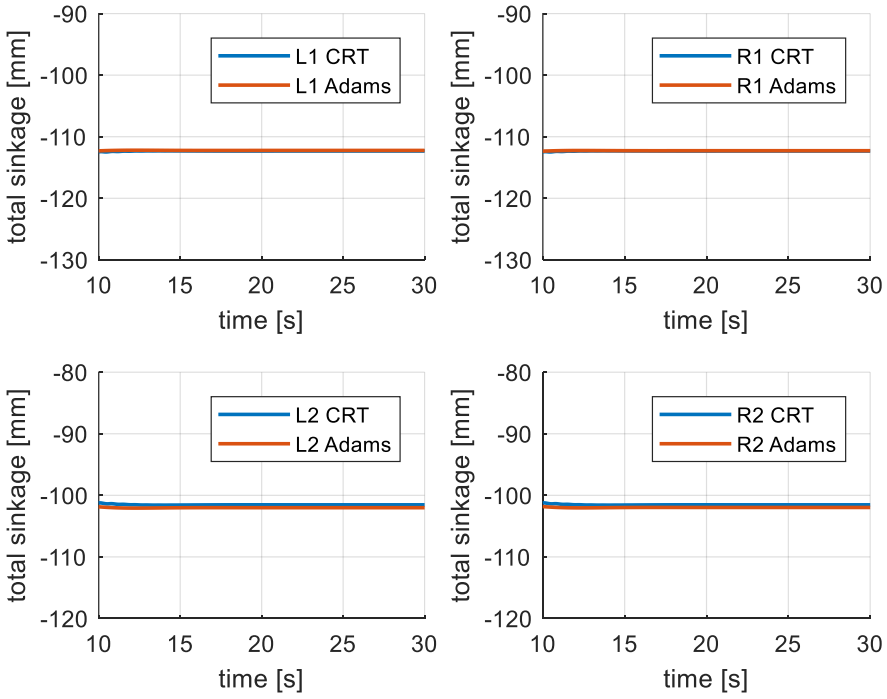

Figure 61: total sinkage (Offline - Constant Speed - Dry Sand)

The normal forces, shown in *Fig. 62*, are slightly different, but the sum of the normal forces at each time step are identical.

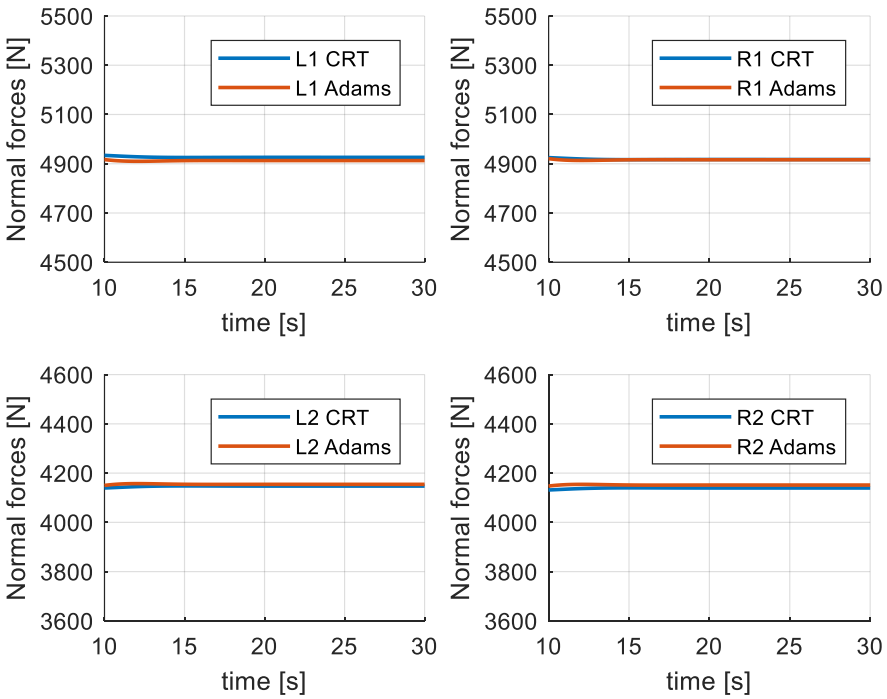

Figure 62: normal forces (Offline - Constant Speed - Dry Sand)

The longitudinal forces (*Fig. 63*) differ more with respect to the other analysed variables: the front wheels differ less than 4 %, while the rear wheels differ 12 % at most. These differences are not excessive for the final goal of this thesis; furthermore, the global trend of all the wheels is identical.

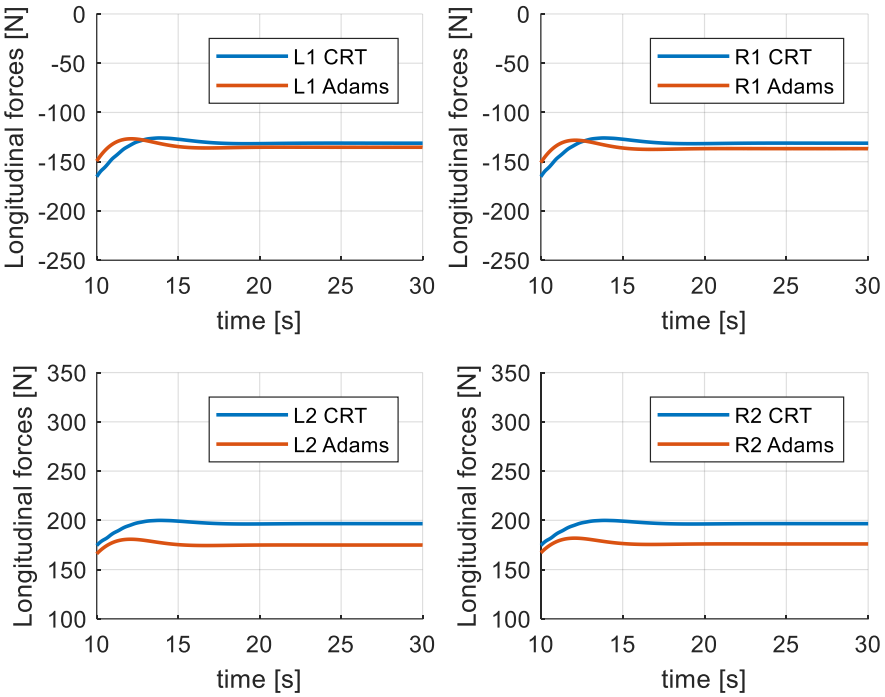

Figure 63: longitudinal forces (Offline - Constant Speed - Dry Sand)

The value of the lateral forces is different because the Adams soft-soil model considers the "bulldozing effect"; however, the trend of the lateral forces is equivalent (*Fig. 64*).

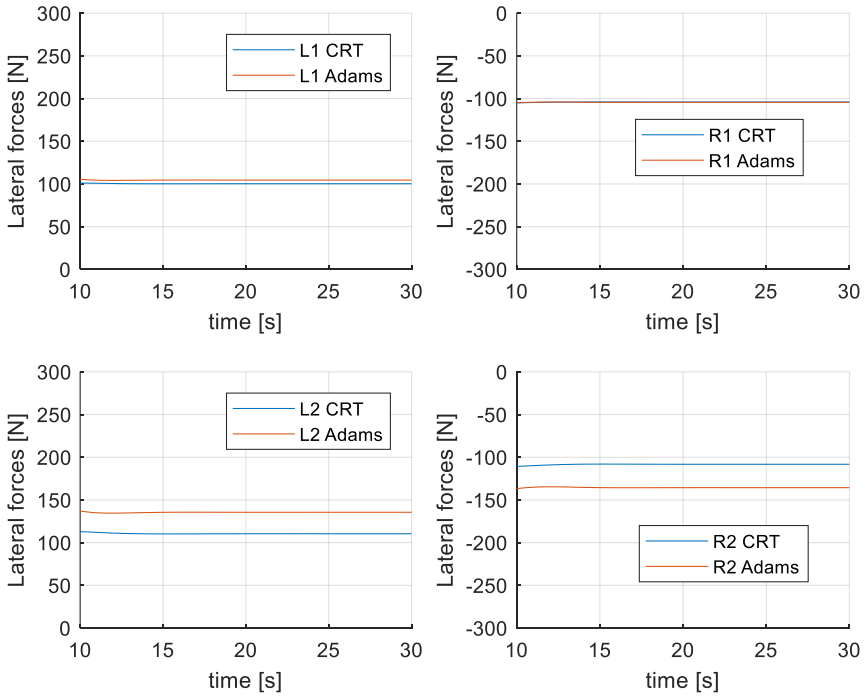

Figure 64: lateral forces (Offline - Constant Speed - Dry Sand)

The value of the drive torque of the off-road model is identical to the Adams/Car simulation (*Fig. 65*).

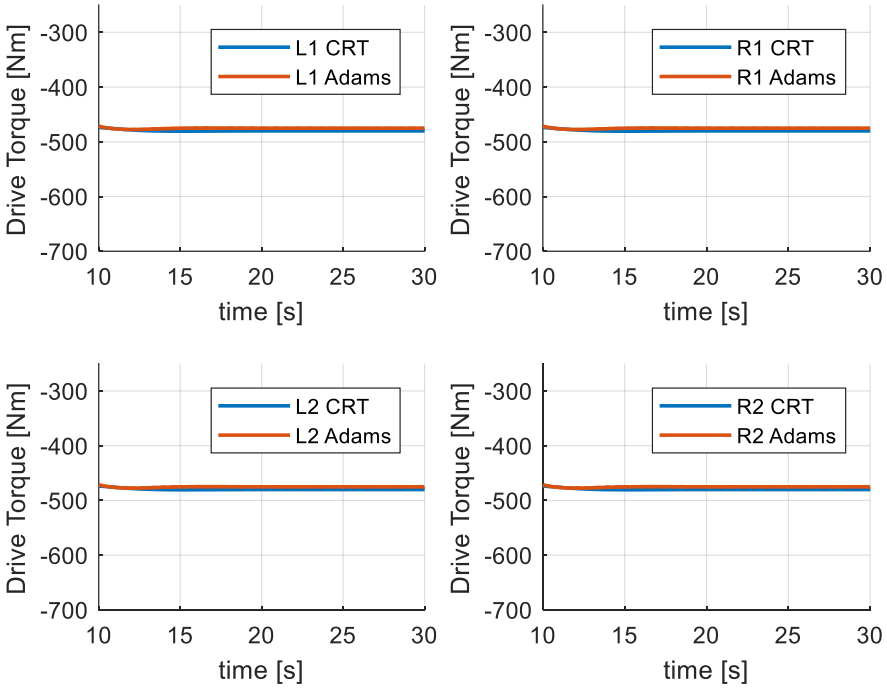

Figure 65: drive torque (Constant Speed - Dry Sand)

8.2.2 Offline Simulation: acceleration – dry sand

The second simulation evaluates the driving manoeuvre at "acceleration" on a "dry sand" (soil data reported in *Tab. 1*).

Based on the following four charts (*Fig. 66-69*), it is evident that both the virtual driver of VI-CarRealTime and the one of Adams/Car carry out almost the same driving manoeuvre:

- speed is almost identical (*Fig. 66*),
- in *Fig. 67*, longitudinal acceleration has a negative spike because the VI-CarRealTime virtual driver releases the throttle for a moment before doing full throttle; in *Fig. 68* is specified the throttle demand;
- the gear does not change during the simulation, in fact in *Fig. 69* the two lines are overlapping.

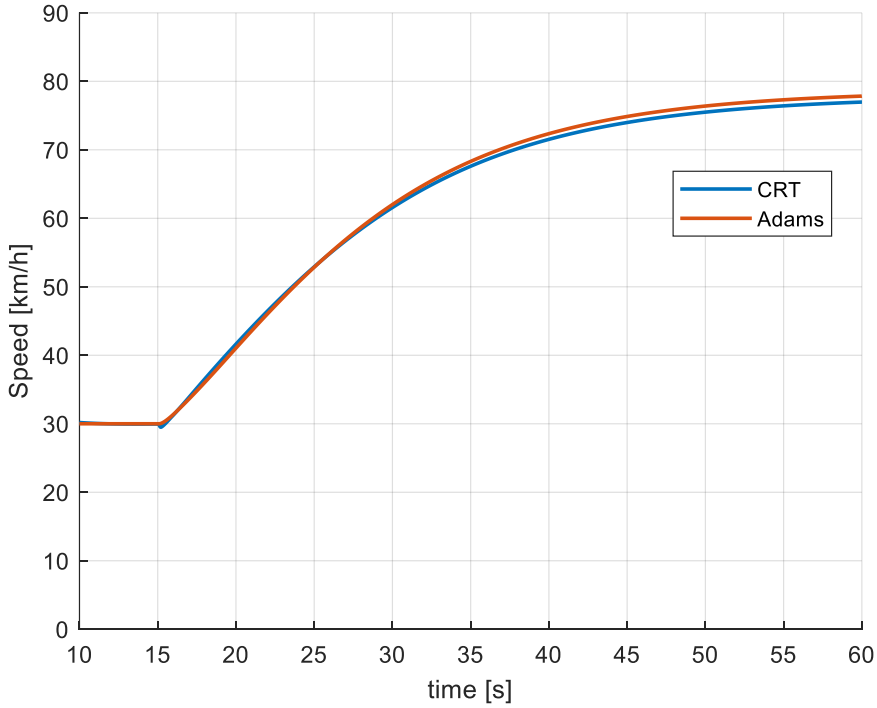

Figure 66: speed (Offline - Acceleration - Dry Sand)

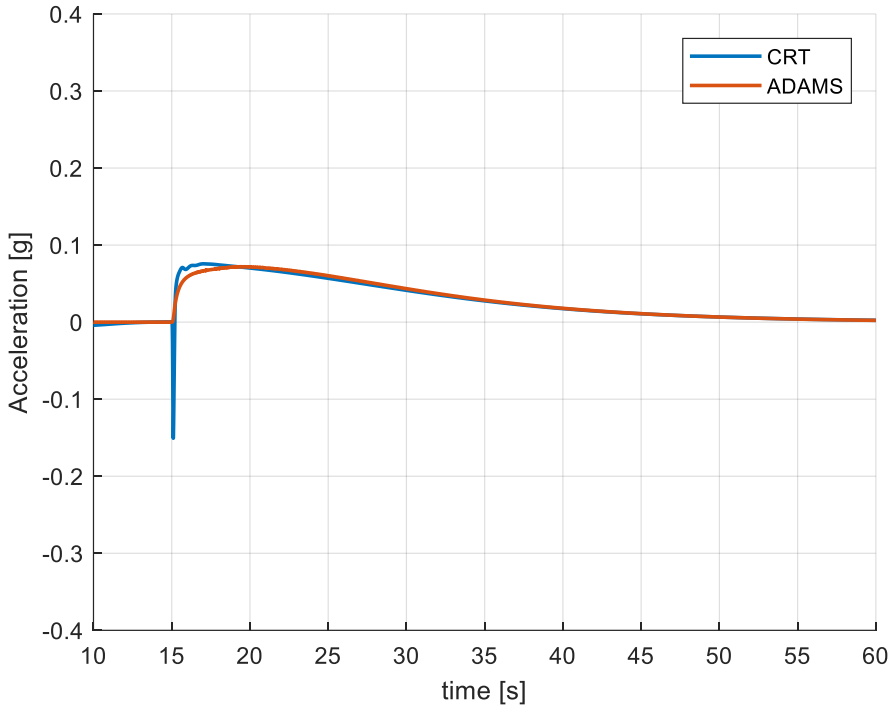

Figure 67: longitudinal acceleration (Offline - Acceleration - Dry Sand)

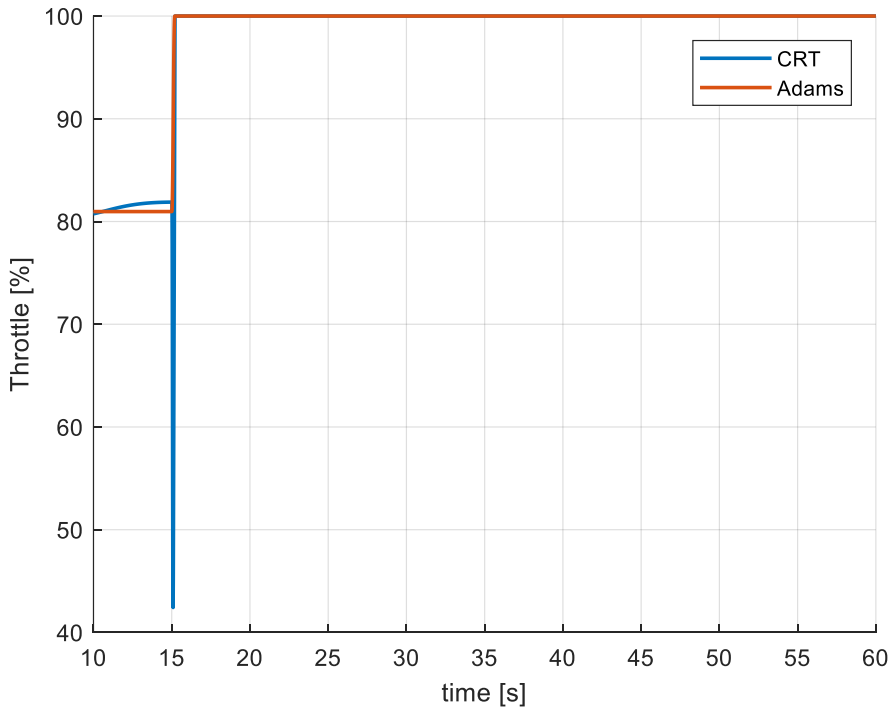

Figure 68: throttle demand (Offline - Acceleration - Dry Sand)

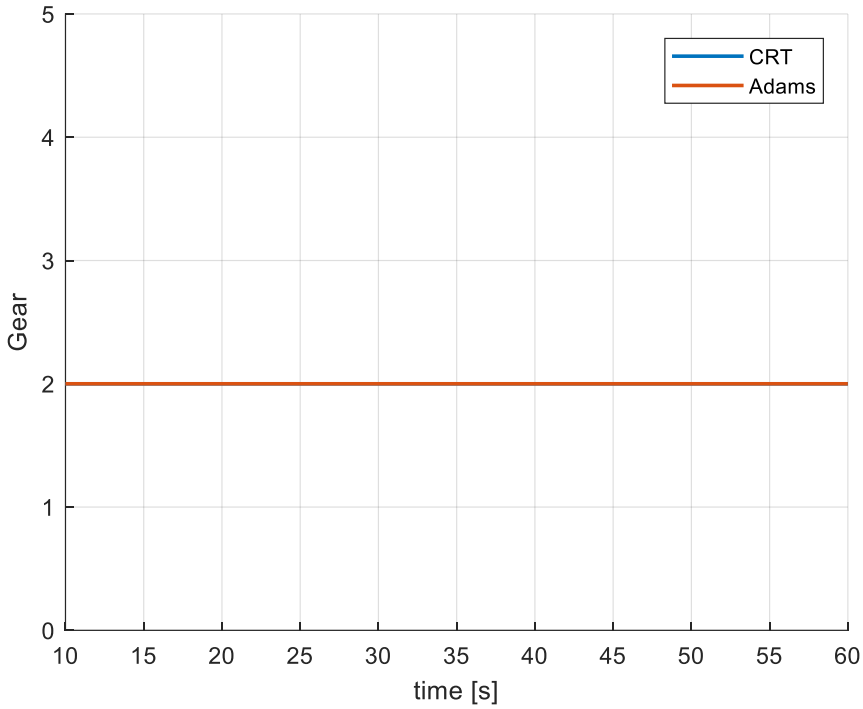

Figure 69: gear demand (Offline - Acceleration - Dry Sand)

In *Fig. 70*, the longitudinal slip has the same trend between the two models; moreover, the longitudinal slip of the rear wheels measures the greatest variance, such as in the first simulation.

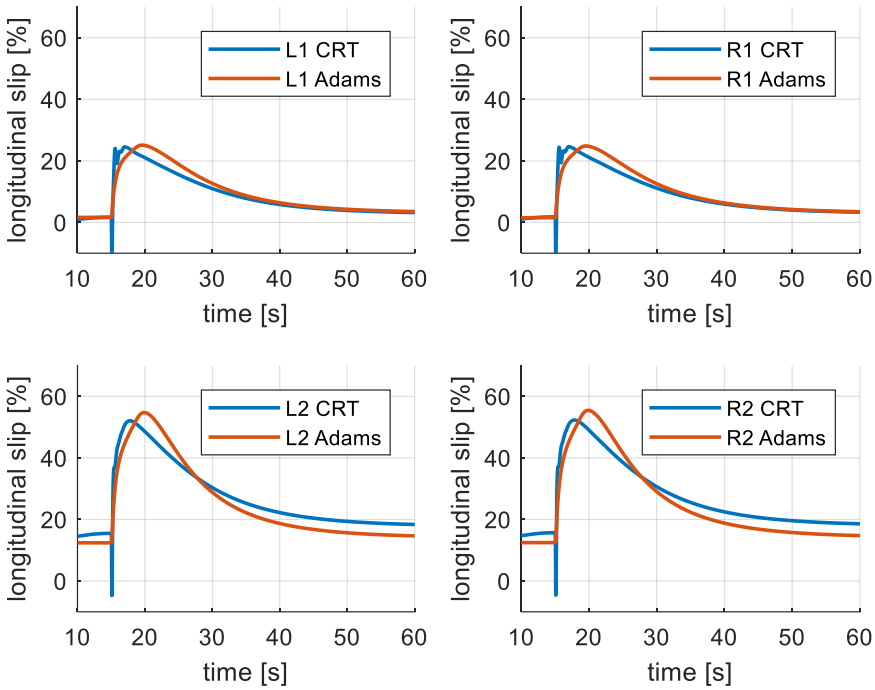

Figure 70: longitudinal slip (Offline - Acceleration - Dry Sand)

Both the entry angle (*Fig. 71*) and the max stress angle (*Fig. 72*) are almost identical to the ones given by Adams/Car. At near the 15s, the driver accelerates causing a load transfer that results in the oscillation of the normal forces (see *Fig. 74*) and therefore of the entry angle.

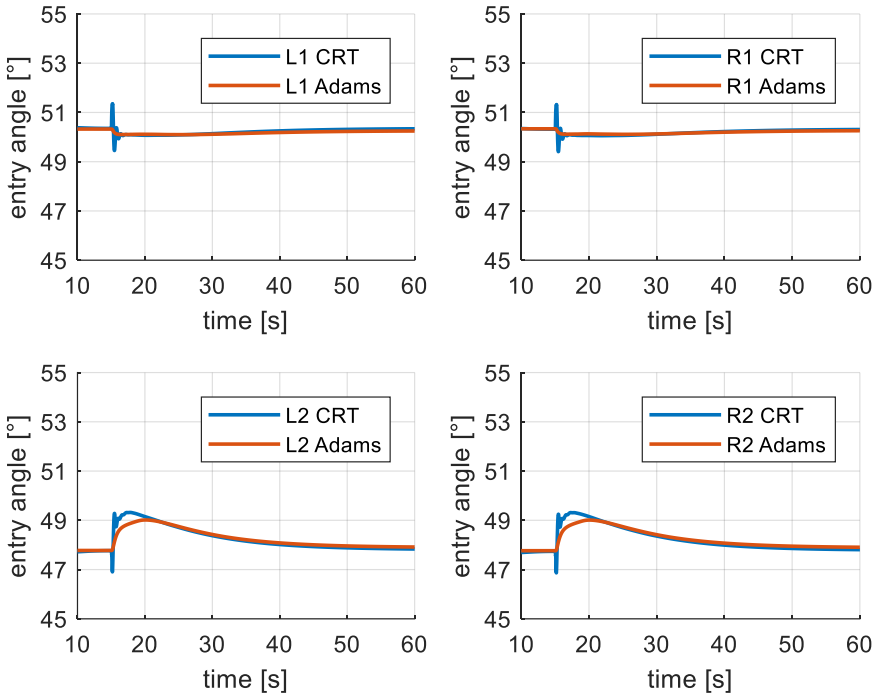

Figure 71: entry angle (Offline - Acceleration - Dry Sand)

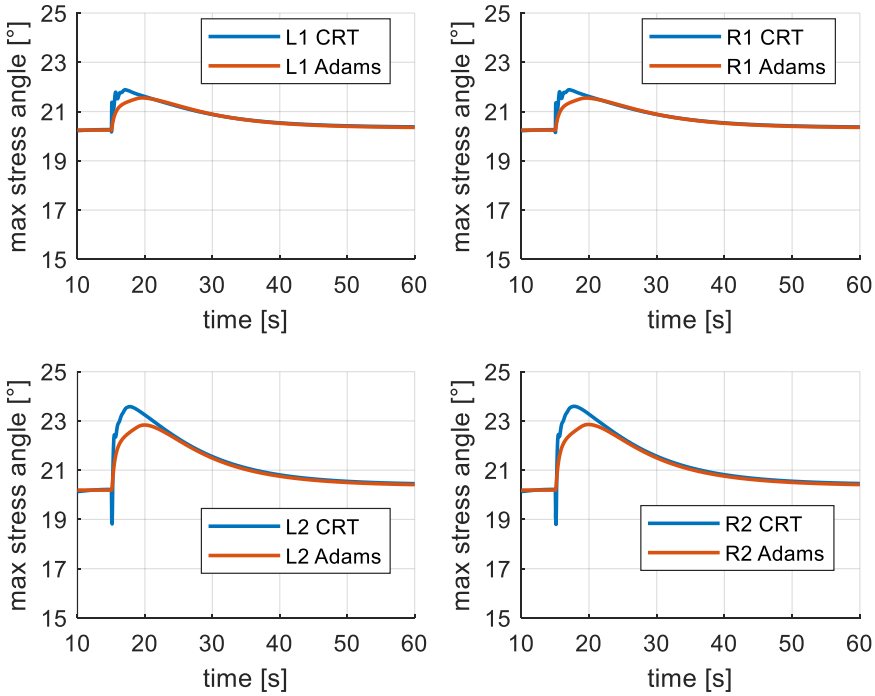

Figure 72: max stress angle (Offline - Acceleration - Dry Sand)

Fig. 73 shows that the vehicle sinks into the soil in almost the same manner.

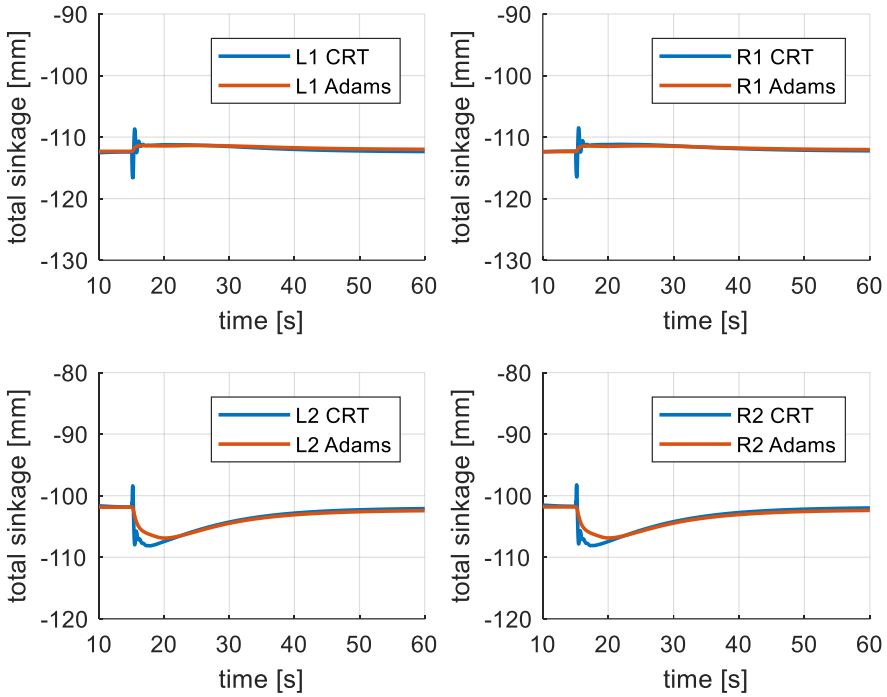

Figure 73: sinkage (Offline - Acceleration - Dry Sand)

The normal forces, shown in *Fig. 74*, are slightly different, but the sum of the normal forces at any time step are identical. It is possible to observe that the Adams/Car model has no oscillations, this difference is due to different solvers used by the software and not because of the model itself. Moreover, *Fig. 74* shows the load transfer from front axle to rear axle due to the longitudinal acceleration.

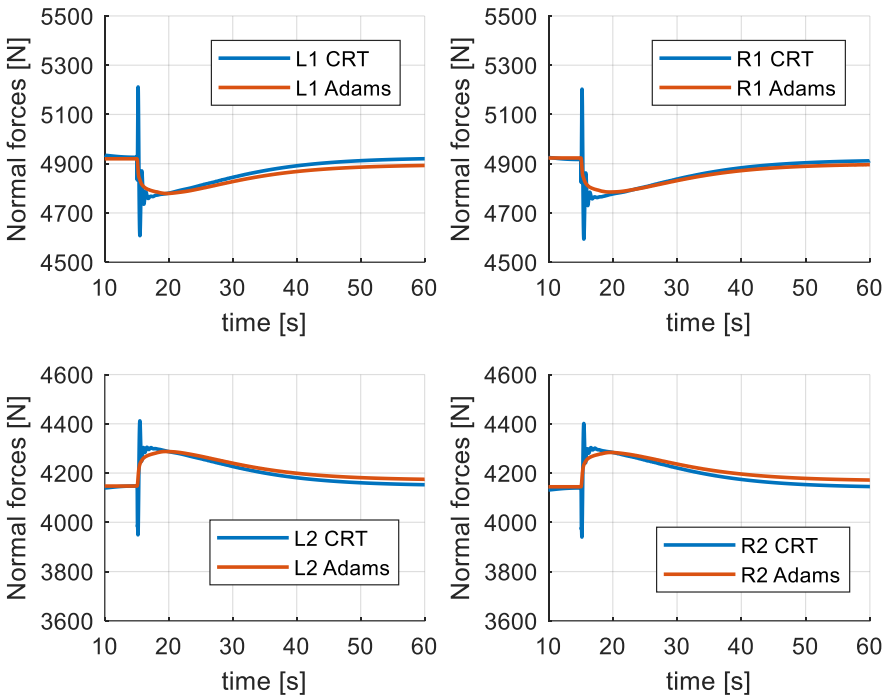

Figure 74: normal forces (Offline - Acceleration - Dry Sand)

In *Fig. 75*, the longitudinal forces have the same trend, and the values are almost the same too. Around the 15s, their behaviour is slightly different, but it is influenced by the normal force oscillations, the longitudinal slip, and entry angle.

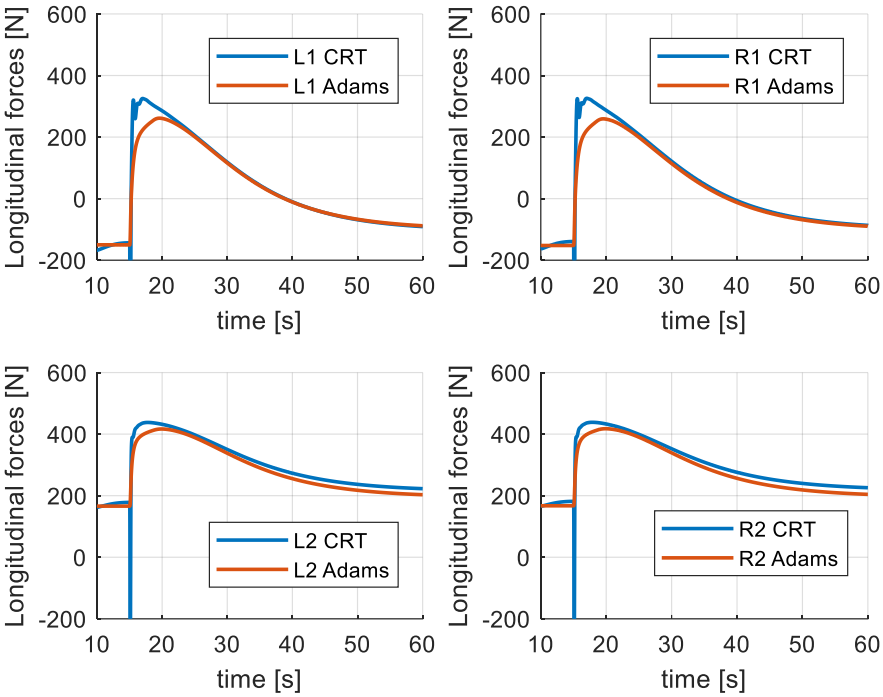

Figure 75: longitudinal forces (Offline - Acceleration - Dry Sand)

The value of the lateral forces is different because the Adams soft-soil model considers the "bulldozing effect"; however, the trend of the lateral forces is equivalent (*Fig. 76*).

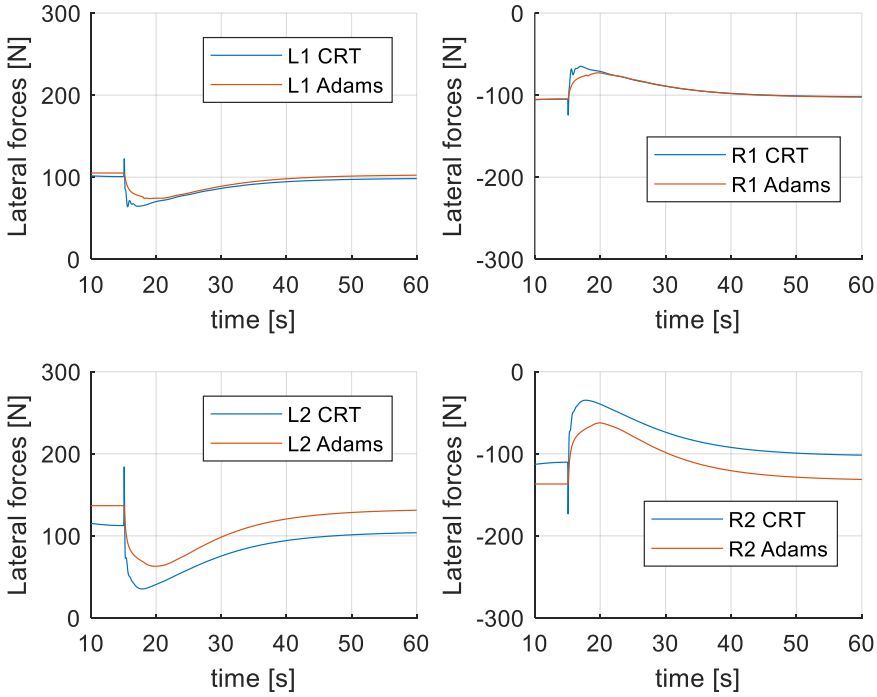

Figure 76: lateral forces (Offline - Acceleration - Dry Sand)

In *Fig. 77*, the drive torque is almost identical; the spike of the CRT model is due to the accelerator release done by the virtual driver.

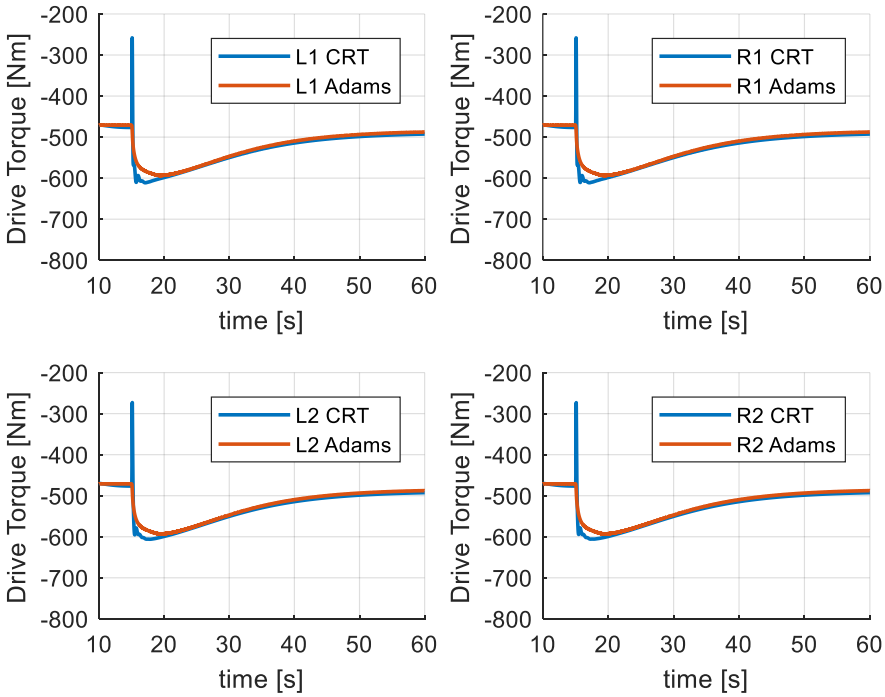

Figure 77: drive torque (Offline - Acceleration - Dry Sand)

8.2.3 Conclusion of offline simulations

Considering all the six performed simulations, it is possible to confirm the accuracy of the developed off-road model because it is well aligned to the results given by the Adams soft soil model.

Since the obtained results, it is possible to proceed to the implementation of the off-road model on dynamic driving simulator and then to analyse the new results.

9 Dynamic Driving Simulator

The term "simulation" indicates an imitation of some real thing, while the term "motion simulation" refers to all about perception: based on this, driving simulation is a type of motion simulation [17].

Driving simulators are widely used by the automotive industry in research and development activities with a positive impact on time and cost, allowing the automotive industry to save money for costly prototypes and road tests.

Depending on the application, there are various driving simulators, starting from a static flat screen with simple steering wheel and pedals to a large dynamic simulator with perfected use of technologies to reflect a virtual world that involves motion systems as well as auditory, and visual environment simulation [18].

During this thesis, it has been used the professional dynamic driving simulator of the company "Danisi Engineering S.r.l." (*Fig. 78*).

The features of the simulator are: 9 degrees of freedom motion platform, low latency (about 15ms from driver action to motion), frequencies up to 50 Hz, large dynamic range with 2.5 g planar and 3.5 g vertical accelerations, on top of large payload to support representative cockpits.

The dynamic driving simulator is composed of a base on which a hexapod, holding up the cockpit, is installed; the base is equipped with an air-bearing system, the hexapod has six electromagnet linear actuators, and the cockpit is derived from a real car, keeping also the actual interiors, steering wheel, etc.

The driver manoeuvres the simulated vehicle like in a real car by the steering wheel, brake and acceleration pedal; moreover, to increase the feeling of reality, the driver commands have a feedback unit to obtain real feel of steering wheel, while for the brake pedal there is a real brake system.

The motion of the simulator is based on an algorithm which aims to give the feeling of driving a real car to the driver. The process of converting the real physical motion of a car into motion simulator inputs is named "motion cueing"; the motion system is controlled by a dedicated software.

Due to the limited space in which the motion has to be represented, the longitudinal motion, which can be very long for a real vehicle, cannot be reproduced without trade-offs. To overcome this limit, through a procedure called "tilt coordination", a continuous longitudinal acceleration or deceleration are represented by introducing a tilting of the cockpit with a rotational acceleration level below the human perception thresholds. Therefore, a component of the gravitational force acts in a longitudinal direction of the vehicle and it simulates longitudinal acceleration or deceleration:

because of a consistent motion illusion given by visual system, the driver in the simulator does not perceive the trick [18].

To reproduce the environment in which the vehicle model is tested, a 7-meter diameter screen and 3 projectors are installed around the cockpit; moreover, to increase the realism of the simulation, a professional sound system is used.

The driver feels the sense of speed through the speed of images and the sound reproduced by the acoustic system.

The image system allows the driver to feel the impression of speed and continuous movement; furthermore, the sound system reproduces the engine and driving noise, representing engine power, engine speed, and driving speed.

Figure 78: dynamic driving simulator (Danisi Engineering S.r.l.)

9.1 SIMulation Workbench

It is necessary to connect different systems or models, that must be run in real-time. Using the software Concurrent's SIMulation Workbench (SimWB), it is possible to connect and to control these following subsystems:

- vehicle model;
- simulator platform;
- motion cueing;
- graphic;
- acoustic systems;
- accessories;
- custom model (such as the developed off-road model).

SimWB is a complete modelling environment for developing and executing in real-time both hardware-in-the-loop and man-in-the-loop simulations [19] .

With SimWB, custom models and other processes can be targeted to different system core and I/O buses for parallel execution. SimWB allows complex simulations to be executed on a single multi-processor platform; furthermore, the simulation loops can run at faster frame rates because SimWB provides fast, direct shared memory access to all parameters and signals needed by simulation [19].

9.2 Off-Road model implementation on Dynamic Simulator

The developed off-road model has been implemented on dynamic driving simulator.

To prepare the off-road model it has been used the software Concurrent's SIMulation Workbench, which allows to easily import models from MATLAB/Simulink without the necessity of inserting hardware-specific S-function blocks.

In fact, SimWB has a specific tool integrated within Simulink environment, SimWB toolkit, that contains the necessary Simulink libraries and interfaces to create an executable suitable for the Concurrent environment.

Using this tool, both inputs and outputs of the vehicle model block have been substituted in RTDB blocks, because the SimWB real-time core is organised around a very fast memory resident database (RTDB) [19].

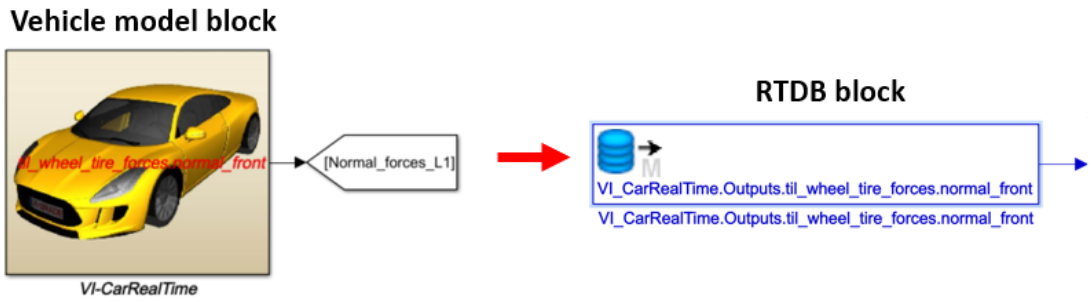

Figure 79: example of RTDB block

Using RTDB blocks, all outputs of the off-road model have been added in the real-time database to post-process them.

All constants of the off-road model, also those included the lookup tables, are initialised using a created script MATLAB. After this operation, the off-road is built and it is compiled by means of SimWB toolkit.

Subsequently, the new off-road model is uploaded on the system and it is ready to run on the dynamic driving simulator using SimWB. It is also necessary to create a specific test that includes all the executables necessary to run the simulation (cueing, vehicle model, simulator, road scenario, etc.)

10 Analysis of Dynamic Driving Simulator Results

The off-road model, prepared according to the above-mentioned procedure, has been tested by a professional driver.

The driver carried out two types of tests on the simulator:

- a subjective evaluation of the off-road model, driving the car on a proving ground without any restriction;
- an objective test, repeating the same driving manoeuvres performed by the virtual driver during offline simulations.

10.1 Driver's feedback

The driver's feedback represents a qualitative and subjective analysis.

During the first session carried out on the simulator, even if the driver had been aware to drive on off-road soil, he would not have known that the test was performed on three different types of off-road soil.

After tests, the driver provided his feedback, confirming to get the feeling of a realistic off-road driving; furthermore, he was able to identify the three different types of soil according to the sequence on which they were simulated. Especially the feeling given by "dry sand" soil was judged very realistic, both in longitudinal and lateral direction; it was immediately recognised as a sand soil by the driver.

10.2 Real-Time Simulation results

The second session of tests allows to obtain results comparable to those obtained by the offline simulation; therefore, by means of the comparison, it is possible to make a quantitative and objective analysis.

Contrary to the virtual driver, the manoeuvres carried out by the driver are affected by the human error: indeed, because of this limit, in the following charts, the results of simulator sessions show some differences with respect to offline results, due to driver inputs, as if it were an experimental acquisition.

In the following paragraph, the simulator outcomes are compared to those obtained by the offline simulation of the off-road model, selecting the most important variables for off-road driving.

Having simulated two driving manoeuvres for each type of terrain, six simulations are run: for the sake of clarity, only the simulations on "dry sand" are reported in the following paragraphs, while the other simulations are available in *Appendix C*.

In each chart, the name "CRT" indicates the results provided by the co-simulation of the off-road model, while the name "DIM" labels the results provided by the dynamic driving simulator.

10.2.1 Real-Time Simulation: constant speed – dry sand

The results of the "constant speed" manoeuvre (see *section 8.1*) on dry sand, carried out on the simulator, are reported here below.

The slightly difference between offline results and simulator outcomes is due to the human error affecting the repetition of the manoeuvre performed by the driver.

In this test, being the car at a higher speed in the initial phase, the driver has to reduce it up to 50 km/h and to maintain it constant; therefore, some outcomes are influenced by the initial condition.

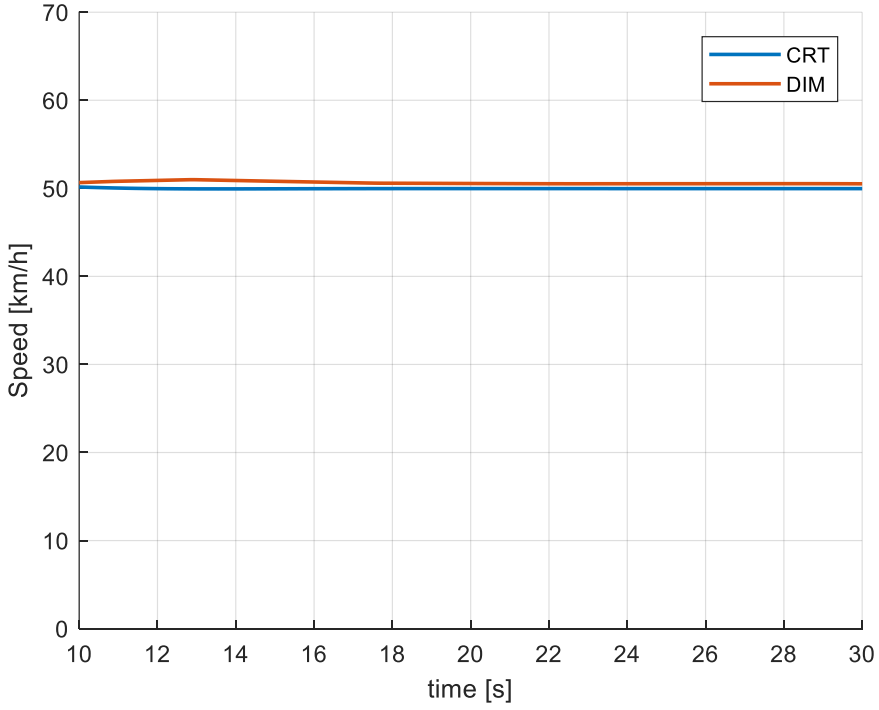

Figure 80: speed (Real-Time - Constant Speed - Dry Sand)

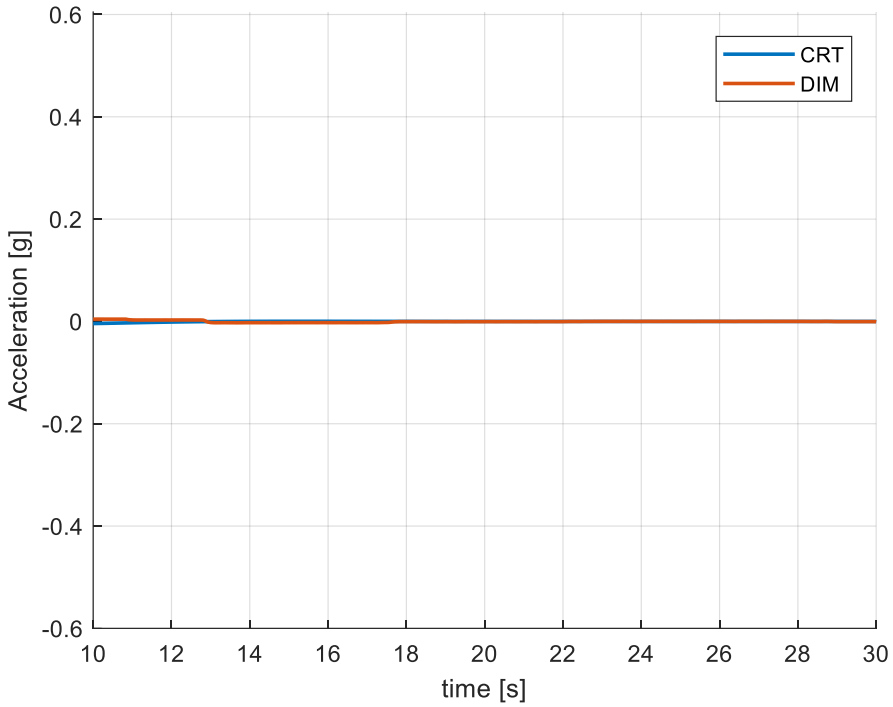

Figure 81: longitudinal acceleration (Real-Time - Constant Speed - Dry Sand)

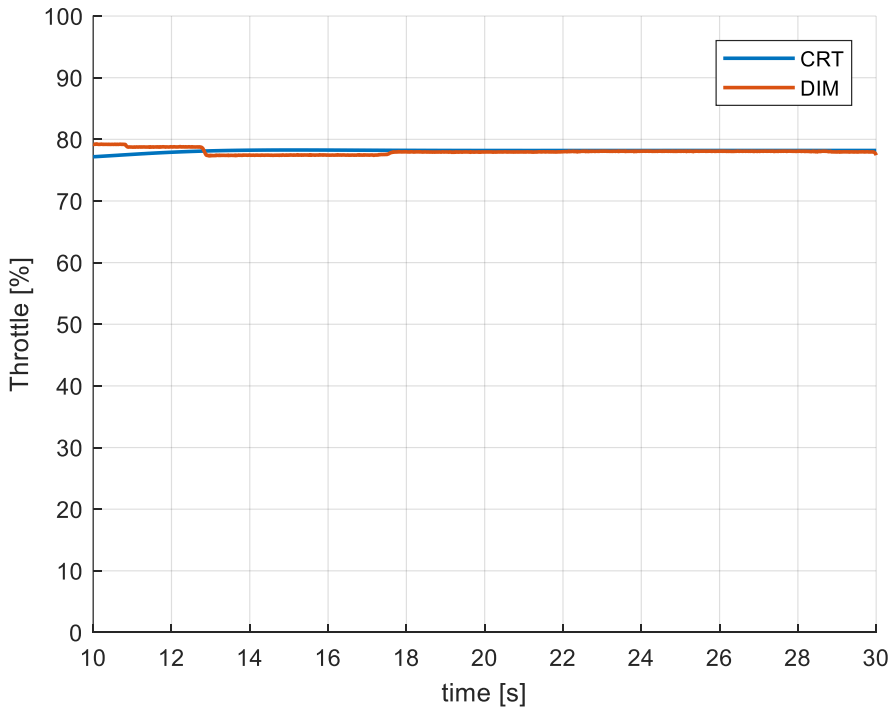

Figure 82: throttle demand (Real-Time - Constant Speed - Dry Sand)

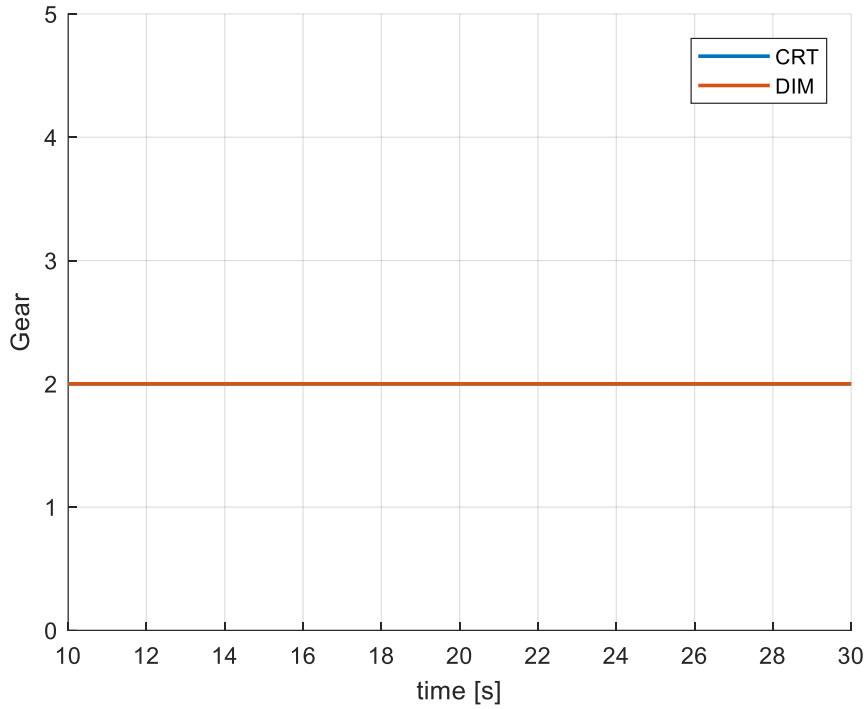

Figure 83: gear demand (Real-Time - Constant Speed - Dry Sand)

The longitudinal slip (*Fig. 84*) is influenced by the initial condition of the test: indeed, the line, which represents the simulator outcomes (DIM), starts from a higher value with respect to the offline simulation.

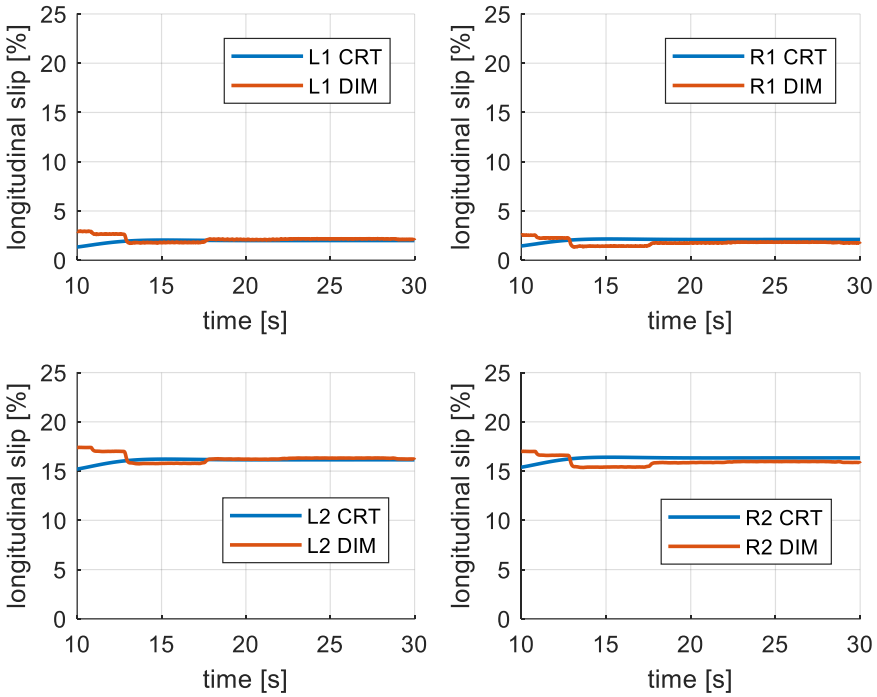

Figure 84: longitudinal slip (Real-Time - Constant Speed - Dry Sand)

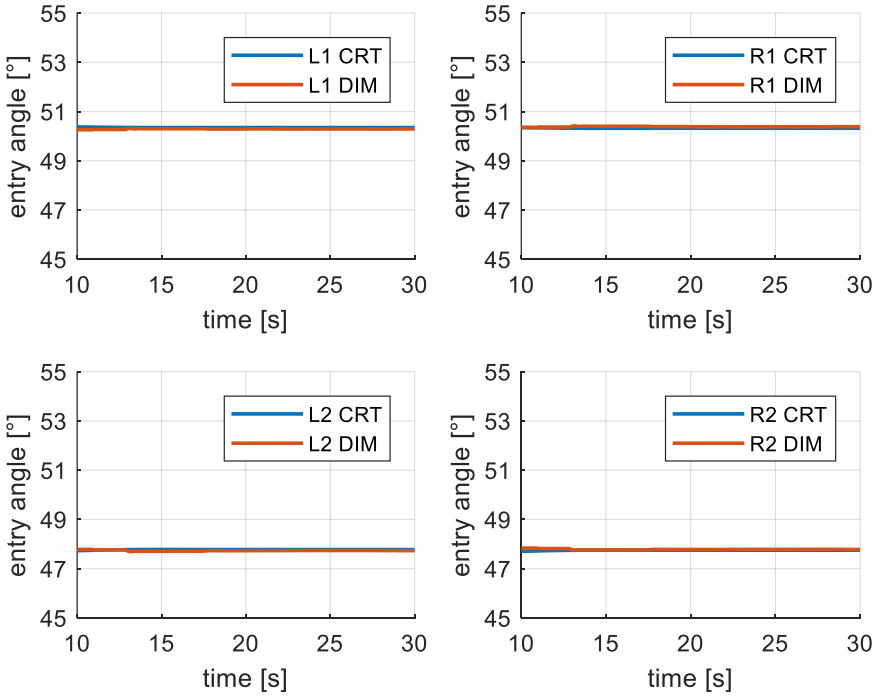

Figure 85: entry angle (Real-Time - Constant Speed - Dry Sand)

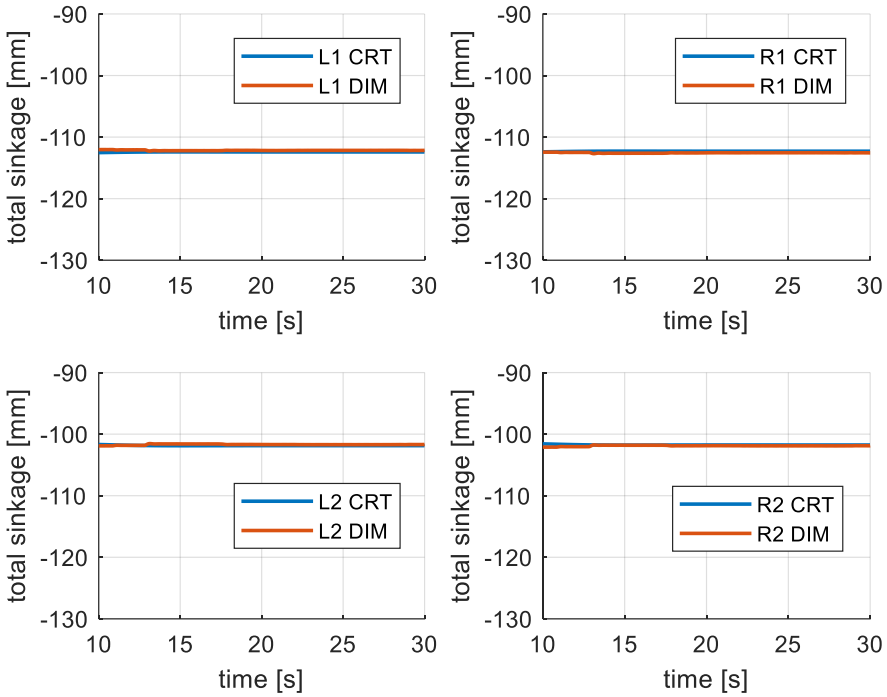

Figure 86: sinkage (Real-Time - Constant Speed - Dry Sand)

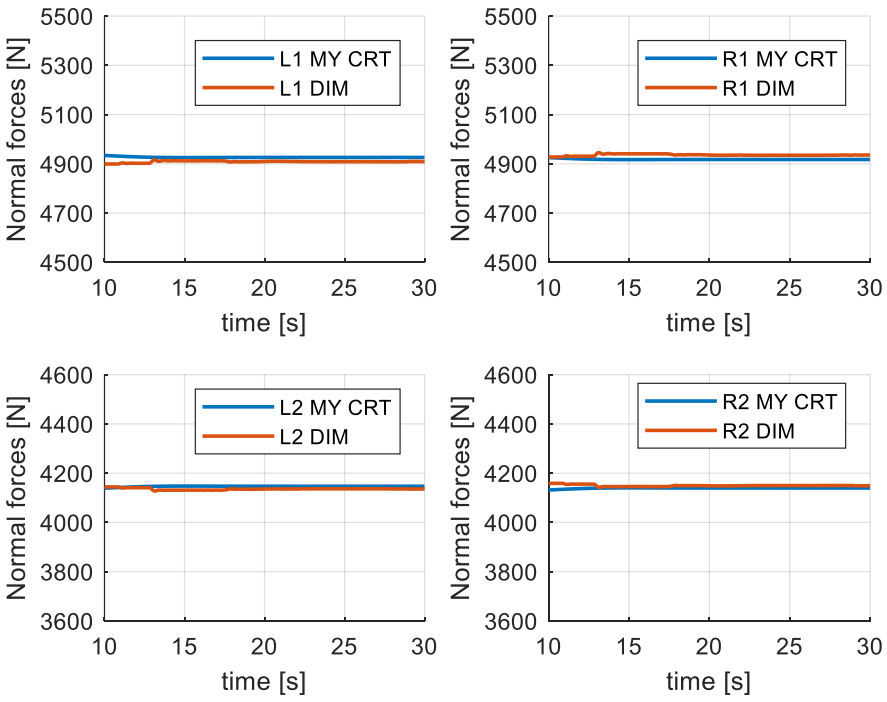

Figure 87: normal forces (Real-Time - Constant Speed - Dry Sand)

The longitudinal forces (*Fig. 88*) have the same trend of the longitudinal slip: the initial condition affects both them in the same way.

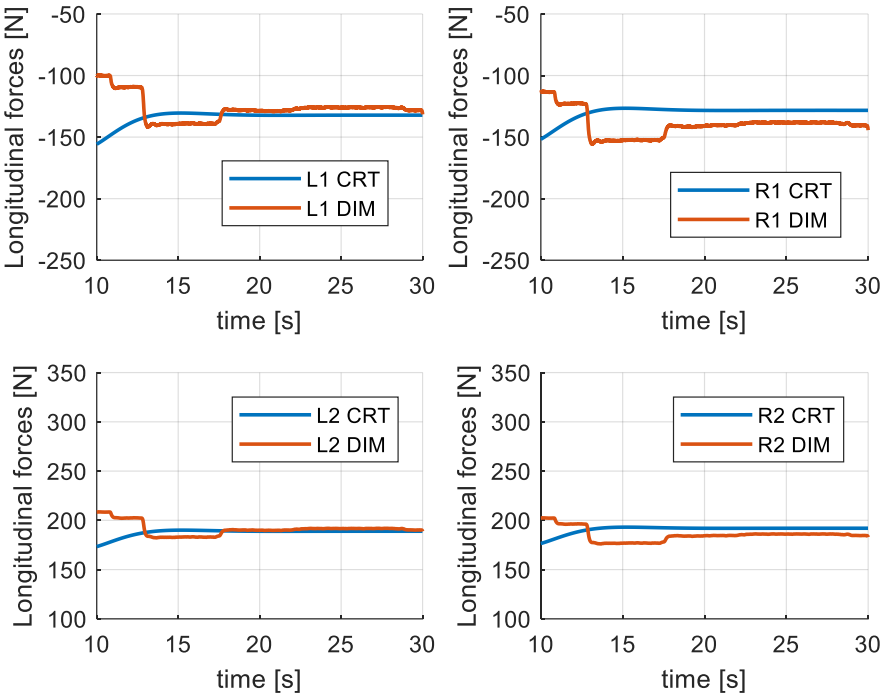

Figure 88: longitudinal forces (Real-Time - Constant Speed - Dry Sand)

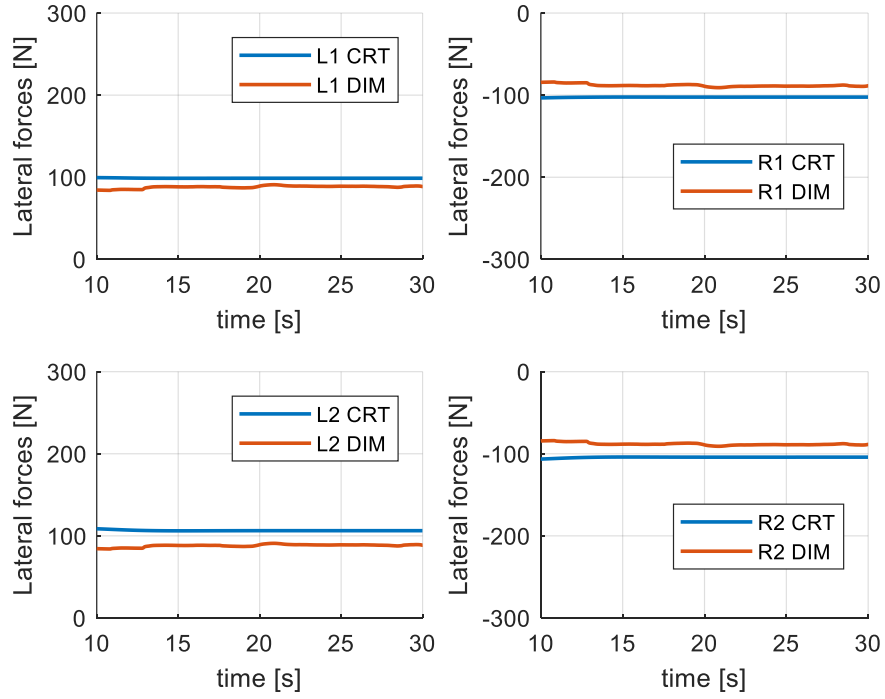

Figure 89: lateral forces (Real-Time - Constant Speed - Dry Sand)

Also, the drive torque is influenced by the initial condition: thus, considering the absolute value of the drive torque, in this case the outcomes given by the simulator start at a higher value with respect to the offline simulation.

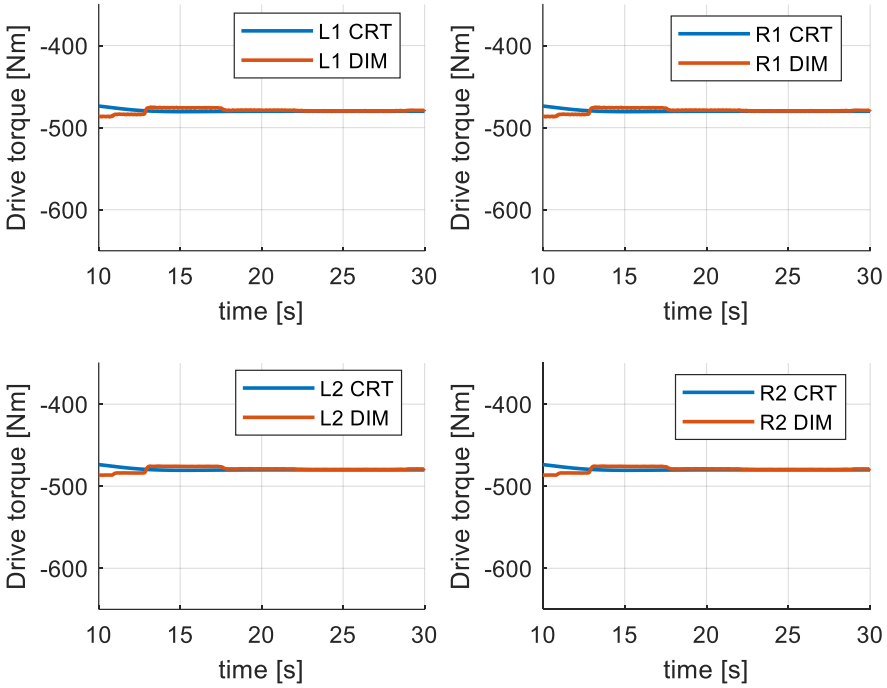

Figure 90. drive torque (Real-Time - Constant Speed - Dry Sand)

10.2.2 Real-Time Simulation: acceleration – dry sand

The results of the "acceleration" manoeuvre (see *section 8.1*) on dry sand, carried out on the simulator, are reported here below.

Contrary to the plot reported in *section 8.2.2*, the following charts show data starting from the moment at which the manoeuvre records the full throttle, without considering the initial constant speed.

On the simulator, for a technical issue, the value of the throttle demand (*Fig. 93*) is limited at 98%: notwithstanding this, it does not affect the quality of results.

Considering the following charts, it is possible to confirm that the off-road model faithfully follows the outcomes given by the offline simulation.

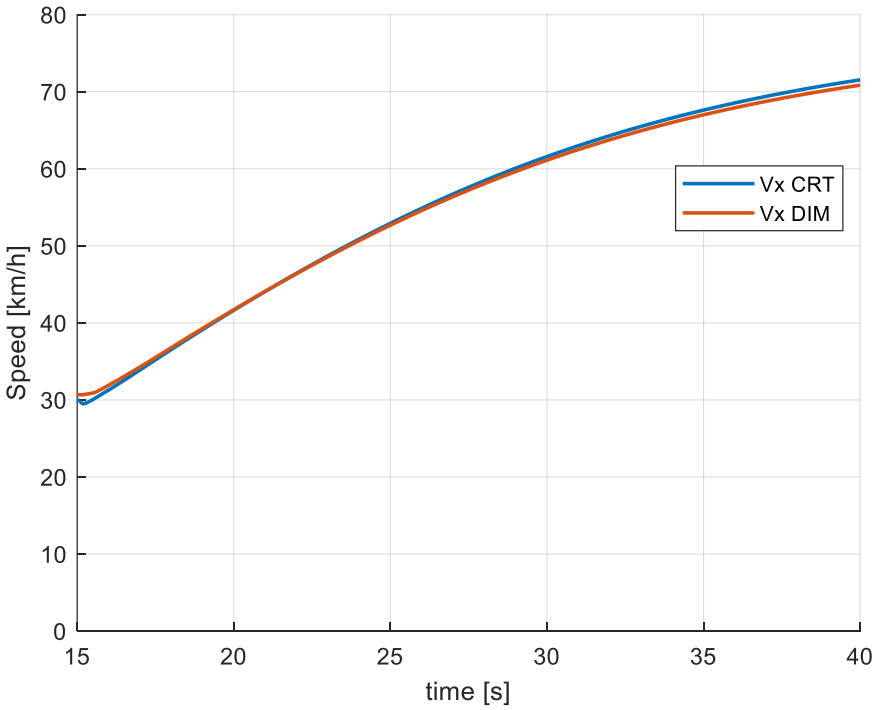

Figure 91: speed (Real-Time - Acceleration - Dry Sand)

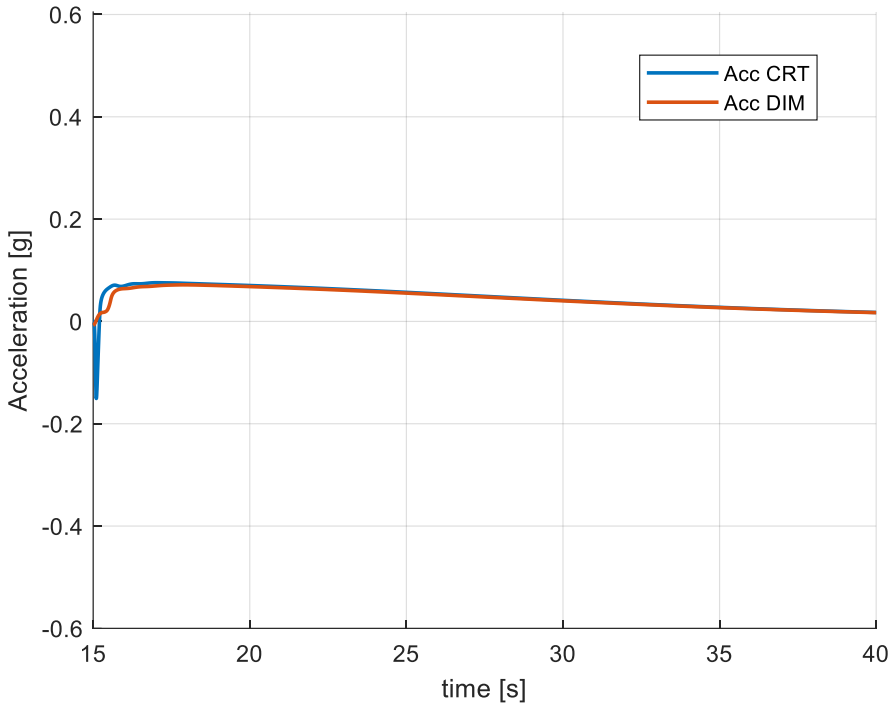

Figure 92: longitudinal acceleration (Real-Time - Acceleration - Dry Sand)

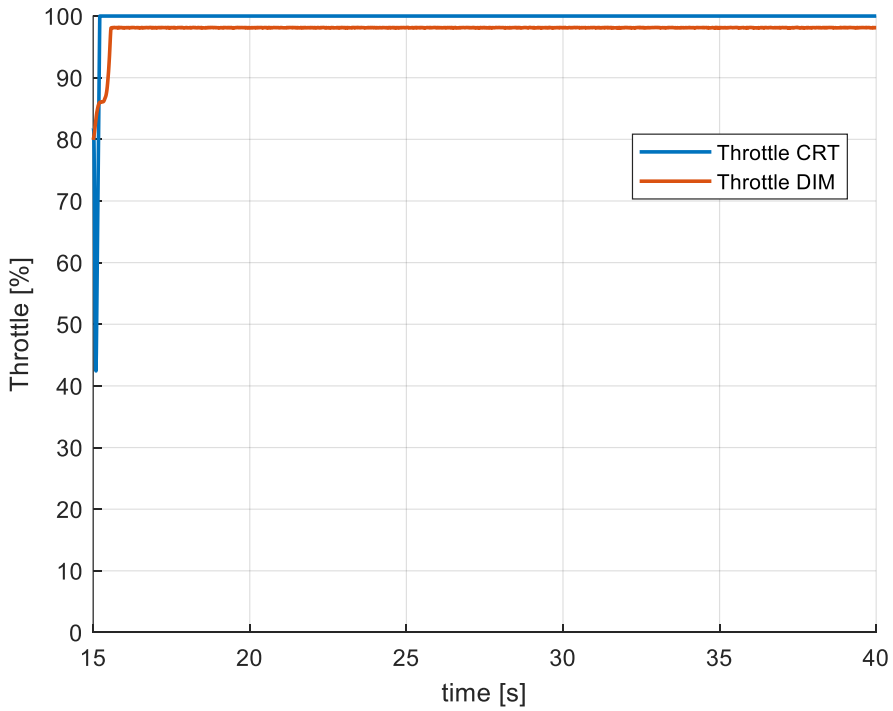

Figure 93: throttle demand (Real-Time - Acceleration - Dry Sand)

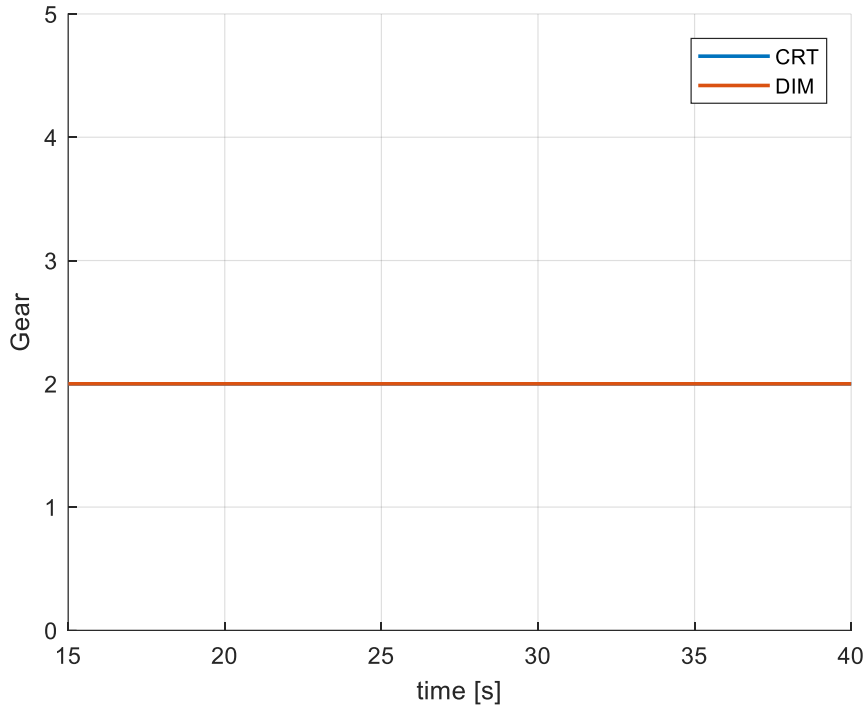

Figure 94: gear demand (Real-Time - Acceleration - Dry Sand)

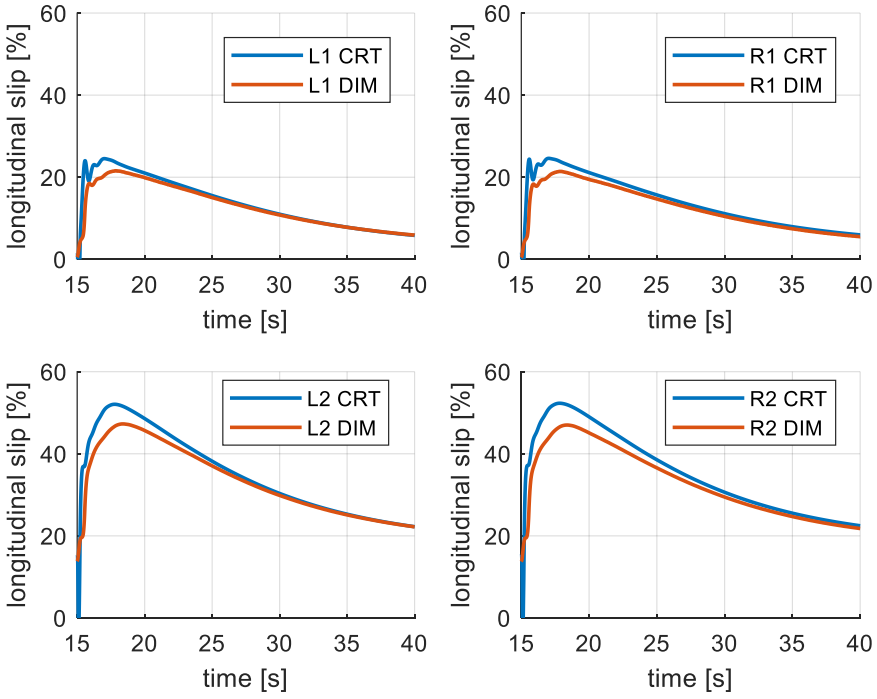

Figure 95: longitudinal slip (Real-Time - Acceleration - Dry Sand)

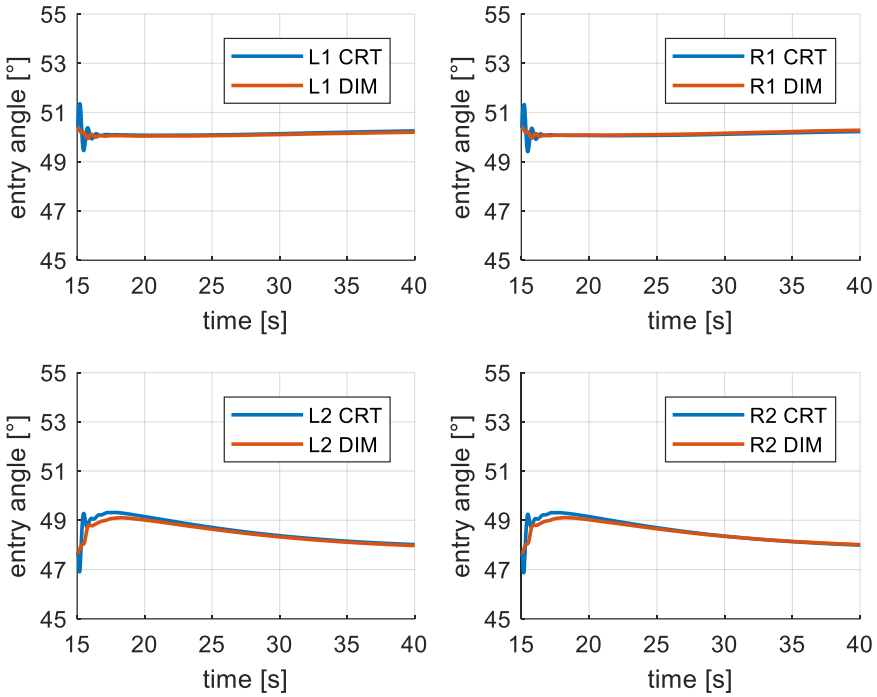

Figure 96: entry angle (Real-Time - Acceleration - Dry Sand)

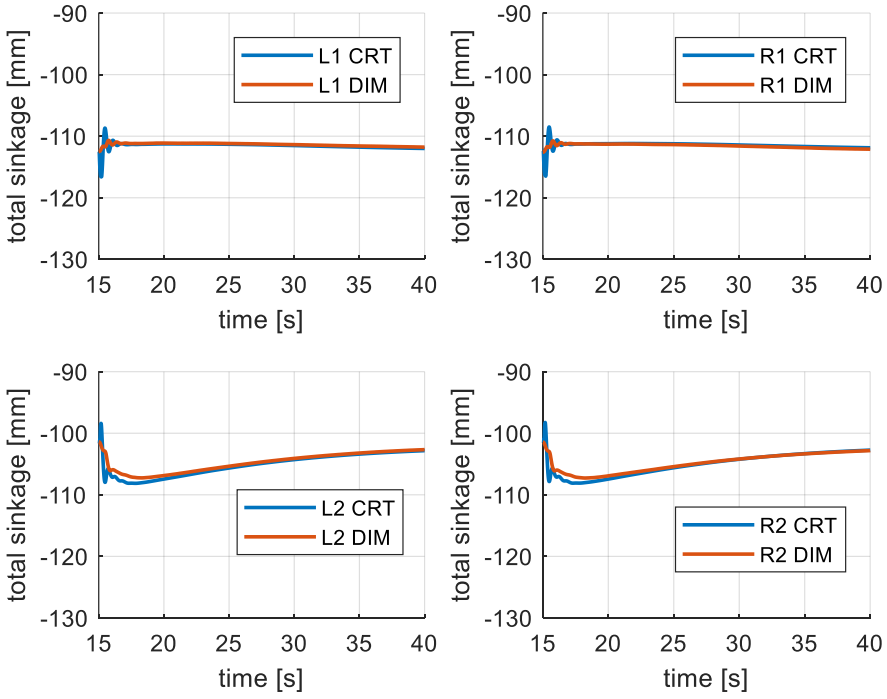

Figure 97: sinkage (Real-Time - Acceleration - Dry Sand)

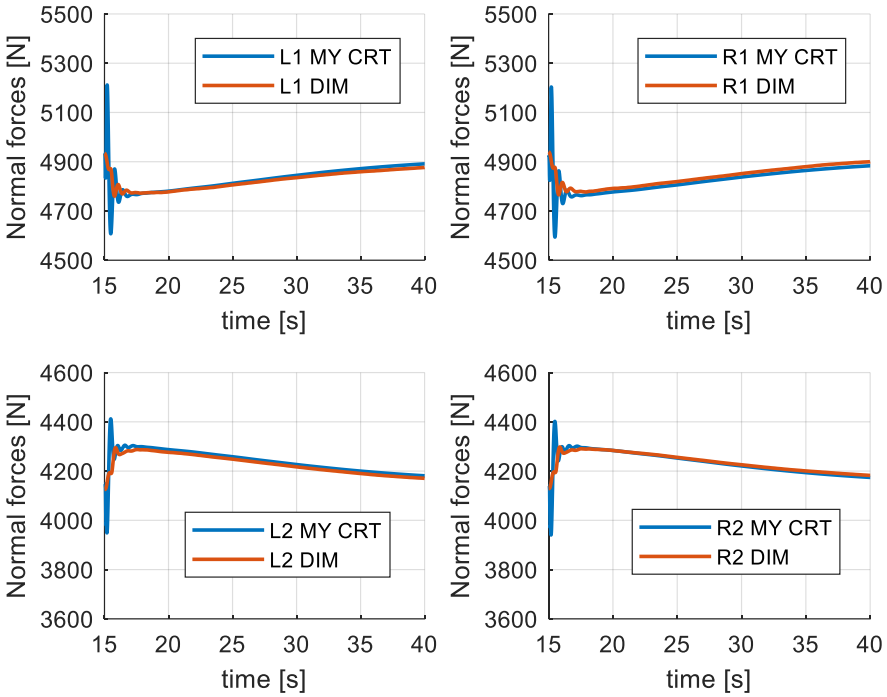

Figure 98: normal forces (Real-Time - Acceleration - Dry Sand)

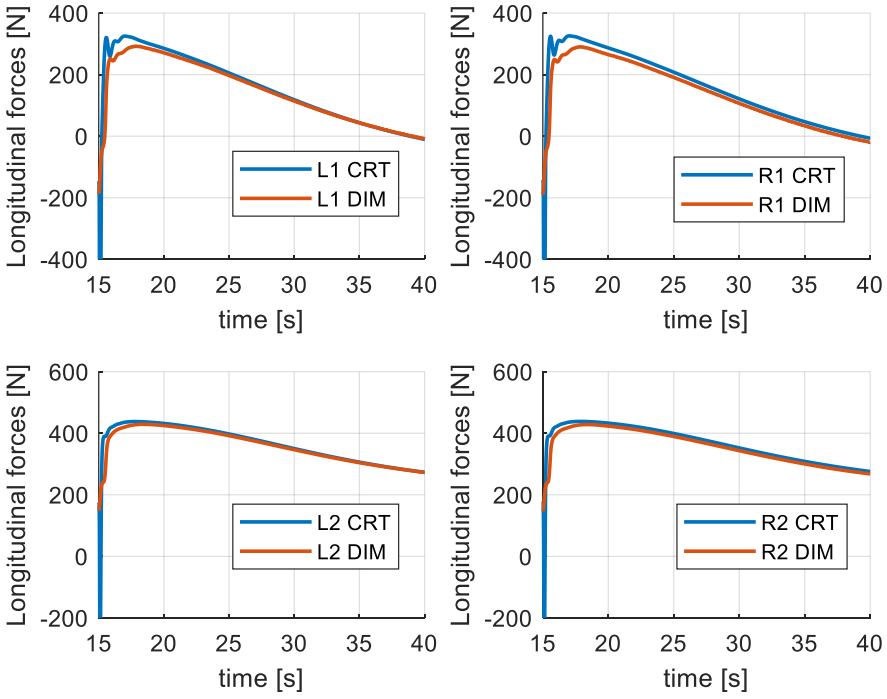

Figure 99: longitudinal forces (Real-Time - Acceleration - Dry Sand)

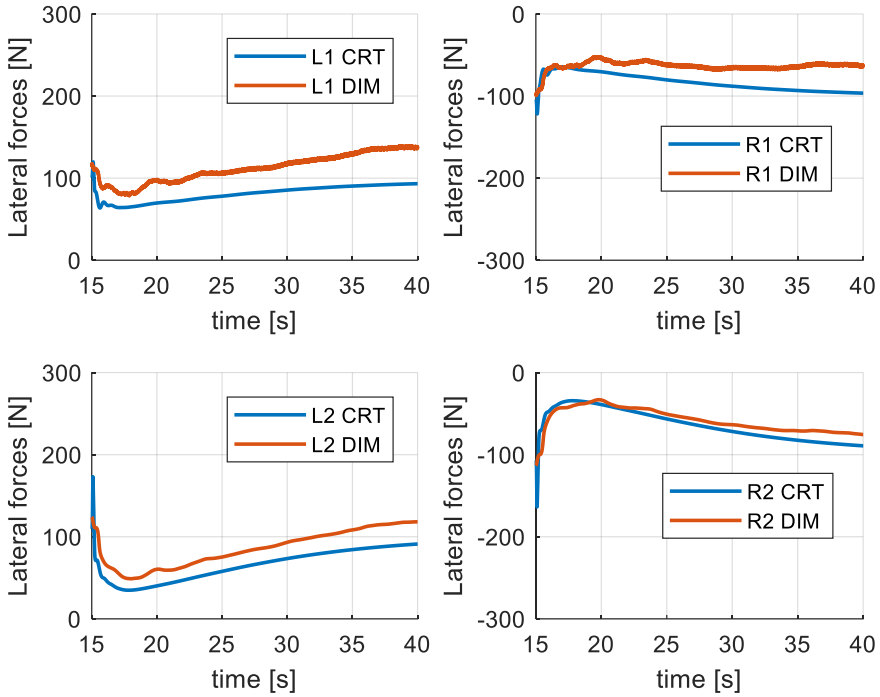

Figure 100: lateral forces (Real-Time - Acceleration - Dry Sand)

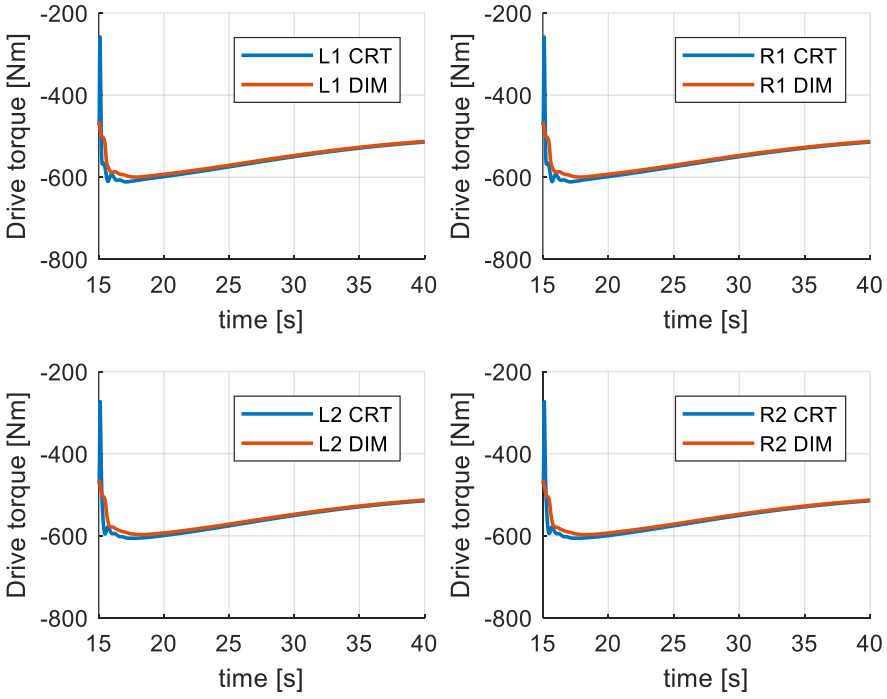

Figure 101: driver torque (Real-Time - Acceleration - Dry Sand)

11 Conclusion and Future Works

11.1 Conclusion

In this thesis an off-road tyre model has been developed to simulate the off-road driving, suitable to run in real-time on professional dynamic driving software.

The aim to obtain a realistic off-road driving on the simulator has been achieved: the results and driver's feedback are satisfying.

The off-road model is capable to run in co-simulation with any vehicle model, after due changes to connect it with the chosen specific vehicle model.

The opportunity to simulate the off-road driving has several advantages because it allows:

- to analyse vehicle performance on different soils;
- to improve the vehicle design process, early detecting some possible issues;
- to save money and time for prototypes and for off-road tests;
- to verify and to repeat systematically some difficult manoeuvres on particular soil conditions;
- to train the drivers to manoeuvre in off-road conditions;
- to reduce the time needed to develop off-road systems and controls, improving also their quality.

The purpose to obtain a realistic model, as much as possible, allows to improve the quality of the results given by the simulations; therefore, it increases the above-mentioned advantages.

Moreover, the off-road model can be useful to evaluate the performance of rover vehicles.

11.2 Future works

Even if the development and implementation of the off-road tyre model for driving simulator was satisfactory, the hypothesis made (see *section 5.1*) highlight some of the possible future development works:

- the model could be extended to flexible tyre, allowing to increase the validity range of the model;
- to implement the multi-pass effect, allowing even a more realistic behaviour;
- to improve the lateral force modelling, also introducing the bulldozing effect;

A remarkable work would be to conduct field tests to experimentally validate the proposed model; unfortunately, the Covid-19 pandemic did not allow to perform tests.

Another noteworthy activity, although challenging to conduct, is to investigate some correlations between soil parameters, coefficient of friction and pneumatic tyre type. This could be conducted together with the above-mentioned validation of the model and it could allow also to develop a method for identifying soil parameters to be used in simulation, increasing the accuracy and reliability of off-road models.

Appendix A: MATLAB script

```
%function to calculate tyre forces and moments

function[Fx,Fy,Fz,Drive_torque] =
Forces_Moments(Sd,costanti,teta_e,alfa)

Ru=costanti(1);       %tyre radius
b=costanti(2);        %tyre width
teta_r=costanti(3);   %exit angle
k_x=costanti(4);      %shear deformation
c=costanti(5);        %soil cohesion
phi=costanti(6);      %angle of internal friction of the soil
k_c=costanti(7);      %cohesion related soils parameter
k_phi=costanti(8);    %angle of internal friction related soils
parameter
n=costanti(9);        %sinkage exponet
gamma_s=costanti(10); %soil density
c0=costanti(11);      %coefficients related to teta_N
c1=costanti(12);      %coefficients related to teta_N
k_y=costanti(13);     %lateral shear deformation

teta_N=(c0+c1*abs(Sd))*teta_e;
teta=linspace(teta_r,teta_e,100);

j_x=Ru.*((teta_e-teta)-(1-Sd)*(sin(teta_e)-sin(teta)));
j_y=Ru.*(1-Sd).*(teta_e-teta).*tan(alfa);

sigma_n2=(Ru^n)*((k_c/b)+k_phi)*((cos(teta)-
cos(teta_e)).^n).*(teta>=teta_N);
sigma_n1=(Ru^n)*((k_c/b)+k_phi)*((cos(teta_e-(((teta-
teta_r)/(teta_N-teta_r))*(teta_e-teta_N)))-
cos(teta_e)).^n).*(teta<teta_N);
sigma_n= sigma_n1 + sigma_n2; %normal stress

tau_x=(c+(sigma_n.*tan(phi))).*(1-exp(-j_x/k_x));
tau_y=(c+(sigma_n.*tan(phi))).*(1-exp(-j_y/k_y));

Fx=Ru*b*(trapz(teta,(tau_x.*cos(teta)))-
trapz(teta,(sigma_n.*sin(teta))));

Fy=Ru*b*(trapz(teta,(tau_y)));

Fz=Ru*b*(trapz(teta,sigma_n.*cos(teta))+trapz(teta,tau_x.*sin(
teta)));

Drive_torque=((Ru^2)*b*(trapz(teta,tau_x)));

end
```

Appendix B: offline simulation results

With reference to the offline simulations performed on the other two types of soil, here below the charts are reported.

Being the charts very similar to those obtained for the simulation on the sand, which have been already analysed and showed in *section 8.2.1* and *8.2.2*, as for the following charts, comments are reported in case of exception only.

Offline Simulation: constant speed – LETE sand

As for the simulation with the "constant speed" manoeuvre (see *section 8.1*) on "LETE sand" (soil data reported in *Tab. 2*), the results are reported here below.

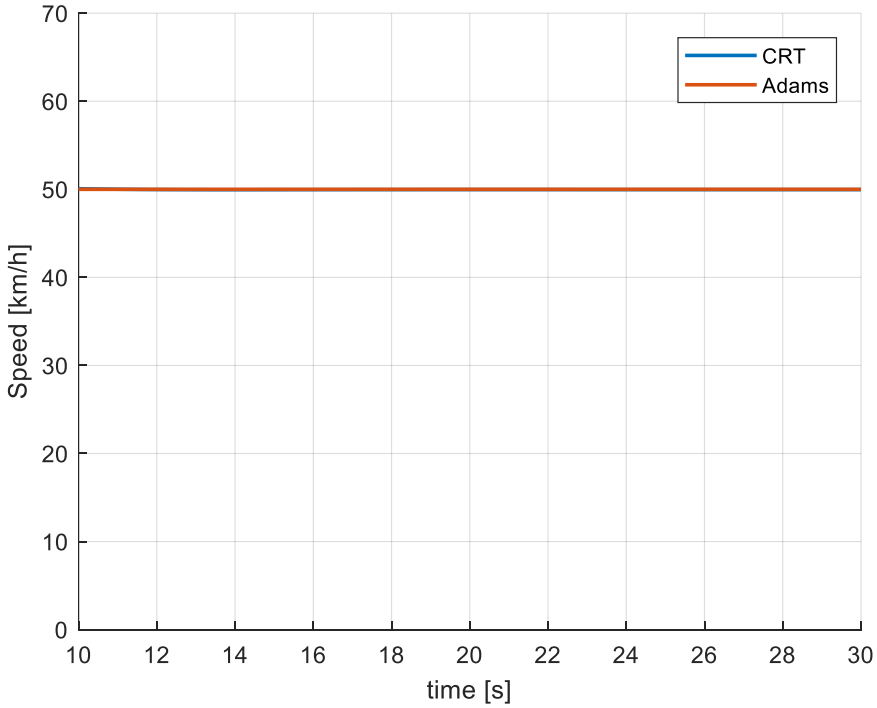

Figure 102: speed (Offline - Constant Speed - LETE Sand)

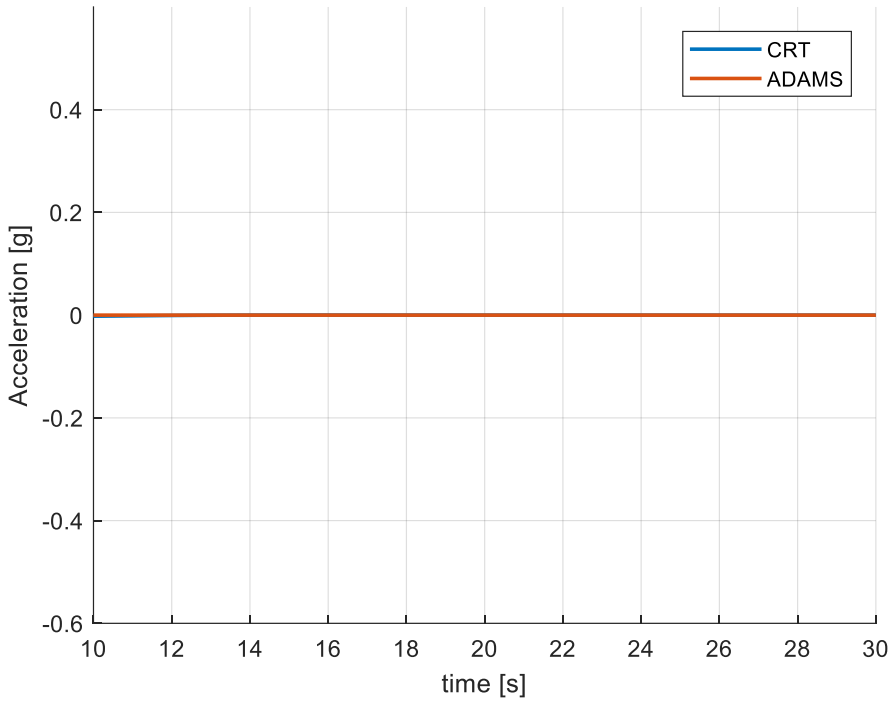

Figure 103: longitudinal acceleration (Offline - Constant Speed - LETE Sand)

The value of the opening throttle (*Fig. 104*) is less than the value obtained in the first simulation (7.2.1).

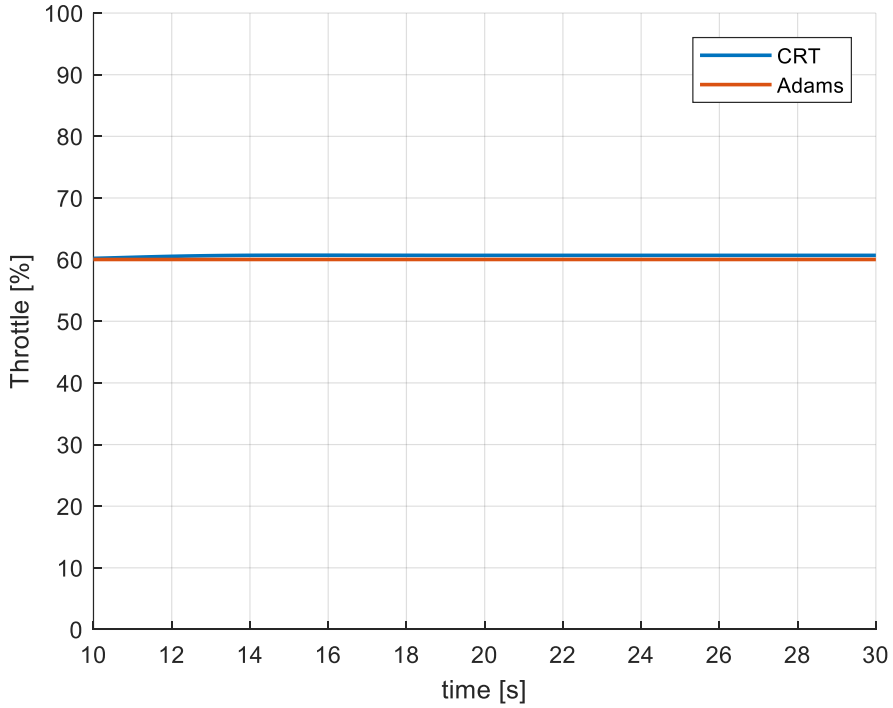

Figure 104: throttle demand (Offline - Constant Speed - LETE Sand)

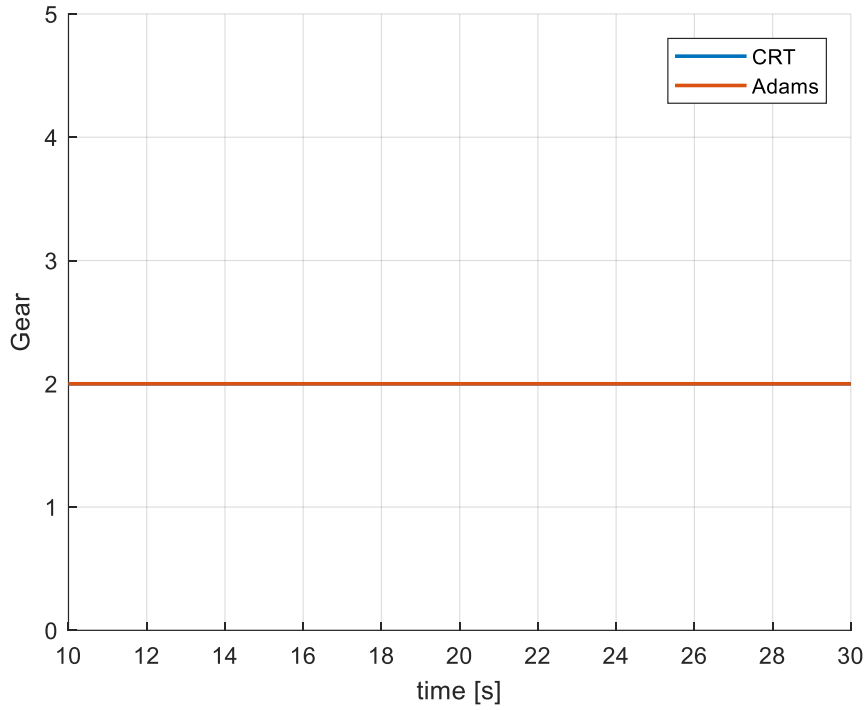

Figure 105: gear demand (Offline - Constant Speed - LETE Sand)

The longitudinal slip (*Fig. 106*), especially of the rear wheels, is more similar to Adams results than the first simulation.

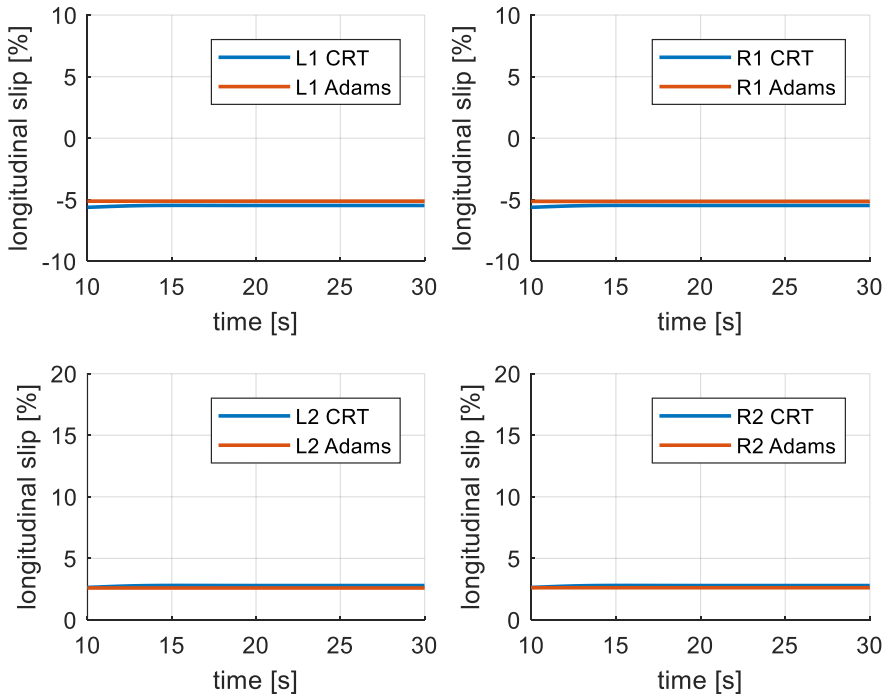

Figure 106: longitudinal slip (Offline - Constant Speed - LETE Sand)

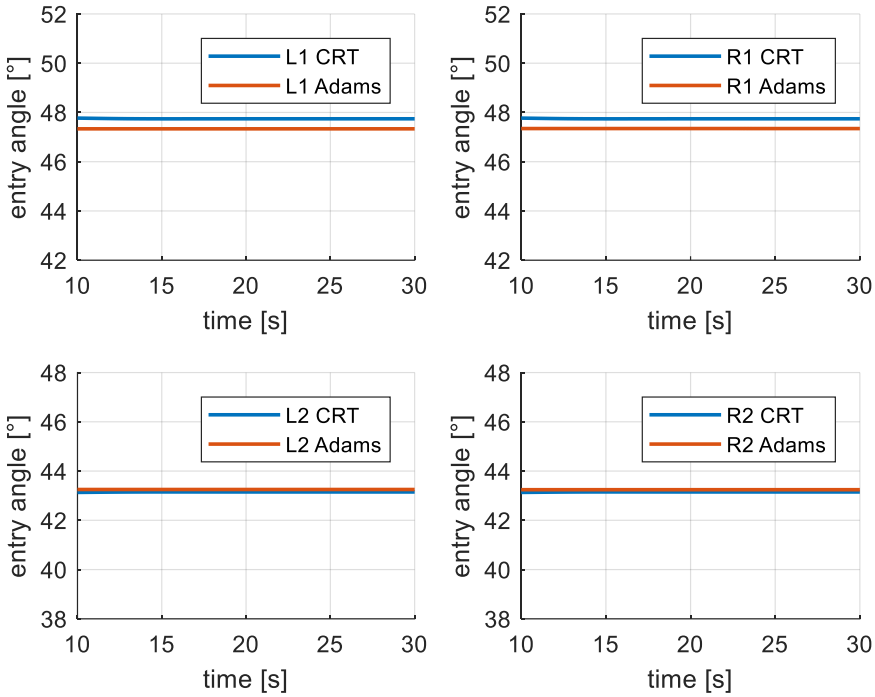

Figure 107: entry angle (Offline - Constant Speed - LETE Sand)

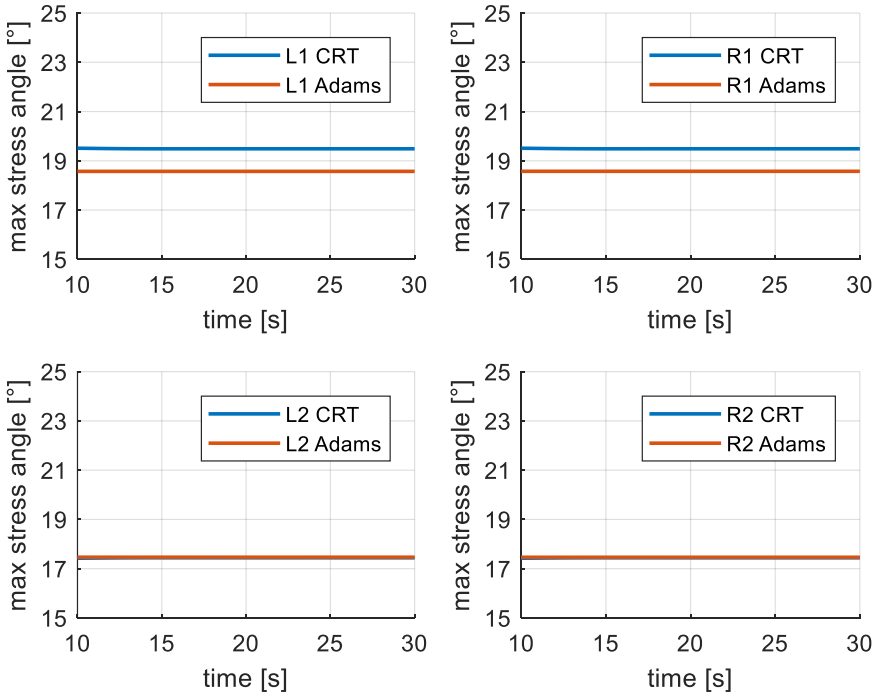

Figure 108: max stress angle (Offline - Constant Speed - LETE Sand)

Fig. 109 shows that the vehicle sinks less on the LETE Sand than on the dry sand.

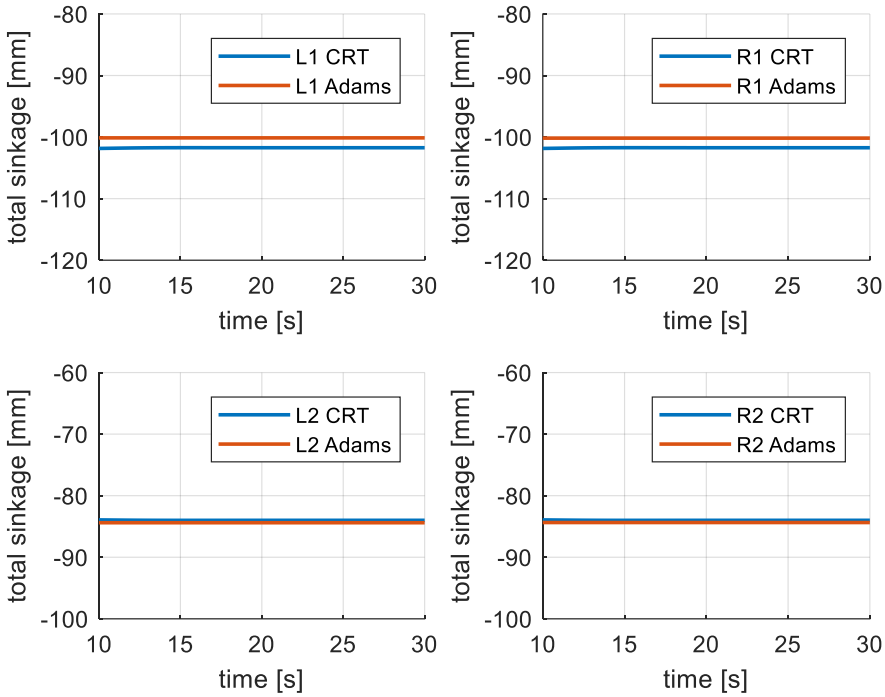

Figure 109: sinkage (Offline - Constant Speed - LETE Sand)

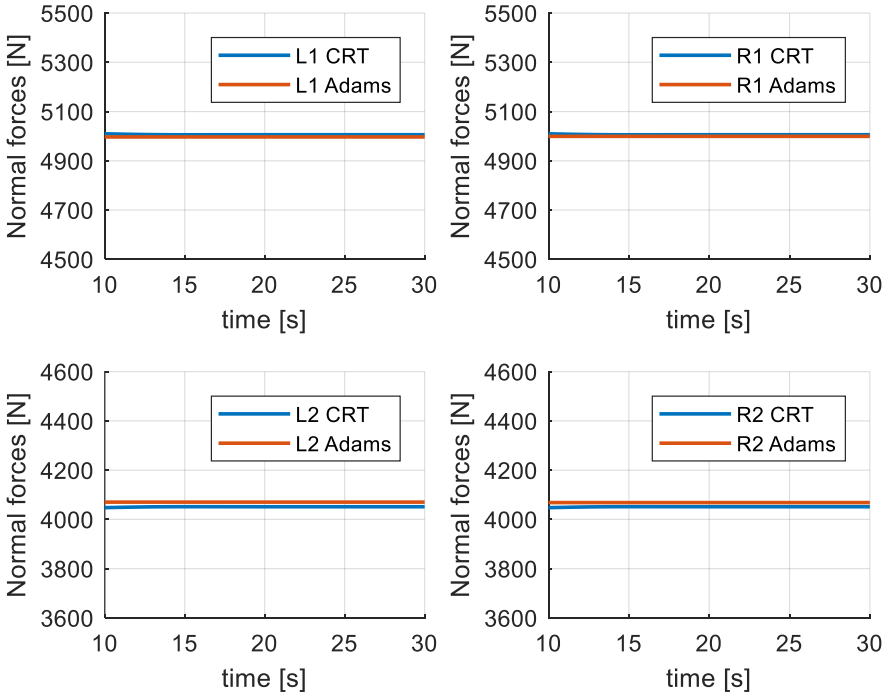

Figure 110: normal forces (Offline - Constant Speed - LETE Sand)

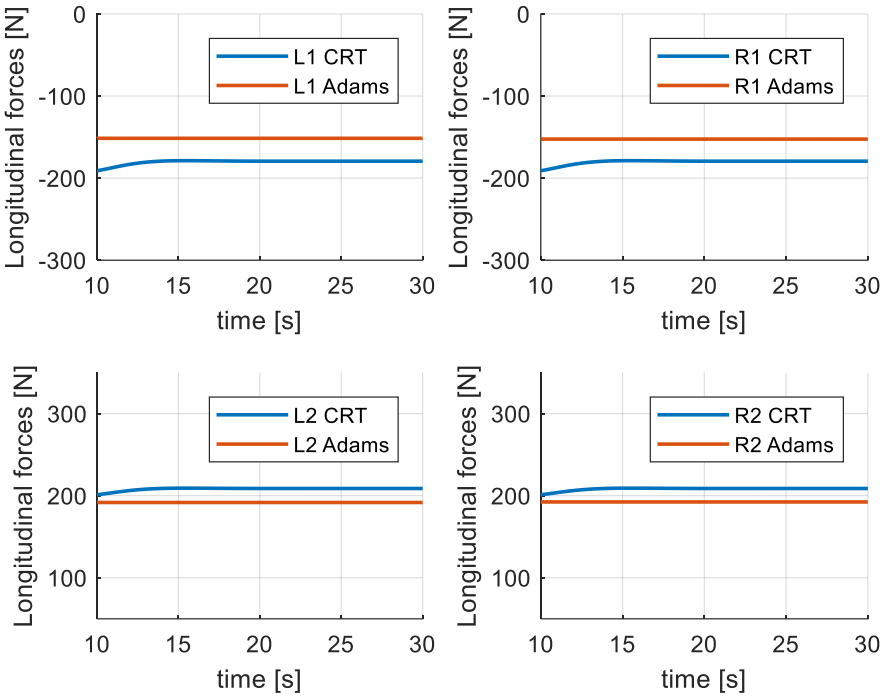

Figure 111: longitudinal forces (Offline - Constant Speed - LETE Sand)

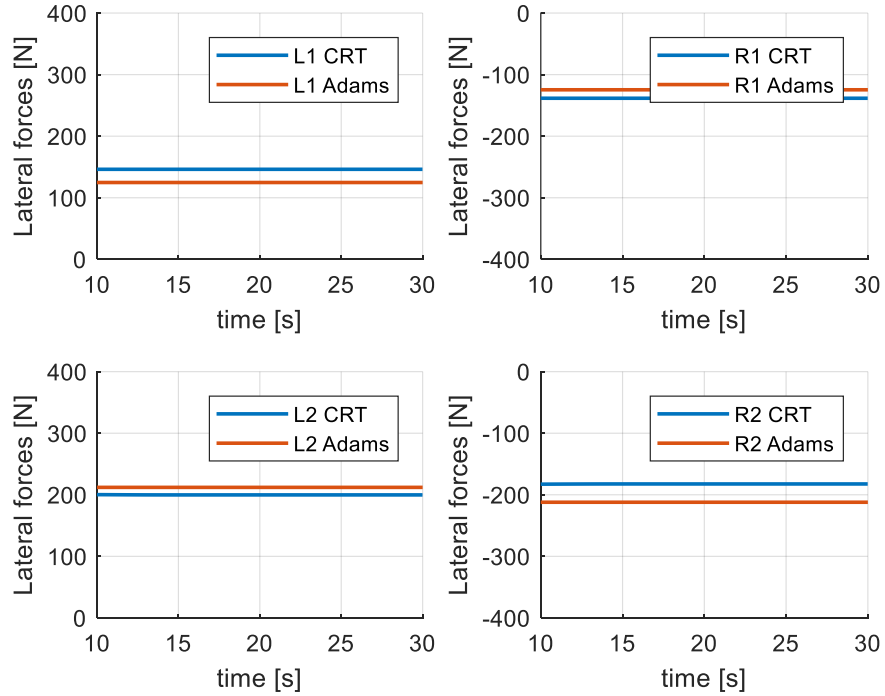

Figure 112: lateral forces (Offline - Constant Speed - LETE Sand)

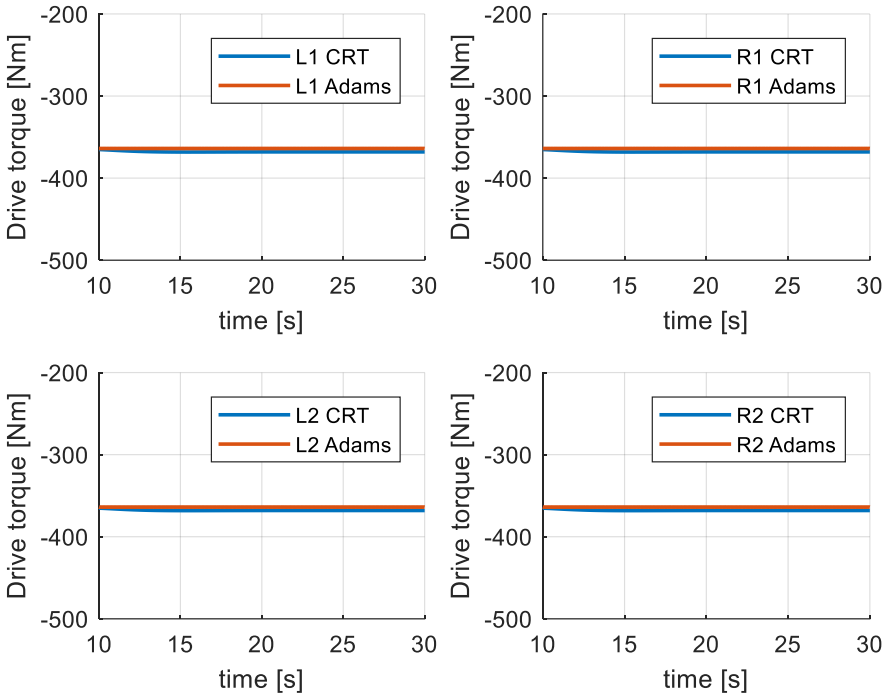

Figure 113: drive torque (Offline - Constant Speed - LETE Sand)

Offline Simulation: acceleration – LETE sand

As for the simulation with the "acceleration" manoeuvre (see *section 8.1*) on "LETE sand" (soil data reported in *Tab. 2*), the results are reported here below.

On the LETE sand, the vehicle is capable to reach speeds greater than 100 km/h. Around the 40s second, the driver changes the gear: the Adams virtual driver executes the gear shift releasing the accelerator, while the VI-CarRealTime driver doesn't.

During the shift gear, the different behaviour, between the two drivers, is due to a different clutch model used by Adams, that influences the results. In fact, in some charts, close to the 40s second, it is possible to observe a spike of the Adams results curve.

Despite some differences between the results of two models, the comparison shows the reliability of the developed off-road model.

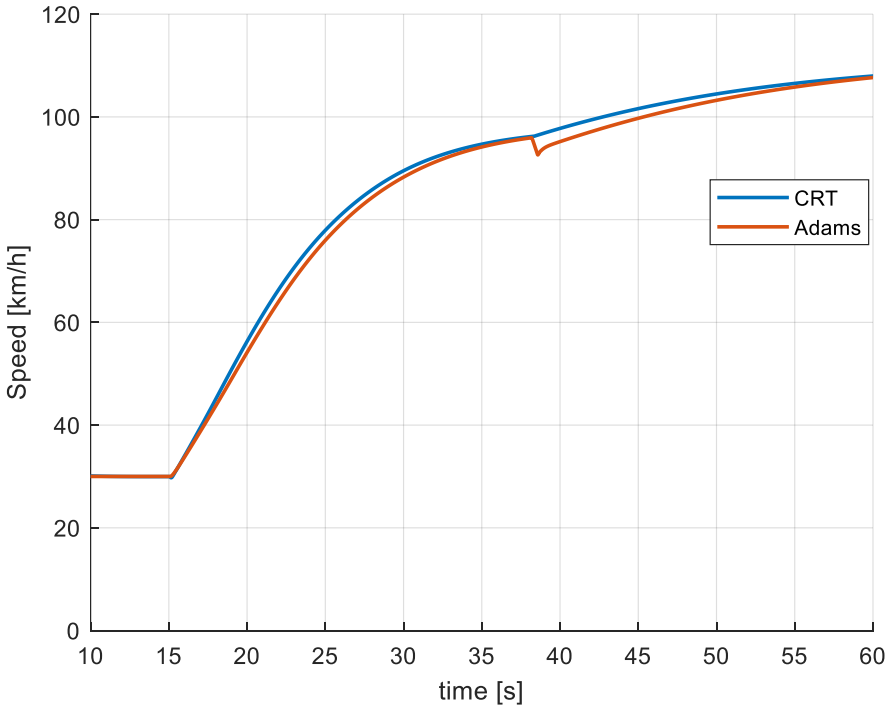

Figure 114: speed (Offline - Acceleration - LETE Sand)

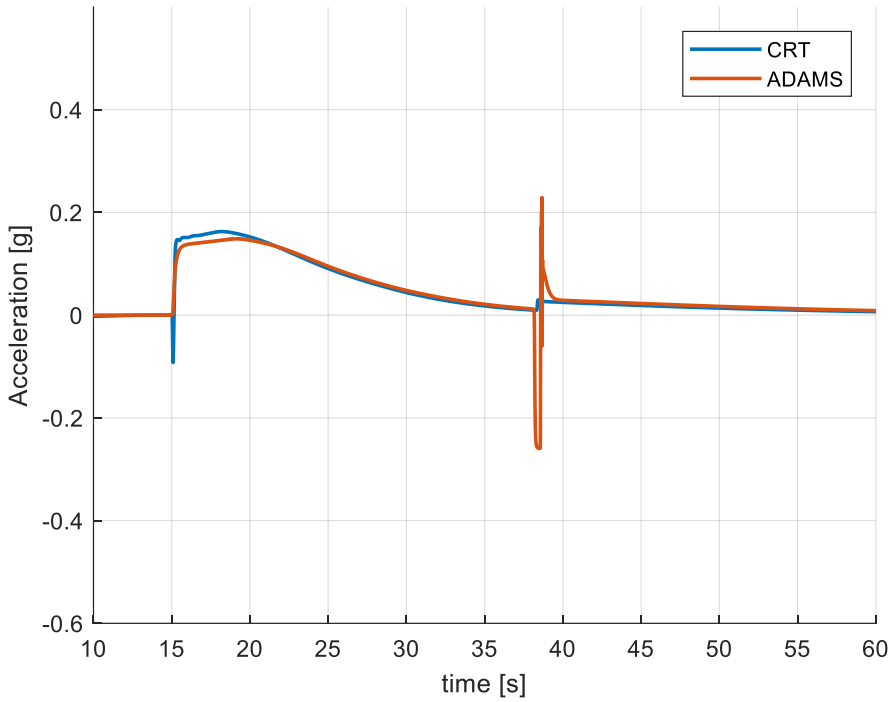

Figure 115: longitudinal acceleration (Offline - Acceleration - LETE Sand)

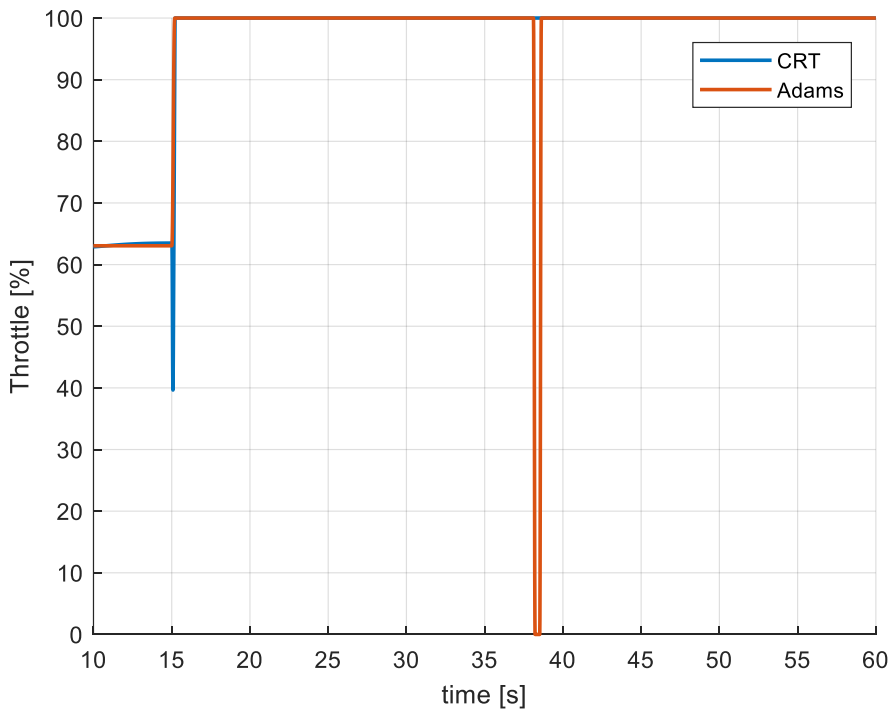

Figure 116: throttle demand (Offline - Acceleration - LETE Sand)

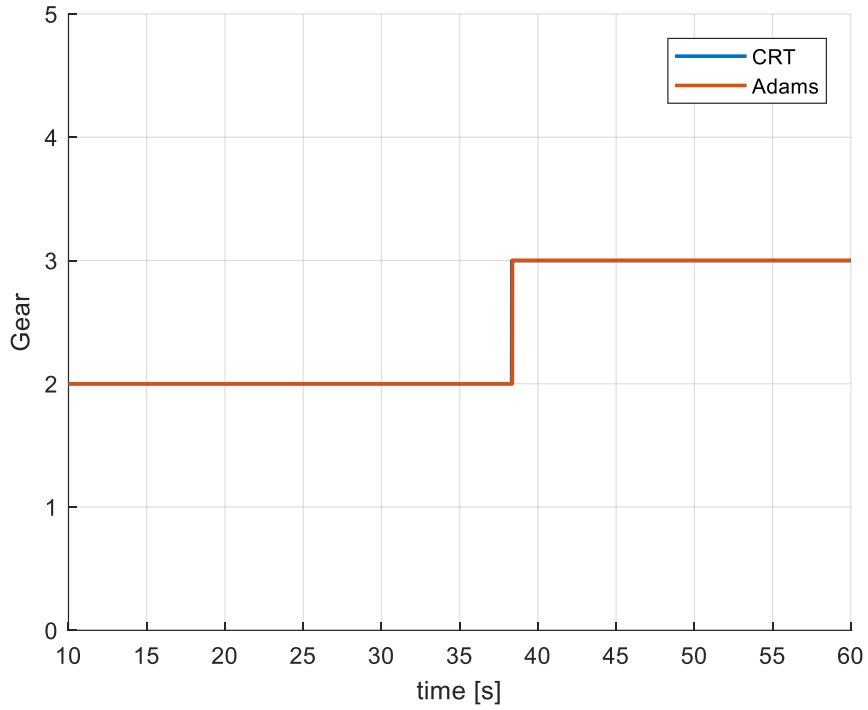

Figure 117: gear demand (Offline - Acceleration - LETE Sand)

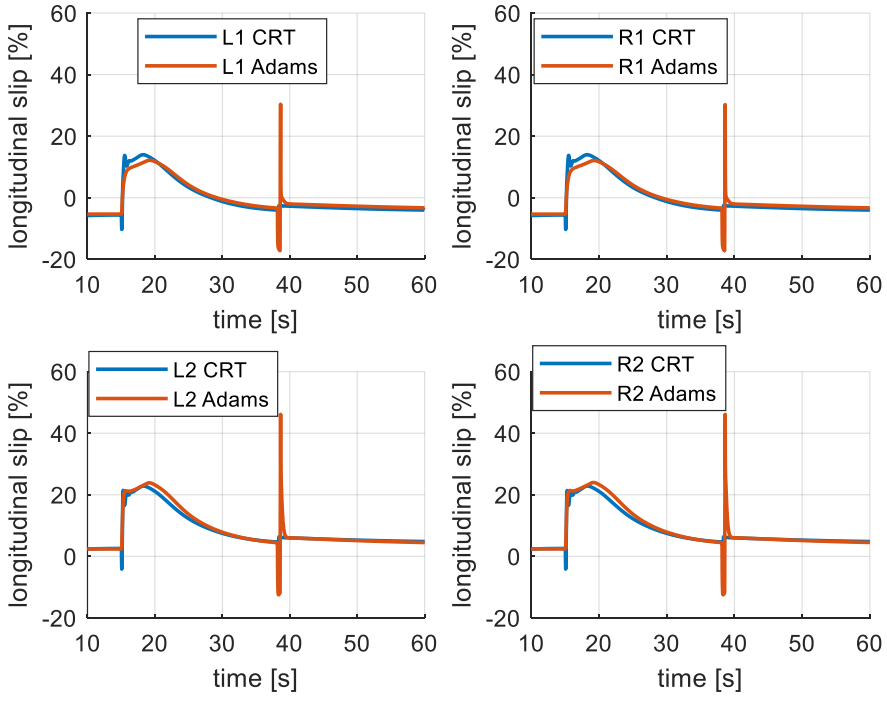

Figure 118: longitudinal slip (Offline - Acceleration - LETE Sand)

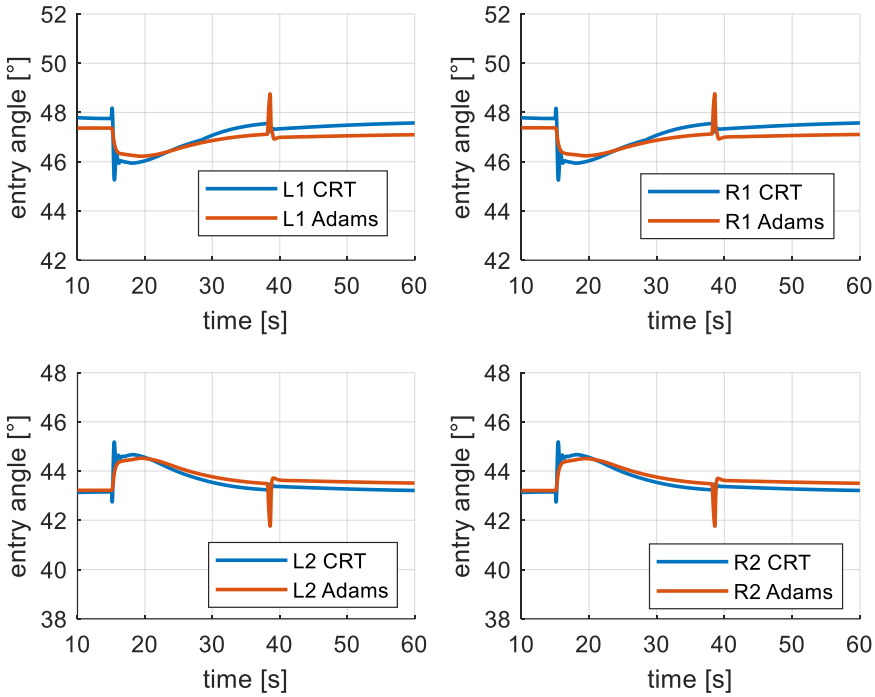

Figure 119: entry angle (Offline - Acceleration - LETE Sand)

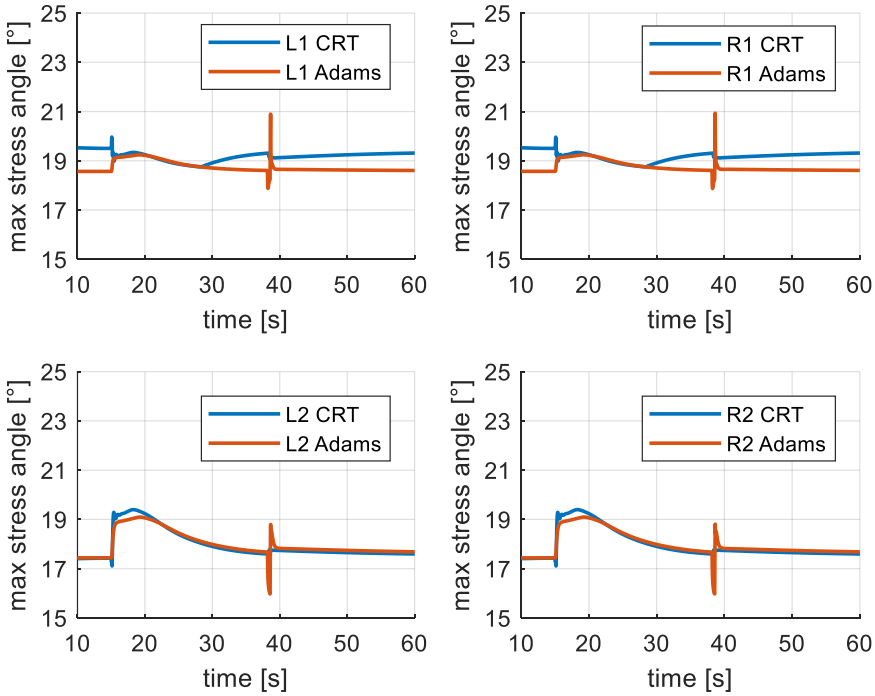

Figure 120: max stress angle (Offline - Acceleration - LETE Sand)

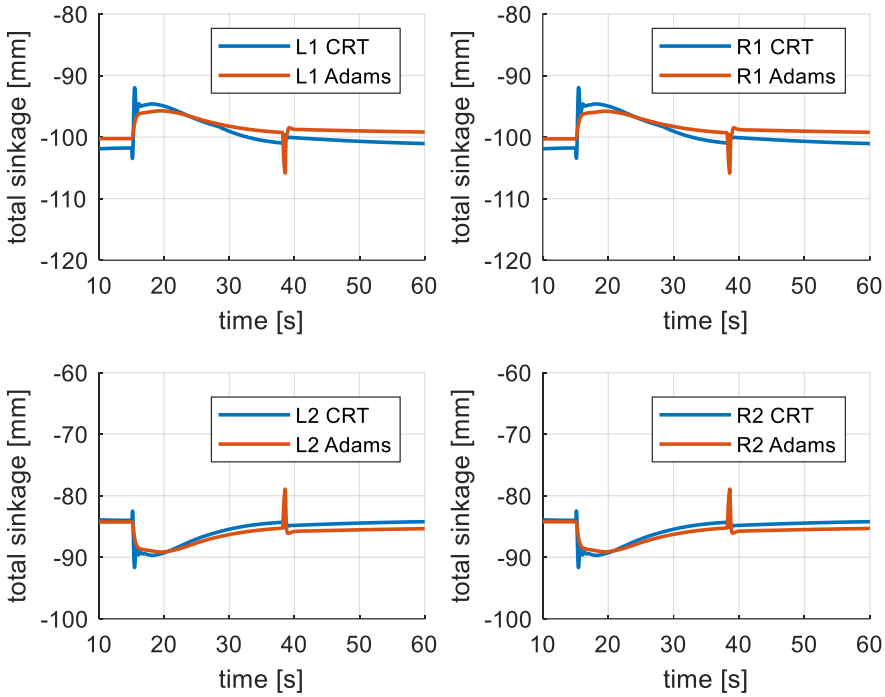

Figure 121: sinkage (Offline - Acceleration - LETE Sand)

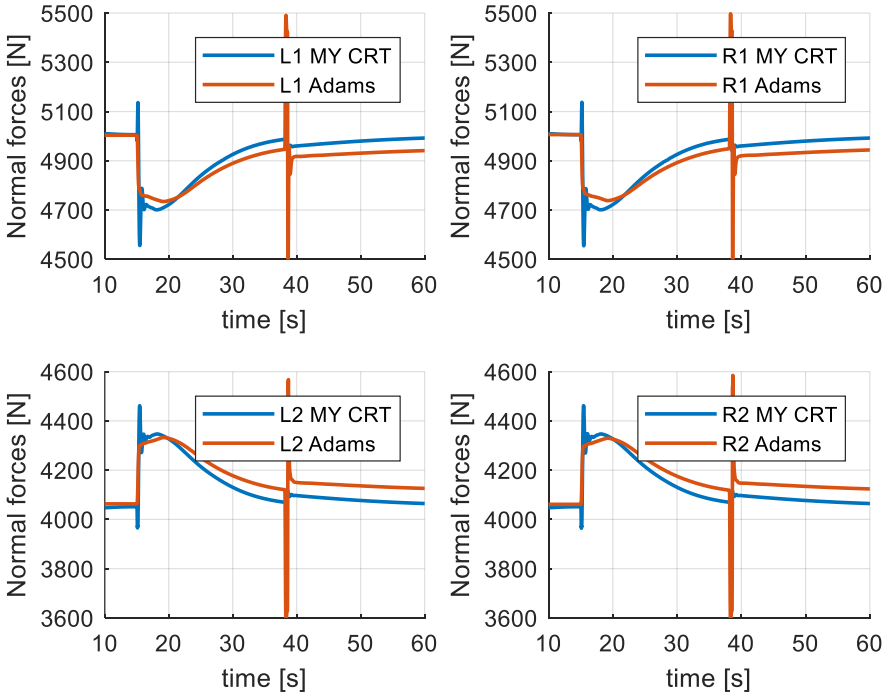

Figure 122: normal forces (Offline - Acceleration - LETE Sand)

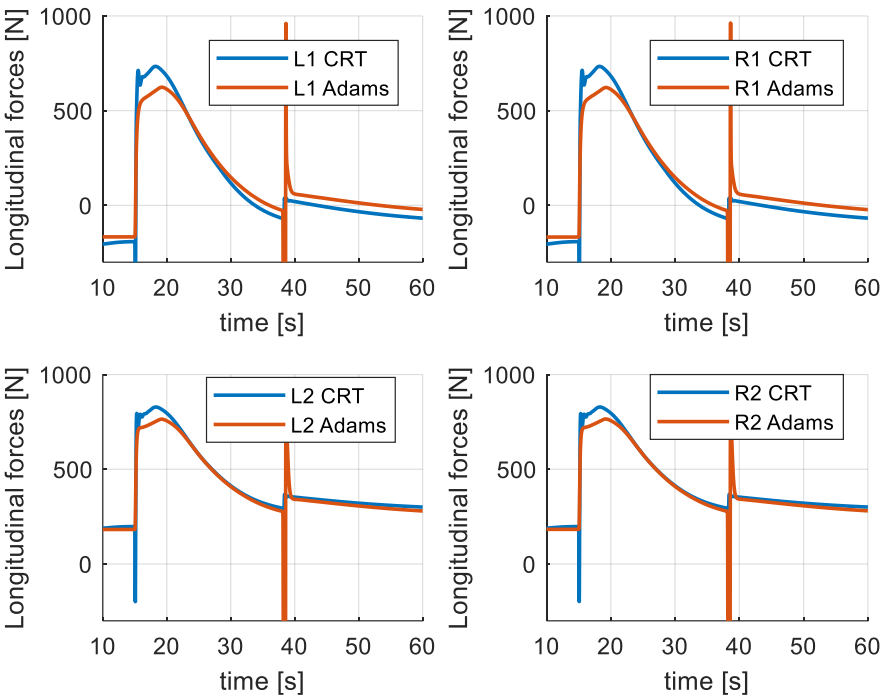

Figure 123: longitudinal forces (Offline - Acceleration - LETE Sand)

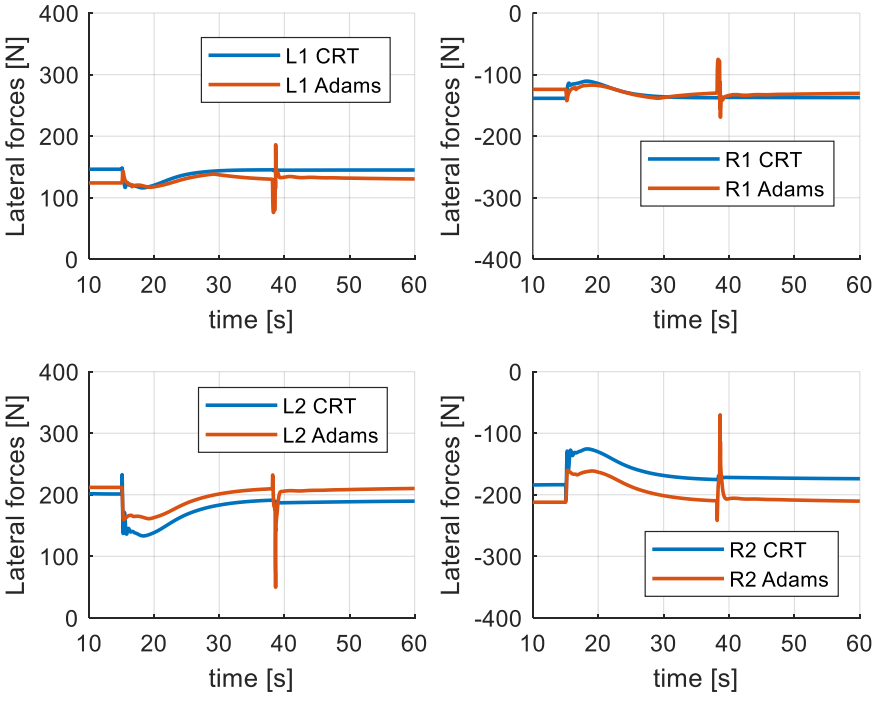

Figure 124: lateral forces (Offline - Acceleration - LETE Sand)

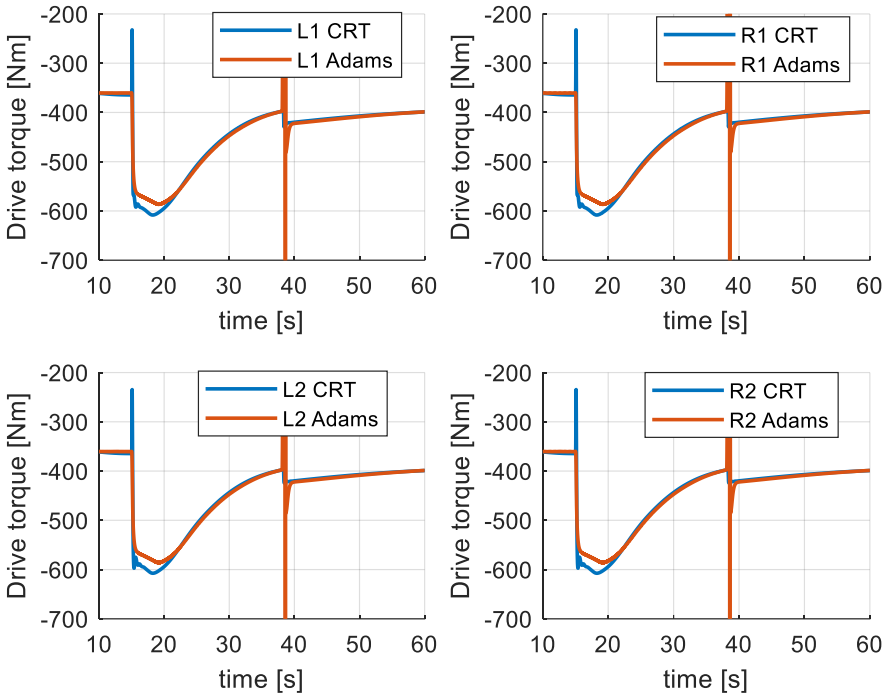

Figure 125: drive torque (Offline - Acceleration - LETE Sand)

Offline Simulation: constant speed – loam sand

As for the simulation with the "constant speed" manoeuvre (see *section 8.1*) on "loam sand" (soil data reported in *Tab. 3*), the results are reported here below.

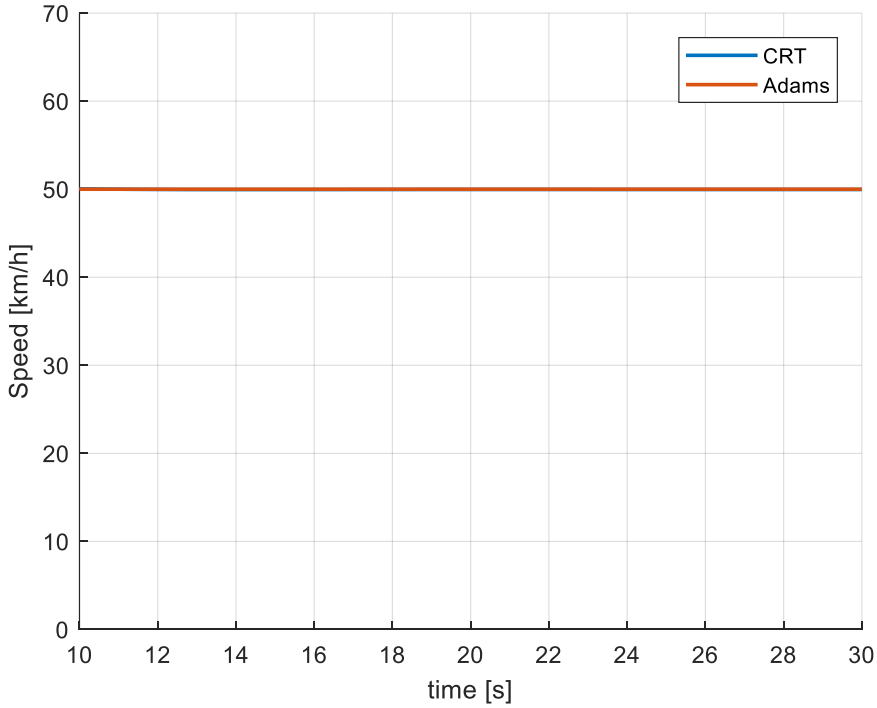

Figure 126: speed (Offline - Constant Speed - Loam Sand)

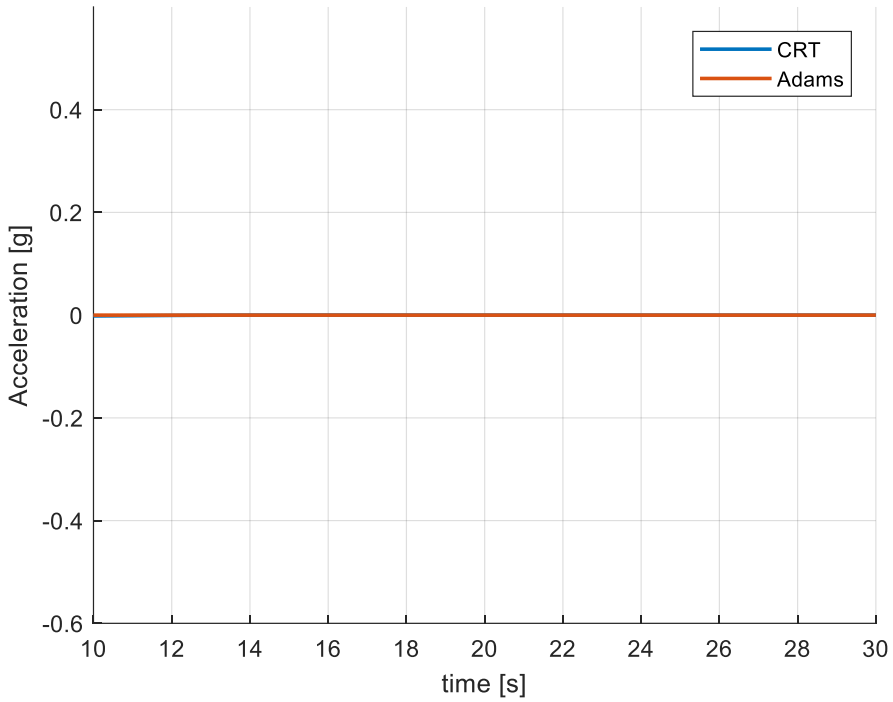

Figure 127: longitudinal acceleration (Offline - Constant Speed - Loam Sand)

In *Fig. 128*, it is observable that the value of the opening throttle is less than the value obtained by the simulation performed on "LETE sand".

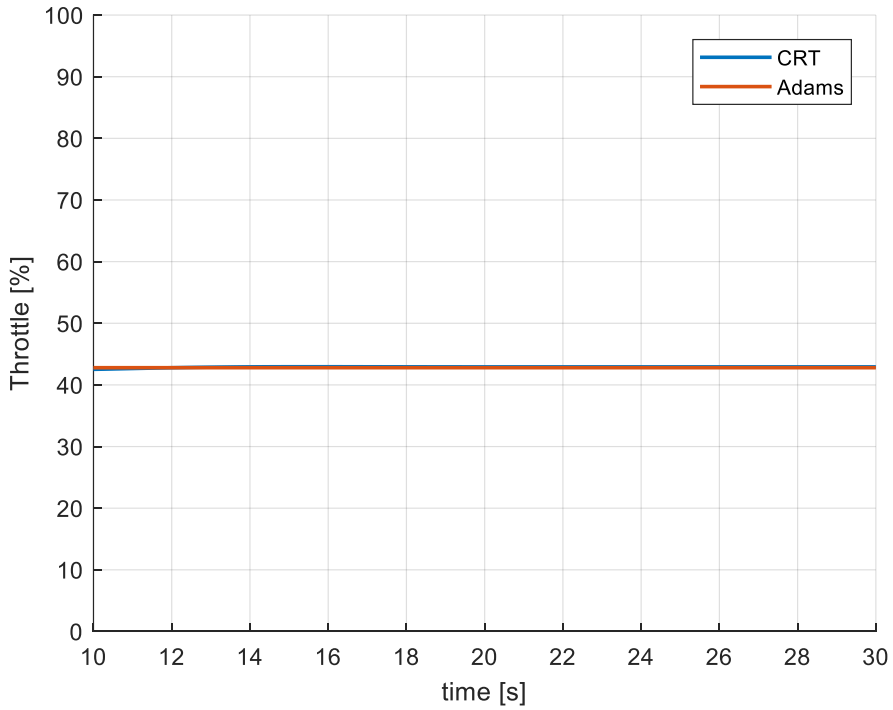

Figure 128: throttle demand (Offline - Constant Speed - Loam Sand)

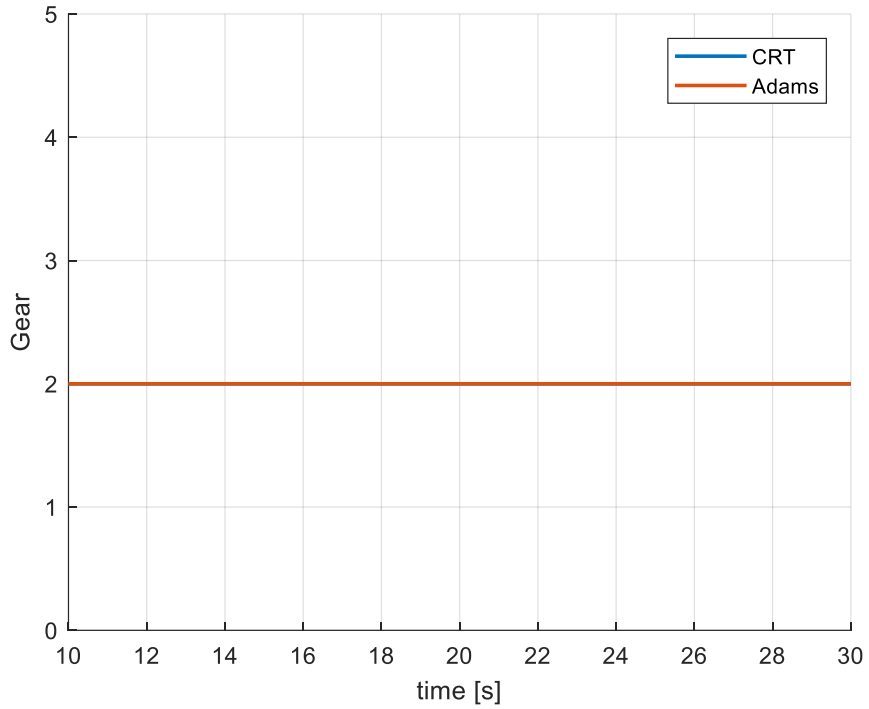

Figure 129: gear demand (Offline - Constant Speed - Loam Sand)

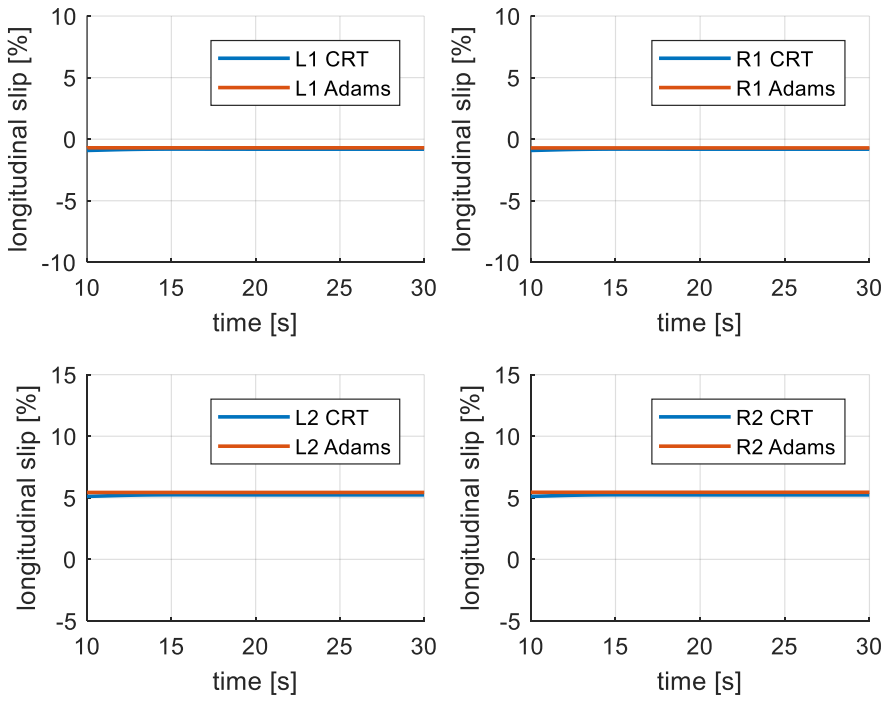

Figure 130: longitudinal slip (Offline - Constant Speed - Loam Sand)

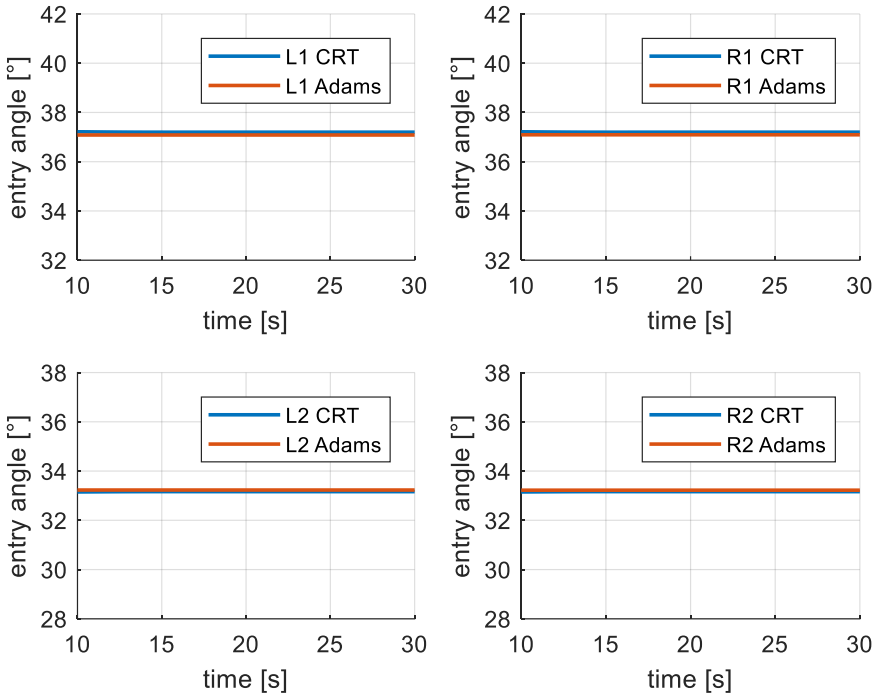

Figure 131: entry angle (Offline - Constant Speed - Loam Sand)

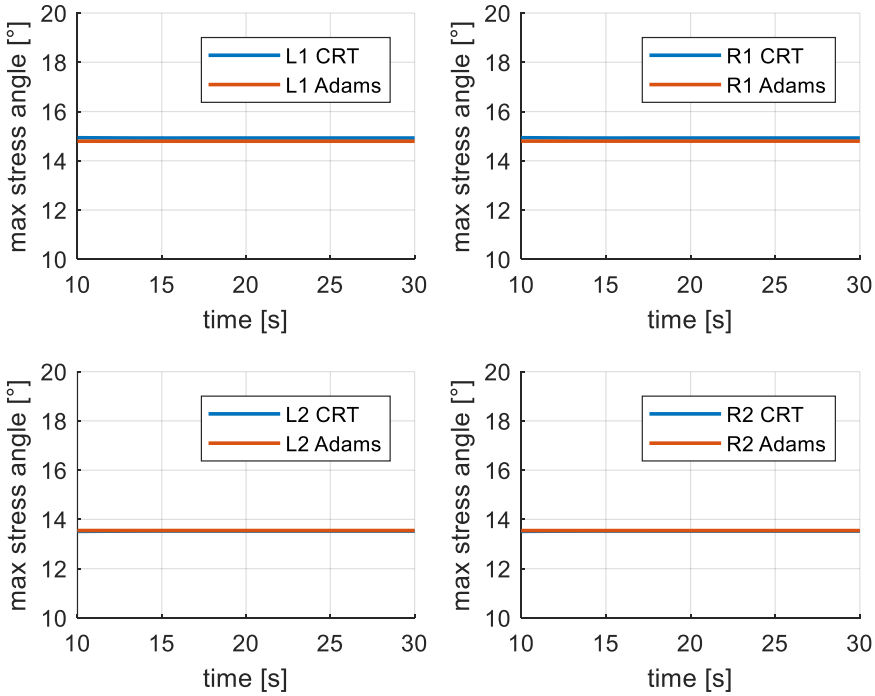

Figure 132: max stress angle (Offline - Constant Speed - Loam Sand)

Fig. 133 shows that the vehicle sinks less on the loam sand than on the LETE sand.

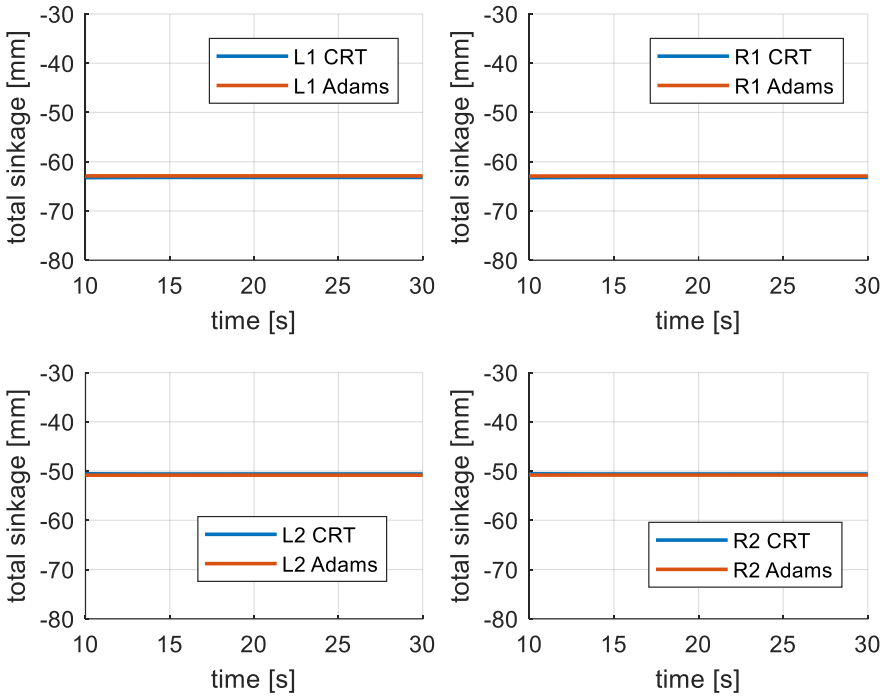

Figure 133: sinkage (Offline - Constant Speed - Loam Sand)

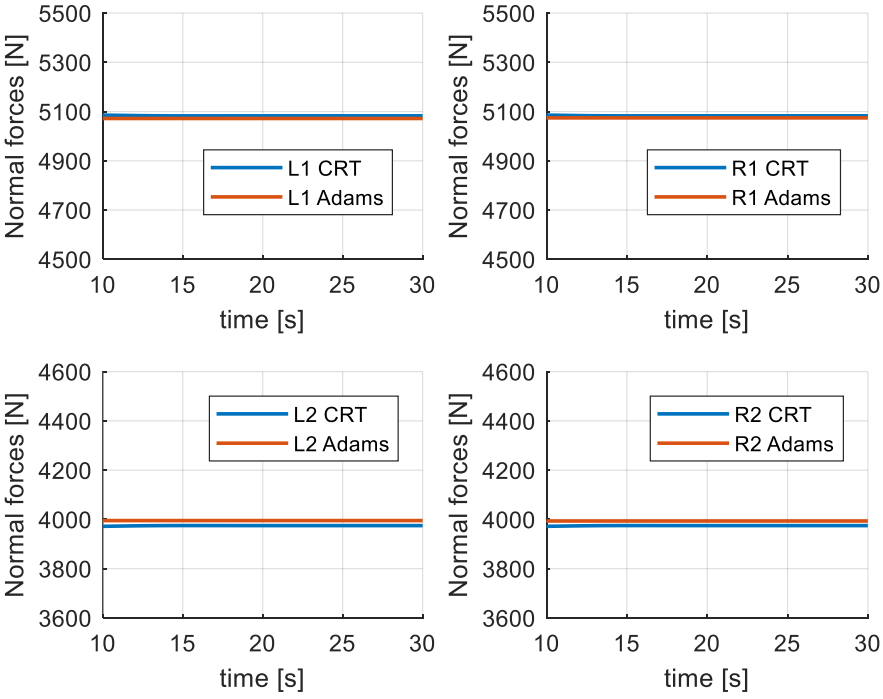

Figure 134: normal forces (Offline - Constant Speed - Loam Sand)

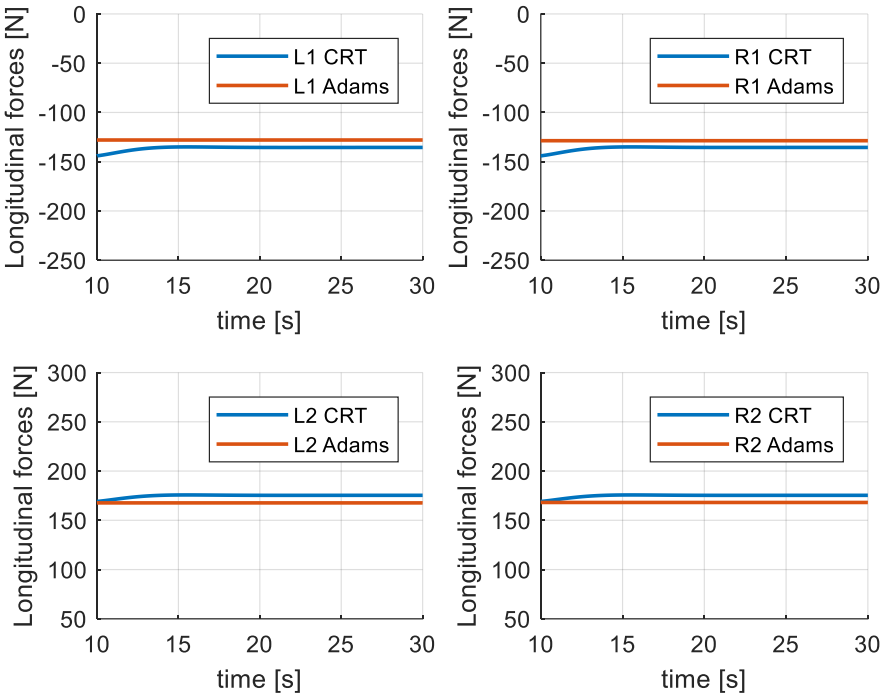

Figure 135: longitudinal forces (Offline - Constant Speed - Loam Sand)

Since the vehicle sinks less, the bulldozing effect has a lower impact, therefore the lateral forces (*Fig. 136*) are more similar to Adams results than in the other simulation.

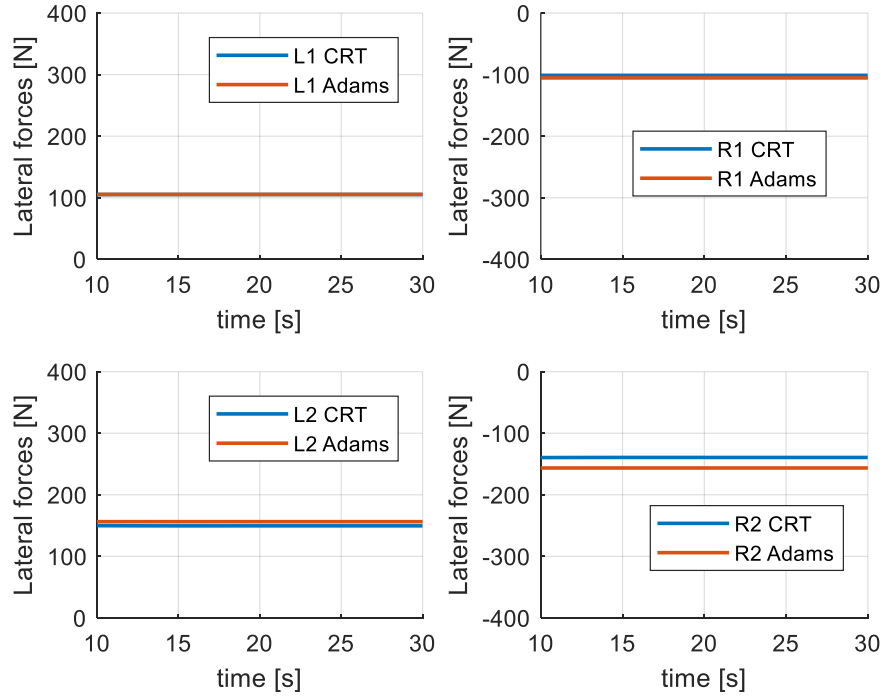

Figure 136: lateral forces (Offline - Constant Speed - Loam Sand)

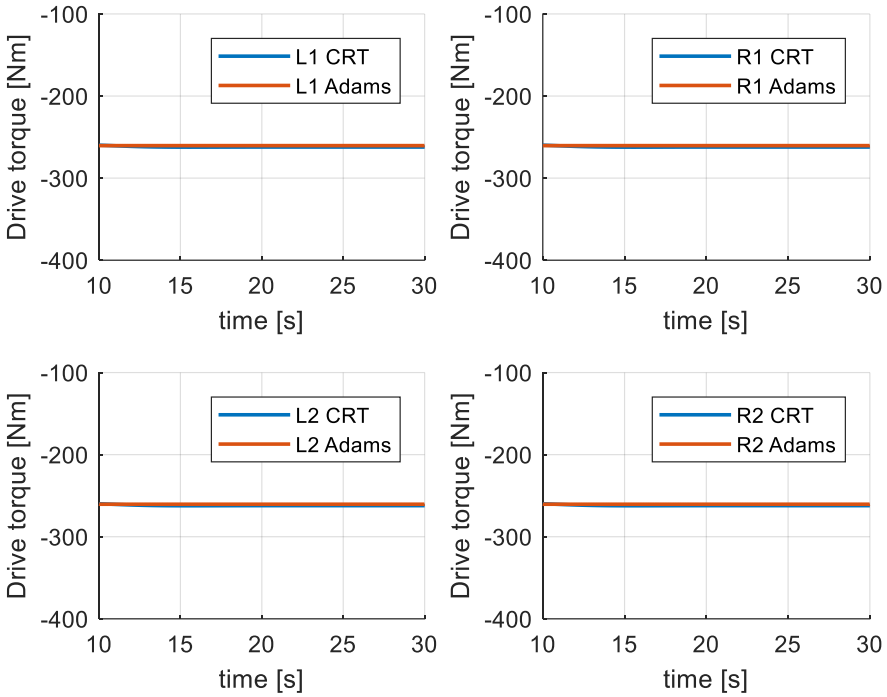

Figure 137: drive torque (Offline - Constant Speed - Loam Sand)

Offline Simulation: acceleration – loam sand

As for the simulation with the "acceleration" manoeuvre (see *section 8.1*) on "loam sand" (soil data reported in *Tab. 3*), the results are reported here below.

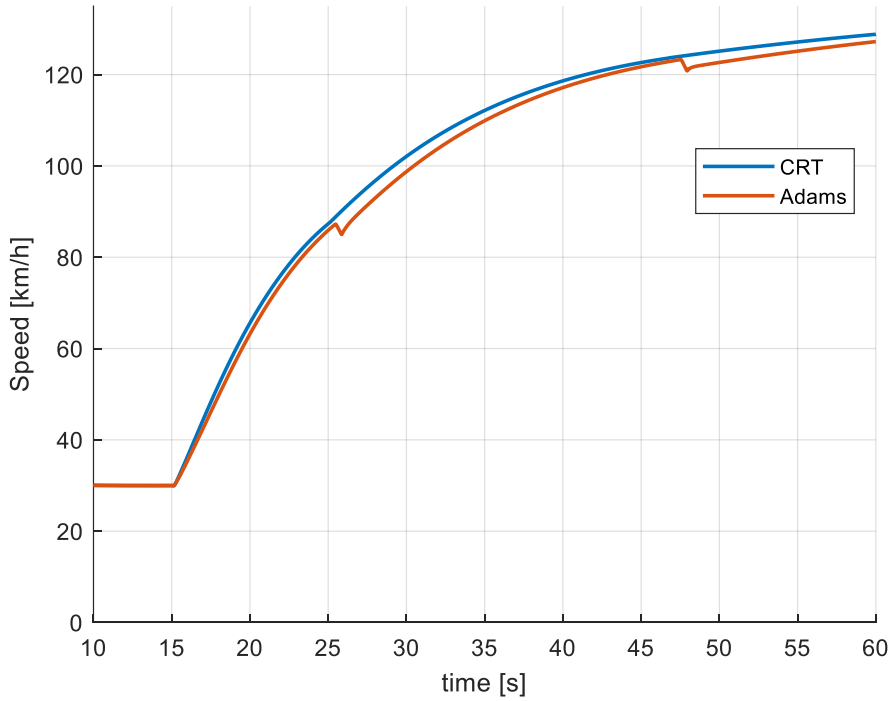

Figure 138: speed (Offline - Acceleration - Loam Sand)

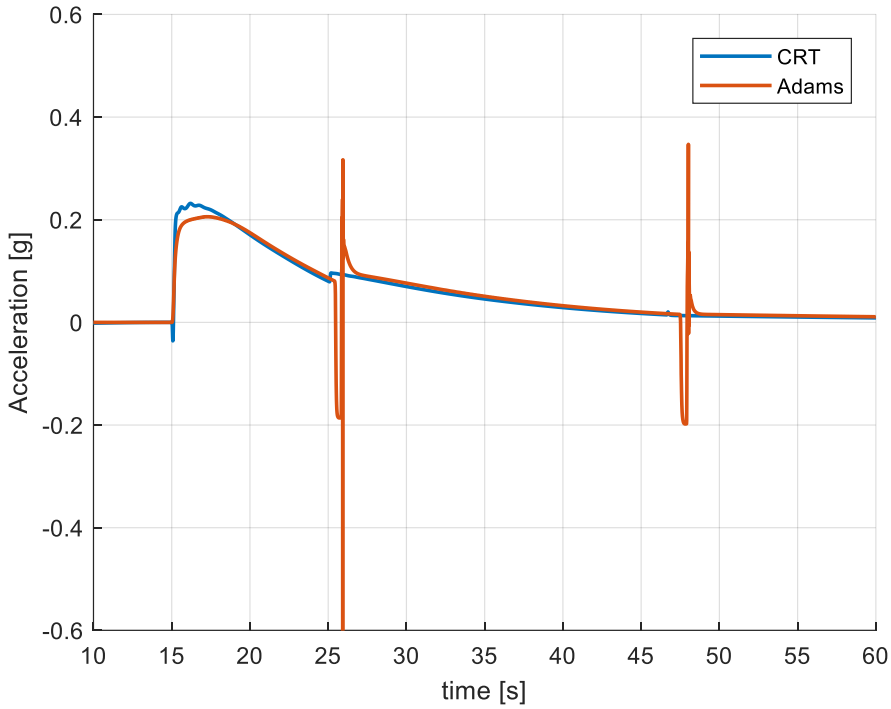

Figure 139: longitudinal acceleration (Offline - Acceleration - Loam Sand)

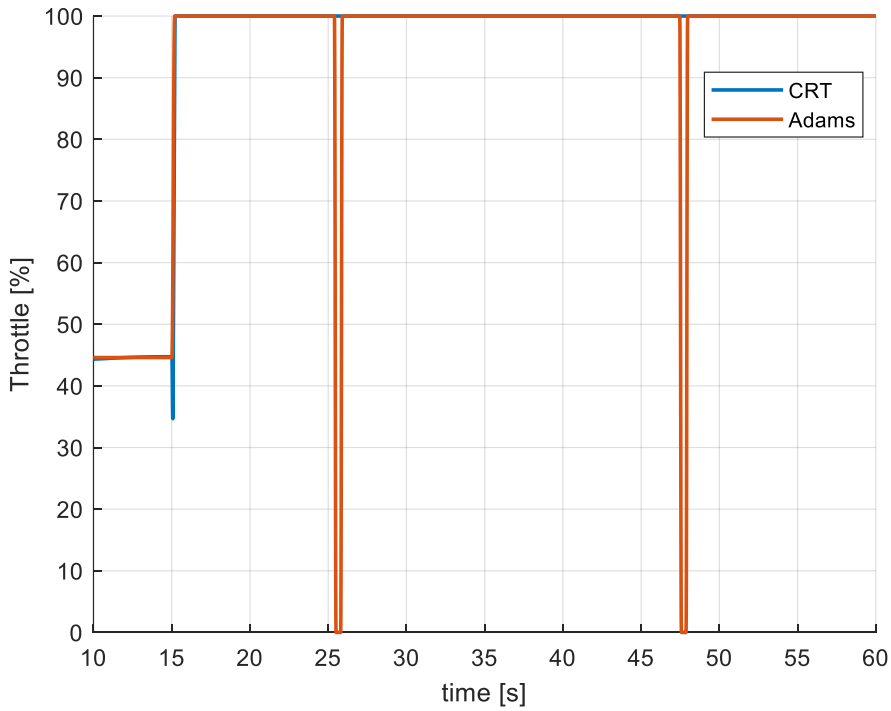

Figure 140: throttle demand (Offline - Acceleration - Loam Sand)

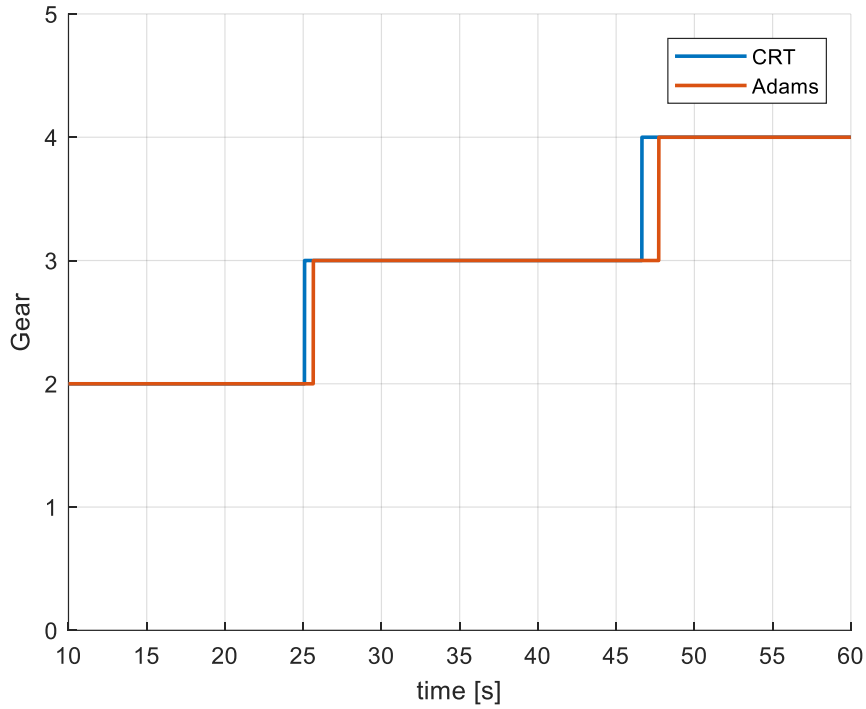

Figure 141: gear demand (Offline - Acceleration - Loam Sand)

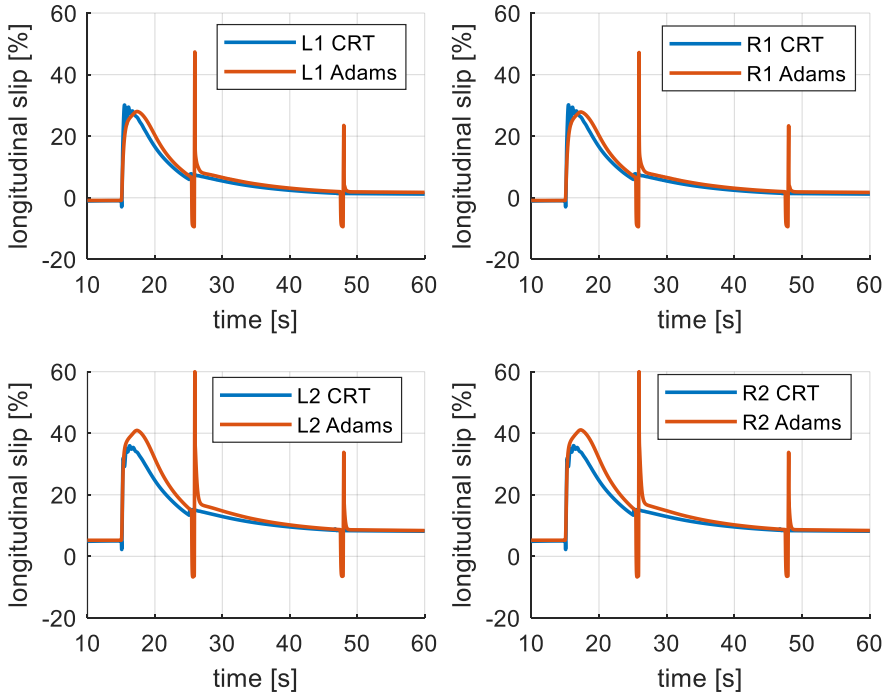

Figure 142: longitudinal slip (Offline - Acceleration - Loam Sand)

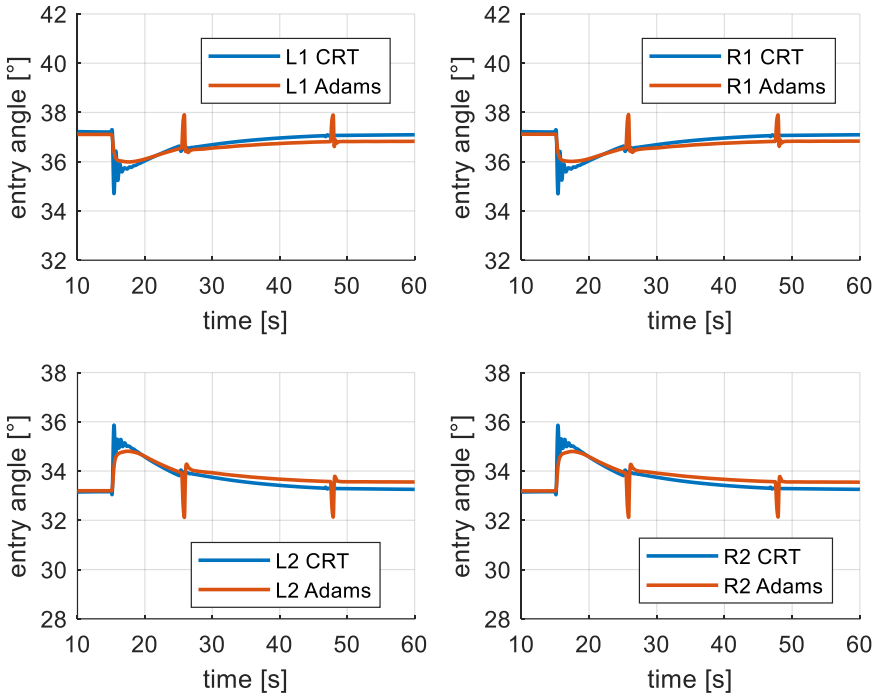

Figure 143: entry angle (Offline - Acceleration - Loam Sand)

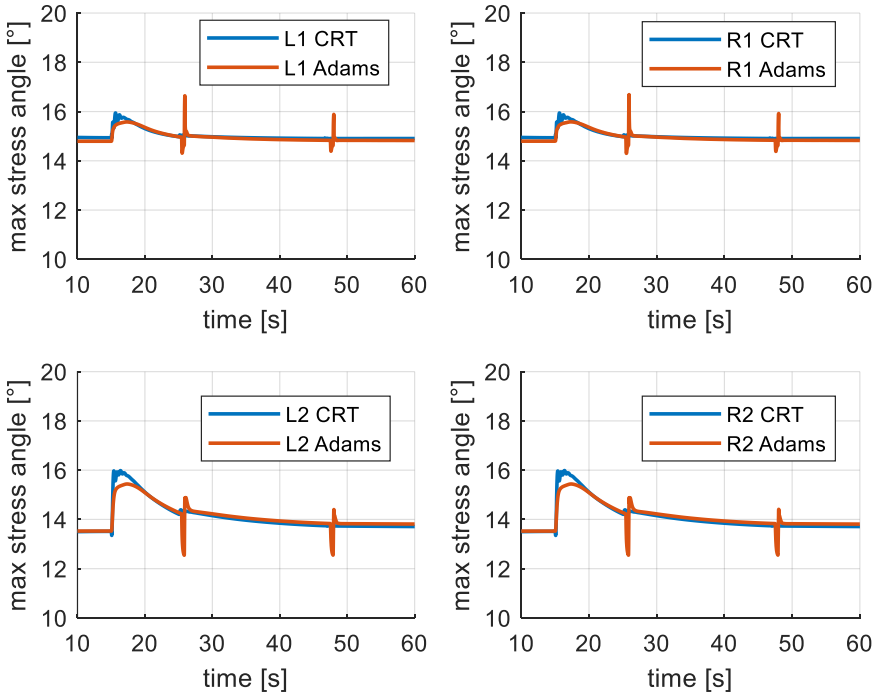

Figure 144: max stress angle (Offline - Acceleration - Loam Sand)

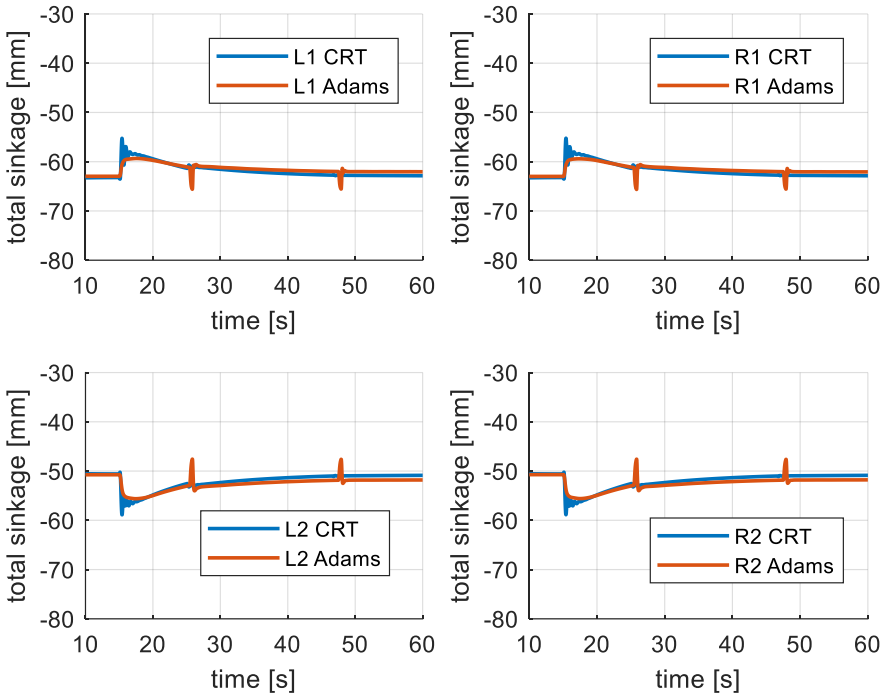

Figure 145: sinkage (Offline - Acceleration - Loam Sand)

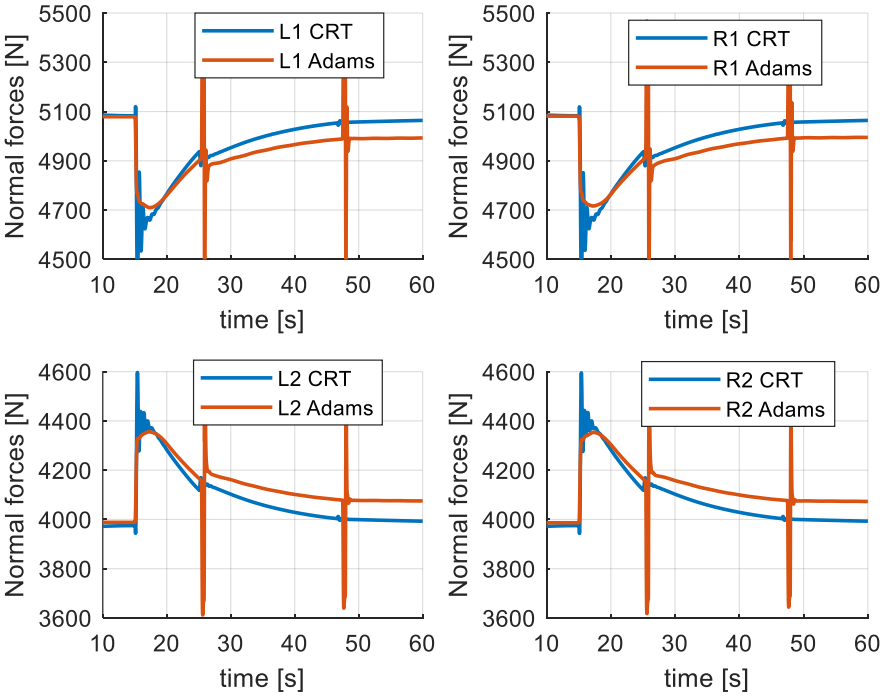

Figure 146: normal forces (Offline - Acceleration - Loam Sand)

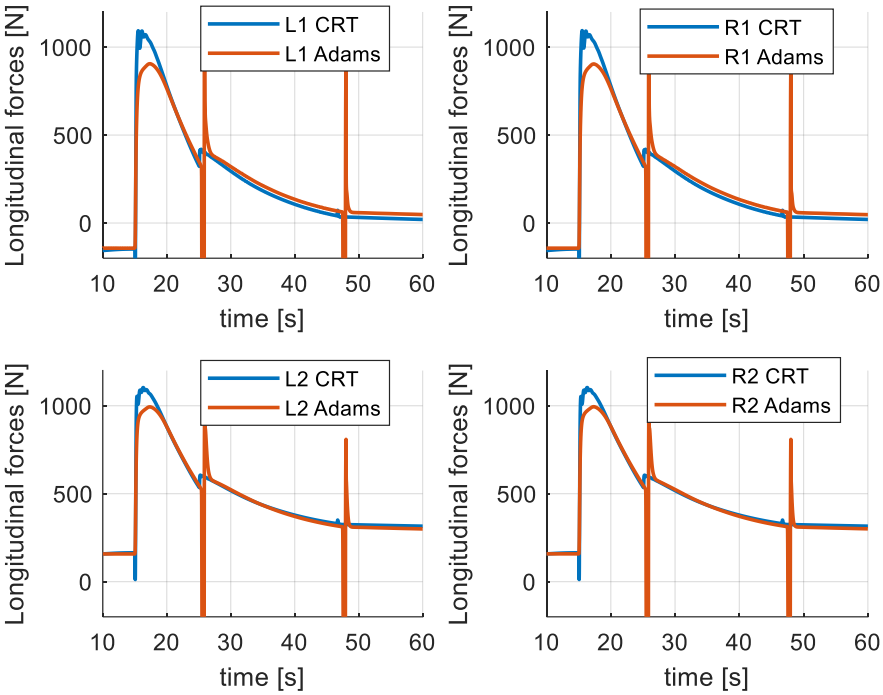

Figure 147: longitudinal forces (Offline - Acceleration - Loam Sand)

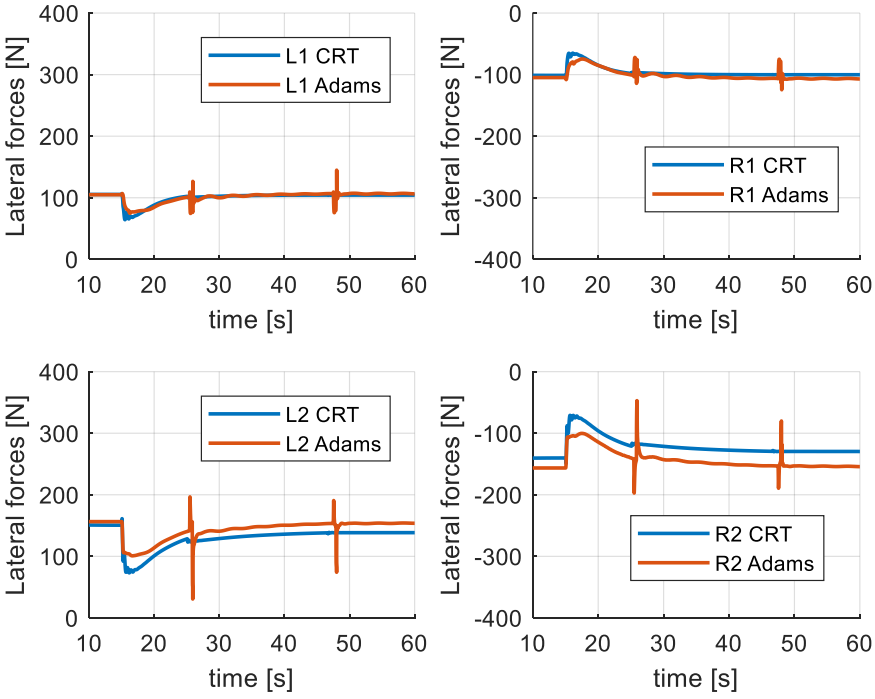

Figure 148: lateral forces (Offline - Acceleration - Loam Sand)

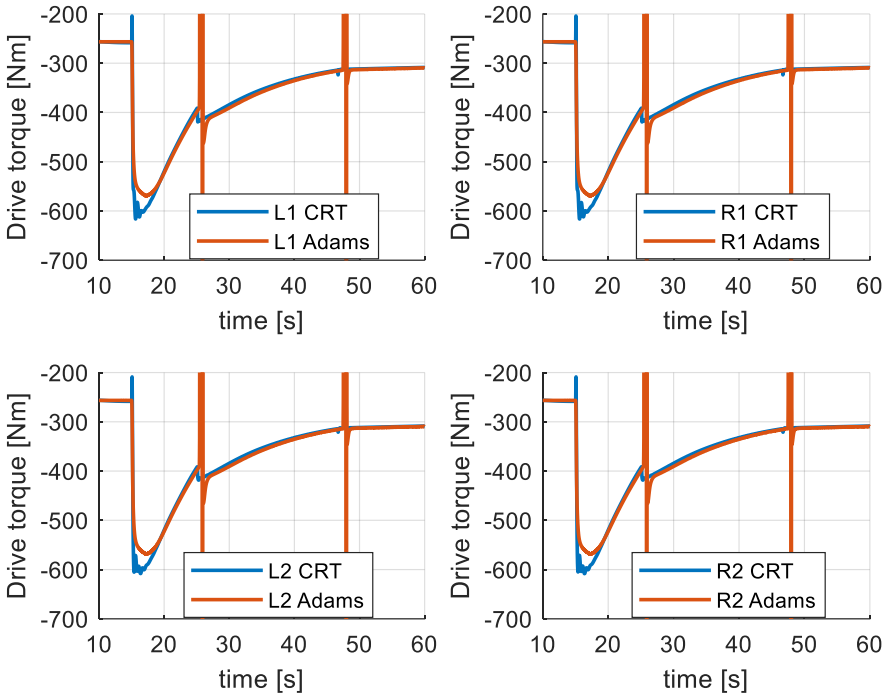

Figure 149: drive torque (Offline - Acceleration - Loam Sand)

Appendix C: dynamic driving simulator results

With reference to the simulations carried out on the dynamic driving simulator for the other two types of soil, here below the charts are reported: it is worth to highlight that, in this case, the charts are very similar to those obtained for the real-time simulation on the sand, which have been already analysed and showed in *section 10.2.1* and *10.2.2*.

Real-Time Simulation: constant speed – LETE sand

As for the simulation with the "constant speed" manoeuvre (see *section 8.1*) on "LETE sand" (soil data reported in *Tab. 2*), the results are reported here below.

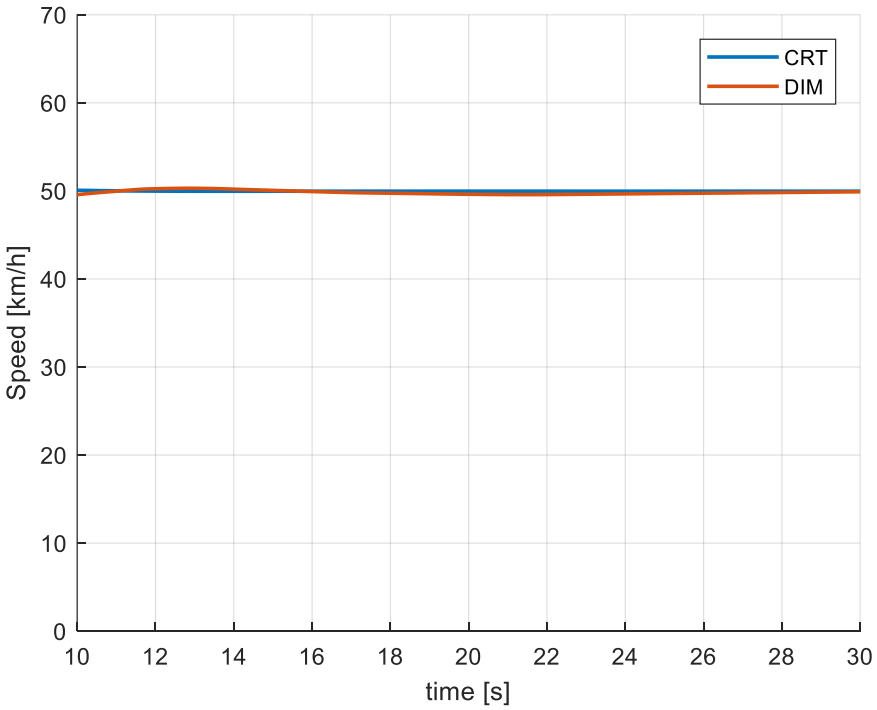

Figure 150: speed (Real-Time - Constant Speed - LETE Sand)

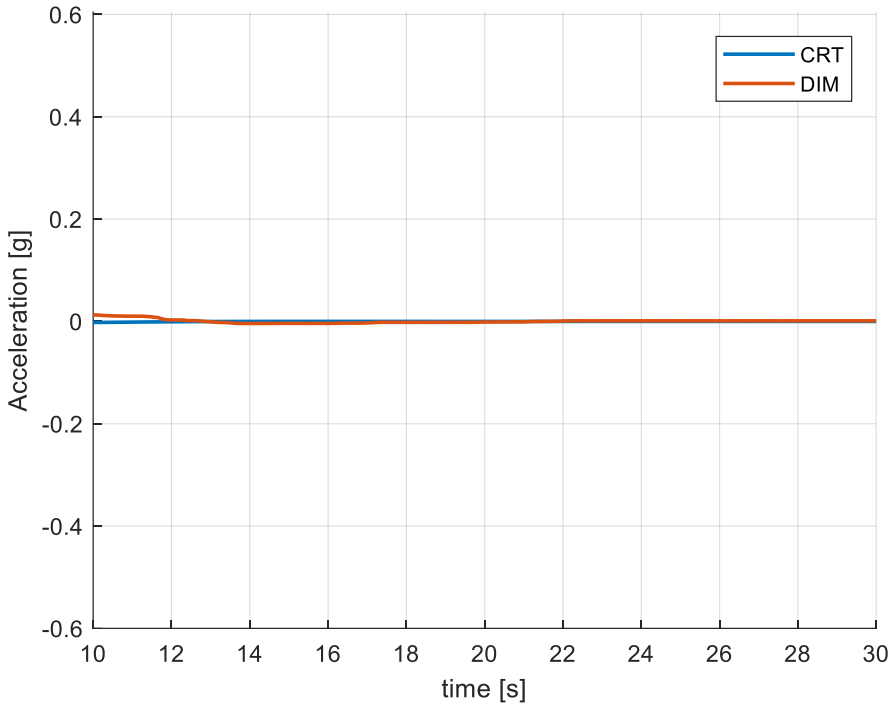

Figure 151: longitudinal acceleration (Real-Time - Constant Speed - LETE Sand)

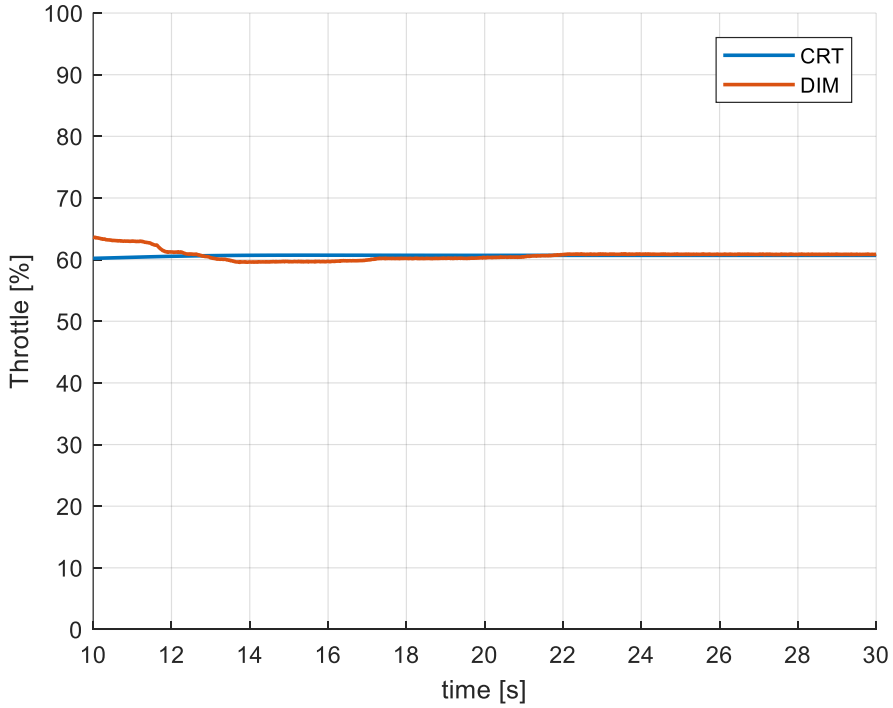

Figure 152: throttle demand (Real-Time - Constant Speed - LETE Sand)

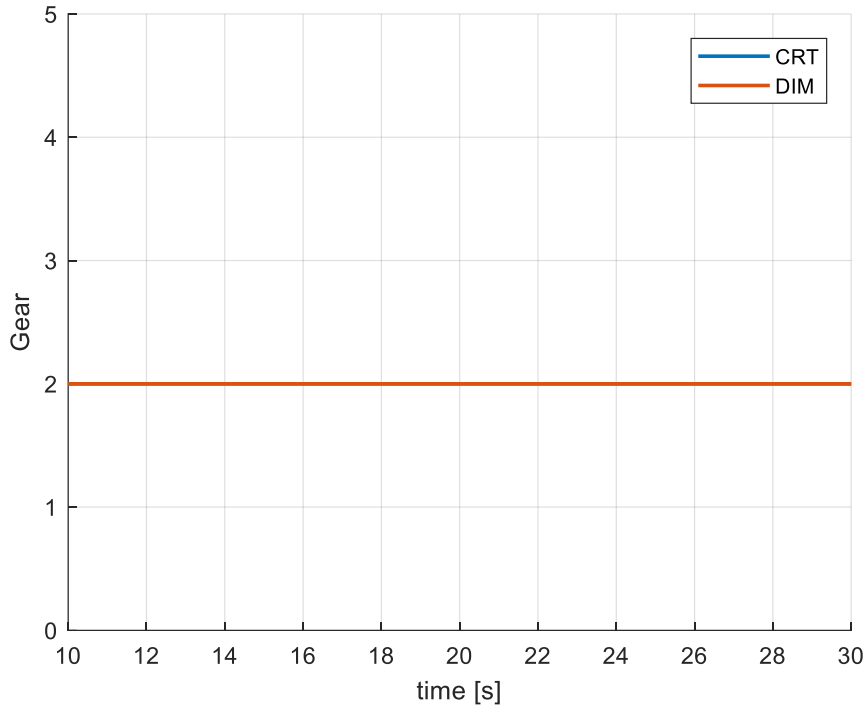

Figure 153: gear demand (Real-Time - Constant Speed - LETE Sand)

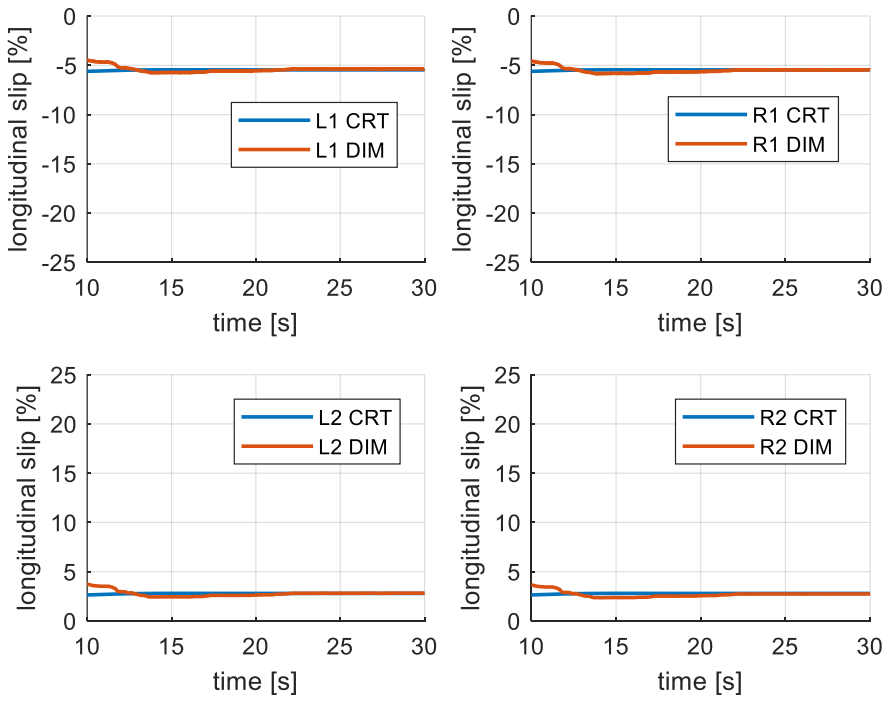

Figure 154: longitudinal slip (Real-Time - Constant Speed - LETE Sand)

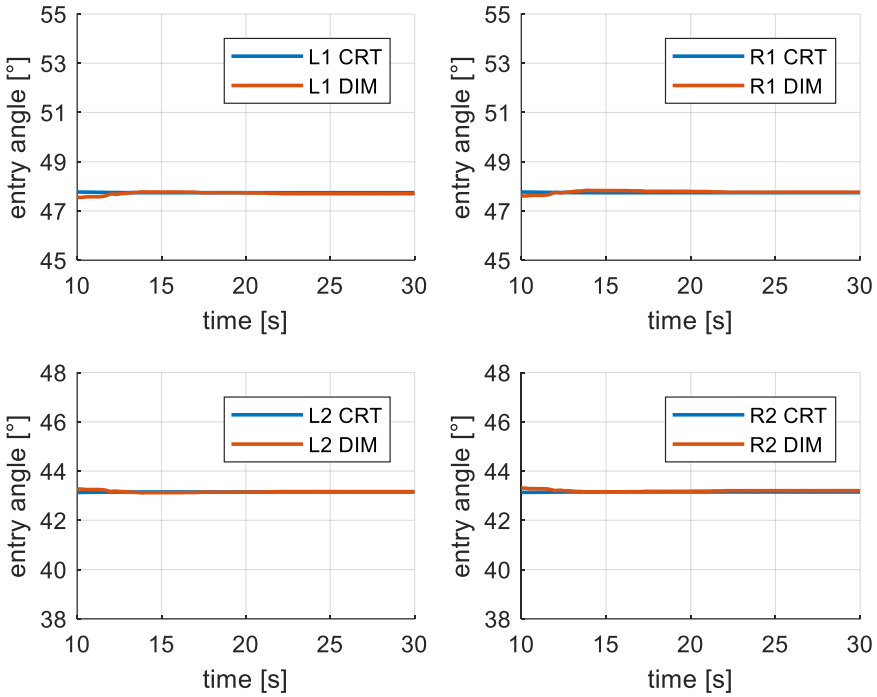

Figure 155: entry angle (Real-Time - Constant Speed - LETE Sand)

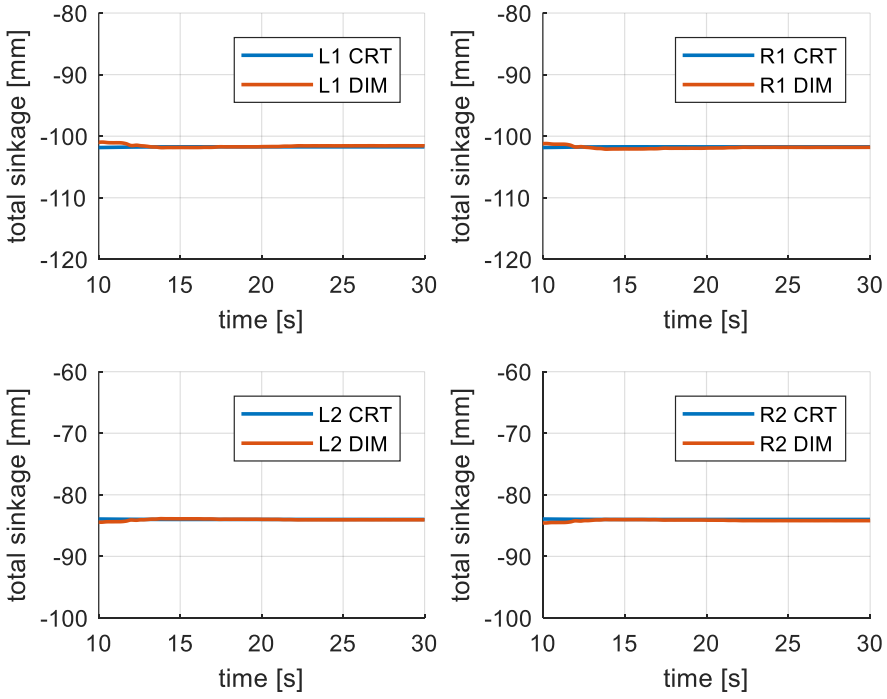

Figure 156: sinkage (Real-Time - Constant Speed - LETE Sand)

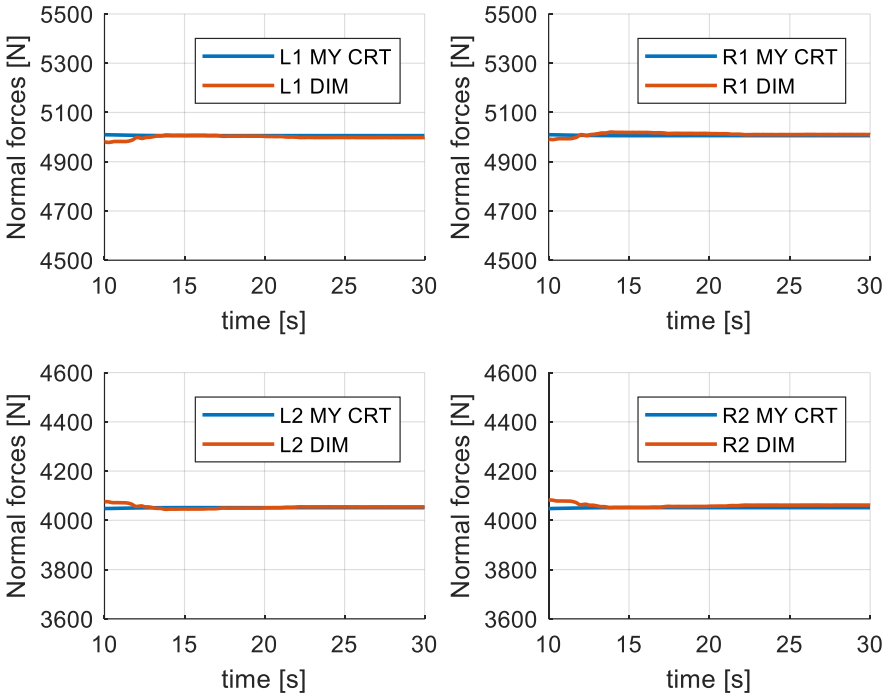

Figure 157: normal forces (Real-Time - Constant Speed - LETE Sand)

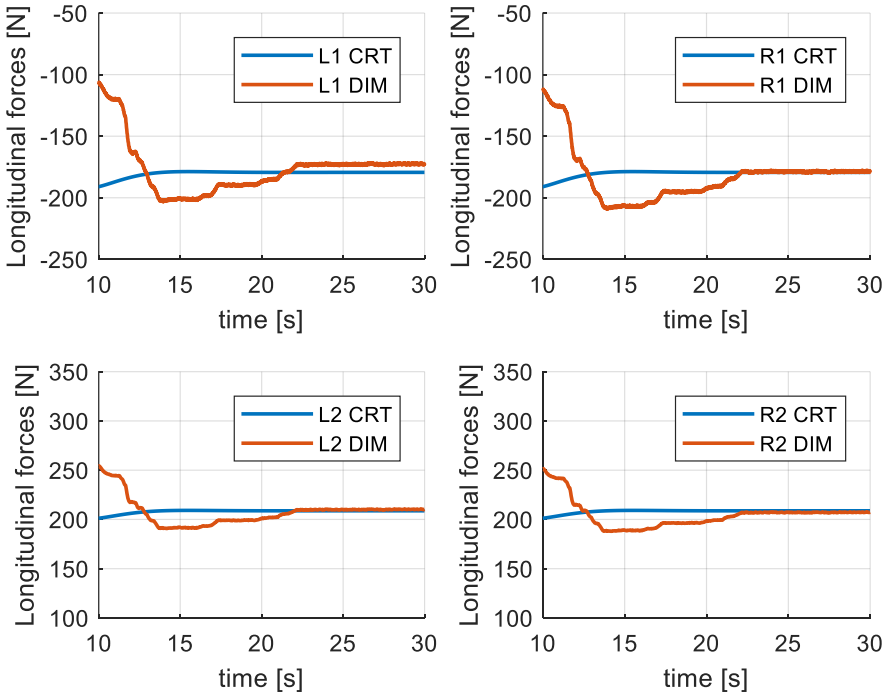

Figure 158: longitudinal forces (Real-Time - Constant Speed - LETE Sand)

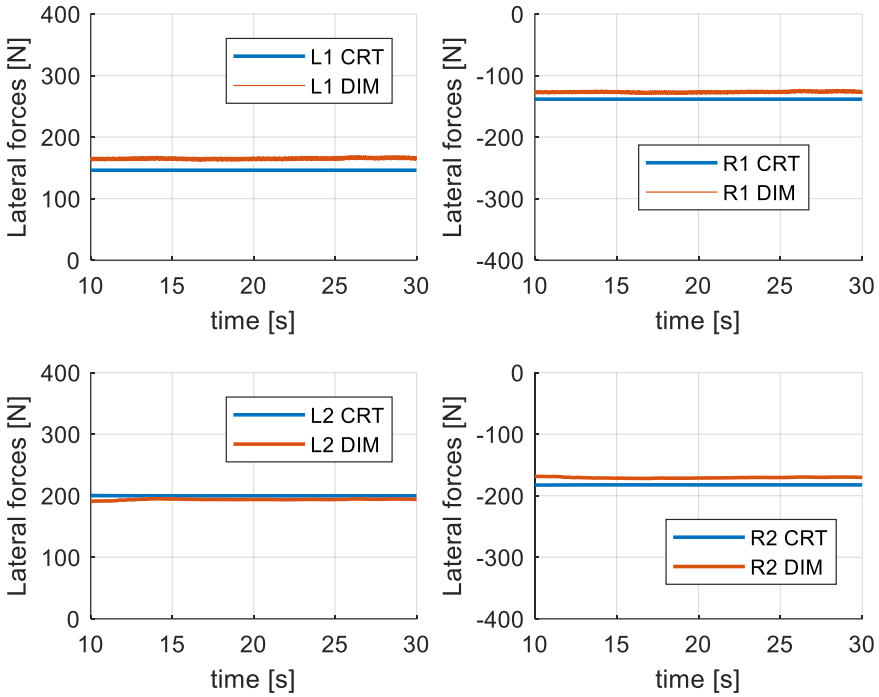

Figure 159: lateral forces (Real-Time - Constant Speed - LETE Sand)

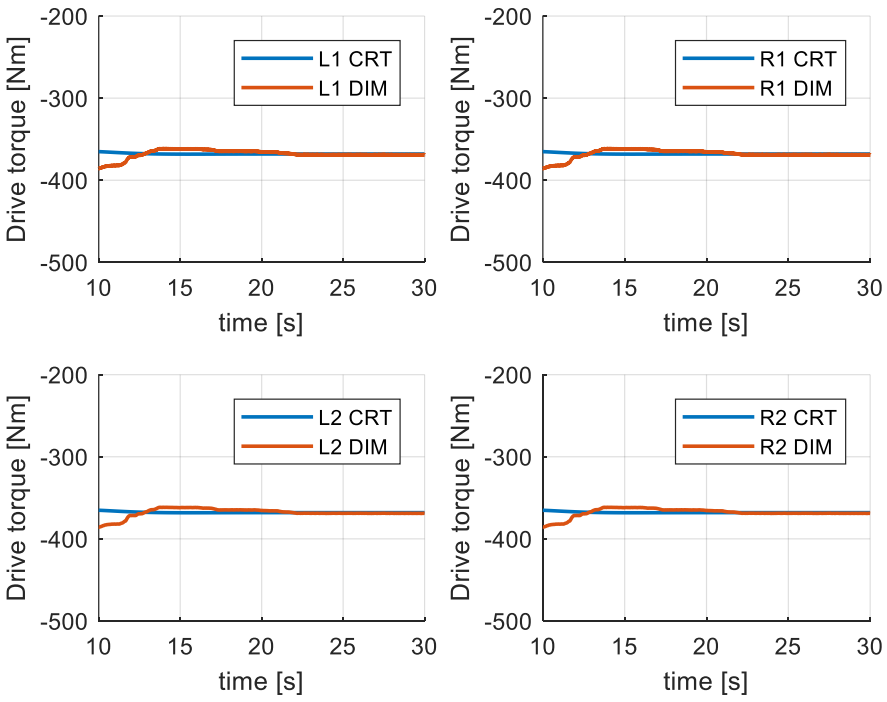

Figure 160: drive torque (Real-Time - Constant Speed - LETE Sand)

Real-Time Simulation: acceleration -LETE sand

As for the simulation with the "acceleration" manoeuvre (see *section 8.1*) on "LETE sand" (soil data reported in *Tab. 2*), the results are reported here below.

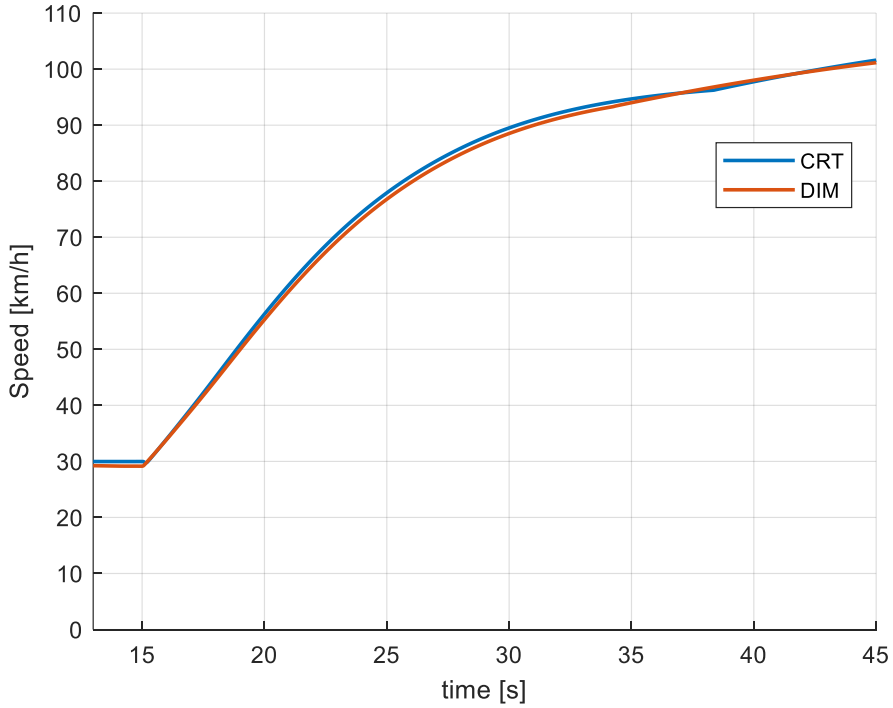

Figure 161: speed (Real-Time - Acceleration - LETE Sand)

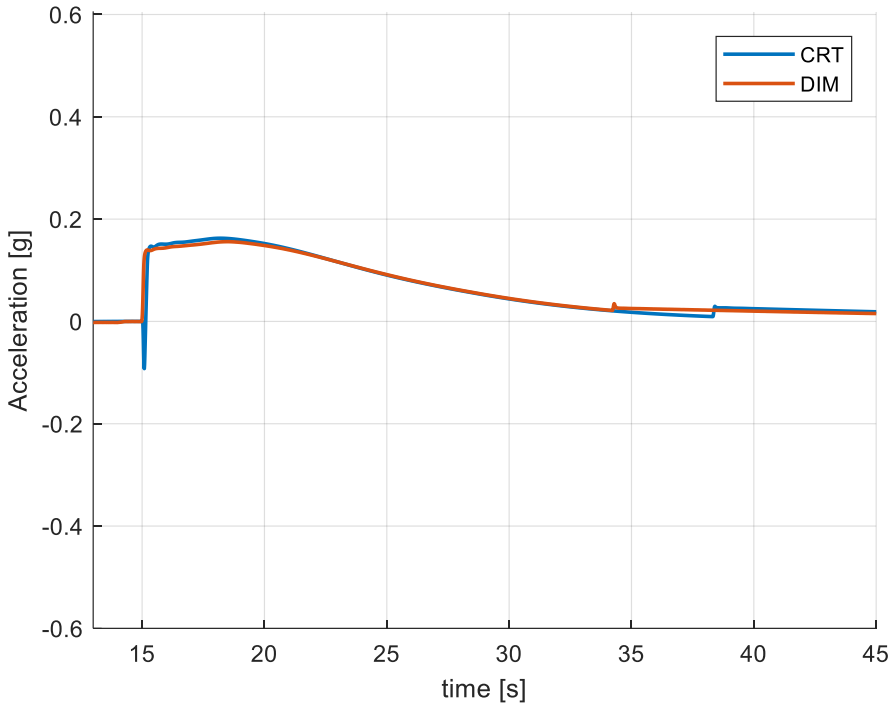

Figure 162: longitudinal acceleration (Real-Time - Acceleration - LETE Sand)

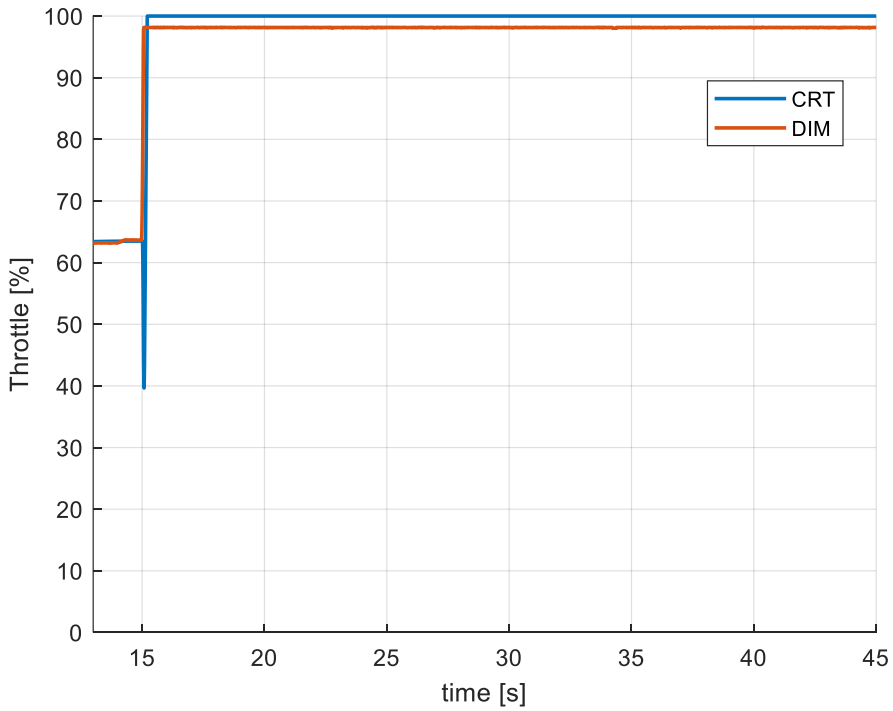

Figure 163: throttle demand (Real-Time - Acceleration - LETE Sand)

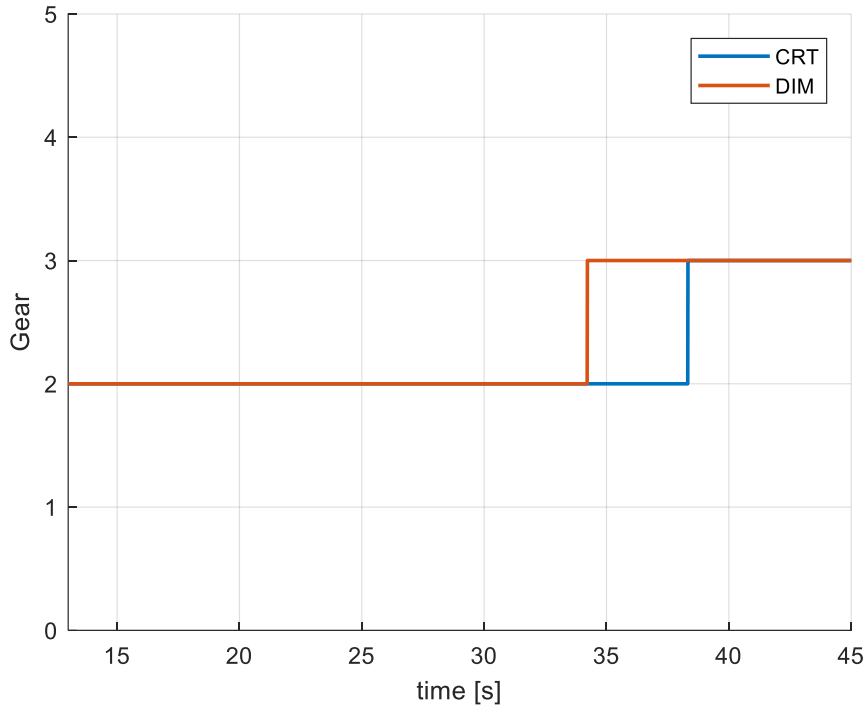

Figure 164: gear demand (Real-Time - Acceleration - LETE Sand)

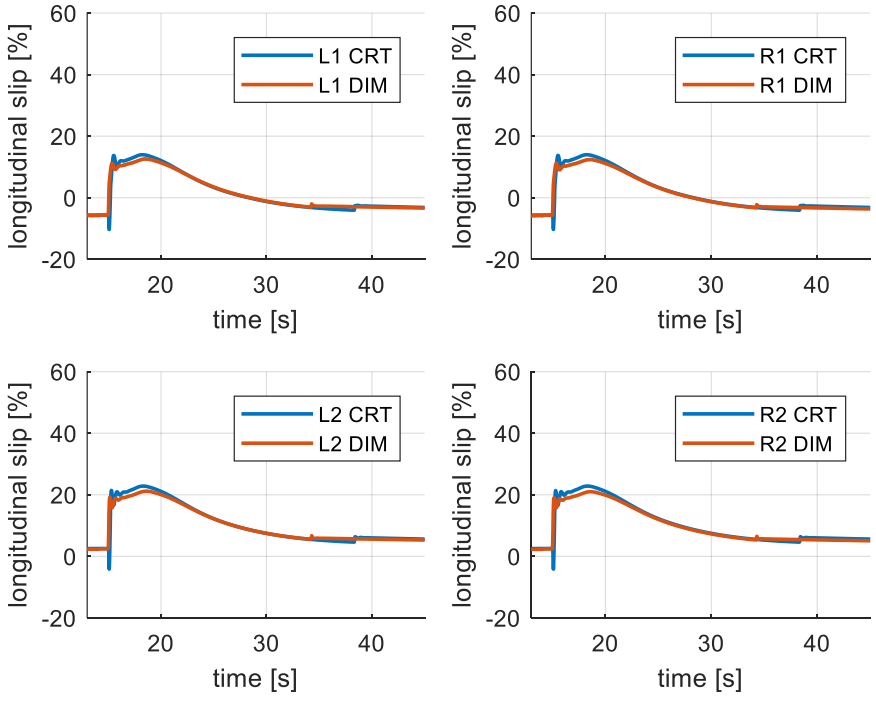

Figure 165: longitudinal slip (Real-Time - Acceleration - LETE Sand)

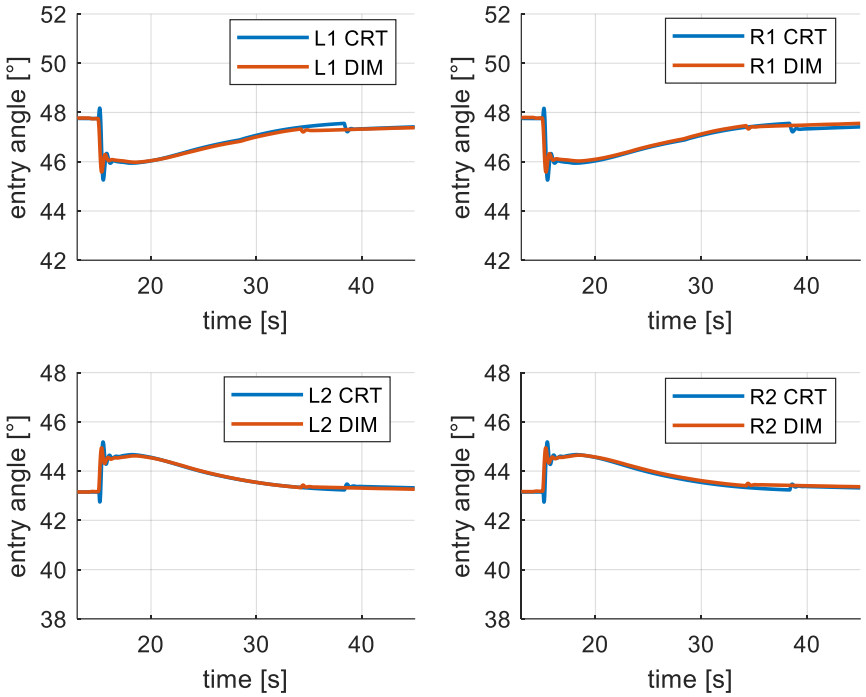

Figure 166: entry angle (Real-Time - Acceleration - LETE Sand)

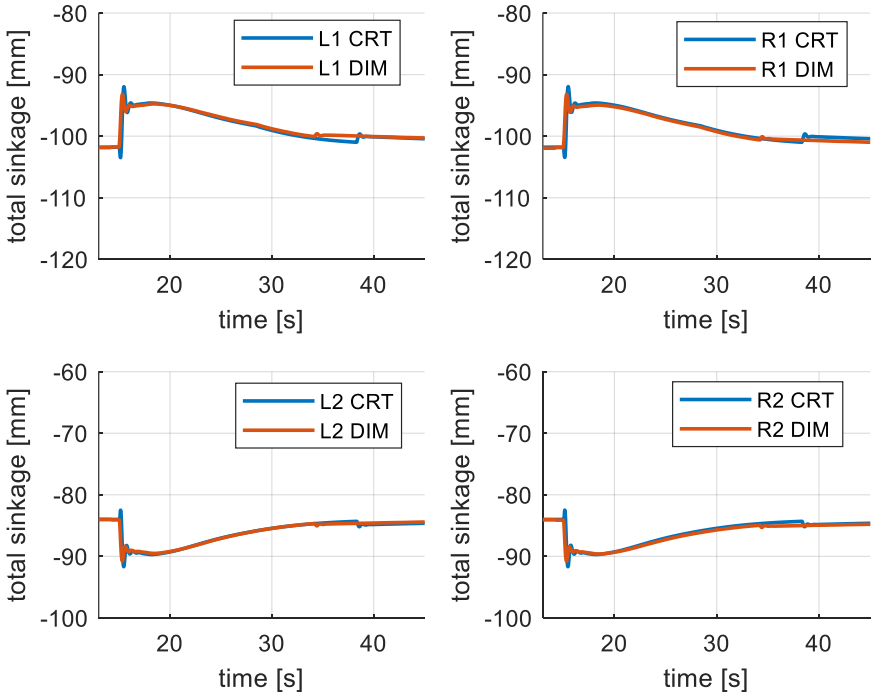

Figure 167: sinkage (Real-Time - Acceleration - LETE Sand)

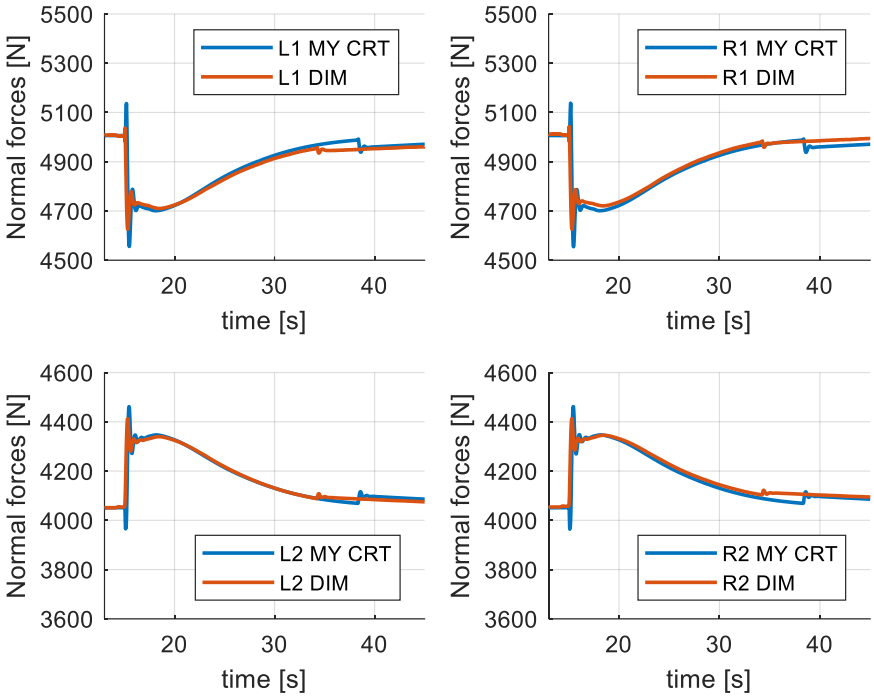

Figure 168: normal forces (Real-Time - Acceleration - LETE Sand)

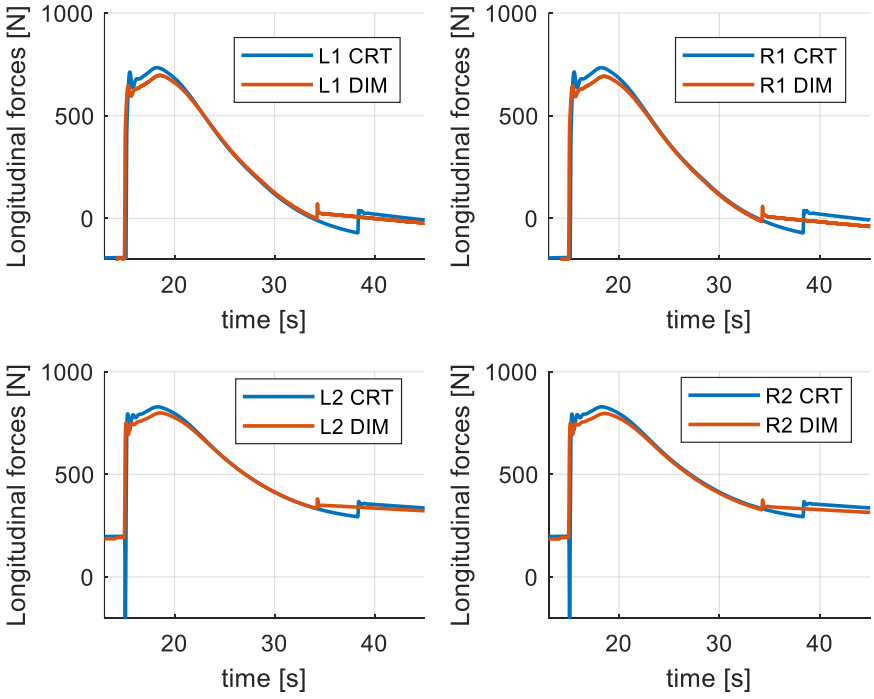

Figure 169: longitudinal forces (Real-Time - Acceleration - LETE Sand)

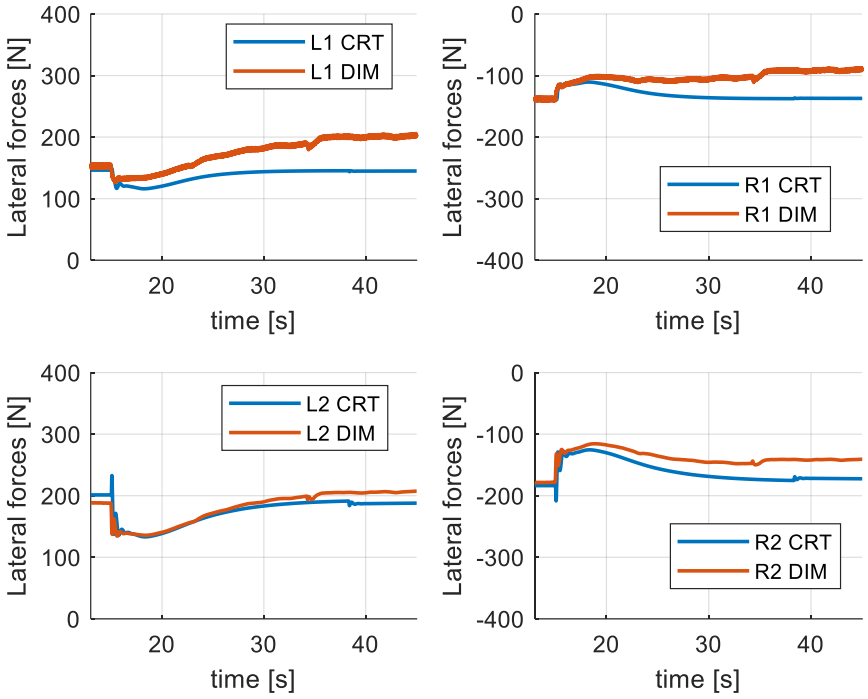

Figure 170: lateral forces (Real-Time - Acceleration - LETE Sand)

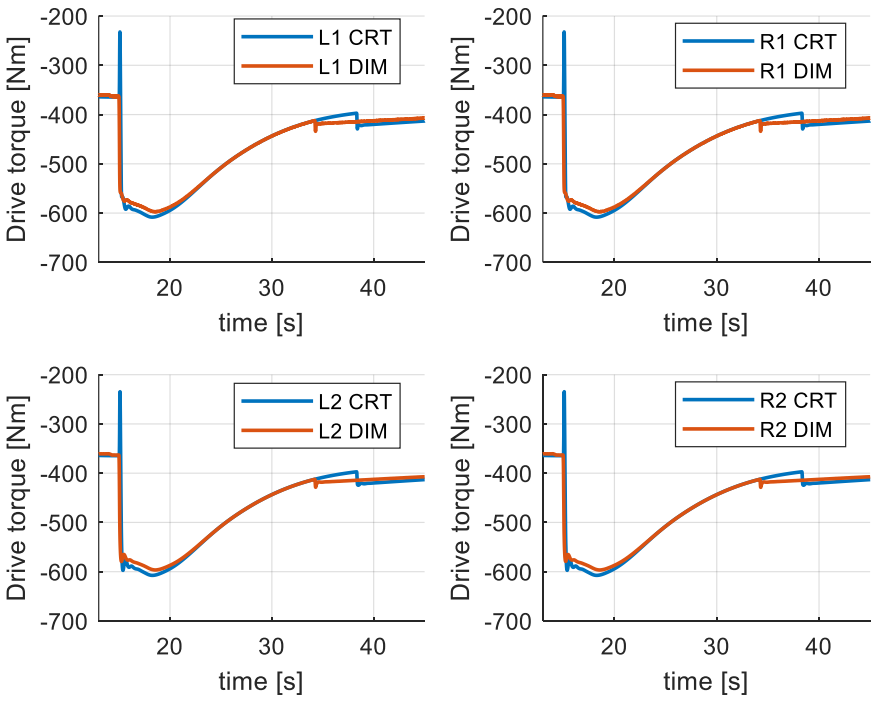

Figure 171: drive torque (Real-Time - Acceleration - LETE Sand)

Real-Time Simulation: constant speed – loam sand

As for the simulation with the "constant speed" manoeuvre (see *section 8.1*) on "loam sand" (soil data reported in *Tab. 3*), the results are reported here below.

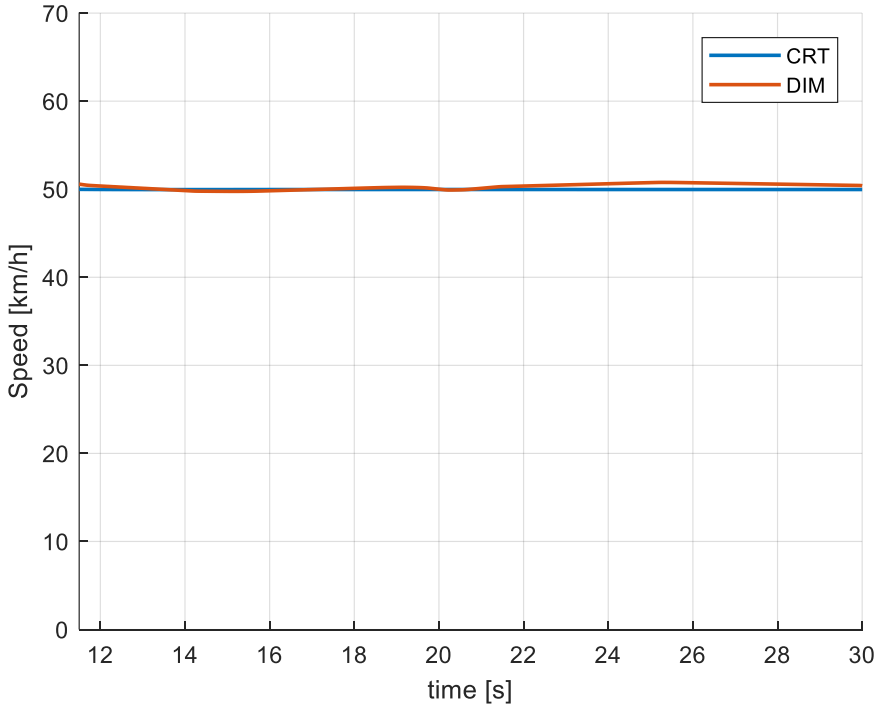

Figure 172: speed (Real-Time - Constant Speed - Loam Sand)

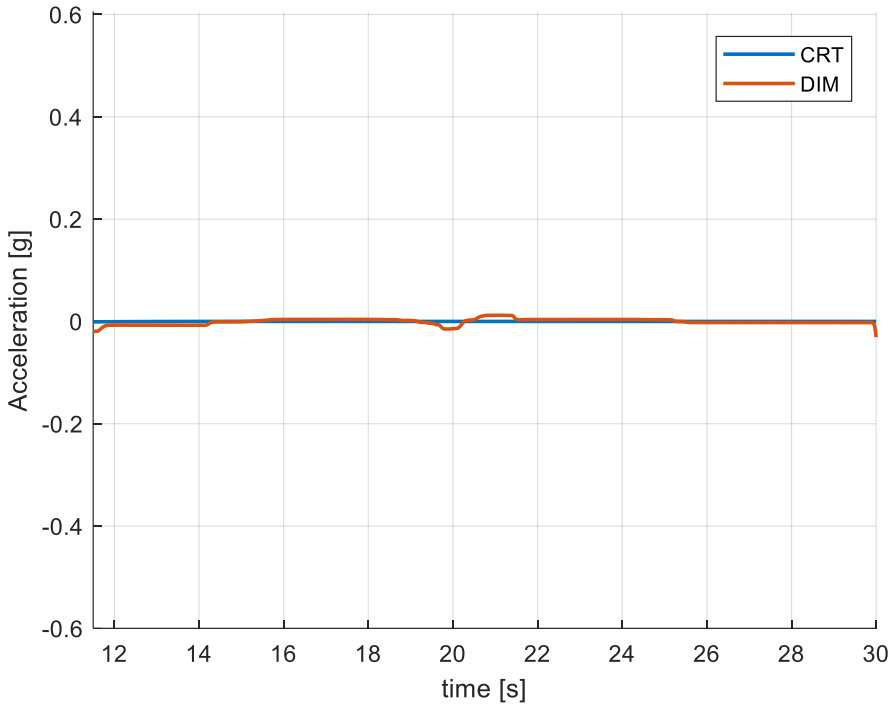

Figure 173: longitudinal acceleration (Real-Time - Constant Speed - Loam Sand)

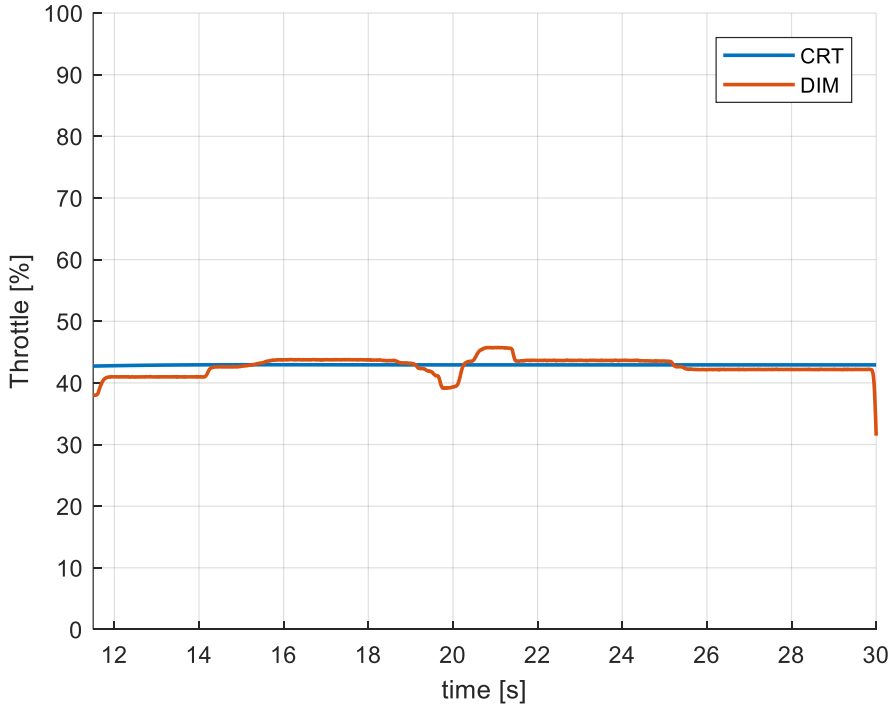

Figure 174: throttle demand (Real-Time - Constant Speed - Loam Sand)

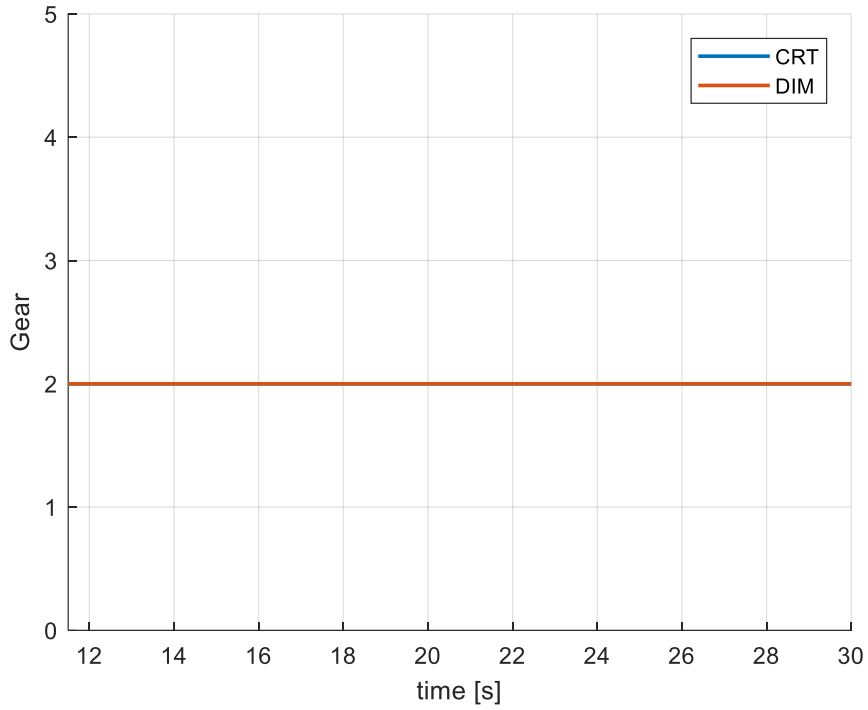

Figure 175: gear demand (Real-Time - Constant Speed - Loam Sand)

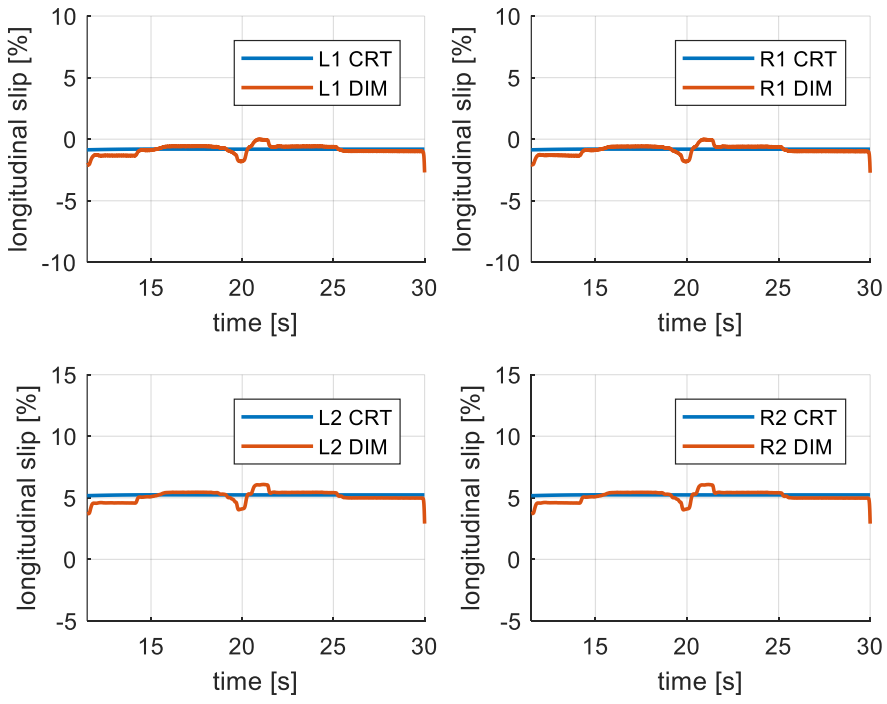

Figure 176: longitudinal slip (Real-Time - Constant Speed - Loam Sand)

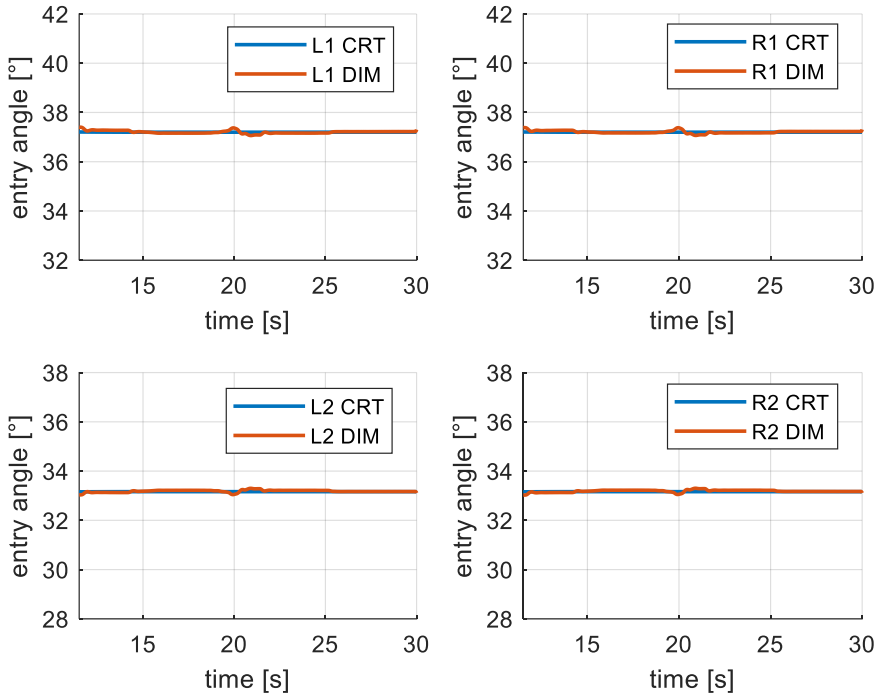

Figure 177: entry angle (Real-Time - Constant Speed - Loam Sand)

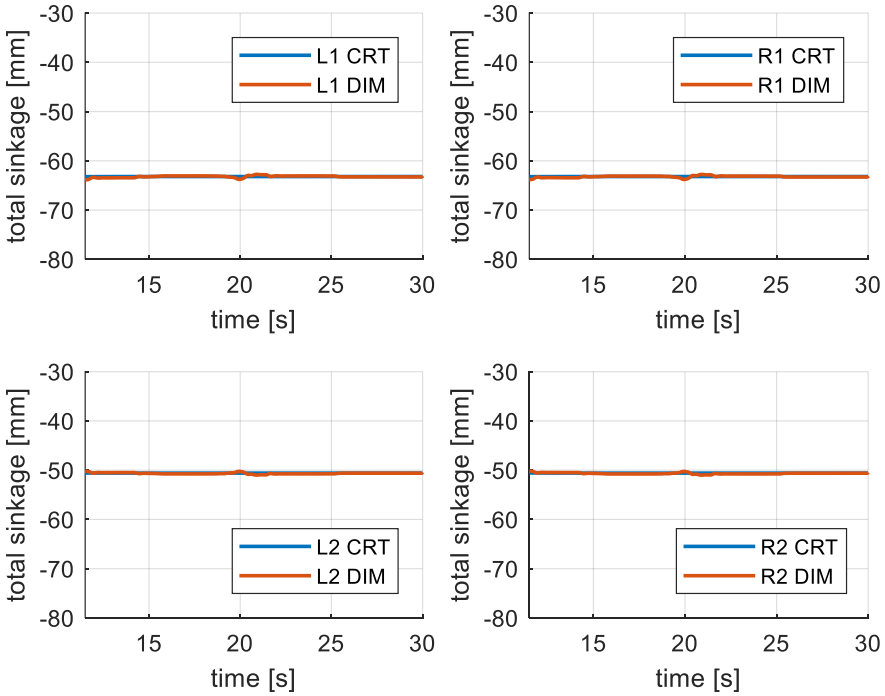

Figure 178: sinkage (Real-Time - Constant Speed - Loam Sand)

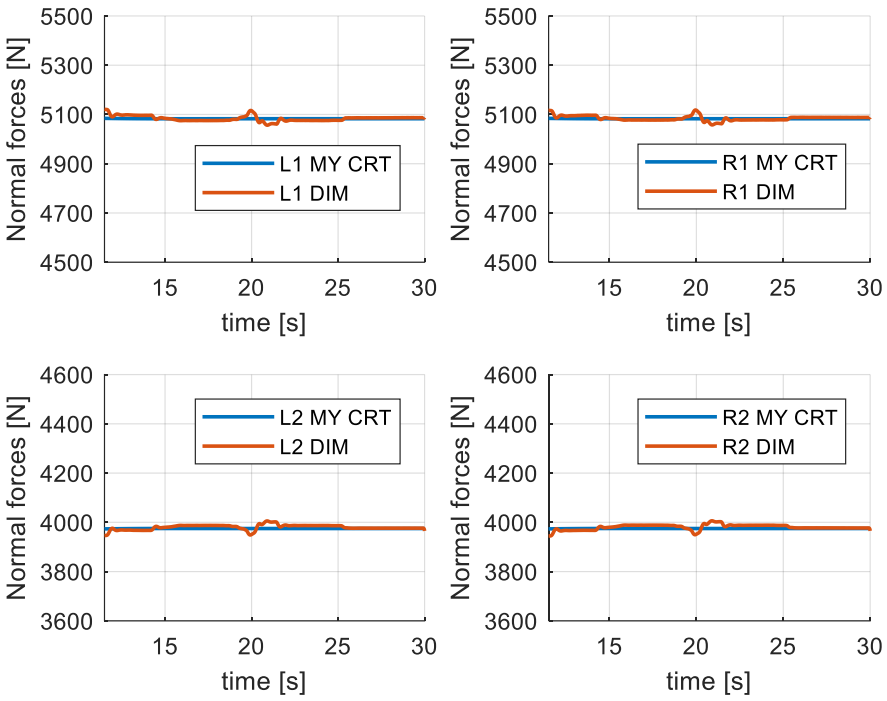

Figure 179: normal forces (Real-Time - Constant Speed - Loam Sand)

Observing the unusual behaviour of longitudinal forces (*Fig. 180*), it is possible to notice the influence of boundary conditions: indeed, the trend is caused by the trend of throttle demand.

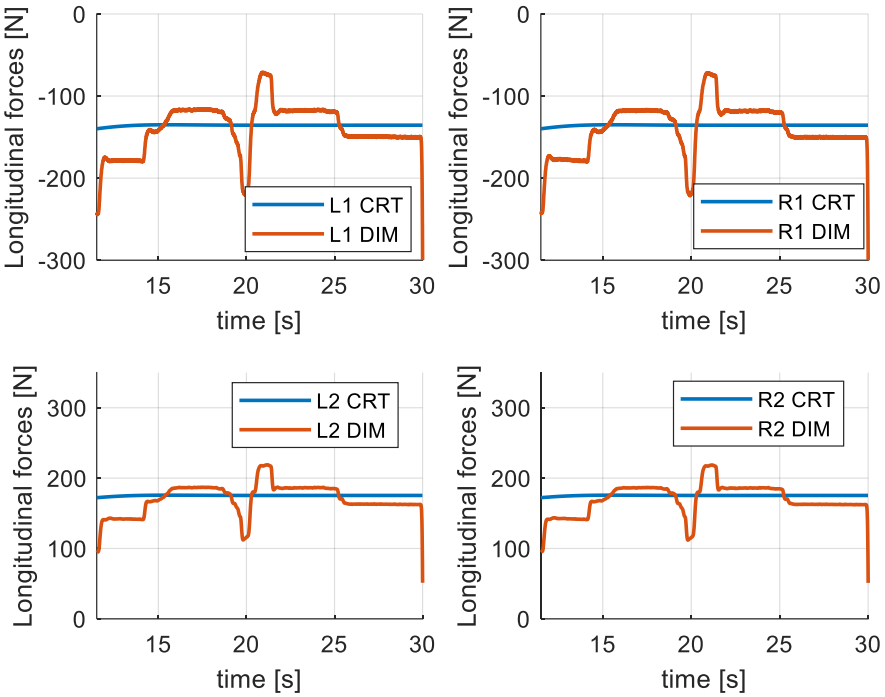

Figure 180: longitudinal forces (Real-Time - Constant Speed - Loam Sand)

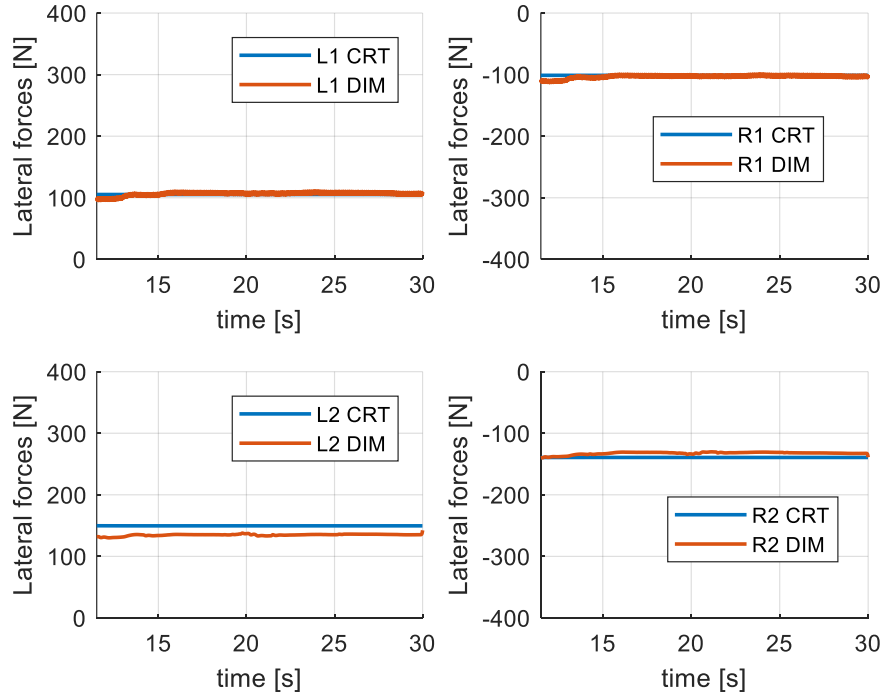

Figure 181: lateral forces (Real-Time - Constant Speed - Loam Sand)

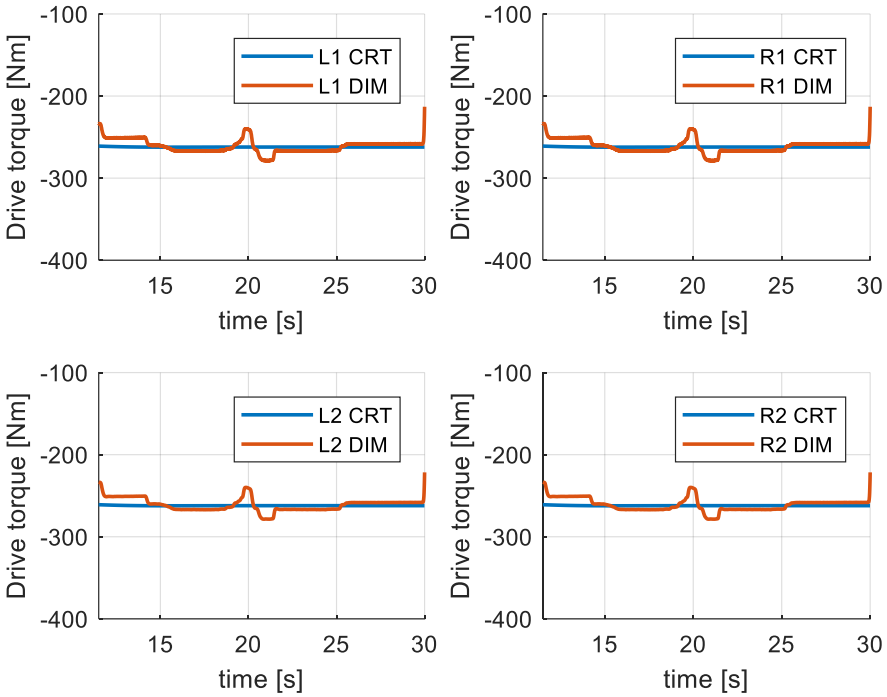

Figure 182: drive torque (Real-Time - Constant Speed - Loam Sand)

Real-Time Simulation: acceleration – loam sand

As for the simulation with the "acceleration" manoeuvre (see *section 8.1*) on "loam sand" (soil data reported in *Tab. 3*), the results are reported here below.

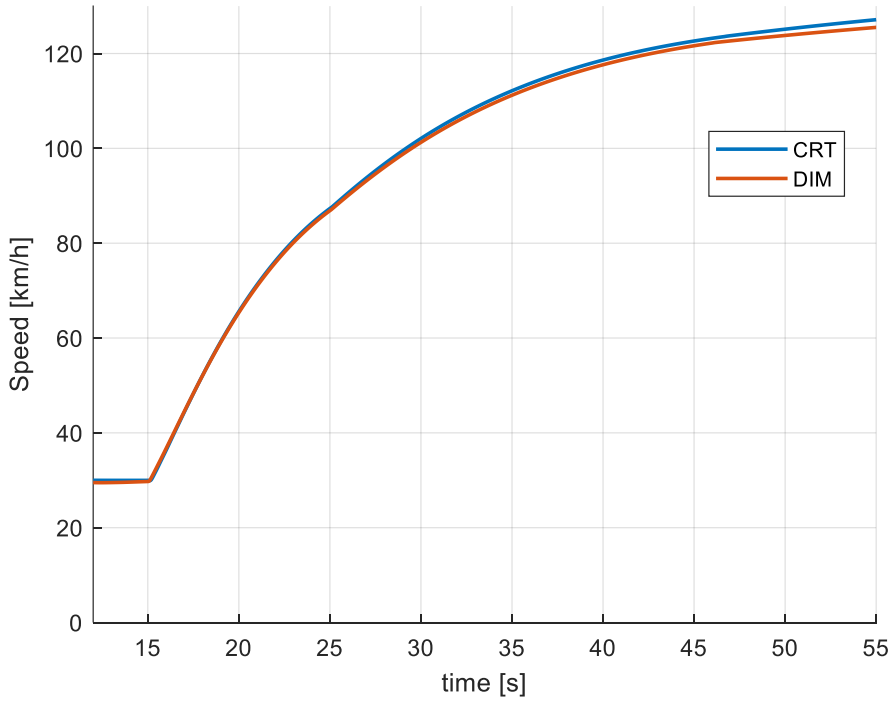

Figure 183: speed (Real-Time - Acceleration - Loam Sand)

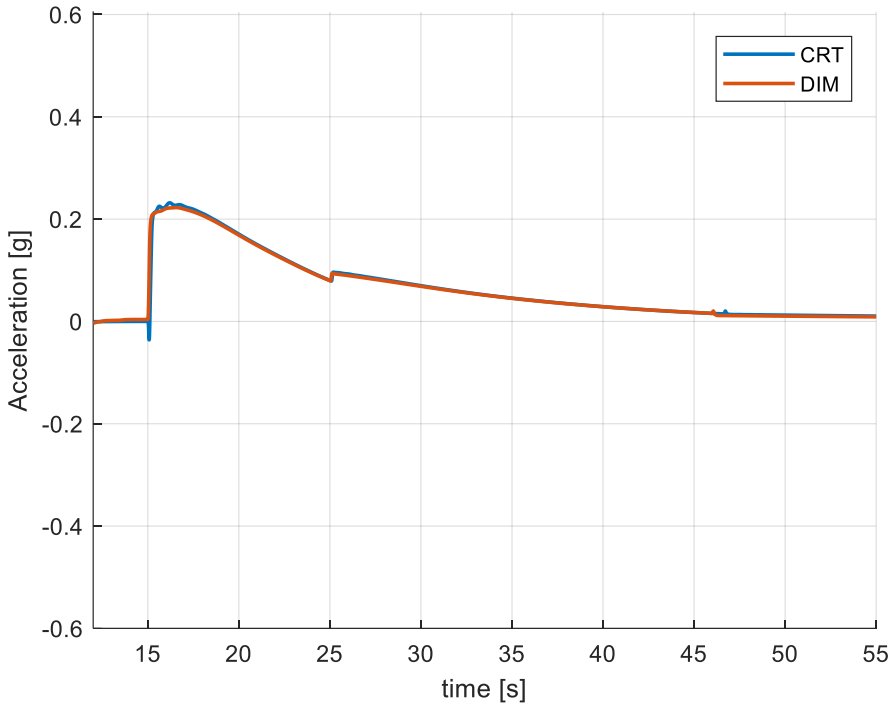

Figure 184: longitudinal acceleration (Real-Time - Acceleration - Loam Sand)

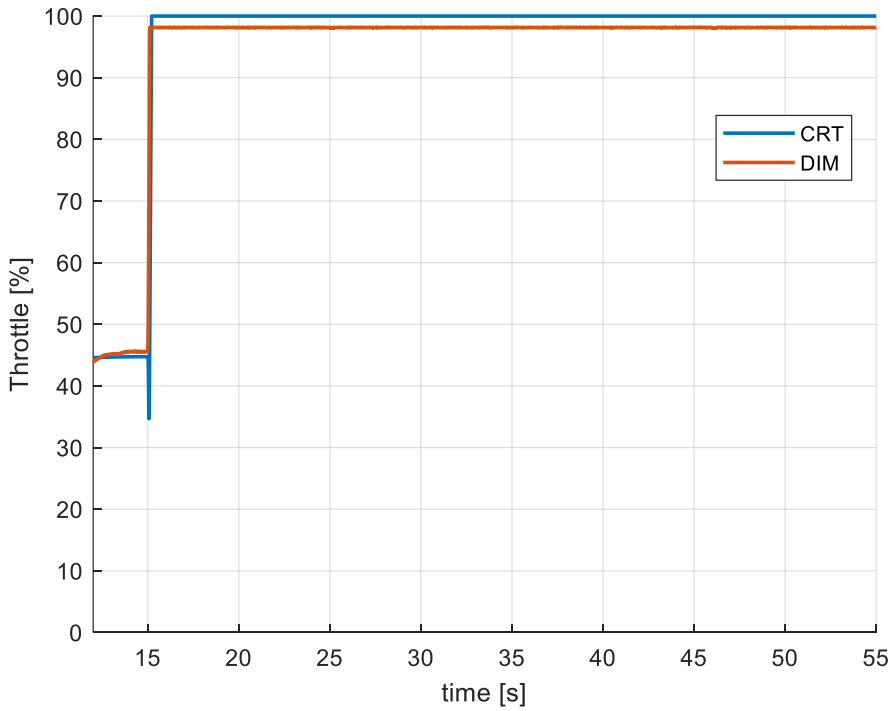

Figure 185: throttle demand (Real-Time - Acceleration - Loam Sand)

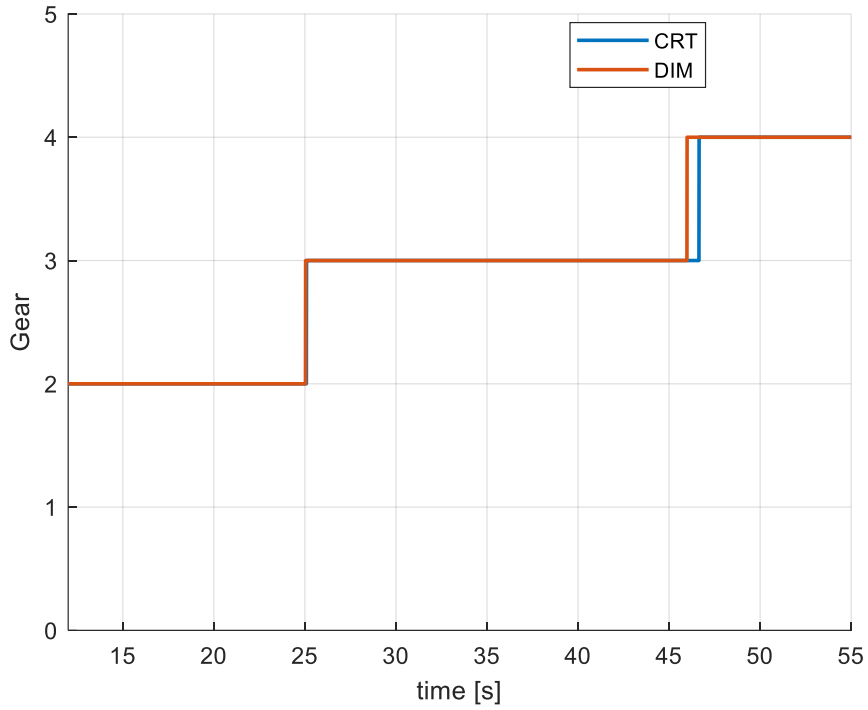

Figure 186: gear demand (Real-Time - Acceleration - Loam Sand)

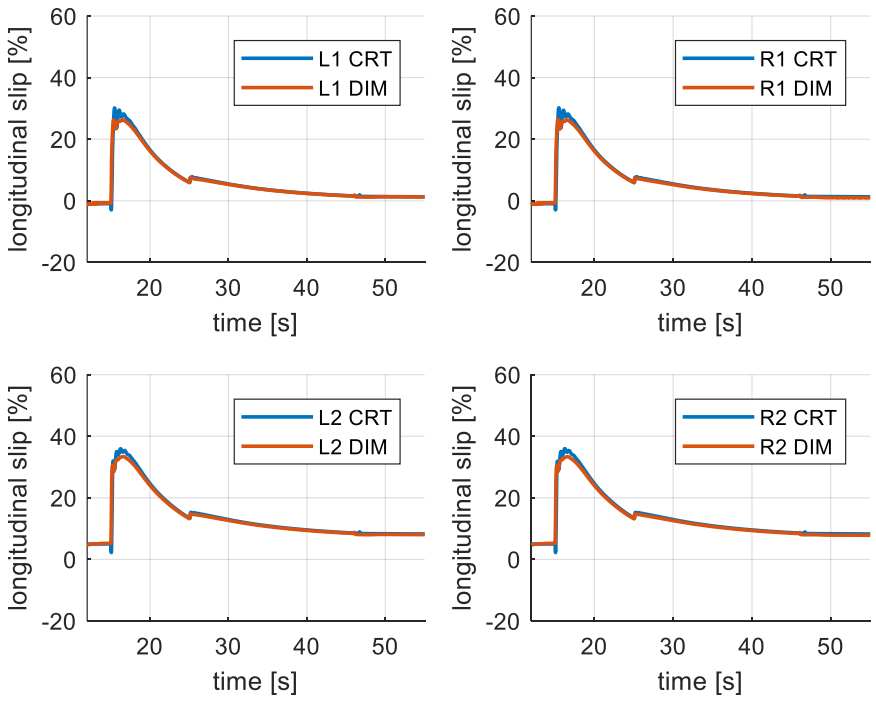

Figure 187: longitudinal slip (Real-Time - Acceleration - Loam Sand)

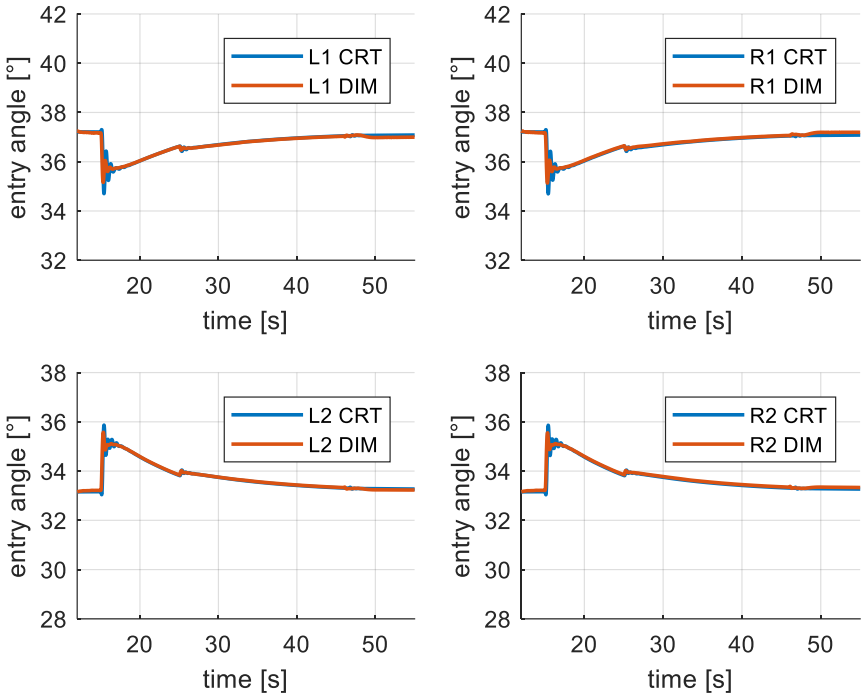

Figure 188: entry angle (Real-Time - Acceleration - Loam Sand)

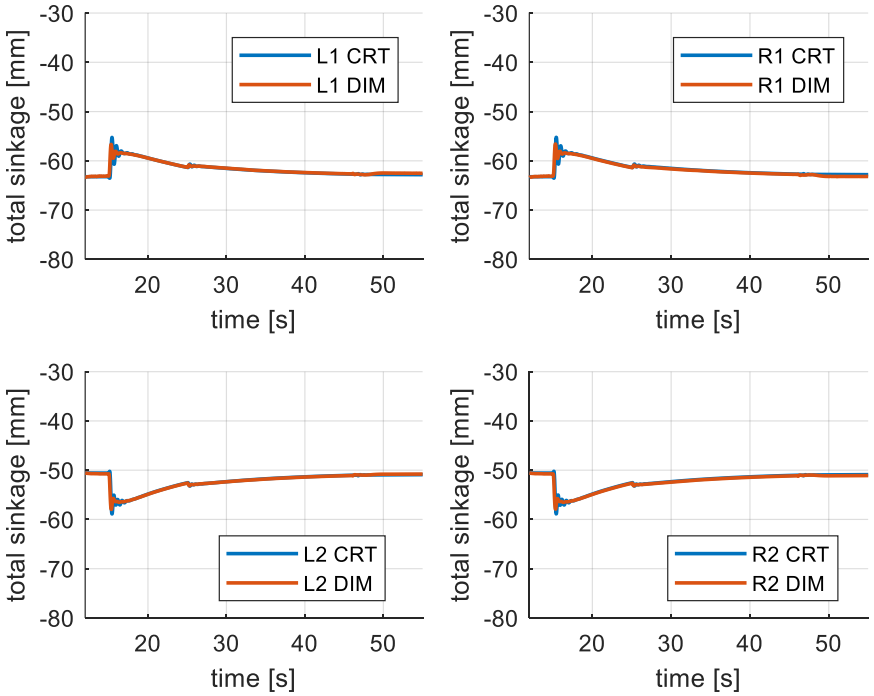

Figure 189: sinkage (Real-Time - Acceleration - Loam Sand)

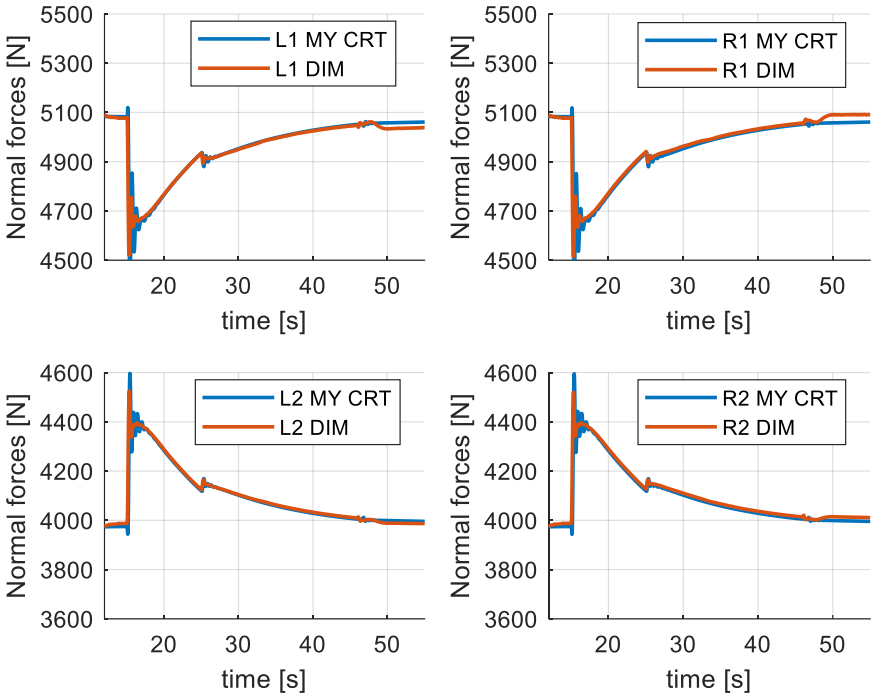

Figure 190: normal forces (Real-Time - Acceleration - Loam Sand)

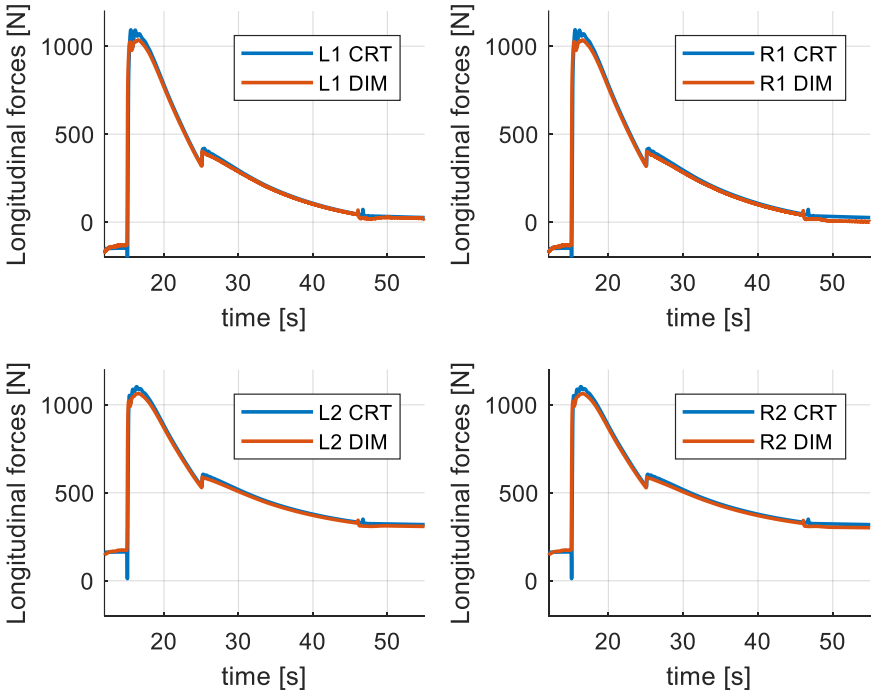

Figure 191: longitudinal forces (Real-Time - Acceleration - Loam Sand)

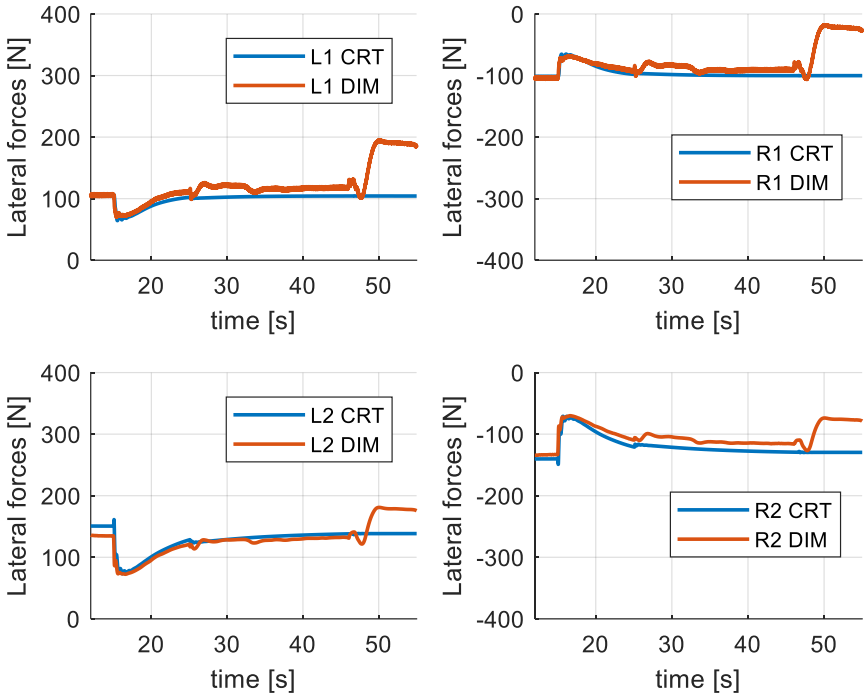

Figure 192: lateral forces (Real-Time - Acceleration - Loam Sand)

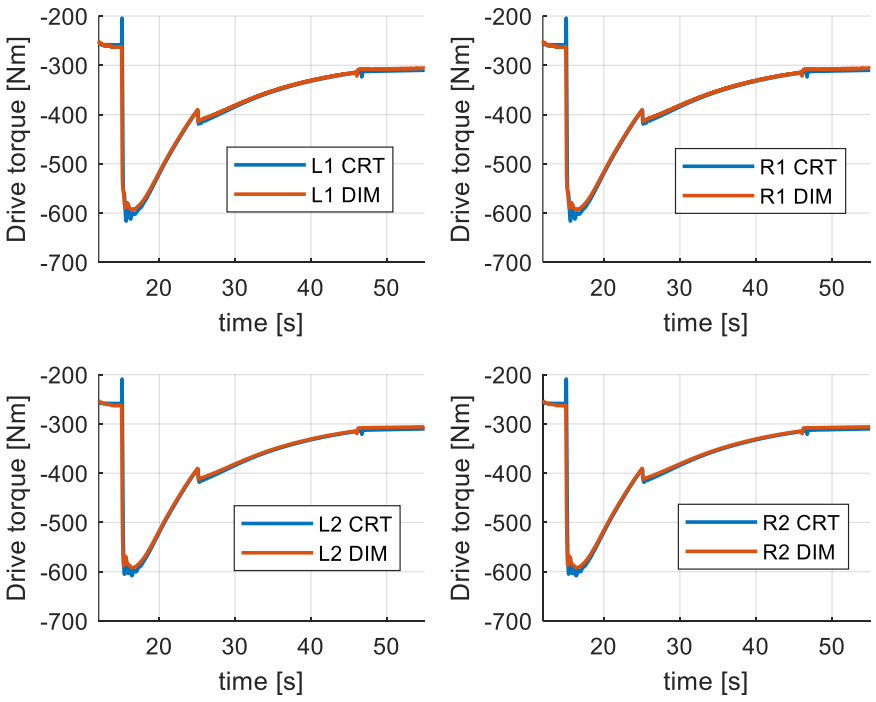

Figure 193: drive torque (Real-Time - Acceleration - Loam Sand)

Bibliography

[1] J. Y. Wong, Terramechanics and Off-Road vehicle engineering, 2010.

[2] S. Taheri, C. Sandu, S. Taheri, E. Pinto and D. Gorsich, "A technical survey on Terramechanics models for tire-terrain interaction used in modeling and simulation of wheeled vehicles," *Journal of Terramechanics,* 2015.

[3] B. J.-Y. Chan, "Development of an Off-Road capable tire model for vehicle dynamics simulations," 2008.

[4] B. J. Chan and C. Sandu, "Development of a 3-D quasi-steady-state tyre model for on-road and off-road vehicle dynamics simulations: Part II – off-road rigid wheel model," 2014.

[5] B. J. Chan and C. Sandu, "Development of a 3-D quasi-steady-state tyre model for on-road and off-road vehicle dynamics simulations: Part III – off-road flexible tyre model," 2014.

[6] C. Senatore and C. Sandu, "Off-road tire modeling and the multi-pass effect for dyamics simulation," *Journal of Terramechanics,* 2011.

[7] W. C. Smith, "Modeling of Wheel-Soil Interaction for Small Ground Vehicles," 2014.

[8] J.-y. Wong and A. R. Reece, "Prediction of rigid wheel performance based on the analysis of soil-wheel stresses: part I (performance of driven rigid wheels)," *Journal of Terramechanics,* 1967.

[9] C. Harnisch, B. Lach, R. Jakobs, M. Troulis and O. Nehls, "A new tyre–soil interaction model for vehicle simulation on deformable ground," *Vehicle System Dynamic,* 2011.

[10] I. C. Holm, "Multi-pass behaviour of pneumatic tires," *Journal of Terramechanics,* 1969.

[11] E. Hegedus, "A simplified method for the determination of bulldozing resistance," *Land Locomotion Research Laboratory, Army Tank Automotive Command Report,* 1960.

[12] K. Terzaghi, P. Ralph B. and M. Gholamreza, Soil mechanics in engineering practice. 3rd ed., New York: John Wiley & Sons, 1996.

[13] D. R. P. Hettiaratchi and A. R. Reece, "Symmetrical three-dimensional soil failure," *Journal of Terramechanics,* 1967.

[14] MSC Software Corporation, *Adams/Car - Soft-Soil tire model - Documentation (Guide).*

[15] "https://it.mathworks.com/help/simulink," [Online].

[16] GmnH VI-grade, *VI-CarRealTime 19.0 Documentation (Guide),* 2019.

[17] Slob, "State of the Art Driving Simulators, a literature survey," Eindohoven, 2008.

[18] W. Hermann, H. Stephan, L. Felix and S. Christina, Handbook of Driver Assistance Systems, Springer Reference, 2016.

[19] [Online]. Available: https://www.concurrent-rt.com/products/simulation-workbench/#literature.